

**Development of Chemical Modulators for Heat Shock Protein 70 (Hsp70): a  
Potential Therapeutic Target for Tauopathies**

**by**

**Yoshinari Miyata**

A dissertation submitted in partial fulfillment  
of the requirements for the degree of  
Doctor of Philosophy  
(Chemical Biology)  
in The University of Michigan  
2012

Doctoral Committee:

Associate Professor Jason E. Gestwicki, Chair  
Assistant Professor Ivan P. Maillard  
Assistant Professor Zaneta Nikolovska-Coleska  
Assistant Professor Matthew B. Soellner

© Yoshinari Miyata

---

2012

To my family

## **Acknowledgements**

First and foremost, I am deeply grateful to Dr. Jason Gestwicki, who has been a great mentor for the last five years of my graduate studies. Soon after I started rotating in his lab, I became fascinated by his passion and vision for research. He has always been very understanding and offered me great advice not only on science but also on career development, which significantly helped me develop my career path. I feel that I am truly lucky to have the opportunity to work with him. I am very thankful to current and former members of the Gestwicki lab. Lyra Chang has taught me how to clone, express/purify proteins and develop assays, which are key in early stages of my thesis project. Chris Evans has helped me start the MKT-077 project and given me advice on chemical synthesis. Srikanth Patury and Andrea Thompson have provided valuable suggestions in assay development. Jennifer Rauch has provided much help in completing the methylene blue mechanism project. Sharan Srinivasan has helped with modeling of Hsp72 mutants. Finally, Xiaokai Li has expanded the library of MKT-077 derivatives, which allowed us to derive initial structure-activity-relationships.

I am also grateful to my thesis committee members. They have provided me valuable feedback as I progress through my thesis project.



I would also like to thank our collaborators Martha Larsen and Thomas McQuade for their help in running the high-throughput screens, Dr. Erik Zuiderweg and Aikaterini Rousaki for the NMR and docking experiments, Dr. Andrew Lieberman and Adrienne Wang for the polyQ AR experiments, Dr. Duxin Sun and Sarah Lee for pharmacokinetic experiments, Dr. Chad Dickey and his laboratory at the University of South Florida for *in vitro* and *in vivo* tau stability assays, and Dr. Jeffrey Brodsky and Sandlin Seguin at the University of Pittsburgh for conducting ATPase assays for MKT-077 derivatives.

Last but not least I would like to thank my parents and my wife, Valbona, for their understanding, continuous support and encouragement. I could not have accomplished this work without them.

## Table of Contents

<b>Dedication</b>	ii
<b>Acknowledgements</b>	iii
<b>List of Figures</b>	xv
<b>List of Tables</b>	xix
<b>List of Abbreviations</b>	xx
<b>Abstract</b>	xxiv
<b>Chapter</b>	
<b>1 Introduction: Heat Shock Protein 70 as a Potential Therapeutic Target for Tauopathies</b>	1
1.1 Abstract	1
1.2 Introduction to tau and tauopathies	2
1.3 Current therapies for tauopathies	4
1.4 The molecular chaperone Hsp70 and Hsp90	6
1.4.1 Molecular chaperones regulate proteostasis	6
1.4.2 Heat shock protein 70 (Hsp70)	7
1.4.3 Heat shock protein 90 (Hsp90)	10
1.4.4 Heat shock protein 27 (Hsp27)	11
1.4.5 The Hsp70-Hsp90 chaperone cycle	12

1.5 Tau regulation by molecular chaperones	14
1.5.1 Tau turnover is controlled by molecular chaperones	14
1.5.2 Tau and Hsp70	16
1.5.3 Tau and Hsp90	17
1.5.4 Tau and small heat shock proteins	18
1.5.5 Tau and BAGs	19
1.5.6 Tau and Hsp110	19
1.5.7 Tau and FKBP51	20
1.6 Models for tau quality control and future opportunities for drug discovery	20
1.6.1 The role of ATP hydrolysis and substrate dwell time	21
1.6.2 Selecting abnormal tau for degradation	23
1.6.3 Control over protein-protein interactions in the Hsp70/Hsp90 complexes	25
1.6.4 Induction of a stress response	26
1.7 Future perspective	27
1.8 References	29
<b>2 Development of High Throughput Screens for Hsp70 and Identification of Chemical Activators and Inhibitors</b>	<b>40</b>
2.1 Abstract	40
2.1.1 Hsp70s are involved in human diseases	41
2.1.2 Co-chaperones of Hsp70 regulates its ATPase activity	41
2.1.3 Our strategy to identify chemical modulators of Hsp70	42

2.2 Results	43
2.2.1 Fluorescent, energy transfer method has enhanced sensitivity for inorganic phosphate	43
2.2.2 Fluorescence method has superior performances in pilot screens	45
2.2.3 High throughput screen for inhibitors of DnaK's ATPase activity	47
2.2.4 Compound 3c binds DnaK, favors high affinity binding to luciferase and blocks DnaK's stimulation by DnaJ	53
2.2.5 Screening of natural product extracts	55
2.2.6 Screenign of known bioactive compounds	57
2.3 Discussion	59
2.3.1 Miniaturization of colorimetric assay by energy transfer	59
2.3.2 High throughput screen and characterization of a hit compound	60
2.3.3 Conclusion	61
2.4 Materials and Methods	62
2.4.1 Reagents	62
2.4.2 Small molecule libraries	62
2.4.3 High throughput ATPase assay – absorbance method	63
2.4.4 High throughput ATPase assay – fluorescence in white plates	64
2.4.5 Tryptophan fluorescence assay	64
2.4.6 Enzyme-linked immunosorbent assay	65
2.4.7 Construction of natural product extract library and screening against DnaK/DnaJ complex	66
2.4.8 Identification of the active component from tea	66

2.4.9 Identification of chemical modulators of Hsp70 from MS2000 library	67
2.5 Appendices	
2.5.1 Characterization of the white plate, fluorescence assay	69
2.5.2 Occasional outliers in white, opaque microtiter plates	70
2.5.3 Characterization of active component from white tea and identification as (-)-epicatechin-3-gallate	71
2.6 References	72
<b>3 Pharmacological Manipulation of Hsp70 by Methylene Blue</b>	<b>75</b>
3.1 Abstract	75
3.1.1 Abnormal tau causes neurodegenerative diseases	76
3.1.2 Molecular chaperones regulate the turnover of substrates, such as tau, through a poorly understood mechanism	77
3.1.3 New inhibitors and activators of Hsp70 might provide new opportunities for understanding Hsp70's role in tau stability	77
3.2 Results	79
3.2.1 Inhibiting Hsp70 leads to tau degradation, activating Hsp70 leads to tau accumulation	79
3.2.2 AC causes proteasomal degradation of tau	82
3.2.3 Hsp70 inhibition does not cause stress response	84
3.2.4 Overexpression of Hsp70 enhances the efficacy of Hsp70 inhibitors, suggesting that Hsp70 is a major target in cells	85
3.2.5 Hsp70 inhibitors cause rapid reduction of tau levels	87

3.2.6 Hsp70 inhibitors reduce the level of tau mutants that are resistant to Hsp90 inhibitors	89
3.2.7 Hsp70 inhibitors reduce tau levels in a mouse model of AD	92
3.2.8 MB and H <sub>2</sub> O <sub>2</sub> irreversibly inhibit Hsp72 but not Hsc70	93
3.2.9 MB oxidizes Cys306 of Hsp72	96
3.2.10 Hsp72 Cys to Ser mutations confer resistance to MB	97
3.2.11 C267D mutation causes a conformational change and disrupts nucleotide binding	98
3.2.12 Cys to Asp mutations “phenocopies” MB treatment in vitro and in cells	101
3.3 Discussion	103
3.3.1 Chemical modulators of Hsp70 provide insight into chaperone-mediated regulation of tau turnover	115
3.3.2 Hsp70 inhibitors, unlike Hsp90 inhibitors, do not activate a stress response	104
3.3.3 Mechanism by which MB inhibits Hsp70	105
3.3.4 Conclusion	107
3.4 Materials and Methods	108
3.4.1 Reagents, cell lines and general methods	108
3.4.2 Measurement of tau levels in cell culture	109
3.4.3 Tau and Hsp70 interaction in the presence of ATP-γS	109
3.4.4 Measurement of tau levels in brain slices and transgenic mice	110
3.4.5 LDH assay	111

3.4.6 Oxidation of Hsp72/Hsc70	111
3.4.7 ATPase activity	111
3.4.8 Preparation of dimedone-modified Hsp72	111
3.4.9 Mass spectrometry	112
3.4.10 Modeling of Hsp72 C267D	112
3.5 Appendices	114
3.5.1 MB-mediated oxidation of Hsp72 is irreversible	114
3.5.2 Stress inducible, but not constitutive forms of the Hsp70 family contain a unique, reactive cysteine at position 306	115
3.5.3 CD spectra of Hsp72 serine point mutants	116
3.5.4 Hydrogen bond and hydrophobic interactions are lost in Hsp72 C267D modeled structure	117
3.5.5 C267D and C306 mutants have impaired ATP binding and are more flexible	118
3.6 References	119
<b>4 Exploring MKT-077 as a Scaffold for Hsp70 Modulators</b>	
4.1 Abstract	123
4.1.1 MKT-077 as a candidate Hsp70 inhibitor	124
4.2 Results	125
4.2.1 MKT-077 binds Hsc70 NBD with 1:1 stoichiometry	125
4.2.2 MKT-077 binds ADP-state of Hsc70 NBD	126
4.2.3 MKT-077 binds Hsc70 NBD with a $K_D$ in the low micromolar	128
4.2.4 AUTODOCK simulations suggest how MKT-077 binds Hsc70	128

4.2.5 The MKT-077 binding site is conserved in Hsp70 isoforms	130
4.2.6 Analysis of the MKT-077 binding site	131
4.2.7 MKT-077 inhibits ATPase activity and stabilizes ADP-like conformation	132
4.2.8 MKT-077 reduces tau level in HeLa cells and is a useful compound for probing structure-function relationships in the Hsp70 system	134
4.2.9 YM1 increases Hsp70 binding to denatured luciferase	135
4.2.10 YM1 competes with Hip for binding	138
4.2.11 Hip and YM1 promote clearance of AR 112Q	139
4.2.12 YM1 enhances clearance of polyQ AR via proteasomal degradation	141
4.2.13 YM1 rescues AR aggregation phenotype in <i>D. melanogaster</i>	144
4.2.14 YM8 is BBB permeable	145
4.2.15 Synthesis and evaluation of neutral MKT-077 derivatives	148
4.3 Discussion	151
4.3.1 MKT-077 binds Hsp70 at an interface of two lobes and stabilizes its ADP form	151
4.3.2 MKT-077 analogs serve as an artificial co-chaperone and promote clearance of AR 112Q	152
4.3.3 Structure-based design leads to the development of high-affinity MKT-077 derivatives with BBB permeability	153
4.4 Materials and Methods	154



4.4.1 Reagents and cell lines	154
4.4.2 Protein preparation	154
4.4.3 NMR assignment	155
4.4.4 NMR titrations	156
4.4.5 Docking computations	157
4.4.6 Molecular dynamics	159
4.4.7 Docking evaluation	159
4.4.8 Partial proteolysis	161
4.4.9 Luciferase binding assay	162
4.4.10 Hip competition binding assay	162
4.4.11 Cell culture and transfection	163
4.4.12 Analysis of protein expression	163
4.4.13 Immunofluorescence	164
4.4.14 Drosophila stocks and phenotypes	164
4.4.15 Statistics	165
4.4.16 Pharmacokinetic sampling	165
4.4.17 Extraction of YM8	165
4.4.18 LC-MS/MS analysis	166
4.4.19 Calibration standards of YM8 for LC-MS/MS analysis	166
4.4.20 Pharmacokinetic analysis	167
4.4.21 Plasma protein binding	167
4.4.22 Synthesis of MKT-077 and YM1	168
4.4.23 Synthesis of biotinylated YM1 probes	168

4.4.24 Synthesis of neutral MKT-077 derivatives	169
4.5 Appendices	175
4.5.1 800 MHz $^1\text{H}$ - $^{15}\text{N}$ TROSY spectrum of 250 $\mu\text{M}$ $^{15}\text{N}$ , $^2\text{H}$ , $^{13}\text{C}$ Hsc70 NBD in the ADP state (residues 1-387)	175
4.5.2 Compilation of chemical shift changes in the $^1\text{H}$ - $^{15}\text{N}$ TROSY spectra	176
4.5.3 Nucleotide-dependent conformational changes in Hsp70 NBD	177
4.5.4 HSc70 (HSPA8) residues in contact with the five MKT-077 docking families, shown in the context of the human Hsp70 (HSPA) paralogs	178
4.5.5 Residues with chemical shift changes and their distances from MKT-077 in the orientation modeled by AUTODOCK	179
4.5.6 Hormone and glutamine length-dependent polyQ AR oligomerization in Tet-ON PC12 cells	180
4.6 References	181
<b>5 Conclusions and Future Directions</b>	
5.1 Conclusions	184
5.2 Future Directions	188
5.2.1 Identifying co-chaperones that are involved in “low affinity” and “high-affinity” complexes	188
5.2.2 Identifying modulators of protein-protein interactions	190
5.2.3 Optimizing neutral MKT-077 derivatives as drug leads	191
5.3 Final thoughts	192



## List of Figures

1.1	Domain architecture of heat shock protein 70 (Hsp70)	8
1.2	Hsp70, Hsp90 and the chemical structures of select inhibitors	9
1.3	Model of Hsp70, Hsp90 Cycling	14
1.4	Schematic overview of tau quality control by molecular chaperones	15
2.1	Model for converting an absorbance assay into a fluorescence quenching method	44
2.2	Comparison of screening performances between absorbance and fluorescence methods.	46
2.3	Screening of 55,400 samples	48
2.4	Hits identified in the screen	51
2.5	Compound 3c binds DnaK and blocks DnaJ-stimulated ATPase activity	53
2.6	Compound 3c interferes with DnaK-DnaJ and is active against human Hsp70s.	55
2.7	Screening of plant extracts against the DnaK-DnaJ system reveals epicatechin-3-gallate as the major inhibitor in white tea	56
2.8	Identification of both activators and inhibitors of the ATPase activity of Hsp70	58
3.1	Inhibitors of Hsp70 decreases tau levels, activators protect it	80

3.2	Hsp70 modulators do not alter the levels of $\alpha$ -synuclein and TDP-43	81
3.3	Nucleotide state of Hsp70 regulates tau binding and inhibitor-mediated reductions in tau occur via proteasomal degradation	82
3.4	Hsp70 modulators do not change the level of tau aggregation	83
3.5	Reductions in tau are independent of a stress response or an increase in Hsp70 expression	84
3.6	Increasing Hsp70 levels enhances Hsp70 inhibitor efficacy	86
3.7	Celastrol enhances Hsp70 inhibitor efficacy	87
3.8	Tau is rapidly degraded in response to Hsp70 inhibitors	88
3.9	Phospho- and mutant tau species are differentially affected by Hsp70 inhibition	91
3.10	Hsp70 inhibition reduces endogenous and over-expressed tau levels in multiple neuronal models.	92
3.11	The ATPase activity of Hsp72, but not Hsc70, is sensitive to oxidation	94
3.12	Hsp72 is oxidized by MB at specific cysteine residues	96
3.13	Serine mutants of Hsp72 are resistant to MB treatment in ATPase and cell-based assays	98
3.14	Modeling of Hsp72 C267D reveals structural changes in residues that contact nucleotide	99
3.15	Homology model of Hsp72 C306D NBD	100
3.16	Pseudo-oxidation mutants phenocopy MB treatment	102
4.1	Chemical structure of MKT-077	124
4.2	Details of some of the chemical shift changes in the TROSY	126

	spectrum of Hsc70	
4.3	Mapping of the chemical shift changes of MKT-077 on the structure of Hsc70 NBD	127
4.4	Fractional shifts upon addition of MKT-077 in the <sup>15</sup> N, <sup>2</sup> H-labeled Hsc70	128
4.5	Results of AUTODOCK	129
4.6	Four families of docking poses	130
4.7	Best docking pose of MKT-077 on Hsc70	132
4.8	MKT-077 inhibits J-protein-stimulated ATPase activity of yeast Hsp70 (Ssa1p)	133
4.9	MKT-077 favors the ADP-bound conformation of Hsc70, as measured by limited trypsin proteolysis	133
4.10	MKT-077 promotes the clearance of phosphorylated tau (pS395/404) and total tau levels in HeLaC3 cells	135
4.11	Chemical structure of YM1	136
4.12	YM1 promotes binding of Hsp70 to denatured luciferase and stabilizes ADP-bound form	137
4.13	Chemical structures of biotinylated YM1 probes	138
4.14	YM1-biotin specifically binds Hsp72	138
4.15	YM1 and Hip bind competitively to Hsp70	139
4.16	Hip promotes clearance of AR112Q via proteasomal degradation	140
4.17	YM1 diminishes AR112Q aggregation	141
4.18	YM1 promotes clearance of AR112Q	142

4.19	YM1 promotes proteasomal degradation of AR112Q in an Hsp70 dependent manner	143
4.20	YM1 rescues the rough eye phenotype in Drosophila expressing AR52Q	144
4.21	Chemical structure of YM8	145
4.22	YM8 competes with YM1-biotin and reduces tau levels	147
4.23	Synthetic scheme for neutral MKT-077 derivatives	147
4.24	Chemical structures of compounds 15 and 16	149
4.25	Potential contacts between the pyridinium moiety of MKT-077 and Hsc70	150
5.1	Utilizing chemical probes to identify chaperone complex in the high-affinity ADP-state	189
5.2	Flow cytometry assay	190
5.3	FRET-like binding assay	191

## List of Tables

4.1	Distribution of YM1 and YM8 in CD-1 mice	146
4.2	Chemical structures of neutral MKT-077 derivatives and their activity	148



## List of Abbreviations

AC	Azure C
AD	Alzheimer's disease
ADP	Adenosine-5'-disphosphate
ALS	Amyolateral sclerosis
AMP-PNP	Adenosine-5'-( $\beta$ , $\gamma$ -imido)triphosphate
AR	Androgen receptor
ATP	Adenosine-5'-triphosphate
BAG	BCL2-associated athanogene
BBB	Blood-brain barrier
CD	Circular dichroism
Cdk5	Cyclin-dependent kinase 5
CFTR	Cystic fibrosis transmembrane regulator
CHIP	C-terminus of Hsc70-interacting protein
CNS	Central nervous system
CTD	C-terminal domain
DHT	Dihydroxytestosterone
DMSO	Dimethylsulfoxide
ECG	Epicatechin-3-gallate

ELISA	Enzyme linked immunosorbent assay
ERAD	ER-associated degradation
FRET	Fluorescence resonance energy transfer
FKBP	FK506-binding protein
FTDP-17	Frontotemporal dementia with parkinsonism linked to chromosome 17
GA	Geldanamycin
Gsk3 $\beta$	Glycogen synthase kinase 3 $\beta$
Hip	Hsp70 interacting protein
HOP	Hsp70/Hsp90 organizing protein
Hsc70	Heat shock cognate 70
HSE	Heat shock element
HSF1	Heat shock factor 1
Hsp110	Heat shock protein 110
Hsp27	Heat shock protein 27
Hsp70	Heat shock protein 70
Hsp90	Heat shock protein 90
HTS	High throughput screening
IDP	Intrinsically disordered protein
LTP	Long-term potentiation
MAPK2	Microtubule affinity regulating kinase 2
MAPT	Microtubule associating protein tau
MB	Methylene blue

MD	Molecular dynamics
MG	Malachite green
MY	Myricetin
NBD	Nucleotide binding domain
NEF	Nucleotide exchange factor
NMDA	N-methyl-D-aspartate
NTF	Neurofibrillary tangle
NMR	Nuclear magnetic resonance
NTD	N-terminal domain
PHF	Paired helical filament
polyQ	polyglutamine
PP5	Protein phosphatase 5
PPA2	Pyrophosphatase 2
PPI	Protein-protein interaction
PPase	Peptidylprolyl isomerase
PSP	Progressive supranuclear palsy
QR	Quinaldine red
RIPA	Radioimmunoprecipitation assay
SAR	Structure activity relationship
SBD	Substrate binding domain
SBMA	Spinal and bulbar muscular atrophy
TDP-43	TAR-DNA binding protein
TPR	Tetratricopeptide repeat

TROSY	Transverse relaxation optimized spectroscopy
UPS	Ubiquitin-proteasome system
VHL	von Hippel-Lindau

## **ABSTRACT**

### **Development of Chemical Modulators for Heat Shock Protein 70 (Hsp70): a Potential Therapeutic Target for Tauopathies**

**by**

**Yoshinari Miyata**

**Chair: Jason E. Gestwicki**

Tauopathies are a class of neurodegenerative disorders, which affect millions of people worldwide. These diseases are characterized by the accumulation of protein aggregates composed of abnormally modified variants of the microtubule-binding protein tau. Despite extensive efforts, there is currently no cure for these devastating diseases.

The goal of this study is to understand whether heat shock protein 70 (Hsp70) may be an under-explored target for tauopathies. Hsp70 is a molecular chaperone that plays important roles in protein quality control, including the turnover of misfolded polypeptides. However, the molecular mechanisms of tau quality control were not known and it wasn't clear how pharmacological inhibition

of Hsp70 might impact tau accumulation. In this thesis, we review the literature linking Hsp70 to tau and hypothesize that inhibiting the ATPase activity of Hsp70 might lead to the degradation of aberrant tau by favoring the triage pathway (Chapter 1). To test this hypothesis, we developed a new high-throughput screen platform and identified promising inhibitors, including methylene blue (MB) (Chapter 2). MB inhibited the ATPase activity of Hsp70 and, consistent with the major hypothesis, caused a dramatic, Hsp70-dependent reduction in the accumulation of tau in cellular and animal models of tauopathy. In mechanistic studies, we found that MB inhibits Hsp70 by selectively oxidizing two key cysteine residues in the chaperone (Chapter 3). To further explore this process, we developed a parallel chemical series of Hsp70 inhibitors based on the known anti-cancer agent, MKT-077. We found that these compounds inhibit the ATPase activity of Hsp70 and, like MB, they dramatically reduce tau levels (Chapter 4). However, the MKT-077 analogs acted by a distinct mechanism: binding to the ADP-bound form of Hsp70 and allosterically blocking nucleotide cycling. Together, these studies suggest that Hsp70 normally protects tau from degradation, while inhibitors lead to its rapid degradation.

In summary, we have used a chemical biology approach to show that Hsp70 plays a critical role in tau stability and inhibitors reduce tau levels. Thus, this work suggests a potential path towards new treatments for tauopathies. In addition, these findings provide molecular insights into how Hsp70 mediates protein quality control.

## **Chapter 1**

### **Introduction: Heat Shock Protein 70 as a Potential Therapeutic Target for Tauopathies**

#### **1.1 Abstract**

Tau is a microtubule-associated protein that accumulates in at least fifteen different neurodegenerative disorders, which are collectively referred to as tauopathies. In these diseases, tau is often hyperphosphorylated and found in aggregates, including paired helical filaments (PHFs), neurofibrillary tangles (NFTs) and other abnormal oligomers. Tau aggregates are associated with neuron loss and cognitive decline, which suggests that this protein can somehow evade normal quality control, allowing it to aberrantly accumulate and become proteotoxic. Consistent with this idea, recent studies have shown that molecular chaperones, such as Hsp70 and Hsp90, counteract tau accumulation and neurodegeneration in disease models. These molecular chaperones are major components of the protein quality control systems and they are specifically involved in the decision to retain or degrade many proteins, including tau and its modified variants. Thus, one potential way to treat tauopathies might be to either

accelerate interactions of abnormal tau with these quality control factors or tip the balance of triage towards tau degradation. In this chapter, we summarize recent findings and suggest models for therapeutic intervention.

## **1.2 Introduction to Tau and Tauopathies.**

Tauopathies are a family of neurodegenerative disorders characterized by the appearance of aggregates of the microtubule associating protein tau (MAPT/tau). These diseases include Alzheimer's disease (AD), the most common neurodegenerative disorder, as well as devastating diseases such as frontotemporal dementia with parkinsonism linked to chromosome 17 (FTDP-17) and progressive supranuclear palsy (PSP) [1-5]. In these diseases, tau is found in aggregates termed paired-helical filaments (PHFs) [6, 7], which assemble into the neurofibrillary tangles (NFTs) that were originally described as "senile" plaques in the neurons of AD patients [8].

Numerous observations have converged on a model in which tau aggregation is important for the clinical symptoms of AD and other tauopathies. For example, tau pathology closely correlates to neuron loss and cognitive deficits [9, 10]. Further, the post-translationally modified forms of tau (e.g. hyperphosphorylated and/or proteolyzed) that are enriched in PHFs and NFTs are also more prone to self-assemble *in vitro* [11]. Finally, FTDP-17 is directly linked to point mutations, such as P301L, that make tau more aggregation-prone. Together, these observations have led to the hypothesis that aggregation and abnormal



accumulation of tau aggregates are significant contributing factors in tauopathies.

Tau is a cytosolic protein that is abundantly expressed in neurons and found in at least thirteen splice isoforms in the brain [12, 13]. Its major cellular function is to stabilize microtubules and this activity has been found to be essential for axonal transport [14]. Interestingly, tau belongs to a class of intrinsically disordered proteins (IDPs) whose free structures are believed to be best represented by an ensemble of possible orientations with weak preference for any specific structural motif [15-18]. However, tau is likely to adopt local structure when bound to microtubules. This interaction occurs through the microtubule-binding repeats of tau, with the 3R and 4R splice isoforms having either three or four repeats, respectively. Consistent with the importance of this domain, mutations in the microtubule-binding repeats have been found to weaken tau binding, reducing microtubule stability and sometimes leading to neuron loss [19, 20].

Phosphorylation of tau by the kinases, GSK3 $\beta$ , Cdk5 and MARK2, is a major regulator of its microtubule interactions [21-24]. GSK3 $\beta$  is a proline-directed, serine/threonine kinase involved in many signaling pathways, including signaling downstream of wnt, insulin and many G-protein coupled receptors [25]. Cdk5 is another serine/threonine kinase involved in multiple pathways, including NMDA receptor and growth factor signaling. Cdk5 exists in two complexes in post mitotic neurons, a pro-survival complex with p35 (Cdk5-p35) and an apoptotic complex with p25 (Cdk5-p25), the latter of which has stronger kinase activity [22, 26, 27].

Together, GSK3 $\beta$  and Cdk5 are thought to be major kinases of tau in the brain [28]. Importantly, MARK2-based phosphorylation of tau is accelerated by the priming activity of either Cdk5 or GSK3 $\beta$  [29], suggesting that tau phosphorylation involves a series of ordered kinase events. In general, phosphorylation of tau reduces its affinity for microtubules [30], while dephosphorylation via enzymes such as PP2A and PP5, restores binding [30, 31]. This reversible cycle of association and dissociation is a normal cellular process that facilitates axonal transport [30-33]. However, hyperphosphorylated forms of tau are more prone to aggregate, which might decrease their solubility and remove them from normal cycling [34]. Further, proteolytic processing of tau, by caspases, calpains and other enzymes, can significantly accelerate hyperphosphorylation and facilitate aggregation [35]. Thus, tauopathies might be considered as involving an imbalance in the normal processing of tau, which affects its microtubule binding, aggregation propensity, phosphorylation status and, ultimately, its turnover.

### **1.3 Current Therapies for Tauopathies.**

There are no cures for any tauopathy. Neuroprotective agents, such as acetylcholinesterase inhibitors and NMDA (*N*-methyl-D-aspartate) antagonists, have been approved for use in the clinic based on their ability to slow the rate of cognitive decline in patients with moderate to severe AD (reviewed in [36]). However, long term strategies for tauopathies will likely need to focus on impacting the underlying, disease-causing accumulation of modified and

aggregated tau (reviewed in [37, 38]). For example, because of the importance of phosphorylation, there are a number of kinase inhibitors being explored as therapeutics for tauopathies [39]. Whether this strategy will be able to improve cognition without adverse effects on other cellular processes remains to be determined. Nevertheless, some studies targeting kinases have demonstrated promising early efficacy in patients (reviewed in [40]). In addition to kinase inhibitors, compounds that directly block the aggregation of tau are also being explored as potential therapeutics [41]. These efforts have produced early-stage molecules of multiple different chemical classes, including rhodanine-based inhibitors, phenylthiazolyhydrazides, N-phenylamines, anthraquinones, benzothiazoles, phenothiazines and polyphenols [41]. However, recent studies suggest that intermediate, soluble oligomers of tau might best correlate with disease, suggesting that any anti-aggregation strategy will have to selectively reduce the levels of these structures [42-44].

Another possible way to treat tauopathies may be to manipulate the quality control pathways that regulate tau turnover. This hypothesis is based on the idea that tauopathies result, in part, from a failure of neurons to properly recognize and remove hyperphosphorylated and/or aggregated tau. All proteins, including tau, are subject to extensive regulation by the cellular quality control pathways, which carefully control the balance between protein expression and turnover to maintain healthy protein homeostasis (or proteostasis). Interestingly, tau clearance is known to be impaired in the aging brain [45], supporting the idea

that diminished quality control might be conducive to certain tauopathies, such as AD, which are linked to aging. Based on this idea, one might imagine that pharmacologically accelerating tau degradation as a possible strategy to overcome aging-dependent deficits in quality control and relieve tauopathies. Recent evidence suggests that tau is essential for the neurotoxicity of amyloid beta, providing a possible link between these classic AD targets and further suggesting that reductions in tau levels might be important via multiple, beneficial mechanisms [46-48]. In this chapter, we will discuss some recent advances in this direction and discuss the strengths and challenges of this strategy. However, it is likely useful to first introduce the structure, function and “druggability” of some of the key components of the quality control pathways: the molecular chaperones.

#### **1.4 The Molecular Chaperones Hsp70 and Hsp90**

##### **1.4.1 Molecular Chaperones Regulate Proteostasis**

Molecular chaperones are abundant and highly conserved proteins that assume an important role in protein quality control [49, 50]. Several members of the chaperone family are upregulated in response to stress and, thus, these factors have been termed heat shock proteins (Hsps). The expression of Hsps is regulated by heat shock factor 1 (HSF1), which, under stress conditions, becomes associated with heat shock elements (HSEs) to elevate the transcription of Hsps and other proteins [51]. Each class of Hsp is named according to its molecular weight; Hsp27, Hsp70, Hsp90, etc. These proteins are

thought to serve individual functions, while collectively they monitor most aspects of protein synthesis, folding, trafficking and assembly of multi-protein complexes (reviewed in [52]). Importantly, the Hsps are also critical at the end of a protein's life, as they facilitate turnover by the proteasome system and the clearance of proteotoxic aggregates by autophagy [53]. Even under normal conditions, as much as 30% of newly synthesized polypeptides are degraded [54], suggesting that all proteins are in equilibrium between folding and degradation, a balance that is maintained, in part, by the Hsp molecular chaperones.

#### **1.4.2 Heat Shock Protein 70 (Hsp70)**

Hsp70 is a major component in protein quality control and, as discussed below, a key factor in tau turnover. There are multiple, highly conserved Hsp70s in humans and members of this family of chaperones are abundant in all major organelles and the cytosol. Each Hsp70 is composed of a nucleotide binding domain (NBD) and a substrate binding domain (SBD) (**Figure 1.1**) [55]. The NBD contains two lobes comprising a deep nucleotide-binding cleft that binds ATP. The SBD can be further divided into beta-sandwich and alpha-helical lid subdomains, the latter of which contains a motif characterized by the amino acids EEVD that binds to tetratricopeptide repeat (TPR) domains. The NBD hydrolyzes ATP, while the SBD binds to hydrophobic regions of polypeptides via the beta-sandwich subdomain [56]. It is thought that Hsp70 promiscuously binds to many hydrophobic polypeptides [57, 58], including regions of tau adjacent to the

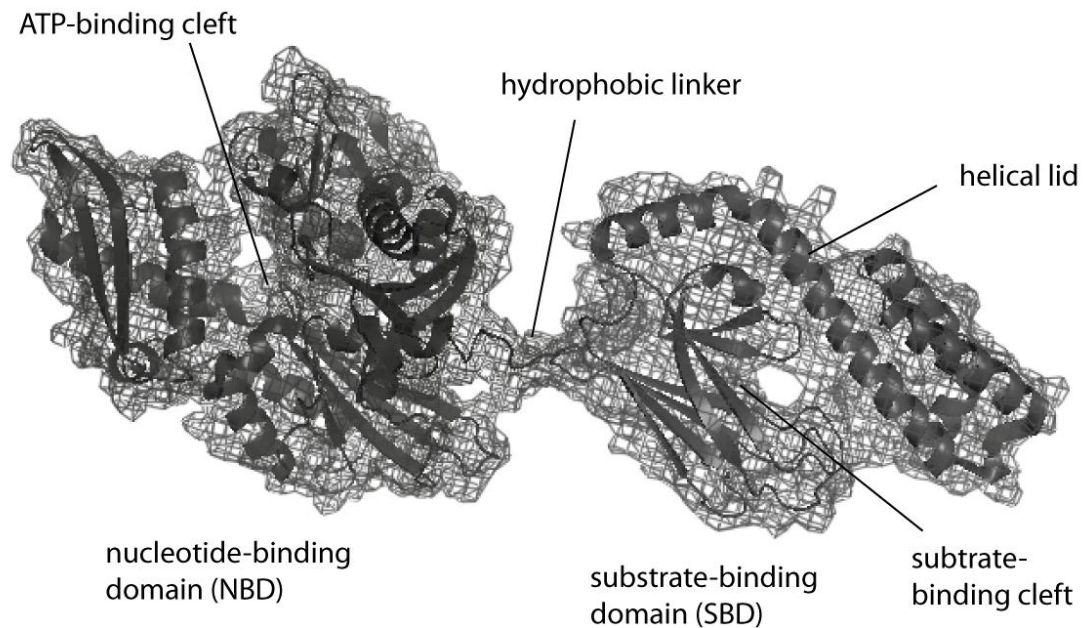


**Figure 1.1 Domain architecture of heat shock protein 70 (Hsp70).** An N-terminal nucleotide-binding domain (NBD) contains the nucleotide binding and hydrolysis center. The substrate-binding domain (SBD), which binds to exposed hydrophobic polypeptides, is attached through a short linker. The C-terminus of the SBD is mostly helical subdomain, which is termed the “lid”. The prokaryotic Hsp70, DnaK, is shown (PDB code #2HKO), but the general architecture appears to be conserved amongst prokaryotic and eukaryotic family members.

microtubule-binding repeats [59]. A flexible linker connects the NBD and SBD and these domains appear to communicate via allostery. For example, with ATP bound to the NBD, the SBD has a weaker binding affinity for substrate polypeptides. The intrinsic ATPase activity of Hsp70 is very weak ( $\sim 0.2$  nmol/ $\mu$ g/min) [60] and, under physiological conditions, it is regulated by co-chaperones, including J-proteins and nucleotide exchange factors (NEFs). Briefly, J-proteins cause a conformational change in Hsp70s that accelerates ATP hydrolysis [61], while NEFs facilitate ADP release [62]. Finally, TPR domain-containing proteins are co-chaperones that bind to the EEVD motif and help dictate the fate of substrates bound to Hsp70. Thus, Hsp70s are part of a multi-protein complex that utilizes coordinated ATPase activity and multiple co-

chaperone partners to shape interactions with misfolded substrates.

Hsp70 has been the subject of recent efforts to develop chemical inhibitors [52, 63] and a number of high throughput screening efforts have been reported [60, 64-67]. Drug development on this emerging target is still in its early stages, with only a few potent and/or selective inhibitors described [68]. In my thesis work, I have been involved in many of the most recent efforts to target Hsp70 and those studies will be described in Chapters 2, 3 and 4. Briefly, most of the currently available chemical probes target the ATPase activity of Hsp70, through either

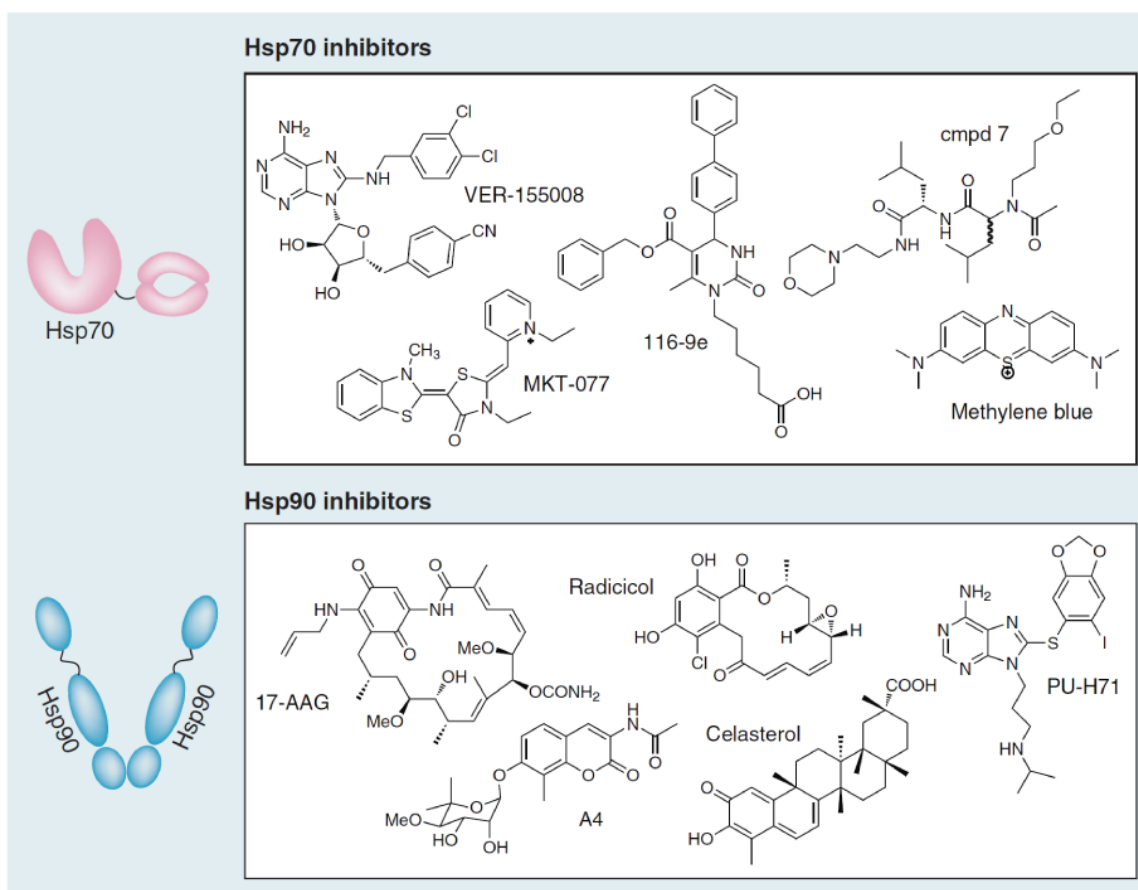


Figure 1.2 Hsp70, Hsp90 and the chemical structures of select inhibitors.

competitive or non-competitive, allosteric mechanisms (**Figure 1.2**). For example, VER-155008 is an ATP-competitive compound developed by structure-guided design [69, 70]. However, there is an indirect relationship between ATP turnover and chaperone functions [71], suggesting that other aspects of Hsp70 function might also be worth exploring for drug discovery. For example, other members of the Gestwicki laboratory have identified compounds that operate at protein-protein interfaces to disrupt interactions with co-chaperones, such as 116-9e [65, 72, 73]. Other inhibitors target the SBD to block binding to substrates, such as compound 7 [74, 75]. As might be expected given the diverse mechanisms of these compounds, known Hsp70 inhibitors represent a variety of chemical classes, including dihydropyrimidines, adenosine analogs, polyamines and others (**Figure 1.2**) [52, 63]. Moreover, many of these inhibitors, including methylene blue and MKT-077, have poorly understood mechanisms as will be discussed in Chapters 3 and 4.

### **1.4.3 Heat Shock Protein 90 (Hsp90)**

Hsp90 has three domains, a 25 kDa N-terminal domain (NTD) connected by a flexible, charged linker to the 40 kDa middle domain (MD) and a 12 kDa C-terminal domain (CTD) [76-83]. These three domains contain an ATP binding pocket, a substrate peptide-binding site, and a TPR domain-binding EEVD motif, respectively. Recent structural studies have suggested that Hsp90 functions as a homodimer in which the CTDs of two Hsp90 molecules are in contact at the bottom of the "V-shaped" open conformer. As in the case of Hsp70, co-



chaperones of Hsp90, such as Aha1, cdc37 and TPR-domain containing proteins, regulate its ATPase activity and control its conformational transitions (reviewed in [84]). Hsp90 is thought to have a more restricted set of substrates than Hsp70, but these clients include a number of important kinases and signaling proteins.

Because of its client pool, Hsp90 has become an established anti-cancer target, with a number of selective and potent inhibitors available [85, 86]. Work on Hsp90 inhibitors benefited from the early discovery of the natural product, geldanamycin, which competes with ATP and induces destabilization of Hsp90-bound proteins [87]. Since this discovery, a number of high-affinity analogs, such as 17-AAG, and alternative synthetic scaffolds, including radicicol and PU-H71, have since been reported (**Figure 1.2**) [85, 88]. These compounds bind in either the N-terminal ATP binding site (*e.g.* 17-AAG, radicicol, PU-H71) [89] or C-terminal (*e.g.* novobiocin, A4) [90, 91] dimerization domain and they show great promise as both anti-cancer compounds and research tools for understanding Hsp90 biology. Several Hsp90 inhibitors are currently in clinical trials, all of which target the N-terminal domain [92]. More recently, there has also been interest in developing compounds, such as celastrol (**Figure 1.2**), that selectively disrupt association of co-chaperones with Hsp90 as an alternative way to control chaperone activity [93-96].

#### **1.4.4 Heat Shock Protein 27 (Hsp27)**

Hsp27 is a member of the small heat shock protein family of molecular chaperones that contain a highly conserved crystallin domain. These proteins are ATP-independent chaperones that undergo homo-oligomerization in response to stress [97, 98]. Small heat shock proteins have been imaged by electron microscopy and these studies have revealed that some of these oligomers are ordered polyhedrons [99]. Further, gel filtration and centrifugation studies have suggested that Hsp27 exists as an ensemble of oligomers, which range in size from dimers to approximately 32mers or greater. Binding of susceptible substrates to the surface of these Hsp27 oligomers is thought to limit stress-induced aggregation and, thus, this chaperone is considered a “holdase”. To allow substrate release, Hsp27 oligomerization is reversible, a process that is regulated, at least in part, by phosphorylation. Like Hsp90 and Hsp70, Hsp27 plays important pro-survival roles; however, no drug-like molecules have been reported that target its activities or protein-protein interactions.

#### **1.4.5 The Hsp70-Hsp90 Chaperone Cycle**

During protein quality control, Hsp70, Hsp90 and Hsp27 (and their co-chaperones) often work in concert. If prolonged misfolding is detected, the chaperones shuttle the protein to a degradation endpoint, such as the proteasome or autophagy. This general model arises, in large part, from a series of seminal experiments on the Hsp70/Hsp90 chaperone system and how it regulates the nuclear hormone receptors [100, 101]. In this model, a J-protein (also known as an Hsp40) is thought to facilitate high affinity, substrate-binding to

Hsp70 by coordinating substrate delivery and ATP turnover (**Figure 1.3**) [60].

The action of a NEF then releases the substrate [49], which can either achieve its proper folding outcome, re-enter the Hsp70-based ATPase cycle, or be fated for subsequent steps in quality control. In these latter cases, an Hsp70-bound substrate can be transferred to Hsp90 via HOP (Hsp70/Hsp90 organizing protein) [102, 103]. Alternatively, either Hsp70 or Hsp90 can recruit the ubiquitin E3 ligase, CHIP, to degrade the bound substrate [104]. During this triage process, certain substrates are known to require additional co-chaperones at distinct steps. For example, the co-chaperones cdc37, a peptidylprolyl isomerase (PPIase) family member and p23 are all critical for the transfer of kinases to Hsp90 and maturation of the active protein [76, 105]. In addition, Hsp90's hydrolysis of ATP, which is stimulated by Aha1, facilitates polypeptide release [82, 106] and transfer to CHIP or other E3 ligases [107, 108]. Thus, protein quality control is thought to involve a series of "checkpoint" steps that monitor substrate folding and enact triage decisions. These steps are defined by ATP/ADP cycling, changes in tertiary and quaternary structure, and fluctuation in the identity of associated co-chaperones.

Although both Hsp70 and Hsp90 can promote degradation of client proteins, it has recently been shown that, functionally, the Hsp70 complex often dominates triage decisions [85, 107, 109]. Thus, Hsp70 may function as a primary checkpoint prior to entering the Hsp90-based complex for maturation. In this model, it may be helpful to picture protein quality control as three phases of (a) J

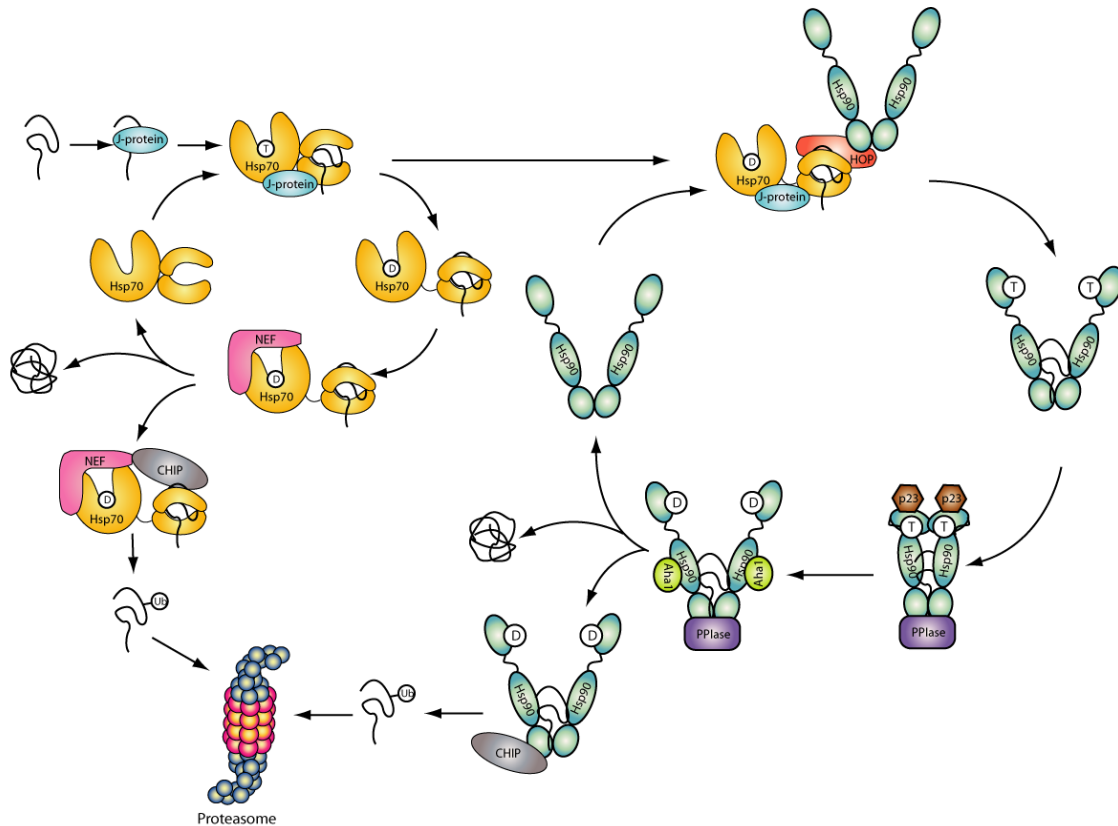


**Figure 1.3 Model of Hsp70-Hsp90 cycling.** Unfolded or misfolded substrates enter the chaperone cycle by engaging in interactions with J proteins, which recruit Hsp70 family chaperones. The ATPase cycle of Hsp70 can result in substrate folding, triage through the proteasome or “hand-off” to the Hsp90 system. The ATPase cycle of Hsp90 refines folding and stabilizes the active form of many kinases and transcription factors. In addition, the Hsp90 cycle makes triage decisions, through CHIP-mediated ubiquitination and degradation.

protein-directed recruitment, (b) primary folding and triage in the Hsp70 complex and (c) secondary folding and function in the Hsp90 system (**Figure 1.3**). In theory, any of these steps might contain suitable drug targets for tauopathies.

## 1.5 Tau Regulation by Molecular Chaperones

### 1.5.1 Tau Turnover is Controlled by Molecular Chaperones

Tau cycling on/off microtubules and its proteolytic turnover are assisted by molecular chaperones and, thus, these proteins play an important role in its normal homeostasis [110, 111]. However, under potentially proteotoxic conditions, the post-translational modifications or mutations that damage tau’s

affinity for microtubules and favor its aggregation are thought to generate a molecular “danger signal” that specifically alerts the quality control system [112, 113]. As discussed above, this system then “decides” to retain or degrade that substrate. In the tauopathy disease scenario, imbalances in this decision for abnormal tau appear to allow accumulation, proteotoxicity and neuron loss (Figure 1.4). In the next sections, we will review the evidence suggesting an

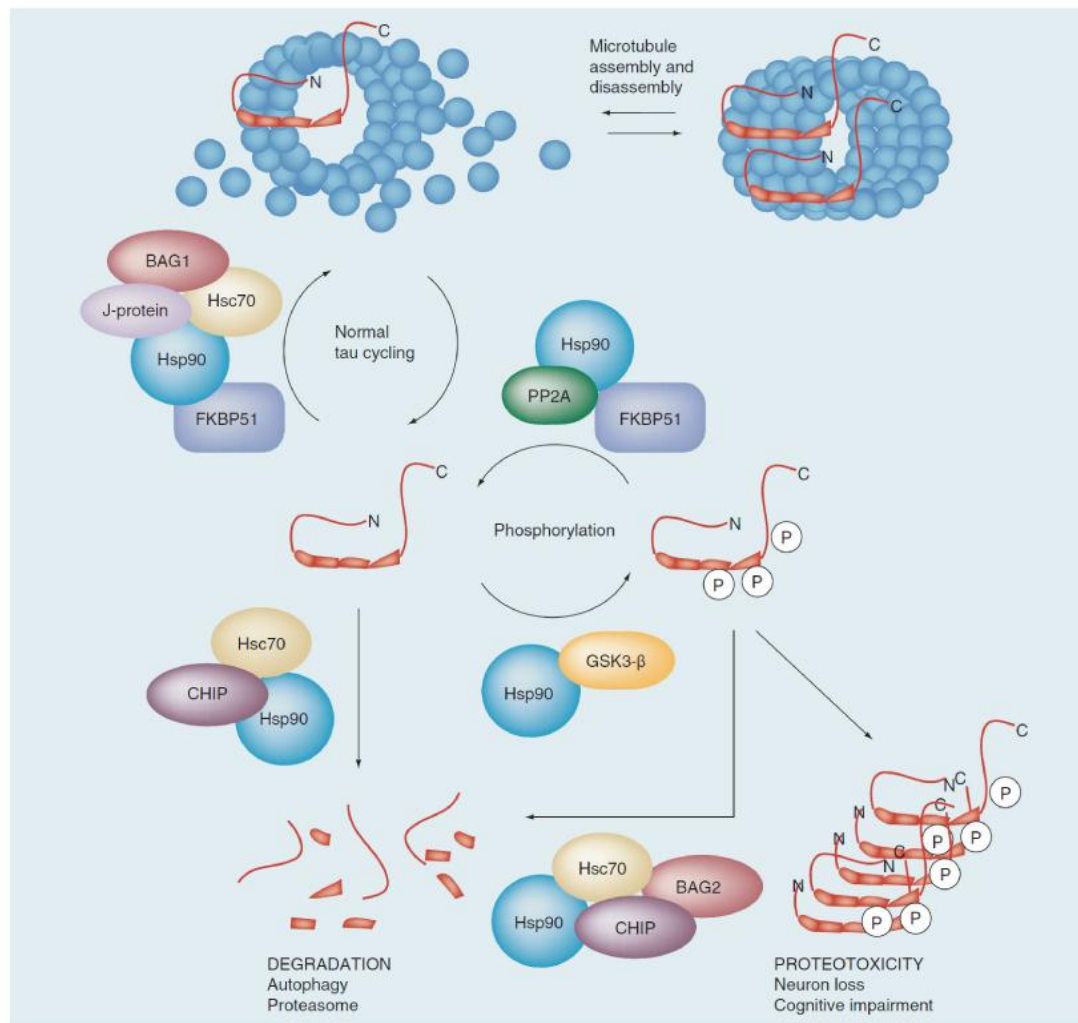


**Figure 1.4 Schematic overview of tau quality control by molecular chaperones.** From the microtubule-bound pool, tau might be released in a form that is capable of re-binding microtubule (termed “cycling tau”). Alternatively, hyperphosphorylated and aggregation-prone tau might accumulate. Chaperones are involved in all stages of cycling tau, in mediating phosphorylation and in making triage decisions.

essential “decision making” role for molecular chaperones in tau quality control. Also, we will discuss findings that suggest Hsp70 and Hsp90 could be drug targets for tauopathies.

### **1.5.2 Tau and Hsp70**

Hsp70s have been shown to both (a) stabilize binding of tau to microtubules [114] and (b) promote its degradation in combination with CHIP [115, 116]. For example, recent work has demonstrated that Hsc70, the constitutive cytosolic form of Hsp70s, dynamically regulates the association of tau with microtubules [112]. These activities arise via direct binding of Hsp70s to the microtubule binding repeats of tau [59]. This central role for Hsp70 family members in regulating tau cycling and triage suggests possible ways of tipping the balance. In fact, recent work from our group, some of which is described in more detail in Chapter 3, has shown that inhibition of the ATPase activity of Hsp70/Hsc70 promotes proteasomal degradation of tau; whereas activation results in tau accumulation [117]. Furthermore, one of these inhibitors was able to reduce phospho-tau levels and improve cognition in a transgenic mouse model [44]. Interestingly, these effects were observed without apparent toxicity, induction of HSF1 activity or adverse health effects on the animals, providing preliminary evidence that targeting Hsp70 may be a surprisingly viable pharmacological approach. However, many critical questions remain. For example, what is the molecular mechanism(s) by which inhibition of Hsp70 leads to tau degradation? How does Hsp70 selectively recognize abnormal tau from a pool of normal,

cycling tau? Speculative models to account for these interesting observations are elaborated upon below.

### **1.5.3 Tau and Hsp90**

Hsp90 was also shown to increase association of tau with microtubules [114], however, its binding is not well characterized and it isn't known whether this is a direct or indirect process. For example, it has recently been shown that Hsp90 promotes tau's phosphorylation by its ability to stabilize GSK3 $\beta$  [118]. These data may suggest that Hsp90 allows accumulation of pathogenic tau species. However, this issue is more complicated, because other work has shown that chemical inhibition of Hsp90 by 17-AAG and other inhibitors reduces cellular levels of two phospho-tau species, pS202/T205 and pS396/S404, both of which are relevant to AD pathogenesis [119]. In response to the inhibitors, tau clearance occurs via CHIP-mediated, proteasomal degradation [119-121]. In addition, other mutant forms of tau have also been particularly susceptible to Hsp90 inhibition, while wild type tau is not [122]. Interestingly, it was recently found that reducing the levels of Akt, another client of the Hsp90/CHIP complex, facilitates tau degradation [123], suggesting a synchronized balance between competing Hsp90 substrates that may be driven, in part, by their relative abundance or susceptibility to Hsp90 binding.

Together, multiple studies suggest that Hsp90 regulates the stability of both phospho- and mutant-tau. However, a greater effort needs to be made to

elucidate the mechanisms driving the apparent preservation of aggregation-prone isoforms. Potential mechanisms and research avenues will be discussed in more detail below, but one interesting idea comes from studies implicating Hsp90 as a driving force in evolution via its ability to preserve mutant proteins [124]. If Hsp90 can buffer against mutations, whether deleterious or beneficial, then this suggests that it might be adopting a similar role in tau pathogenesis. In other words, Hsp90 inhibition may be able to “de-evolve” the chaperone system to clear proteotoxic tau species.

#### **1.5.4 Tau and Small Heat Shock Proteins**

Hsp27 has emerged as a potential target for tau regulation based on early findings that it preferentially binds to phosphorylated and hyperphosphorylated tau and promotes their clearance [125, 126]. However, astrocyte-derived Hsp27 has been shown to promote tau accumulation and Hsp27 associates with tau tangles in a mouse model [127, 128], suggesting a more complex relationship. Recently, our group demonstrated that viral delivery of wildtype Hsp27 into the brains of tau-transgenic mice reduced tau levels and rescued long-term potentiation (LTP) deficits. Conversely, delivery of a mock-phosphorylated mutant Hsp27 caused increased tau levels [129]. This study suggests that Hsp27 may need to cycle between phosphorylated and de-phosphorylated states to promote tau clearance, perhaps explaining the apparent contradictions observed previously. Until more is known about the structure and biology of Hsp27, and why certain multimeric states are necessary for its chaperoning abilities, it will



likely remain an elusive target.

### **1.5.5 Tau and BAGs**

Proteins containing BAG domains, such as BAG1 and BAG2, have been found to function as NEFs for Hsp70s [62]. BAG1 is up-regulated in the hippocampus of AD patients [130], where it associates with tau and increases tau levels in cooperation with Hsp70 [131]. BAG1 silencing decreases tau levels, consistent with a critical role for this co-chaperone in protecting tau from degradation. However, another related BAG family member, BAG2, interacts with Hsp70 and tau but, unlike BAG1, it appears to be involved in clearing phosphorylated tau [132]. Thus, it appears that different BAG family members can have distinct and dramatic impacts on the fate of Hsp70-bound tau. Moreover, these studies suggest that pharmacologically enhancing BAG2 or inhibiting BAG1 might be expected to decrease tau levels. However, the best way to leverage this information isn't yet clear.

### **1.5.6 Tau and Hsp110**

Recent work has defined Hsp110 as another nucleotide exchange factor for Hsp70s [133, 134]. This co-chaperone is of interest in tauopathies because Hsp110 knockout mice show an age-dependent accumulation of phosphorylated tau in the hippocampus [135]. Because little is known about direct binding of Hsp110 to tau or its specific effects on substrate selection by Hsp70s, it isn't yet clear how these findings might be translated to therapeutics.

### **1.5.7 Tau and FKBP51**

Recently, the co-chaperone FKBP51 (FK506-binding protein 51 kDa) has been implicated as a modulator of tau binding to microtubules. FKBP51 contains a peptidyl-prolyl cis-trans isomerase (PPIase) domain as well as a TPR domain; thus it can be recruited to the Hsp90 system where it catalyzes isomerization of proline residues in chaperone-bound substrates. In relation to tau biology, FKBP51 enhances the association of Hsp90 with tau, co-localize with tau in murine neurons, co-immunoprecipitate with tau in AD tissue samples, and increase with age in an AD mouse model [136]. These interactions may be functionally important because silencing FKBP51 reduces tau and phosphorylated-tau levels [136]. In addition, the PPIase activity of FKBP51 was necessary for tau-related, microtubule formation in a *Xenopus* oocyte model, suggesting that this co-chaperone is not only interacting with tau but that its enzymatic activity is important. Finally, FKBP51-Hsp90 complex has been proposed to be responsible for the interaction of tau with phosphatases, helping to restore binding to microtubules [137]. Together, these studies suggest that an Hsp90-FKBP51 complex assists normal cycling of tau via multiple mechanisms. Moreover, because high affinity inhibitors of FKBP51 (such as FK506) are well known, these findings suggest important avenues for therapeutic intervention [138].

## **1.6 Models for Tau Quality Control and Future Opportunities for Drug Discovery**

Together, these genetic and pharmacological studies suggest that targeting molecular chaperones may be a way to reduce phosphorylated tau levels and treat tauopathies. In fact, preliminary support for this idea has been provided using chemical inhibitors of Hsp70 and Hsp90 in model systems [44, 117, 120, 121]. However, there are many open questions about the best way to proceed on the path to therapeutics. How do you develop drugs that reduce abnormal tau levels without impacting global proteostasis? Is it possible to selectively induce a BAG2-Hsp70 or CHIP-Hsp90 complex to accelerate tau degradation? In part, these deceptively simple questions arise from our relatively poor understanding of how normal triage decisions are made by the Hsp70/Hsp90 chaperone systems. How are substrates normally selected? What structural transitions lead to normal substrate turnover? What features of a substrate are important for communicating its failed folding to the chaperones? Here, we will briefly provide some plausible models that are consistent with the available findings. These discussions, while admittedly oversimplified, are intended to act as a framework for guiding future therapeutic efforts.

### **1.6.1 The Role of ATP Hydrolysis and Substrate Dwell Time**

From a medicinal chemist's perspective, targeting the ATP-binding site of either Hsp70 or Hsp90 has significant advantages, because the nucleotide-binding pockets are deep, well-defined clefts (for a recent, in-depth review of this concept see: [68]). Moreover, as mentioned above, inhibitors of the ATPase activities of either Hsp70 or Hsp90 have been found to reduce tau levels, supporting the

general promise of this approach [44, 117, 120, 121]. However, the mechanisms that correlate changes in nucleotide state with substrate degradation are not clear. In general, it is thought that inhibition of ATP cycling will lead to release of the substrate to the degradation pathways because of the allostery between nucleotide state and substrate-binding affinity. However, what is the structure and composition of the early degradation complex? How does it differ from the folding or retention complex? We propose that if we better understood the molecular and structural underpinnings of this triage decision, we might be able to develop therapeutic strategies that best target abnormal tau for turnover with minimal toxicity.

One potential model linking ATPase inhibitors to changes in tau fate is based on the relative partitioning of substrates onto the Hsp70/Hsp90 chaperones [139]. As discussed earlier, both of these chaperones hydrolyze ATP and use this cycling to regulate their affinity for substrates. Thus, substrate “dwell time” in the chaperone-bound state will depend, in part, on nucleotide turnover rate and the relative abundance of the ATP- and ADP-bound forms [140]. It seems possible that folding-competent proteins, on average, might be more transiently associated with the Hsp70/Hsp90 complex, while misfolded substrates could be “stalled” and have increased dwell time. In this model, accumulation of an Hsp70-substrate complex (either via treatment with chemical inhibitors or because of intrinsic properties of the substrate) might allow enough time for a degradation factor (e.g. CHIP) to bind and facilitate polyubiquitination. This idea is supported

by the findings that inhibitors of Hsp70's ATPase activity favor degradation of tau, while activators (which would presumably promote ATP cycling) lead to net retention [73, 117]. Similarly, AdaSGC, which inhibits J-protein stimulated Hsp70 ATPase activity, promotes escape of  $\Delta F508$  cystic fibrosis transmembrane regulator (CFTR) from ER-associated degradation (ERAD) [142]. For studies on Hsp90 inhibitors, this model also has some support. For example, Hsp90 inhibitors cause degradation of tau and many cancer-related substrates [85]. Moreover, these compounds were found to prolong binding of Hsp90 to a model substrate, which was sufficient to promote its degradation [141]. Together, these studies suggest that degradation factors, such as CHIP, might be particularly recruited to chaperones in a "stalled" conformation that is enforced by prolonged ATP/ADP binding or another, yet uncharacterized, structural signal. This "degradation cue" seems likely to be additionally impacted by a variety of other factors, including the context of the client, availability of co-chaperones and, possibly, the organelle environment. The fact that Hsp70 inhibitors reduce tau levels without affecting other likely Hsp70 substrates, such as  $\alpha$ -synuclein or TDP-43 in the same cells, generally supports the idea that substrates are actively involved in dictating their own fate [117]. Direct measurements of substrate dwell times in cells will likely be required to clarify the impact of this variable on quality control decisions.

### **1.6.2 Selecting Abnormal Tau for Degradation**

The context-sensitive activity of the chaperone systems naturally gives rise to a

model in which they can “sense” molecular features of their substrates, such as aggregation-propensity. This model is consistent with the data that hyperphosphorylated tau appears to be specifically selected for degradation by some chaperone machines, such as the Hsp90-FKBP51 complex, without effects on normal tau [132, 136]. How does this selectivity arise? This question is important because any future therapy will likely need to reduce abnormal tau levels with minimal impact on total tau or global proteostasis. One potential insight comes from the observation that there are more than 40 distinct J-proteins in humans [143]. These co-chaperones are thought to be especially important for client selection and recruitment into the early Hsp70 triage complex. Because mammals express over forty J proteins, dozens of NEFs, hundreds of TPRs and other co-chaperones, combinatorial assembly will quickly permit a vast array of possible Hsp70/Hsp90 chaperone complexes. Thus, in this hypothetical and speculative model, groups of related substrates (e.g. hyperphosphorylated tau isoforms) might be expected to depend on a dedicated set of complexes. A major prediction of this model, then, is that targeting the “right” chaperone complex with small molecules might allow selective degradation of abnormal tau without adverse effects on other targets. However, this model is likely too simple. In addition to the composition of the targeted chaperone complex, cellular outcomes are likely to be influenced by the relative substrate expression levels, age, cellular folding capacity, current flux through the degradation pathways and cell type [144].

### **1.6.3 Control Over Protein-Protein Interactions in the Hsp70/Hsp90 Complexes**

Because substrate fate is thought to be dependent on a series of “hand-offs” between dynamic, multi-protein chaperone complexes (as in Figure 2), another option for controlling the fate of tau might be to specifically target key protein-protein interactions. Consistent with this idea, data from our group and others has suggested that chemical modulators of co-chaperone interactions “tip” the equilibrium and alter tau levels [72, 73, 117]. This general idea has been observed in other systems as well. For example, the Hsp90 inhibitor geldanamycin, mimics ADP binding but it also inhibits recruitment of p23, which is a necessary step in client maturation [145]. Interestingly, p23 deletion causes hypersensitivity to geldanamycin and its over-expression exhibits a protective effect [146], suggesting that these chemical and co-chaperone factors are antagonistic. Together, these data suggest that blocking recruitment of specific co-chaperones or facilitating the assembly of others might directly impact client fate. In fact, this is believed to be what occurs during natural triage steps [147]. For example, BAG-2 inhibits client ubiquitination by CHIP by interfering with the interaction between CHIP and E2 ubiquitin-conjugating enzymes [148]. In another example, McClellan, et al. showed that von Hippel-Lindau (VHL) tumor-suppressor protein requires Hsp70 for its folding and degradation whereas Hsp90 is only required for degradation [149]. HOP was also required for degradation, indicating that transfer of VHL from the Hsp70 complex to Hsp90 is a necessary part of its degradation pathway. To the medicinal chemist or

chemical biologist, these studies suggest numerous potential opportunities for achieving desired outcomes by manipulating protein contacts within the chaperone system.

Although there are significant challenges related to targeting protein-protein interactions (PPIs), significant advances have been achieved in the past decade [150, 151]. Emerging experimental methods, such as NMR-based fragment screening, are producing robust compounds [152] and comprehensive cheminformatics analyses have started to elucidate the features of good PPI inhibitors [151]. Because of these advances, PPI inhibitors are being identified with increasing frequency, even in the Hsp70/Hsp90 systems [73, 153]. For example, previous members of the Gestwicki laboratory found that dihydropyrimidine-based molecules can either force the association of a prokaryotic Hsp70 with its J protein partner or, with a relatively modest change in chemical structure, related compounds could block this contact [73]. These early studies suggest that the chaperone complexes might be amenable to chemical prodding, perhaps altering the fate of substrates, such as tau, that pass through this quality control system.

#### **1.6.4 Induction of a Stress Response**

Over the past decade, induction of Hsps has been shown to ameliorate proteotoxicity caused by misfolded proteins [154-159]. Accordingly, pharmacological activation of the heat shock response may be another viable strategy for the treatment of tauopathies. Towards that eventual goal, several



compounds that activate HSF1 have been reported (reviewed in [160]). However, the mechanisms that link HSF1 induction to improved proteostasis are not yet clear. In the case of HSF1 inducers, it seems plausible that the resulting conditions (e.g. elevated levels of Hsp70/90) influence the average dwell time of misfolded substrates on chaperones, leading to improved capacity to degrade damaged proteins. Additionally, high concentrations of chaperones, including Hsp27, might protect misfolded proteins from engaging in off-pathway, proteotoxic interactions. Because N-terminal Hsp90 inhibitors often induce a stress response, this mechanism may be particularly important in the response of abnormal tau to those compounds.

### **1.7 Future Perspective**

What does the future hold for molecular chaperones as therapeutic targets for tauopathies? As emphasized throughout these discussions, we expect that more detailed insights into the cellular and molecular mechanisms of protein quality control will allow us to safely promote the turnover of abnormal tau. Based on our current knowledge, it seems likely that these eventual therapies will include compounds targeting the ATP-binding clefts of Hsp70/90. These compounds might prolong the dwell time of abnormal tau on the chaperones, promoting their degradation. However, to achieve low toxicity, this list of possible drugs may also include molecules that target other regions on Hsp70 and Hsp90, especially co-chaperone binding surfaces that influence the selection of substrates. Finally, other chaperones, such as small heat shock proteins, remain under-explored as

drug target because they lack obvious binding sites. Finding ways to target these factors, with directly or via induction of a heat shock response, may expand our ability to accelerate tau turnover and ameliorate tauopathies.

In this dissertation work, we approach some of these key questions by developing new, allosteric inhibitors of Hsp70 and exploring their effects on tau stability. In Chapter 2, we describe a new screening paradigm for specifically finding inhibitors of protein-protein interactions in the Hsp70 complex. In Chapter 3, we explore the mechanism of one promising Hsp70 inhibitor, methylene blue. In Chapter 4, we describe the mechanism of MKT-077, another promising allosteric inhibitor of Hsp70. Further, in these Chapters, we describe the effects of these compounds on tau stability and clarify the mechanisms linking Hsp70 function to tau turnover. Finally, in Chapter 5, we provide a perspective on the future of Hsp70 as a drug target in tauopathies.

## **Notes**

This chapter is based on a manuscript written by Miyata, Y., Koren, J.<sup>3<sup>rd</sup></sup>, Kiray, J., Dickey, C.A. and Gestwicki, J.E. that was published as “Molecular chaperones and regulation of tau quality control: strategies for drug discovery in tauopathies” in *Future Medicinal Chemistry*, (2011) 3(12), 1523-1537.

## 1.8 References

1. Feany MB, & Dickson DW: Neurodegenerative disorders with extensive tau pathology: A comparative study and review. *Ann Neurol* 40(2), 139-148 (1996).
2. Feany MB, Ksiezak-Reding H, Liu WK, *et al.*: Epitope expression and hyperphosphorylation of tau protein in corticobasal degeneration: Differentiation from progressive supranuclear palsy. *Acta Neuropathol* 90(1), 37-43 (1995).
3. Goedert M, Spillantini MG, Crowther RA, *et al.*: Tau gene mutation in familial progressive subcortical gliosis. *Nat Med* 5(4), 454-457 (1999).
4. Hutton M, Lendon CL, Rizzu P, *et al.*: Association of missense and 5'-splice-site mutations in tau with the inherited dementia ftdp-17. *Nature* 393(6686), 702-705 (1998).
5. Mattila P, Togo T, & Dickson DW: The subthalamic nucleus has neurofibrillary tangles in argyrophilic grain disease and advanced alzheimer's disease. *Neurosci Lett* 320(1-2), 81-85 (2002).
6. Alonso AC, Grundke-Iqbal I, & Iqbal K: Alzheimer's disease hyperphosphorylated tau sequesters normal tau into tangles of filaments and disassembles microtubules. *Nat Med* 2(7), 783-787 (1996).
7. Hernandez F, & Avila J: Tauopathies. *Cell Mol Life Sci* 64(17), 2219-2233 (2007).
8. Grundke-Iqbal I, Iqbal K, Tung YC, *et al.*: Abnormal phosphorylation of the microtubule-associated protein tau (tau) in alzheimer cytoskeletal pathology. *Proc Natl Acad Sci U S A* 83(13), 4913-4917 (1986).
9. Ramsden M, Kotilinek L, Forster C, *et al.*: Age-dependent neurofibrillary tangle formation, neuron loss, and memory impairment in a mouse model of human tauopathy (p301l). *J Neurosci* 25(46), 10637-10647 (2005).
10. Santacruz K, Lewis J, Spire T, *et al.*: Tau suppression in a neurodegenerative mouse model improves memory function. *Science* 309(5733), 476-481 (2005).
11. Chun W, & Johnson GV: The role of tau phosphorylation and cleavage in neuronal cell death. *Front Biosci* 12(733-756) (2007).
12. Andreadis A: Tau gene alternative splicing: Expression patterns, regulation and modulation of function in normal brain and neurodegenerative diseases. *Biochim Biophys Acta* 1739(2-3), 91-103 (2005).
13. Mandelkow E, von Bergen M, Biernat J, & Mandelkow EM: Structural principles of tau and the paired helical filaments of alzheimer's disease. *Brain Pathol* 17(1), 83-90 (2007).
14. Gustke N, Trinczek B, Biernat J, Mandelkow EM, & Mandelkow E: Domains of tau protein and interactions with microtubules. *Biochemistry* 33(32), 9511-9522 (1994).
15. Mukrasch MD, Bibow S, Korukottu J, *et al.*: Structural polymorphism of 441-residue tau at single residue resolution. *PLoS Biol* 7(2), e34 (2009).
16. Dyson HJ, & Wright PE: Intrinsically unstructured proteins and their functions. *Nat Rev Mol Cell Biol* 6(3), 197-208 (2005).

17. Narayanan RL, Durr UH, Bibow S, *et al.*: Automatic assignment of the intrinsically disordered protein tau with 441-residues. *J Am Chem Soc* 132(34), 11906-11907 (2010).
18. Uversky VN: Flexible nets of malleable guardians: Intrinsically disordered chaperones in neurodegenerative diseases. *Chem Rev* 111(2), 1134-1166 (2011).
19. Hasegawa M, Smith MJ, & Goedert M: Tau proteins with ftdp-17 mutations have a reduced ability to promote microtubule assembly. *FEBS Lett* 437(3), 207-210 (1998).
20. Jordan MA: Mechanism of action of antitumor drugs that interact with microtubules and tubulin. *Curr Med Chem Anticancer Agents* 2(1), 1-17 (2002).
21. Anderton BH, Betts J, Blackstock WP, *et al.*: Sites of phosphorylation in tau and factors affecting their regulation. *Biochem Soc Symp* 67), 73-80 (2001).
22. Hashiguchi M, Saito T, Hisanaga S, & Hashiguchi T: Truncation of cdk5 activator p35 induces intensive phosphorylation of ser202/thr205 of human tau. *J Biol Chem* 277(46), 44525-44530 (2002).
23. Liu F, Iqbal K, Grundke-Iqbal I, & Gong CX: Involvement of aberrant glycosylation in phosphorylation of tau by cdk5 and gsk-3beta. *FEBS Lett* 530(1-3), 209-214 (2002).
24. Lund ET, McKenna R, Evans DB, Sharma SK, & Mathews WR: Characterization of the in vitro phosphorylation of human tau by tau protein kinase ii (cdk5/p20) using mass spectrometry. *J Neurochem* 76(4), 1221-1232 (2001).
25. Engmann O, & Giese KP: Crosstalk between cdk5 and gsk3beta: Implications for alzheimer's disease. *Front Mol Neurosci* 2(2) (2009).
26. Hisanaga S, & Endo R: Regulation and role of cyclin-dependent kinase activity in neuronal survival and death. *J Neurochem* 115(6), 1309-1321 (2010).
27. Patrick GN, Zukerberg L, Nikolic M, *et al.*: Conversion of p35 to p25 deregulates cdk5 activity and promotes neurodegeneration. *Nature* 402(6762), 615-622 (1999).
28. Flaherty DB, Soria JP, Tomasiewicz HG, & Wood JG: Phosphorylation of human tau protein by microtubule-associated kinases: Gsk3beta and cdk5 are key participants. *J Neurosci Res* 62(3), 463-472 (2000).
29. Kosuga S, Tashiro E, Kajioka T, *et al.*: Gsk-3beta directly phosphorylates and activates mark2/par-1. *J Biol Chem* 280(52), 42715-42722 (2005).
30. Mandelkow EM, Thies E, Trinczek B, Biernat J, & Mandelkow E: Mark/par1 kinase is a regulator of microtubule-dependent transport in axons. *J Cell Biol* 167(1), 99-110 (2004).
31. Thies E, & Mandelkow EM: Missorting of tau in neurons causes degeneration of synapses that can be rescued by the kinase mark2/par-1. *J Neurosci* 27(11), 2896-2907 (2007).
32. Drewes G, Ebner A, Preuss U, Mandelkow EM, & Mandelkow E: Mark, a novel family of protein kinases that phosphorylate microtubule-associated

- proteins and trigger microtubule disruption. *Cell* 89(2), 297-308 (1997).
33. Trinczek B, Ebner A, Mandelkow EM, & Mandelkow E: Tau regulates the attachment/detachment but not the speed of motors in microtubule-dependent transport of single vesicles and organelles. *J Cell Sci* 112 ( Pt 14)(2355-2367 (1999).
  34. Gong CX, & Iqbal K: Hyperphosphorylation of microtubule-associated protein tau: A promising therapeutic target for alzheimer disease. *Curr Med Chem* 15(23), 2321-2328 (2008).
  35. de Calignon A, Fox LM, Pitstick R, *et al.*: Caspase activation precedes and leads to tangles. *Nature* 464(7292), 1201-1204 (2010).
  36. Lleo A, Greenberg SM, & Growdon JH: Current pharmacotherapy for alzheimer's disease. *Annu Rev Med* 57(513-533 (2006).
  37. Lee VM, & Trojanowski JQ: Progress from alzheimer's tangles to pathological tau points towards more effective therapies now. *J Alzheimers Dis* 9(3 Suppl), 257-262 (2006).
  38. Schneider A, & Mandelkow E: Tau-based treatment strategies in neurodegenerative diseases. *Neurotherapeutics* 5(3), 443-457 (2008).
  39. Mazanetz MP, & Fischer PM: Untangling tau hyperphosphorylation in drug design for neurodegenerative diseases. *Nat Rev Drug Discov* 6(6), 464-479 (2007).
  40. Maccioni RB, Farias G, Morales I, & Navarrete L: The revitalized tau hypothesis on alzheimer's disease. *Arch Med Res* 41(3), 226-231 (2010).
  41. Bulic B, Pickhardt M, Schmidt B, *et al.*: Development of tau aggregation inhibitors for alzheimer's disease. *Angew Chem Int Ed Engl* 48(10), 1740-1752 (2009).
  42. Cowan CM, Bossing T, Page A, Shepherd D, & Mudher A: Soluble hyperphosphorylated tau causes microtubule breakdown and functionally compromises normal tau in vivo. *Acta Neuropathol* 120(5), 593-604 (2010).
  43. Cowan CM, Chee F, Shepherd D, & Mudher A: Disruption of neuronal function by soluble hyperphosphorylated tau in a drosophila model of tauopathy. *Biochem Soc Trans* 38(2), 564-570 (2010).
  44. O'Leary JC, 3rd, Li Q, Marinec P, *et al.*: Phenothiazine-mediated rescue of cognition in tau transgenic mice requires neuroprotection and reduced soluble tau burden. *Mol Neurodegener* 5(45 (2010).
  45. Dickey C, Kraft C, Jinwal U, *et al.*: Aging analysis reveals slowed tau turnover and enhanced stress response in a mouse model of tauopathy. *Am J Pathol* 174(1), 228-238 (2009).
  46. Ittner LM, & Gotz J: Amyloid-beta and tau--a toxic pas de deux in alzheimer's disease. *Nat Rev Neurosci* 12(2), 65-72 (2011).
  47. Rapoport M, Dawson HN, Binder LI, Vitek MP, & Ferreira A: Tau is essential to beta -amyloid-induced neurotoxicity. *Proc Natl Acad Sci U S A* 99(9), 6364-6369 (2002).
  48. Vossel KA, Zhang K, Brodbeck J, *et al.*: Tau reduction prevents abeta-induced defects in axonal transport. *Science* 330(6001), 198 (2010).
  49. Bukau B, Weissman J, & Horwich A: Molecular chaperones and protein

- quality control. *Cell* 125(3), 443-451 (2006).
50. Tyedmers J, Mogk A, & Bukau B: Cellular strategies for controlling protein aggregation. *Nat Rev Mol Cell Biol* 11(11), 777-788 (2010).
  51. Akerfelt M, Morimoto RI, & Sistonen L: Heat shock factors: Integrators of cell stress, development and lifespan. *Nat Rev Mol Cell Biol* 11(8), 545-555 (2010).
  52. Patury S, Miyata Y, & Gestwicki JE: Pharmacological targeting of the hsp70 chaperone. *Curr Top Med Chem* 9(15), 1337-1351 (2009).
  53. Ketterer N, Dreiseidler M, Tawo R, & Hohfeld J: Chaperone-assisted degradation: Multiple paths to destruction. *Biol Chem* 391(5), 481-489 (2010).
  54. Schubert U, Anton LC, Gibbs J, *et al.*: Rapid degradation of a large fraction of newly synthesized proteins by proteasomes. *Nature* 404(6779), 770-774 (2000).
  55. Bertelsen EB, Chang L, Gestwicki JE, & Zuiderweg ER: Solution conformation of wild-type e. Coli hsp70 (dnak) chaperone complexed with adp and substrate. *Proc Natl Acad Sci U S A* 106(21), 8471-8476 (2009).
  56. Zhu X, Zhao X, Burkholder WF, *et al.*: Structural analysis of substrate binding by the molecular chaperone dnak. *Science* 272(5268), 1606-1614 (1996).
  57. Flynn GC, Pohl J, Flocco MT, & Rothman JE: Peptide-binding specificity of the molecular chaperone bip. *Nature* 353(6346), 726-730 (1991).
  58. Rudiger S, Germeroth L, Schneider-Mergener J, & Bukau B: Substrate specificity of the dnak chaperone determined by screening cellulose-bound peptide libraries. *EMBO J* 16(7), 1501-1507 (1997).
  59. Sarkar M, Kuret J, & Lee G: Two motifs within the tau microtubule-binding domain mediate its association with the hsc70 molecular chaperone. *J Neurosci Res* 86(12), 2763-2773 (2008).
  60. Chang L, Bertelsen EB, Wisen S, *et al.*: High-throughput screen for small molecules that modulate the atpase activity of the molecular chaperone dnak. *Anal Biochem* 372(2), 167-176 (2008).
  61. Laufen T, Mayer MP, Beisel C, *et al.*: Mechanism of regulation of hsp70 chaperones by dnaj cochaperones. *Proc Natl Acad Sci U S A* 96(10), 5452-5457 (1999).
  62. Brodsky JL, & Bracher A: Nucleotide exchange factors for hsp70 molecular chaperones. In: *Networking of chaperones by co-chaperones*. Baltch GL (Ed.), Landes Bioscience, Austin, 26-37 (2007).
  63. Evans CG, Chang L, & Gestwicki JE: Heat shock protein 70 (hsp70) as an emerging drug target. *J Med Chem* 53(12), 4585-4602 (2010).
  64. Kang Y, Taldone T, Clement CC, *et al.*: Design of a fluorescence polarization assay platform for the study of human hsp70. *Bioorg Med Chem Lett* 18(13), 3749-3751 (2008).
  65. Miyata Y, Chang L, Bainor A, *et al.*: High-throughput screen for escherichia coli heat shock protein 70 (hsp70/dnak): Atpase assay in low volume by exploiting energy transfer. *J Biomol Screen* 15(10), 1211-1219 (2010).
  66. Ricci L, & Williams KP: Development of fluorescence polarization assays

- for the molecular chaperone hsp70 family members: Hsp72 and dnaK. *Curr Chem Genomics* 2(90-95) (2008).
67. Wisen S, & Gestwicki JE: Identification of small molecules that modify the protein folding activity of heat shock protein 70. *Anal Biochem* 374(2), 371-377 (2008).
  68. Massey AJ: Atpases as drug targets: Insights from heat shock proteins 70 and 90. *J Med Chem* 53(20), 7280-7286 (2010).
  69. Massey AJ, Williamson DS, Browne H, *et al.*: A novel, small molecule inhibitor of hsc70/hsp70 potentiates hsp90 inhibitor induced apoptosis in hct116 colon carcinoma cells. *Cancer Chemother Pharmacol* 66(3), 535-545 (2010).
  70. Williamson DS, Borgognoni J, Clay A, *et al.*: Novel adenosine-derived inhibitors of 70 kda heat shock protein, discovered through structure-based design. *J Med Chem* 52(6), 1510-1513 (2009).
  71. Chang L, Thompson AD, Ung P, Carlson HA, & Gestwicki JE: Mutagenesis reveals the complex relationships between atpase rate and the chaperone activities of escherichia coli heat shock protein 70 (hsp70/dnaK). *J Biol Chem* 285(28), 21282-21291 (2010).
  72. Chang L, Miyata Y, Ung PM, *et al.*: Chemical screens against a reconstituted multiprotein complex: Myricetin blocks dnaJ regulation of dnaK through an allosteric mechanism. *Chem Biol* 18(2), 210-221 (2011).
  73. Wisen S, Bertelsen EB, Thompson AD, *et al.*: Binding of a small molecule at a protein-protein interface regulates the chaperone activity of hsp70-hsp40. *ACS Chem Biol* 5(6), 611-622 (2010).
  74. Bischofberger P, Han W, Feifel B, Schonfeld HJ, & Christen P: D-peptides as inhibitors of the dnaK/dnaJ/grpE chaperone system. *J Biol Chem* 278(21), 19044-19047 (2003).
  75. Haney CM, Schneider C, Beck B, Brodsky JL, & Domling A: Identification of hsp70 modulators through modeling of the substrate binding domain. *Bioorg Med Chem Lett* 19(14), 3828-3831 (2009).
  76. Ali MM, Roe SM, Vaughan CK, *et al.*: Crystal structure of an hsp90-nucleotide-p23/sba1 closed chaperone complex. *Nature* 440(7087), 1013-1017 (2006).
  77. Krukenberg KA, Bottcher UM, Southworth DR, & Agard DA: Grp94, the endoplasmic reticulum hsp90, has a similar solution conformation to cytosolic hsp90 in the absence of nucleotide. *Protein Sci* 18(9), 1815-1827 (2009).
  78. Krukenberg KA, Forster F, Rice LM, Sali A, & Agard DA: Multiple conformations of e. Coli hsp90 in solution: Insights into the conformational dynamics of hsp90. *Structure* 16(5), 755-765 (2008).
  79. Bron P, Giudice E, Rolland JP, *et al.*: Apo-hsp90 coexists in two open conformational states in solution. *Biol Cell* 100(7), 413-425 (2008).
  80. Southworth DR, & Agard DA: Species-dependent ensembles of conserved conformational states define the hsp90 chaperone atpase cycle. *Mol Cell* 32(5), 631-640 (2008).
  81. Ratzke C, Mickler M, Hellenkamp B, Buchner J, & Hugel T: Dynamics of

- heat shock protein 90 c-terminal dimerization is an important part of its conformational cycle. *Proc Natl Acad Sci U S A* 107(37), 16101-16106 (2010).
82. Pearl LH, & Prodromou C: Structure and mechanism of the hsp90 molecular chaperone machinery. *Annu Rev Biochem* 75(271-294 (2006).
  83. Shiau AK, Harris SF, Southworth DR, & Agard DA: Structural analysis of e. Coli hsp90 reveals dramatic nucleotide-dependent conformational rearrangements. *Cell* 127(2), 329-340 (2006).
  84. Taipale M, Jarosz DF, & Lindquist S: Hsp90 at the hub of protein homeostasis: Emerging mechanistic insights. *Nat Rev Mol Cell Biol* 11(7), 515-528 (2010).
  85. Trepel J, Mollapour M, Giaccone G, & Neckers L: Targeting the dynamic hsp90 complex in cancer. *Nat Rev Cancer* 10(8), 537-549 (2010).
  86. Workman P, Burrows F, Neckers L, & Rosen N: Drugging the cancer chaperone hsp90: Combinatorial therapeutic exploitation of oncogene addiction and tumor stress. *Ann N Y Acad Sci* 1113(202-216 (2007).
  87. Whitesell L, Mimnaugh EG, De Costa B, Myers CE, & Neckers LM: Inhibition of heat shock protein hsp90-pp60v-src heteroprotein complex formation by benzoquinone ansamycins: Essential role for stress proteins in oncogenic transformation. *Proc Natl Acad Sci U S A* 91(18), 8324-8328 (1994).
  88. Taldone T, Sun W, & Chiosis G: Discovery and development of heat shock protein 90 inhibitors. *Bioorg Med Chem* 17(6), 2225-2235 (2009).
  89. Hadden MK, Lubbers DJ, & Blagg BS: Geldanamycin, radicicol, and chimeric inhibitors of the hsp90 n-terminal atp binding site. *Curr Top Med Chem* 6(11), 1173-1182 (2006).
  90. Donnelly A, & Blagg BS: Novobiocin and additional inhibitors of the hsp90 c-terminal nucleotide-binding pocket. *Curr Med Chem* 15(26), 2702-2717 (2008).
  91. Marcu MG, & Neckers LM: The c-terminal half of heat shock protein 90 represents a second site for pharmacologic intervention in chaperone function. *Curr Cancer Drug Targets* 3(5), 343-347 (2003).
  92. Biamonte MA, Van de Water R, Arndt JW, *et al.*: Heat shock protein 90: Inhibitors in clinical trials. *J Med Chem* 53(1), 3-17 (2010).
  93. Allan RK, Mok D, Ward BK, & Ratajczak T: Modulation of chaperone function and cochaperone interaction by novobiocin in the c-terminal domain of hsp90: Evidence that coumarin antibiotics disrupt hsp90 dimerization. *J Biol Chem* 281(11), 7161-7171 (2006).
  94. Li Y, Zhang T, Jiang Y, *et al.*: (-)-epigallocatechin-3-gallate inhibits hsp90 function by impairing hsp90 association with cochaperones in pancreatic cancer cell line mia paca-2. *Mol Pharm* 6(4), 1152-1159 (2009).
  95. Zhang T, Hamza A, Cao X, *et al.*: A novel hsp90 inhibitor to disrupt hsp90/cdc37 complex against pancreatic cancer cells. *Mol Cancer Ther* 7(1), 162-170 (2008).
  96. Zhang T, Li Y, Yu Y, *et al.*: Characterization of celastrol to inhibit hsp90 and cdc37 interaction. *J Biol Chem* 284(51), 35381-35389 (2009).



97. Haslbeck M, Franzmann T, Weinfurter D, & Buchner J: Some like it hot: The structure and function of small heat-shock proteins. *Nat Struct Mol Biol* 12(10), 842-846 (2005).
98. Sun Y, & MacRae TH: Small heat shock proteins: Molecular structure and chaperone function. *Cell Mol Life Sci* 62(21), 2460-2476 (2005).
99. Haslbeck M, Kastenmuller A, Buchner J, Weinkauff S, & Braun N: Structural dynamics of archaeal small heat shock proteins. *J Mol Biol* 378(2), 362-374 (2008).
100. Pratt WB, & Toft DO: Steroid receptor interactions with heat shock protein and immunophilin chaperones. *Endocr Rev* 18(3), 306-360 (1997).
101. Smith DF, & Toft DO: Minireview: The intersection of steroid receptors with molecular chaperones: Observations and questions. *Mol Endocrinol* 22(10), 2229-2240 (2008).
102. Carrigan PE, Nelson GM, Roberts PJ, *et al.*: Multiple domains of the co-chaperone hop are important for hsp70 binding. *J Biol Chem* 279(16), 16185-16193 (2004).
103. Hernandez MP, Sullivan WP, & Toft DO: The assembly and intermolecular properties of the hsp70-hop-hsp90 molecular chaperone complex. *J Biol Chem* 277(41), 38294-38304 (2002).
104. Connell P, Ballinger CA, Jiang J, *et al.*: The co-chaperone chip regulates protein triage decisions mediated by heat-shock proteins. *Nat Cell Biol* 3(1), 93-96 (2001).
105. Pearl LH: Hsp90 and cdc37 -- a chaperone cancer conspiracy. *Curr Opin Genet Dev* 15(1), 55-61 (2005).
106. Panaretou B, Siligardi G, Meyer P, *et al.*: Activation of the atpase activity of hsp90 by the stress-regulated cochaperone aha1. *Mol Cell* 10(6), 1307-1318 (2002).
107. Kundrat L, & Regan L: Balance between folding and degradation for hsp90-dependent client proteins: A key role for chip. *Biochemistry* 49(35), 7428-7438 (2010).
108. Morishima Y, Wang AM, Yu Z, *et al.*: Chip deletion reveals functional redundancy of e3 ligases in promoting degradation of both signaling proteins and expanded glutamine proteins. *Hum Mol Genet* 17(24), 3942-3952 (2008).
109. Stankiewicz M, Nikolay R, Rybin V, & Mayer MP: Chip participates in protein triage decisions by preferentially ubiquitinating hsp70-bound substrates. *FEBS J* 277(16), 3353-3367 (2010).
110. Jinwal UK, Koren J, O'Leary JC, *et al.*: Hsp70 atpase modulators as therapeutics for alzheimer's and other neurodegenerative diseases. *Mol Cell Pharmacol* 2(2), 43-46 (2010).
111. Koren J, 3rd, Jinwal UK, Lee DC, *et al.*: Chaperone signalling complexes in alzheimer's disease. *J Cell Mol Med* 13(4), 619-630 (2009).
112. Jinwal UK, O'Leary JC, 3rd, Borysov SI, *et al.*: Hsc70 rapidly engages tau after microtubule destabilization. *J Biol Chem* 285(22), 16798-16805 (2010).
113. Weaver CL, Espinoza M, Kress Y, & Davies P: Conformational change as

- one of the earliest alterations of tau in alzheimer's disease. *Neurobiol Aging* 21(5), 719-727 (2000).
114. Dou F, Netzer WJ, Tanemura K, *et al.*: Chaperones increase association of tau protein with microtubules. *Proc Natl Acad Sci U S A* 100(2), 721-726 (2003).
  115. Petrucelli L, Dickson D, Kehoe K, *et al.*: Chip and hsp70 regulate tau ubiquitination, degradation and aggregation. *Hum Mol Genet* 13(7), 703-714 (2004).
  116. Shimura H, Schwartz D, Gygi SP, & Kosik KS: Chip-hsc70 complex ubiquitinates phosphorylated tau and enhances cell survival. *J Biol Chem* 279(6), 4869-4876 (2004).
  117. Jinwal UK, Miyata Y, Koren J, 3rd, *et al.*: Chemical manipulation of hsp70 atpase activity regulates tau stability. *J Neurosci* 29(39), 12079-12088 (2009).
  118. Tortosa E, Santa-Maria I, Moreno F, *et al.*: Binding of hsp90 to tau promotes a conformational change and aggregation of tau protein. *J Alzheimers Dis* 17(2), 319-325 (2009).
  119. Dickey CA, Dunmore J, Lu B, *et al.*: Hsp induction mediates selective clearance of tau phosphorylated at proline-directed ser/thr sites but not kxgs (mark) sites. *FASEB J* 20(6), 753-755 (2006).
  120. Dickey CA, Eriksen J, Kamal A, *et al.*: Development of a high throughput drug screening assay for the detection of changes in tau levels -- proof of concept with hsp90 inhibitors. *Curr Alzheimer Res* 2(2), 231-238 (2005).
  121. Dickey CA, Kamal A, Lundgren K, *et al.*: The high-affinity hsp90-chip complex recognizes and selectively degrades phosphorylated tau client proteins. *J Clin Invest* 117(3), 648-658 (2007).
  122. Luo W, Dou F, Rodina A, *et al.*: Roles of heat-shock protein 90 in maintaining and facilitating the neurodegenerative phenotype in tauopathies. *Proc Natl Acad Sci U S A* 104(22), 9511-9516 (2007).
  123. Dickey CA, Koren J, Zhang YJ, *et al.*: Akt and chip coregulate tau degradation through coordinated interactions. *Proc Natl Acad Sci U S A* 105(9), 3622-3627 (2008).
  124. Lindquist S: Protein folding sculpting evolutionary change. *Cold Spring Harb Symp Quant Biol* 74(103-108 (2009).
  125. Kosik KS, & Shimura H: Phosphorylated tau and the neurodegenerative foldopathies. *Biochim Biophys Acta* 1739(2-3), 298-310 (2005).
  126. Shimura H, Miura-Shimura Y, & Kosik KS: Binding of tau to heat shock protein 27 leads to decreased concentration of hyperphosphorylated tau and enhanced cell survival. *J Biol Chem* 279(17), 17957-17962 (2004).
  127. Bjorkdahl C, Sjogren MJ, Zhou X, *et al.*: Small heat shock proteins hsp27 or alphas-crystallin and the protein components of neurofibrillary tangles: Tau and neurofilaments. *J Neurosci Res* 86(6), 1343-1352 (2008).
  128. Schwarz L, Vollmer G, & Richter-Landsberg C: The small heat shock protein hsp25/27 (hspb1) is abundant in cultured astrocytes and associated with astrocytic pathology in progressive supranuclear palsy and corticobasal degeneration. *Int J Cell Biol* 2010(717520 (2010).

129. Abisambra JF, Blair LJ, Hill SE, *et al.*: Phosphorylation dynamics regulate hsp27-mediated rescue of neuronal plasticity deficits in tau transgenic mice. *J Neurosci* 30(46), 15374-15382 (2010).
130. Elliott E, Laufer O, & Ginzburg I: Bag-1m is up-regulated in hippocampus of alzheimer's disease patients and associates with tau and app proteins. *J Neurochem* 109(4), 1168-1178 (2009).
131. Elliott E, Tsvetkov P, & Ginzburg I: Bag-1 associates with hsc70.Tau complex and regulates the proteasomal degradation of tau protein. *J Biol Chem* 282(51), 37276-37284 (2007).
132. Carrettiero DC, Hernandez I, Neveu P, Papagiannakopoulos T, & Kosik KS: The cochaperone bag2 sweeps paired helical filament- insoluble tau from the microtubule. *J Neurosci* 29(7), 2151-2161 (2009).
133. Andreasson C, Fiaux J, Rampelt H, Mayer MP, & Bukau B: Hsp110 is a nucleotide-activated exchange factor for hsp70. *J Biol Chem* 283(14), 8877-8884 (2008).
134. Dragovic Z, Broadley SA, Shomura Y, Bracher A, & Hartl FU: Molecular chaperones of the hsp110 family act as nucleotide exchange factors of hsp70s. *EMBO J* 25(11), 2519-2528 (2006).
135. Eroglu B, Moskophidis D, & Mivechi NF: Loss of hsp110 leads to age-dependent tau hyperphosphorylation and early accumulation of insoluble amyloid beta. *Mol Cell Biol* 30(19), 4626-4643 (2010).
136. Jinwal UK, Koren J, 3rd, Borysov SI, *et al.*: The hsp90 cochaperone, fkbp51, increases tau stability and polymerizes microtubules. *J Neurosci* 30(2), 591-599 (2010).
137. Salminen A, Ojala J, Kaarniranta K, Hiltunen M, & Soininen H: Hsp90 regulates tau pathology through co-chaperone complexes in alzheimer's disease. *Prog Neurobiol* 93(1), 99-110 (2011).
138. Van Duyne GD, Standaert RF, Karplus PA, Schreiber SL, & Clardy J: Atomic structure of fkbp-fk506, an immunophilin-immunosuppressant complex. *Science* 252(5007), 839-842 (1991).
139. Frydman J: Folding of newly translated proteins in vivo: The role of molecular chaperones. *Annu Rev Biochem* 70(603-647 (2001).
140. Arndt V, Rogon C, & Hohfeld J: To be, or not to be--molecular chaperones in protein degradation. *Cell Mol Life Sci* 64(19-20), 2525-2541 (2007).
141. Schneider C, Sepp-Lorenzino L, Nimmesgern E, *et al.*: Pharmacologic shifting of a balance between protein refolding and degradation mediated by hsp90. *Proc Natl Acad Sci U S A* 93(25), 14536-14541 (1996).
142. Park HJ, Mylvaganum M, McPherson A, *et al.*: A soluble sulfogalactosyl ceramide mimic promotes delta f508 cfr escape from endoplasmic reticulum associated degradation. *Chem Biol* 16(4), 461-470 (2009).
143. Kampinga HH, Hageman J, Vos MJ, *et al.*: Guidelines for the nomenclature of the human heat shock proteins. *Cell Stress Chaperones* 14(1), 105-111 (2009).
144. Powers ET, Morimoto RI, Dillin A, Kelly JW, & Balch WE: Biological and chemical approaches to diseases of proteostasis deficiency. *Annu Rev Biochem* 78(959-991 (2009).

145. Smith DF, Whitesell L, Nair SC, *et al.*: Progesterone receptor structure and function altered by geldanamycin, an hsp90-binding agent. *Mol Cell Biol* 15(12), 6804-6812 (1995).
146. Forafonov F, Toogun OA, Grad I, *et al.*: P23/sba1p protects against hsp90 inhibitors independently of its intrinsic chaperone activity. *Mol Cell Biol* 28(10), 3446-3456 (2008).
147. Hohfeld J, Cyr DM, & Patterson C: From the cradle to the grave: Molecular chaperones that may choose between folding and degradation. *EMBO Rep* 2(10), 885-890 (2001).
148. Arndt V, Daniel C, Nastainczyk W, Alberti S, & Hohfeld J: Bag-2 acts as an inhibitor of the chaperone-associated ubiquitin ligase chip. *Mol Biol Cell* 16(12), 5891-5900 (2005).
149. McClellan AJ, Scott MD, & Frydman J: Folding and quality control of the vhl tumor suppressor proceed through distinct chaperone pathways. *Cell* 121(5), 739-748 (2005).
150. Gestwicki JE, & Marinec PS: Chemical control over protein-protein interactions: Beyond inhibitors. *Comb Chem High Throughput Screen* 10(8), 667-675 (2007).
151. Wells JA, & McClendon CL: Reaching for high-hanging fruit in drug discovery at protein-protein interfaces. *Nature* 450(7172), 1001-1009 (2007).
152. Hajduk PJ, Meadows RP, & Fesik SW: Nmr-based screening in drug discovery. *Q Rev Biophys* 32(3), 211-240 (1999).
153. Li Y, Zhang T, Schwartz SJ, & Sun D: New developments in hsp90 inhibitors as anti-cancer therapeutics: Mechanisms, clinical perspective and more potential. *Drug Resist Updat* 12(1-2), 17-27 (2009).
154. Auluck PK, Chan HY, Trojanowski JQ, Lee VM, & Bonini NM: Chaperone suppression of alpha-synuclein toxicity in a drosophila model for parkinson's disease. *Science* 295(5556), 865-868 (2002).
155. Bonini NM: Chaperoning brain degeneration. *Proc Natl Acad Sci U S A* 99 Suppl 4(16407-16411 (2002).
156. Fujimoto M, Takaki E, Hayashi T, *et al.*: Active hsf1 significantly suppresses polyglutamine aggregate formation in cellular and mouse models. *J Biol Chem* 280(41), 34908-34916 (2005).
157. Muchowski PJ, Schaffar G, Sittler A, *et al.*: Hsp70 and hsp40 chaperones can inhibit self-assembly of polyglutamine proteins into amyloid-like fibrils. *Proc Natl Acad Sci U S A* 97(14), 7841-7846 (2000).
158. Wacker JL, Zareie MH, Fong H, Sarikaya M, & Muchowski PJ: Hsp70 and hsp40 attenuate formation of spherical and annular polyglutamine oligomers by partitioning monomer. *Nat Struct Mol Biol* 11(12), 1215-1222 (2004).
159. Wyttenbach A, Sauvageot O, Carmichael J, *et al.*: Heat shock protein 27 prevents cellular polyglutamine toxicity and suppresses the increase of reactive oxygen species caused by huntingtin. *Hum Mol Genet* 11(9), 1137-1151 (2002).
160. Nagai Y, Fujikake N, Popiel HA, & Wada K: Induction of molecular

chaperones as a therapeutic strategy for the polyglutamine diseases. *Curr Pharm Biotechnol* 11(2), 188-197 (2010).

## Chapter 2

### Development of High Throughput Screens for Hsp70 and Identification of Chemical Activators and Inhibitors

#### 2.1 Abstract

As discussed in Chapter 1, Hsp70 is a potential therapeutic target for tauopathies. Despite increasing interest in inhibitors of this canonical molecular chaperone, only a handful of examples have been reported. In order to test a large number of compounds, we developed a new high throughput screening platform in 384-well format, which employs an energy transfer strategy to measure the ATPase activity of Hsp70. Briefly, white 384-well plates emit fluorescence when irradiated at 430 nm. In turn, this intrinsic fluorescence can be quenched by energy transfer with the quinaldine red-based chromophore, which absorbs at 430 nm upon complex formation with inorganic phosphate. Using this platform and a related approach, we screened over 55,000 compounds against the prokaryotic member of Hsp70, DnaK. The assay performance was good ( $Z'$  ~ 0.6, CV ~8%) and new inhibitors were identified. In secondary assays, these compounds either blocked or promoted stimulation of DnaK by its co-chaperone, DnaJ. Thus, this simple

and inexpensive method is suitable for screening against Hsp70-family members and it has provided new chemical probes for studying the role of Hsp70 in tauopathy.

### **2.1.1 Hsp70s are Involved in Human Diseases**

Members of the heat shock protein 70 (Hsp70) family of molecular chaperones are ubiquitously expressed and remarkably well conserved. In both eukaryotes and prokaryotes, Hsp70s play important roles in protein quality control, including during folding, transport and turnover [1]. Chapter 1 focused on the roles of Hsp70 in tauopathies and discussed the potential of these chaperones as drug targets in this class of diseases. However, Hsp70s have been implicated in cancer [2] and a number of protein-misfolding disorders, such as Parkinson's disease [3]. In prokaryotes, the Hsp70 ortholog, DnaK, has been found to be essential for virulence in *Staphylococcus aureus* [4]. Despite these promising observations, a scarcity of drug-like inhibitors has limited in-depth exploration of this chaperone as a therapeutic target for tauopathies or other diseases [5]. The major goal of this Chapter is to develop new methods for identifying chemical compounds that target Hsp70s.

### **2.1.2 Co-Chaperones of Hsp70 Regulates its ATPase Activity**

As discussed in Chapter 1, members of the Hsp70 family are composed of two domains: a substrate-binding domain (SBD) and a nucleotide-binding domain (NBD) [6]. The SBD accommodates short stretches of peptide and it seems to

have a preference for the hydrophobic residues that might be exposed in misfolded or incompletely folded proteins [7]. Binding of the SBD to its substrates is regulated, in part, by the nucleotide state of the adjacent NBD: the ATP-bound form has relatively weak affinity for substrates, while the ADP-bound form binds tightly [8]. However, the intrinsic ATPase activity of these proteins is slow; for example, *Escherichia coli* DnaK, has a  $V_{\max}$  of  $\sim 1$  pmol ATP /  $\mu\text{g}$  enzyme / minute [9]. This modest turnover allows regulation by co-chaperones, such as DnaJ [10]. DnaJ belongs to a family of co-chaperones that bind Hsp70s through a conserved J-domain. This protein-protein contact accelerates ATP turnover through an allosteric mechanism [11].

### **2.1.3 Our Strategy to Identify Chemical Modulators of Hsp70**

In envisioning strategies for inhibiting members of the Hsp70 family, two of their activities become apparent as potential targets [5]. One approach is to inhibit binding of the SBD to its substrates. This strategy is exploited by certain insect-derived, anti-bacterial peptides [12] and a fluorescence polarization-based assay to identify similar compounds has been developed [13]. A separate strategy is to block nucleotide turnover [14,15]. As discussed in Chapter 1, this goal might be accomplished by either directly competing with nucleotide [16] or by inhibiting the protein-protein interactions with the stimulatory co-chaperones. Toward this goal, other members of the Gestwicki group employed the well-known malachite green (MG) reagent to detect ATP hydrolysis by the DnaK-DnaJ combination in 96-well plates [17,18]. This assay identified a number of new Hsp70 inhibitors.



While the MG assay appeared to be a promising way to find new inhibitors of Hsp70 for use in tauopathies, our early attempts to further miniaturize the absorbance platforms to low volume 384-well microtiter plates were frustrated by significantly decreased sensitivity (data not shown). This is a problem because we could not screen larger compound collections using the 96-well format. In this Chapter, we explore whether energy transfer methodology [19] could be used to improve the performance of this assay in low volume.

## **2.2 Results**

### **2.2.1 Fluorescent, Energy Transfer Method Has Enhanced Sensitivity for Inorganic Phosphate.**

The primary technical challenge in performing absorbance assays in high-density formats, such as 384- and 1536-well plates, is that the sensitivity is typically decreased ~2.5 fold by the restrictive well geometry [20,21]. In addition, absorbance assays demand flat, clear-bottomed microtiter plates that consume more reagents than other well geometries (*e.g.* round, concave). However, absorbance assays are often inexpensive and robust, so there is interest in finding ways to adopt them to higher density. One promising approach was reported by Zuck *et al.*, who successfully converted a QR-based phosphate assay for use in 384-well format (**Figure 2.1A**) [19]. They observed that when white, opaque microtiter plates are irradiated at 430 nm, they emit fluorescence in a broad range between approximately 450 and 600 nm (**Figure 2.1B**). Because the QR-complex absorbs light at 530 nm, the emission from wells

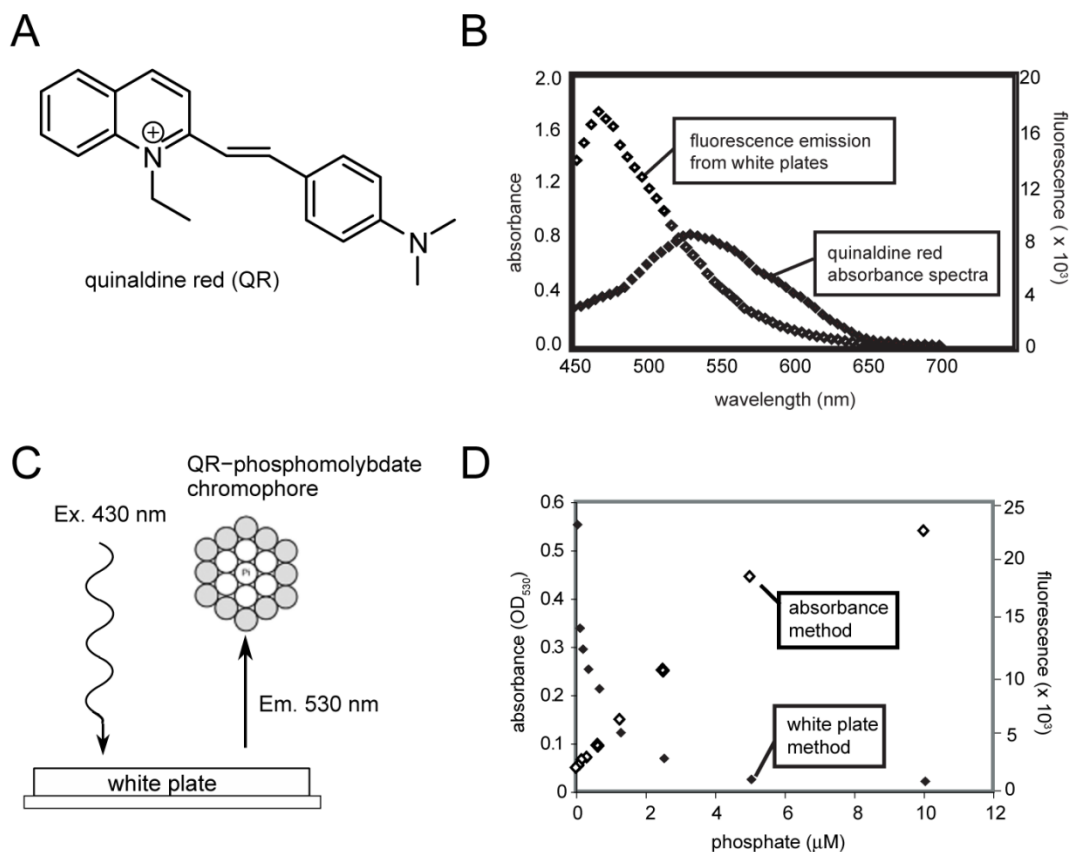


**Figure 2.1 Model for converting an absorbance assay into a fluorescence quenching method.** (A) Chemical structure of quinaldine red (QR). (B) Overlap between QR-phosphomolybdate chromophore and intrinsic fluorescence of white opaque 384-well plates. When irradiated at 430 nm, white plates emit broadly between 450 and 550 nm. (C) Schematic representation of white plate method. Fluorescence emission from white plates is quenched by QR in the presence of molybdate and inorganic phosphate (spheres). (D) Comparison of sensitivity for phosphate between absorbance and fluorescence methods. Results are the average of at least triplicates and error bars are standard error of the mean (some bars are smaller than the symbols).

containing phosphate is quenched; thus, this simple modification converts the absorbance assay into a fluorescence-quenching format (**Figure 2.1C**). Zuck and colleagues found that this strategy improves sensitivity because both the fluorescence emission and excitation are absorbed by the chromophore [19]. Further, the Walt group has explored the mechanistic underpinnings of a similar process, and they found that both radiative and non-radiative energy transfer

events contribute to improved sensing [22].

Before adapting this platform for use against the prokaryotic Hsp70 family member, DnaK, we were interested in discerning the lowest concentration of phosphate that could be robustly detected. Accordingly, we prepared phosphate standard solutions and directly compared the sensitivity of the absorbance- and fluorescence-based methods. For these experiments, we found that the linear detection range of the absorbance method was approximately 0.5 to 5  $\mu\text{M}$  (**Figure 2.1D**), in agreement with previous reports [17]. We found that the white plates gave a linear range of approximately 0.06 to 0.6  $\mu\text{M}$ , an approximately 10-fold improvement in sensitivity.

### **2.2.2 Fluorescence Method Has Superior Performance in Pilot Screens.**

To our knowledge, a high throughput screening application of this fluorescence method has not yet been reported. Therefore, we first performed a pilot screen in 384-well plates to gauge its performance. Briefly, we found that the combination of 0.4  $\mu\text{M}$  DnaK and 0.7  $\mu\text{M}$  DnaJ gave a signal that was linear for at least 2-3 hours when incubated with 1 mM ATP (**Appendix 2.9.1**). From these experiments, we developed a protocol that was adopted from the previous 96-well version (**Figure 2.2A**) [18]. For calculation of Z' scores, we defined the negative control as the signal from enzyme plus DMSO and the positive control as buffer plus DMSO.

Using these conditions, we screened the MS2000 collection of bioactive

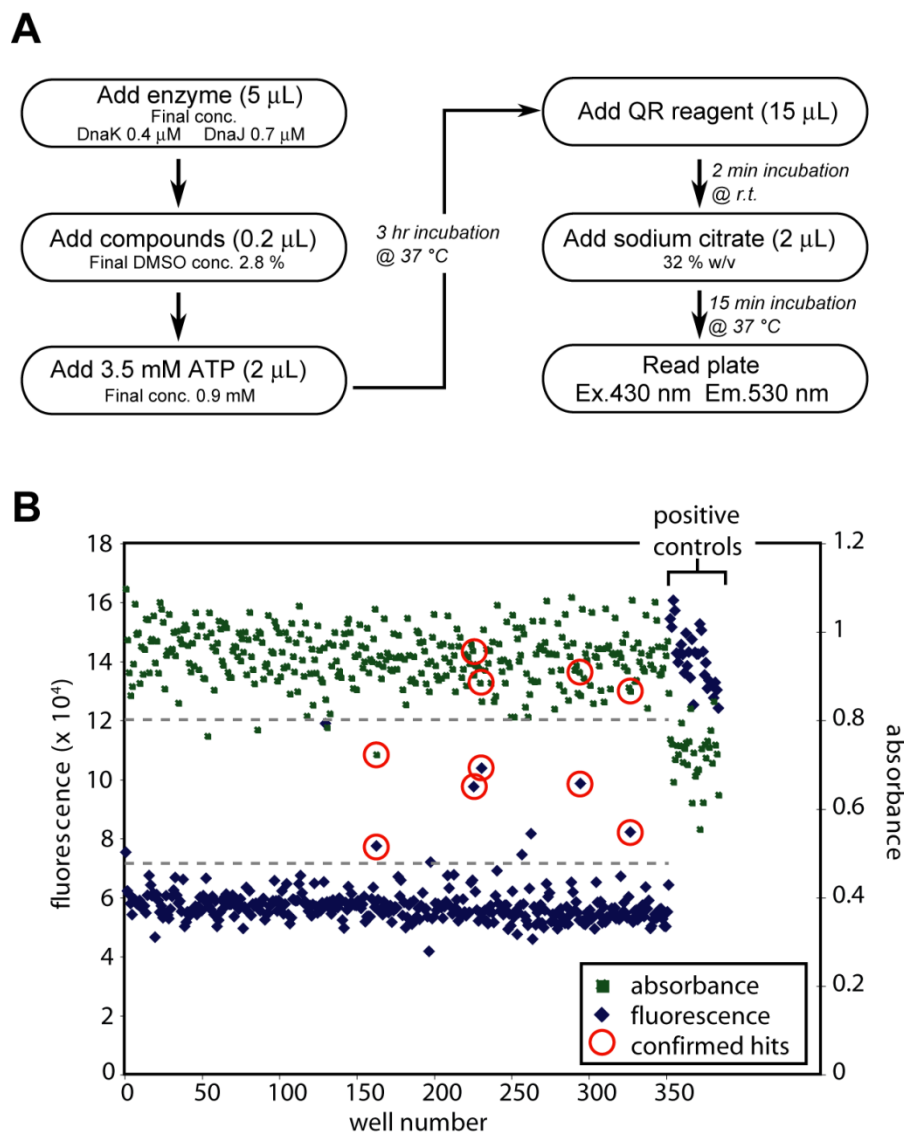


**Figure 2.2 Comparison of screening performances between absorbance and fluorescence methods.** (A) Detailed protocol for fluorescence quenching method in 384-well plates. (B) Representative data from the side-by-side pilot screen for absorbance method and fluorescence method. Each dotted line represents three times standard deviation from the negative control. Data points for known inhibitors (as determined from previous 96-well assays) are circled. Fluorescence based method successfully identified all of the five known inhibitors whereas absorbance based method only detected one. The fluorescence method yielded ~4-fold higher signal-to-noise ratio than the absorbance method.

compounds. This library is known to contain five DnaK inhibitors; thus, it could be used to probe the assay performance [23]. Also, we directly compared the

absorbance and energy transfer methods by splitting the reactions into either clear plates or low volume, white plates. Using this side-by-side approach, we confirmed our previous observations that the absorbance-based assay is a relatively poor HTS method, with a Z' score of approximately 0.2. Moreover, this method only identified one of five known inhibitors and it gave two false positives (**Figure 2.2B**). In contrast, the fluorescence method yielded a Z' score of 0.6 and it correctly identified all five known inhibitors. We also confirmed that the fluorescence method could accurately replicate the IC<sub>50</sub> of one inhibitor (**Appendix 2.9.1C**). Together, these results suggest that the fluorescence method is suitable for screening in low volume 384-well plates.

### **2.2.3 High Throughput Screen for Inhibitors of DnaK's ATPase Activity.**

Based on the promising results from the pilot experiments, we screened an additional 55,400 small molecules and natural product crude extracts against the ATPase activity of DnaK-DnaJ (**Figure 2.3A**). In these experiments, we found that the Z' factors ranged from 0.10 - 0.75 with an average of 0.58 (**Figure 2.3B**). Interestingly, we found that the occasional poor Z' values were partially attributable to plates with intrinsic fluorescence that were either significantly above or below average (**Appendix 2.9.2**). Because these microtiter plates were not originally manufactured for use in fluorescence applications, we expect that the amount of fluorescent material may be unevenly distributed, resulting in occasional plates with higher or lower signal. These unsatisfactory plates (Z' value < 0.4) were excluded from further analyses (3 % of total plates), increasing the average Z' score to 0.60. More recently, we have started “pre-screening”

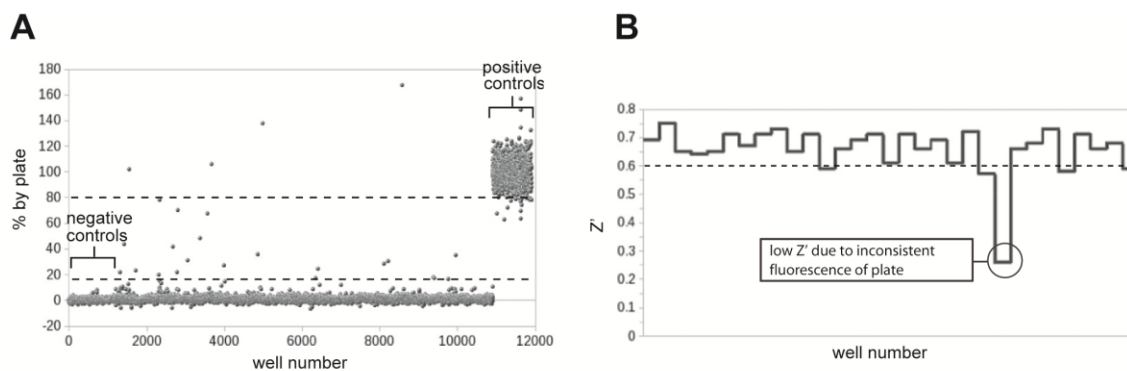


**Figure 2.3 Screening of 55,400 samples.** (A) Representative data from the screening campaign. Positive controls (buffer plus DMSO) and negative controls (enzyme plus DMSO) are shown. Some examples of false positives are clearly shown above the 100% line. (B) Representative Z' values by plate from the screen. The average Z' for the entire screening was 0.58. We observed occasional low Z', which is likely due to plates' irregular fluorescence properties (circled).

fresh, empty plates to remove these outliers.

Samples were screened at a single concentration (between 10 to 40  $\mu\text{M}$ ) against DnaK-DnaJ, with the addition of 0.01% Triton X-100 to minimize false discovery of aggregators. From these screens, samples that exhibited effects of 35% or higher by plate were considered inhibitors. Samples with signals at least 3-times the standard deviation from the negative controls and samples on their given plate were also included. Of 55,400 samples tested, 598 fell into this category (hit rate: 1.1 %). In previous studies by the Gestwicki laboratory, activators of Hsp70s have also proven to be powerful chemical tools [23,24]. With the aim of potentially expanding the number of activators, the HTS results were reviewed for samples with signals of -2.5 standard deviations or lower. Using this modest criterion, 122 unique samples were identified as activators (hit rate: 0.22 %).

To confirm their activities, the samples were subjected to confirmatory retesting

in duplicate. Prior to this experiment, 10 compounds containing a heavy metal and 11 compounds with a molecular weight above 650 Da were excluded, because they were expected to have unfavorable properties. In addition, the natural product extracts were excluded and their analysis will be reported elsewhere. Thus, a total of 508 unique compounds (400 inhibitors and 108 activators) were assayed and 73 inhibitors confirmed. None of the activators confirmed upon retesting, although it should be noted that they only exhibited weak activity in the primary screen and the assay conditions were optimized to identify inhibitors. The Z' factors for the confirmation assay ranged from 0.65 and 0.70.

The confirming structures were subsequently clustered to determine if series were present. Clustering at 65% + similarity with the fingerprints (Unity) and clustering algorithms (Optisim) by Benchware DataMiner produced 55 clusters. It has been shown that a compound with 85% or greater structural similarity to an active compound will have a ~30% probability of also being active [25]. Therefore, we analyzed our internal database of ~150,000 compounds and retrieved structures that have 85% or greater similarity to any of the confirmed inhibitors. Based on this analysis, we selected 76 compounds that belong to three largest clusters for testing in dose dependence assays. These assays were performed using a 2-fold dilution series of eight compound concentrations (1 to 125  $\mu$ M). Of the 127 compounds tested, 70 showed dose dependent inhibition curves. In order to minimize false positives, these 70 compounds were then evaluated for

autofluorescence. Briefly, compounds were excluded if their intrinsic fluorescence (Ex: 430 nm, Em: 530 nm) at 5  $\mu$ M was at least 10% of the positive control or if their dose dependence plateau was above the positive control (see examples in **Figure 2.3A**). These filters excluded 34 samples, leaving 36 unique compounds as potential DnaK-DnaJ inhibitors. These compounds were clustered to reveal six unique chemical scaffolds. Finally, each of these compounds was manually reviewed for the possession of reactive groups such as Michael acceptors, epoxides, and free thiols. However, none of them had such functional groups.

To further evaluate the identified actives, we repurchased four examples that belong to the largest cluster (cluster 1, containing 26 of the 36 remaining compounds); **1a** (4-(4-nitrophenyl)-3a,4,5,9b-tetrahydro-3H-cyclopenta[c]quinoline-6-carboxylic acid) (ChemBridge, cat. 5585430), **1b** (4-(4-chlorophenyl)-3a,4,5,9b-tetrahydro-3H-cyclopenta[c]quinoline-8-carboxylic acid) (ChemDiv, cat. 2374-0013), **1c** (4-(3-(trifluoromethyl)phenyl)-3a,4,5,9b-tetrahydro-3H-cyclopenta[c]quinoline-8-carboxylic acid) (ChemDiv, cat. 5408-1849), **1d** (4-(4-ethylphenyl)-3a,4,5,9b-tetrahydro-3H-cyclopenta[c]quinoline-8-carboxylic acid) (ChemDiv, cat. 6415-0967) (**Figure 2.4A**). Unexpectedly, none of these compounds were inhibitors upon re-testing. These samples were subsequently subjected to a side-by-side assay against the original stock solutions. Interestingly, the two series had significantly different inhibitory profiles; the “old” samples were highly active whereas the repurchased compounds were



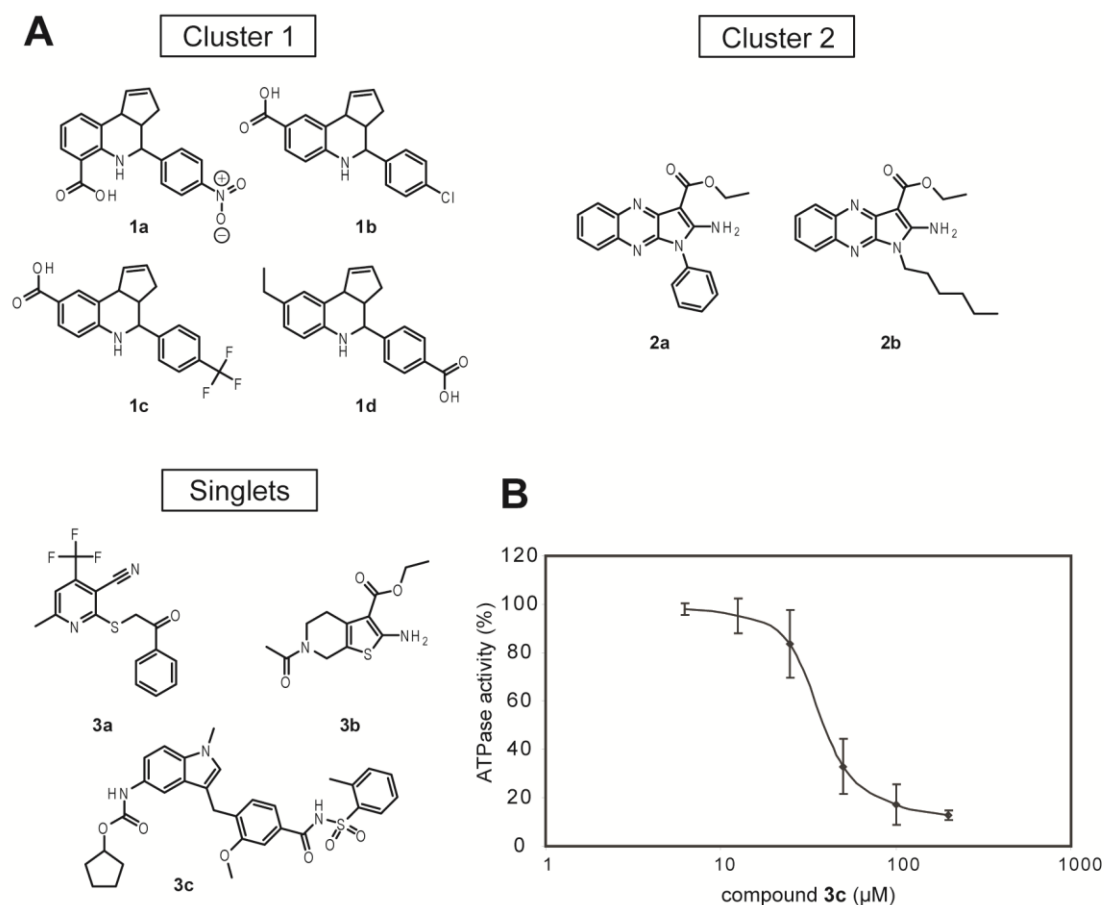


**Figure 2.4 Hits identified in the screen.** (C) Chemical structures of representative active compounds. A total of 36 inhibitors were identified in this screen; 26 cluster I compounds, 6 cluster II and 4 singlets. The structures of the re-tested compounds are shown. (D) Inhibition curve for compound 3c. IC<sub>50</sub> value was calculated to be  $37 \pm 1 \mu\text{M}$ . The assay was performed in triplicates and error bars represent standard error of mean.

inactive. Despite these differences, analysis by mass spectrometry and <sup>1</sup>H NMR suggested that both sets of compounds were relatively pure and that they had the correct molecular formulae. One potential clue to this discrepancy came from observations made during the assay setup, in which we noticed differences in the color of these samples. Specifically, over the span of 5 days at room temperature in DMSO, the re-purchased compounds would eventually become slightly colored. Moreover, these aged samples now had anti-DnaK ATPase activity

upon re-testing. Based on the reported synthesis of this scaffold [26] and the presence of a free acid in the active structures, we suspected that the color difference (and perhaps the activity differences) might arise due to metal chelation. Indeed, treatment with EDTA inhibited the color change and extraction of the "active" form with an EDTA solution led to a loss of its activity (data not shown). Thus, we concluded that the active sample appears to involve a metal and no further investigation was pursued.

Compounds belonging to the other clusters were studied in a similar manner. Briefly, we repurchased two compounds from cluster 2 [**2a** (ethyl 2-amino-1-phenyl-1H-pyrrolo[2,3-b]quinoxaline-3-carboxylate) (ChemDiv, cat. 5122-1769), **2b** (ethyl 2-amino-1-hexyl-1H-pyrrolo[2,3-b]quinoxaline-3-carboxylate) (ChemDiv, cat. 6256-4951)] and the three singlets that were available for resupply [**3a** (6-methyl-2-((2-oxo-2-phenylethyl)thio)-4-(trifluoromethyl)nicotinonitrile) (ChemDiv, cat. 3076-0200), **3b** (ethyl 6-acetyl-2-amino-4,5,6,7-tetrahydrothieno[2,3-c]pyridine-3-carboxylate) (ChemDiv, cat. K813-0112), **3c** (cyclopentyl (3-(2-methoxy-4-((o-tolylsulfonyl)carbamoyl)benzyl)-1-methyl-1H-indol-5-yl) carbamate) (Cayman Chemical Inc., cat. 10008282)]. We confirmed the structure of these compounds by mass spectrometry and then determined their IC<sub>50</sub> values. Compounds **2a**, **2b**, **3a** and **3b** had poor activity (> 500 μM) and were not further pursued. However, compound **3c** inhibited ATPase activity with an IC<sub>50</sub> value of 37 ± 1 μM (**Figure 2.4B**). Previously identified, allosteric Hsp70 inhibitors also have relatively modest, micromolar IC<sub>50</sub> values [5]. Thus, the activity of **3c** is

comparable to some of the known compounds.

## 2.2.4 Compound 3c Binds DnaK, Favors High Affinity Binding to Luciferase and Blocks DnaK's Stimulation by DnaJ

To characterize compound **3c** in secondary assays, we first investigated its ability to directly bind DnaK. Using tryptophan fluorescence, we found that the

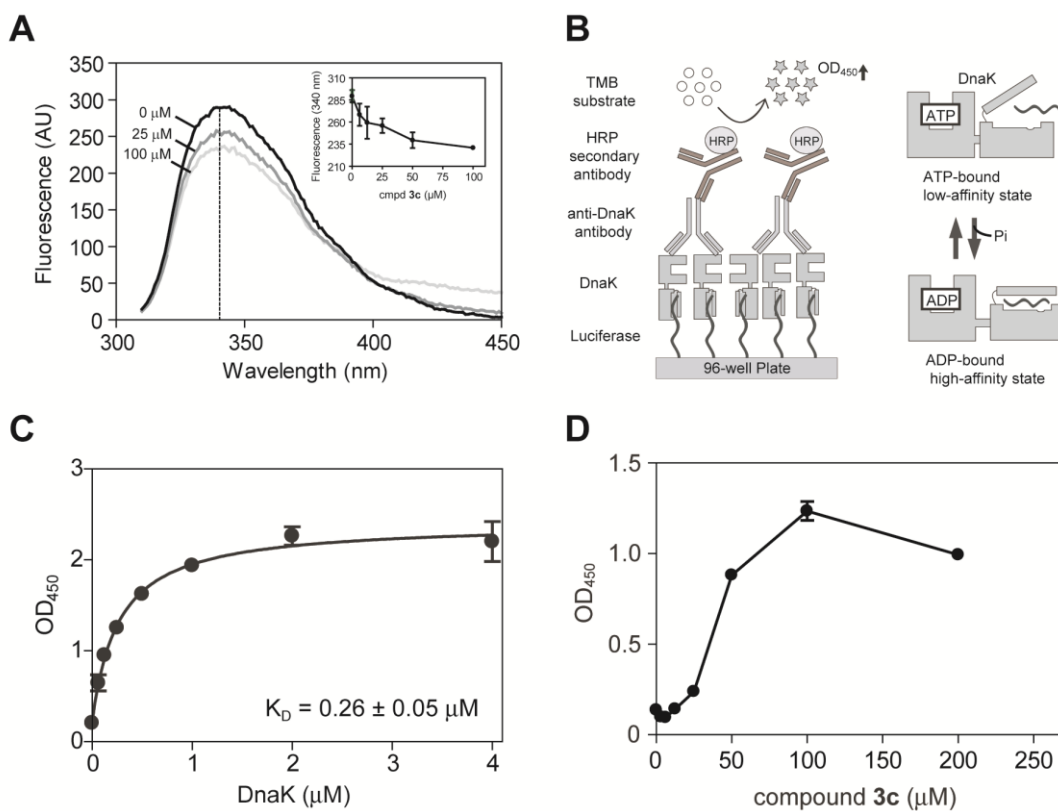


**Figure 2.5 Compound 3c binds DnaK and blocks DnaJ-stimulated ATPase activity.** (A) Tryptophan fluorescence was used to measure binding of compound to DnaK. Protein (5  $\mu\text{M}$  + 1 mM ATP), and compound were pre-incubated for 20 minutes at 37 °C prior to measurement of intrinsic fluorescence (ex 290 nm; em 300-450 nm). Inset: the results of the dose dependence experiments are the average of triplicates and the error bars represent standard error of mean. The dose dependence experiments were carried out at 340 nm (dotted line). (B) On the left is a schematic of the ELISA for DnaK binding to a model substrate, firefly luciferase. On the right is a schematic of the ADP-bound form of DnaK, which binds tighter than the ATP-bound form to substrates. (C) Measurement of DnaK binding to luciferase, using the ELISA approach. The results are the average of duplicates and the error bars represent standard error of mean. (D) Compound 3c favored the high-affinity form of DnaK. The chaperone (0.05  $\mu\text{M}$  DnaK + 1 mM ATP) was treated with 3c at the indicated concentrations for 20 minutes prior to the ELISA.

compound bound the chaperone with an estimated  $K_D$  of  $13 \pm 1.7 \mu\text{M}$ , in relatively good agreement with the  $IC_{50}$  value from the ATPase assay (**Figure 2.5A**). Next, we wanted to explore how compound **3c** might influence the structure of DnaK and, specifically, its interactions with substrates. As mentioned above, the ATP-bound form of DnaK has relatively poor affinity for substrate, while the ADP-bound form has enhanced affinity (**Figure 2.5B**) [8]. To test whether compound **3c** might change DnaK's apparent affinity for substrate, we measured binding of the chaperone to the model substrate, firefly luciferase (**Figure 2.5B**). By this method, the affinity of DnaK for luciferase was  $260 \pm 50$  nM (**Figure 2.5C**) and addition of compound **3c** significantly improved the apparent affinity (**Figure 2.5D**).

Because much of the signal from the ATPase assay is due to the stimulatory activity of the co-chaperone DnaJ, we hypothesized that compound **3c** might alter the interaction between DnaK and DnaJ. To explore that model, we determined the  $K_{0.5}$  of DnaJ to estimate the strength of the protein-protein interaction. In the absence of inhibitor, we found that the  $K_{0.5}$  of DnaJ was  $0.17 \pm 0.01 \mu\text{M}$  (**Figure 2.6A**). Addition of low levels ( $25 \mu\text{M}$ ) of compound **3c** did not significantly alter this value ( $K_{0.5} = 0.18 \pm 0.01 \mu\text{M}$ ). However, higher concentrations ( $50$  or  $100 \mu\text{M}$ ) increased the  $K_{0.5}$  to  $0.96 \pm 0.16 \mu\text{M}$  and greater than  $2 \mu\text{M}$ , respectively (**Figure 2.6A**). These results suggested that binding of compound **3c** to DnaK might interrupt its interactions with DnaJ.

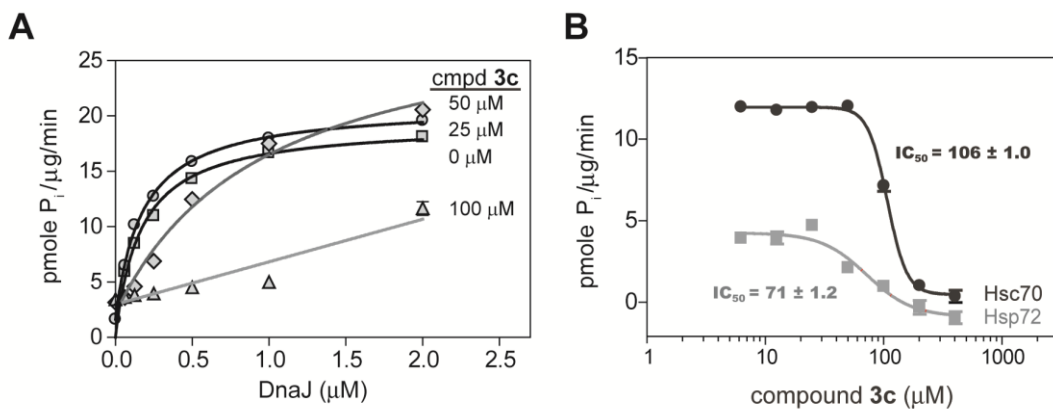


**Figure 2.6 Compound 3c interferes with DnaK-DnaJ and is active against human Hsp70s.** (A) Compound 3c specifically blocked DnaJ-mediated stimulation of ATP turnover by DnaK. The DnaK concentration was 0.6 μM and ATPase activity was measured using the absorbance version of the assay. The results are the average of triplicates and the error bars represent standard error of mean. (B) Compound 3c also inhibited the DnaJ-stimulated ATPase activity of bovine Hsc70 and human Hsp72, as measured using the absorbance version of the assay. The protein concentrations were: Hsc70 or Hsp72 (0.6 μM) and DnaJ (1.0 μM). The results are the average of triplicates and the error bars represent standard error of mean.

Finally, members of the Hsp70 family are highly conserved, with DnaK sharing nearly 50% sequence identity with human Hsp72 (HSPA1A) and bovine Hsc70 (HSPA8). To test whether compound **3c** might inhibit the ATPase activity of these related family members, we carried out dose dependence experiments in the presence of DnaJ. We found that this compound had an IC<sub>50</sub> of 71 ± 1.2 μM for human Hsp72, and an IC<sub>50</sub> of 106 ± 1.0 μM against bovine Hsc70 (**Figure 2.6B**), showing that compound **3c** also inhibits the mammalian isoforms. Together, this screening approach using the reconstituted Hsp70 complex (DnaK-DnaJ) identified an inhibitor that specifically blocks the interaction.

### 2.2.5 Screening of Natural Product Extracts

To explore additional chemical scaffolds that inhibit Hsp70's ATPase activity, we assembled a collection of organic extracts from 36 commercial spices and crude plant materials. For this specific study, we chose to use common plant materials,

containing largely known compounds, to facilitate downstream identification of active components. Also, because the Hsp70 family is highly conserved and expressed in many plant pathogens, we were interested in whether natural product extracts might be particularly enriched for inhibitors of this system.

This collection was arrayed in 96-well plates and screened at 40  $\mu\text{g}/\text{mL}$  using the colorimetric ATPase assay [18]. We used the colorimetric version of the assay (rather than the new fluorescence method) because of the small number of samples. Using this approach, we screened each crude extract in triplicate and

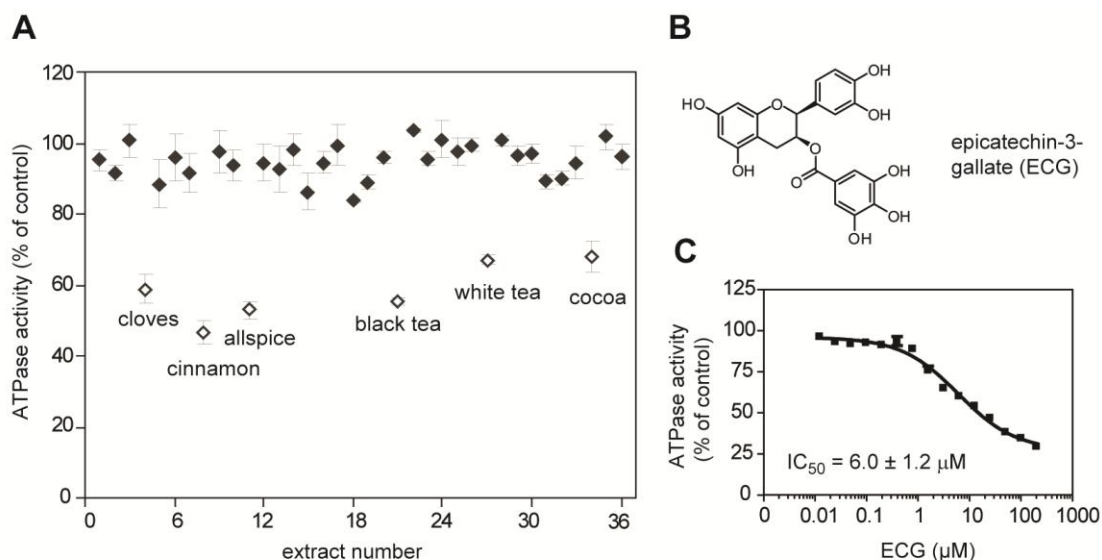


**Figure 2.7 Screening plant extracts against the DnaK-DnaJ system reveals epicatechin-3-gallate as the major inhibitor in white tea.** (A) Results of the screen of natural product extracts (40  $\mu\text{g}/\text{mL}$ ) against the ATPase activity of the DnaK (0.6  $\mu\text{M}$ ) and DnaJ (1  $\mu\text{M}$ ). Each extract was screened in duplicate and the range is shown relative to a solvent control. The active compounds (> 25% inhibition) are shown in open symbols. (B) Chemical structure of ECG. (C) Dose dependent inhibition of DnaK-DnaJ by ECG. The active component of white tea was identified by bio-assay guided fractionation and the structure confirmed by comparing the NMR spectra to an authentic sample (Appendix 2.9.3). The dose dependence experiment was performed against DnaK-DnaJ in triplicate and the error bars represent standard error of the mean.

found that only 6 of 36 extracts (allspice, black tea, cocoa, cinnamon, cloves, and white tea) inhibited ATPase activity by more than 30% (**Figure 2.7A**). Using activity-guided fractionation on reverse phase HPLC columns, we identified the major active component from the white tea extract as epicatechin-3-gallate (ECG) (**Figure 2.7B and Appendix 2.9.3**). ECG is known to be prevalent in this plant [27]. In dose dependence experiments, the  $IC_{50}$  of authentic ECG was  $6.0 \pm 0.9$   $\mu$ M against the DnaK-DnaJ system (**Figure 2.7C**). Based on this finding, we collected 80 related flavonoids and found that myricetin has the best overall inhibitory activity. Subsequent structural and mechanistic studies by Lyra Chang and Eric Bertelsen identified myricetin's binding site on DnaK and demonstrated that the compound specifically blocks the interaction between DnaK and DnaJ (described in more detail in [28]). While flavonoids are known to have a wide range of cellular targets and activity and, thus, they are not ideal chemical tools, identification of the new binding site may aid in These studies confirmed that the ATPase assay against the reconstituted DnaK-DnaJK complex could be used to identify compounds that block protein-protein contacts and "tune" the activity of Hsp70 family chaperones.

### **2.2.6 Screening of Known Bioactive Compounds**

Using the same colorimetric method, we next evaluated a library of 2,800 known bioactive compounds. We expected that this collection might have different compounds than the 55K diverse compounds or the natural product extract collection and, thus, new chemical scaffolds might be found. Using the same

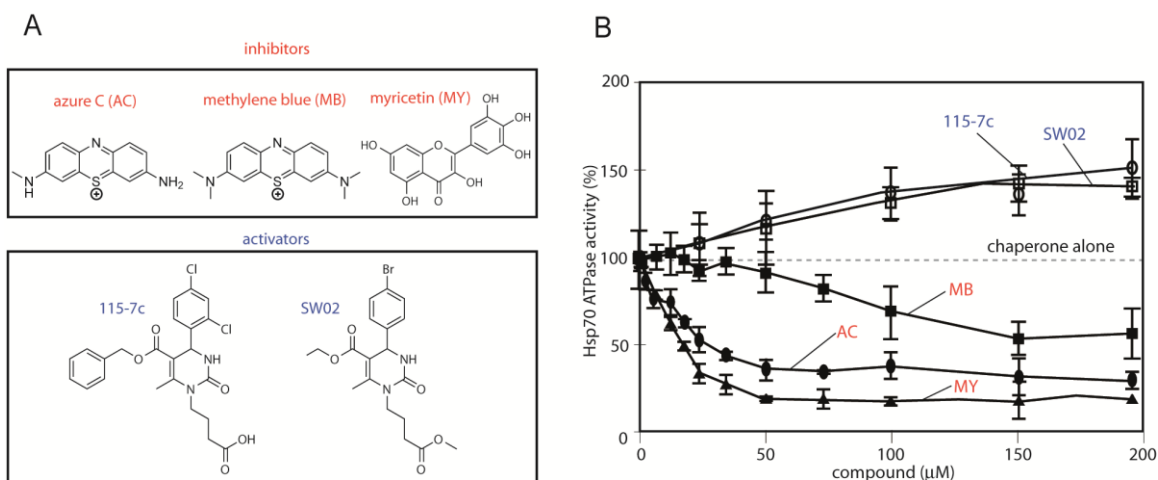


**Figure 2.8** Identification of both activators and inhibitors of the ATPase activity of Hsp70. (A) The chemical structures of the inhibitors and activators are shown. Note that inhibitors were identified from two distinct chemical classes: benzothiazines (MB, AC) and flavones (MY). (B) Dose dependence studies confirm that the dihydropyrimidines (115-7c and SW02) are activators of Hsp70-mediated nucleotide hydrolysis, while the benzothiazines and MY inhibited this activity. Results are the average of triplicates and error is standard deviation.

screening method used above, we screened 2,800 members of the MS2000 and NCC collections of bioactive and FDA-approved compounds. This collection also included ~250 dihydropyrimidines because its scaffold had previously been found to bind Hsp70 [29,30]. These efforts identified five active compounds (0.2% hit rate) belonging to at least three chemical scaffolds (**Figure 2.8A**). These compounds either accelerated or reduced the ATPase activity of human Hsp70. The benzothiazine, methylene blue (MB), its demethylated analogue, azure C (AC [31]) inhibited human Hsp70 by more than 80% with  $IC_{50}$  values of 83, 11  $\mu$ M, respectively (**Figures 2.8B**). In addition, we found myricetin as an inhibitor, supporting our previous finding (see **2.2.5**). We were also able to identify activators of ATPase activity in the dihydropyrimidine family (115-7c and SW02). These compounds increased Hsp70 function by ~ 45% with  $EC_{50}$  values of ~ 120 to 150  $\mu$ M. Together, these experiments, using a new HTS platform and three



different compound collections, provided a suite of chemical probes for Hsp70.

## **2.3 Discussion**

### **2.3.1 Miniaturization of Colorimetric Assay by Energy Transfer**

Absorbance assays are widely used to monitor the activity of ATPases, GTPases, phosphatases and kinases. They are widely used, in part, because they are robust, easy to use and relatively inexpensive. However, these assays are typically performed in cuvettes or medium-density (i.e. 96-well) microtiter plates. While these formats are suitable for some studies, they are not preferred for high throughput screens, especially in low volume. Adopting a method developed by Zuck *et al*, [19], we have successfully converted a QR-based absorbance assay to 384-well format and screened a collection of >55,000 compounds. Although this general method was published in 2005, it remains largely under-evaluated in the screening literature. Rather, other phosphate-detection technologies, such as Phosphate Sensor (Invitrogen, Carlsbad, CA) and Transcreener™ ADP2 kit (Bellbrook Laboratories, Madison, WI) have been more widely used [32]. In our hands, this simple and inexpensive (approximately 1-2 cents / well) fluorescence method was robust and had good assay performance against a weak ATPase. However, it must be emphasized that there is significant potential for interference from autofluorescent or colored compounds, yielding false positives. Also, it should be clearly noted that occasional plates, from multiple manufacturers, produced very poor Z' values due to their inconsistent fluorescence (see **Appendix 2.9.2**). Despite these important concerns, we suspect that this

procedure may be useful in certain settings, especially when cost is a primary concern.

### 2.3.2 High Throughput Screen and Characterization of a Hit Compound

Using the energy transfer methodology, we embarked on a screening strategy against *E. coli* DnaK in combination with its co-chaperone DnaJ. We screened three different collections, including a natural product extract library, a collection of known bioactives and a diversity set. Screening of 55,400 molecules identified compound **3c**, with an IC<sub>50</sub> value of  $37 \pm 1 \mu\text{M}$  (see **Figure 2.4B**) and an affinity of  $13 \pm 1.7 \mu\text{M}$  (see **Figure 2.5A**). Compound **3c** selectively suppressed stimulation by DnaJ, while having little effect on the intrinsic ATPase activity (see **Figure 2.5**). Further, this compound did not block binding of DnaK to luciferase and, rather, it significantly enhanced this interaction (see **Figure 2.5D**). The high affinity form of DnaK is a poor partner for DnaJ [10], which might partially explain the observed behaviors. Future structural studies are expected to provide more insight into the mechanism of this compound and, more broadly, the pathways of allosteric regulation in the DnaK-DnaJ complex.

Additional screening using the previously established colorimetric method identified three chemical scaffolds including flavonoids, phenothiazines and dihydropyrimidines. Importantly, the dihydropyrimidines enhanced ATP turnover by Hsp70 while phenothiazines inhibited it, providing us with tools to “tune” the activity of Hsp70. Although additional work is needed to optimize these

compounds, these screening efforts provided multiple new scaffolds for exploration. In Chapters 3, we will further characterize two of these promising scaffolds.

### **2.3.3 Conclusion**

Previous work by the Gestwicki group had resulted in a 96-well assay that could be used to identify new activators and inhibitors of Hsp70 [18]. This was an important advance because there were very few chemical modulators of Hsp70 known and this platform allowed identification of promising compounds, including dihydropyrimidines. However, this approach wasn't suitable for screening larger collections because of a loss of sensitivity in low volume. In this Chapter, I have developed a QR-based high throughput screening method in 384-well format by taking advantage of intrinsic fluorescent property of microtiter plates. This approach solved the problem of low sensitivity and this method proved to be a rigorous HTS method.

Beyond the technical advance of developing a new screening approach, the work in this Chapter also revealed a number of new chemical scaffolds that either activate or inhibit Hsp70. As discussed in Chapter 1, the biology of Hsp70 is highly dependent on its interactions with co-chaperones, such as J proteins and NEFs. Thus, we were particularly interested in finding molecules that act on the complex between Hsp70 and the J co-chaperones. Accordingly, we performed the screens against the reconstituted complex of DnaK and DnaJ. Consistent

with the assay design, we found that the resulting compounds selectively acted on the DnaK-DnaJ complex (as further discussed in Chapter 3). These molecules may be especially powerful probes for exploring the complex biology of Hsp70 and its roles in tau turnover.

## **2.4 Materials and methods**

### **2.4.1 Reagents**

Unless otherwise specified, all reagents were purchased from Sigma (St. Louis, MO). The dihydropyrimidines 115-7c and SW02 were synthesized as described (Wisén, et al. 2008) *E. coli* DnaK was purified according to published procedures [18]. *E. coli* DnaJ was purified as previously described [33].

### **2.4.2 Small Molecule Libraries.**

The MicroSource MS2000 library contains ~2,000 bioactive compounds with a minimum of 95% purity. Briefly, the collection includes 958 known therapeutic drugs, 629 natural products and derivatives, 343 compounds with reported biological activities and 70 compounds approved for agricultural use. The University of Michigan Center for Chemical Genomics (CCG) small molecule library consists of 16,000 Maybridge HitFinder, 13,000 ChemBridge, 20,000 ChemDiv, 3,000 NCI, 450 NIH Clinical Collection (NCC) compounds and ~20,000 natural product extracts. The activity of promising compounds was confirmed using repurchased samples from original vendors. Compound **3c** was purchased from Cayman Chemical Inc. (Ann Arbor, MI). Compounds were used without

further purification.

### **2.4.3 High Throughput ATPase Assay – Absorbance Method.**

The assay procedure was adopted from previous reports with modifications where indicated [18]. All components other than compounds were added by a Multidrop dispenser (Thermo Fisher Scientific, Inc., Waltham, MA). Stock solutions of 0.05% w/v quinaldine red (QR), 2% w/v polyvinyl alcohol, 6% w/v ammonium heptamolybdate tetrahydrate in 6 M HCl and water were mixed in a 2:1:1:2 ratio to prepare the QR reagent. This reagent was prepared fresh prior to each experiment. For compound screening, a stock solution of DnaK and DnaJ was prepared in assay buffer (100 mM Tris-HCl, 20 mM KCl, and 6 mM MgCl<sub>2</sub>, 0.01% Triton X-100, pH 7.4) so that the final concentration of DnaK was 0.4 μM and DnaJ was 0.7 μM (unless noted). This solution (10 μL) was then added to each well of a 384-well clear plate (Thermo Fisher Scientific, Inc., Waltham, MA). To this solution, 0.4 μL of either compound (1.5 mM) or DMSO was added to each well by Biomek HDR (Beckman, Fullerton, CA). Finally, 4 μL of a 7 mM ATP solution was added to begin the reaction. The plates were then incubated for 3 hrs at 37 °C. After incubation, each well received 40 μL of the QR reagent, allowing 2 min of reaction time, and then quenched by addition of 32% w/v solution of sodium citrate (4 μL). The plates were then incubated for an additional 15 min at 37 °C before measuring absorbance at 530 nm on a PHERAstar plate reader (BMG Labtech, Cary, NC).

#### **2.4.4 High Throughput ATPase Assay – Fluorescence in White Plates.**

The QR reagent was prepared exactly as indicated above. All components other than compounds were added by a Multidrop dispenser (Thermo Fisher Scientific, Inc., Waltham, MA). The DnaK-DnaJ stock solution was prepared so that the final concentration of DnaK was 0.4  $\mu\text{M}$  and DnaJ was 0.7  $\mu\text{M}$  (unless noted). This solution (5  $\mu\text{L}$ ) was then added to each well of a 384-well opaque, white, low-volume, non-sterile, polystyrene 384-well plates (Greiner Bio-One North America Inc., Monroe, NC). To this solution, 0.2  $\mu\text{L}$  of either compound (1.5 mM) or DMSO was added to each well by Biomek HDR (Beckman, Fullerton, CA). Finally, 2  $\mu\text{L}$  of a 3.5 mM ATP solution was added to begin the reaction. The plates were then incubated for 3 hrs at 37 °C. After incubation, each well received 15  $\mu\text{L}$  of the QR reagent, allowing 2 min of reaction time, and then quenched by addition of 32% w/v solution of sodium citrate (2  $\mu\text{L}$ ). These plates were incubated for 15 min at 37 °C and the fluorescence intensity measured (excitation 430 nm, emission 530 nm) on a PHERAstar plate reader. Standard curves were obtained using stock solutions of dibasic potassium phosphate.

#### **2.4.5 Tryptophan Fluorescence Assay.**

The method for measuring binding to DnaK was carried out as previously described [18]. Briefly, DnaK (5  $\mu\text{M}$ ) in 1 mM ATP was incubated with the indicated concentration of compound **3c** in a total volume of 25  $\mu\text{L}$  for 20 min at 37 °C. The emission spectrum between 300 - 450 nm was recorded (excitation at 290 nm) using a SpectraMax M5 microplate reader (Molecular Devices,

Sunnyvale, CA).

#### **2.4.6 Enzyme-linked Immunosorbent Assay.**

The procedure for DnaK binding to luciferase was adapted from a previous report [34]. Briefly, firefly luciferase (0.2 mg/mL) was first incubated with 0.1  $\mu$ M trypsin at 37 °C for 1 hr in HEPES buffer (40 mM HEPES, 8 mM MgCl<sub>2</sub>, 20 mM NaCl, 20 mM KCl, 0.3 mM EDTA, pH 7.2), the reaction was quenched with 1 mM PMSF and diluted to 5  $\mu$ g/mL with PBS buffer (pH 7.4). An aliquot (50  $\mu$ L) was then added to 96-well plates (ThermoFisher brand, clear, non-sterile, flat bottom). After 1 hr of incubation at 37 °C, the wells were washed three times with 100  $\mu$ L PBS-T (0.05% Tween-20). A solution of DnaK (at the indicated concentrations), compound **3c**, and 1 mM ATP was pre-incubated in HEPES with 0.01% Tween for 30 min. From this solution, 50  $\mu$ L was added to wells and allowed to bind for 30 min at room temperature. After washing three times with PBS-T, 5% non-fat milk (w/v) in 100  $\mu$ L TBS-T was used to block the non-specific binding sites. Primary antibody was then added (1:3000 dilution of rabbit anti-DnaK serum in TBS-T, 50  $\mu$ L/well) and the plates were incubated for 1 hr at room temperature. Wells were then washed three times with TBS-T, followed by addition of HRP-conjugated secondary (1:3000 dilution of goat anti-rabbit serum in TBS-T, 50  $\mu$ L/well). After a 1 hr incubation, the wells were washed three times and signal developed for 20 min using the TMB kit from Cell Signaling Technology (Danvers, MA). The absorbance was measured using a SpectraMax M5 microplate reader (Molecular Devices, Sunnyvale, CA) at 450 nm.

#### **2.4.7. Construction of Natural Product Extract Library and Screening Against DnaK/DnaJ Complex**

Approximately 300 mg of powdered natural product was extracted with ~500  $\mu$ L of methanol. After vortexing and 15 minutes of sonication, the samples were centrifuged at 10,000 rpm for 5 minutes and the supernatant collected. After removing the organic solvent, the dried material was suspended in DMSO at 1 mg/mL. The resulting extract library was screened in the ATPase assay at 40  $\mu$ g/ml final concentration, using a previously described protocol [18]. The concentrations of DnaJ and DnaK were 1.0 and 0.6  $\mu$ M, respectively.

#### **2.4.8 Identification of the Active Component from Tea.**

White tea leaves were extracted with EtOAc, MeOH and acetone. The combined extracts were then concentrated *in vacuo* and the residue was partitioned between H<sub>2</sub>O and CH<sub>2</sub>Cl<sub>2</sub>. The organic phase was partitioned between 90% MeOH and *n*-hexanes and the aqueous MeOH fraction was further partitioned between 60% MeOH and CH<sub>2</sub>Cl<sub>2</sub>. Using ATPase assays for bioactivity-guided fractionation, we identified the 60% MeOH fraction as the sample with inhibitory activity against *E. coli* DnaK. This sample was then subjected to ODS flash chromatography (Supelco, Bellefonte, PA) with aqueous MeOH, yielding six fractions. The most active fraction was purified by reversed-phase HPLC (Beckman-coulter, Brea, CA) on Waters Spherisorb ODS-2 using a linear gradient elution of an aqueous MeOH system followed by reversed-phase HPLC with 20% aqueous MeOH. This procedure yielded epicatechin 3-gallate (ECG) as



the major active component. The identification of this compound was confirmed by comparison of the  $^1\text{H}$  NMR spectrum and ESI-MS spectrum with those of an authentic sample purchased from MicroSource (see **Appendix 2.9.**).

#### **2.4.9. Identification of Chemical Modulators of Hsp70 from MS2000 Library.**

High throughput screening of ATPase activity was performed using human Hsp72 and *E.coli* DnaJ as previously described [18]. The pilot collection of compounds was comprised of the commercial MS2000 FDA-approved set (Spectrum) and an internally generated, focused collection of dihydropyrimidines [35]. The statistical parameters of the screen were similar to those previously reported for the prokaryotic Hsp70, DnaK (Z factor  $\sim 0.7$ ; S/N  $> 10$ ; CV  $\sim 8\%$ ). Active compounds were defined as those with at least 30% activity: activators accelerated steady-state ATP hydrolysis at least 30%, while inhibitors reduced this value. This criterion was selected because it represents 3 standard deviations of the DMSO control. Hits were subsequently subject to 8-point dose dependence verification in triplicate and the results analyzed with GraphPad PRISM.

#### **Notes**

This work was partially published in the following manuscripts:

“High-throughput screen for *Escherichia coli* heat shock protein 70 (Hsp70/DnaK): ATPase assay in low volume by exploiting energy transfer” Miyata, Y., Chang, L., Bainor, A., Mcquade, T.J., Walczak, C.P., Zhang, Y., Larsen, M.J., Kirchhoff, P.,

and Gestwicki, J.E.,(2010), *J.Biol.Screen.* 15;1211-1219

“Chemical screens against a reconstituted multiprotein complex: myricetin blocks DnaJ regulation of DnaK through an allosteric mechanism” Chang, L., Miyata, Y., Ung, M.U., Bertelsen, E.B., Mcquade, T.J., Carlson, H.A., Zuiderweg, E.R.P. and Gestwicki, J.E. (2011) *Chem.Biol.* 18;210-221

“Chemical manipulation of Hsp70 ATPase activity regulates tau stability” Jinwal, U.K., Miyata, Y., Koren, J.III., Jones, J.R., Trotter, J.H., Chang, L., O’Leary, J.O., Morgan, D., Lee, D., Shults, C.L., Rousaki, A., Weeber, E.J., Zuiderweg, E.R.P., Gestwicki, J.E. and Dickey, C.A. (2009) *J. Neurosci.* 29 (39); 12079-12088

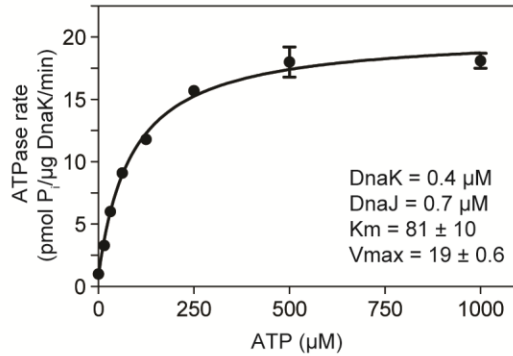
### **Author contributions**

Yoshinari Miyata, Lyra Chang and Jason, E. Gestwicki designed the screens and follow-up experiments. Yoshinari Miyata and Lyra Chang conducted the screens with help from Thomas J. Mcquade, Martha, J. Larsen and Paul Kirchhoff (UM Center for Chemical Genomics) and they also conducted the follow-up experiments. Anthony Bainor and Christopher P. Walczak carried out some of the absorbance-based 384-well plate assay. Yaru Zhang optimized conditions for the ELISA assay. Yoshinari Miyata performed assay-guided purification and identification of active component from tea extract.

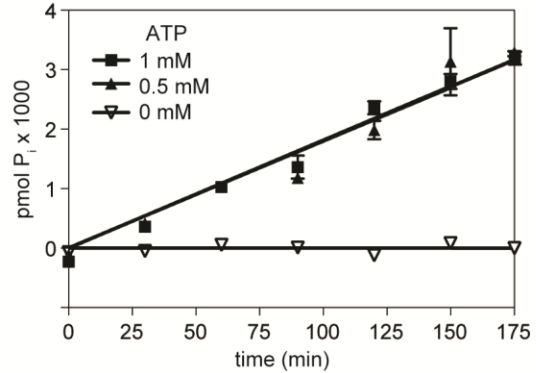
## 2.5 Appendices

### 2.5.1 Characterization of the white plate, fluorescent assay

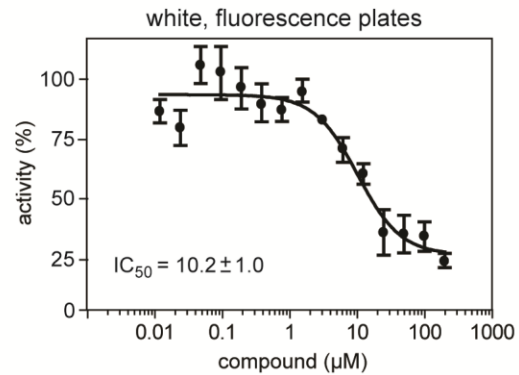
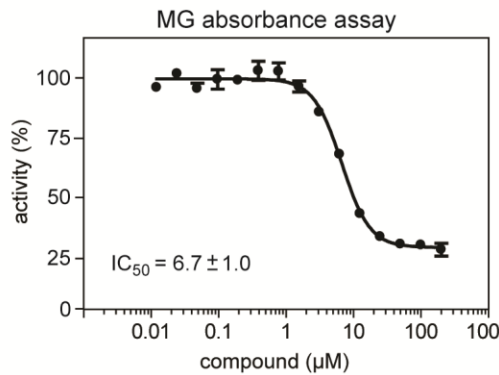
#### A Kinetic parameters of DnaK-DnaJ



#### B Linear range of the DnaK-DnaJ complex



#### C Dose dependence of a known inhibitor by two different ATPase methods

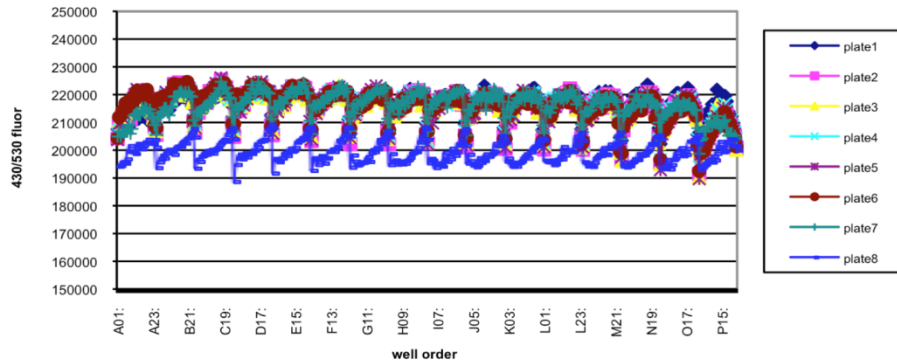


#### Appendix 2.5.1 Characterization of the white plate, fluorescent assay. (A)

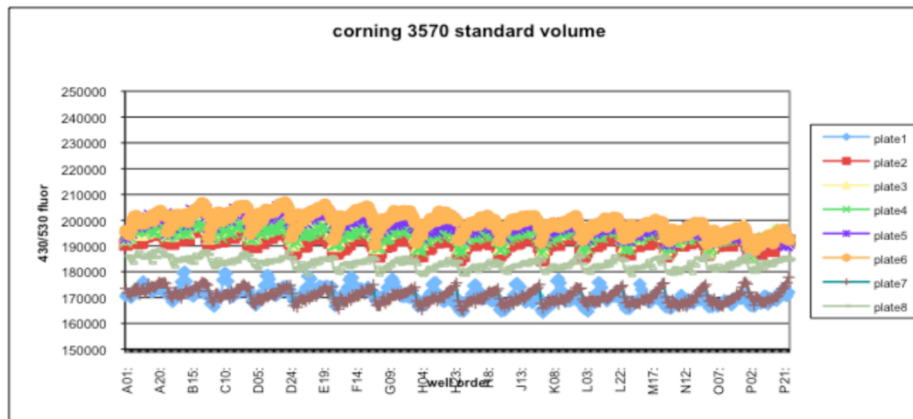
Determination of the kinetic parameters of DnaK-DnaJ in the fluorescence method, under the screening conditions. (B) Determination of the linear range. The concentration of DnaK was 0.4  $\mu$ M and DnaJ was 0.7  $\mu$ M. (C) Direct comparison of the  $IC_{50}$  values of a known inhibitor in the normal, malachite green-based absorbance assay and the white, fluorescent plate assay. The concentration of DnaK was 0.4  $\mu$ M, DnaJ was 0.7  $\mu$ M and ATP was 1 mM. Results are the average of triplicates and the error bars represent standard error of the mean.

## 2.5.2 Occasional outliers in white, opaque microtiter plates.

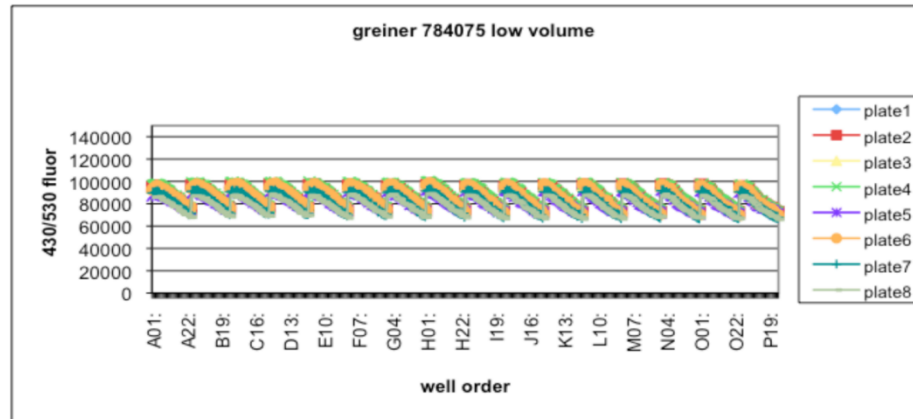
corning 3825 low volume



corning 3570 standard volume



greiner 784075 low volume

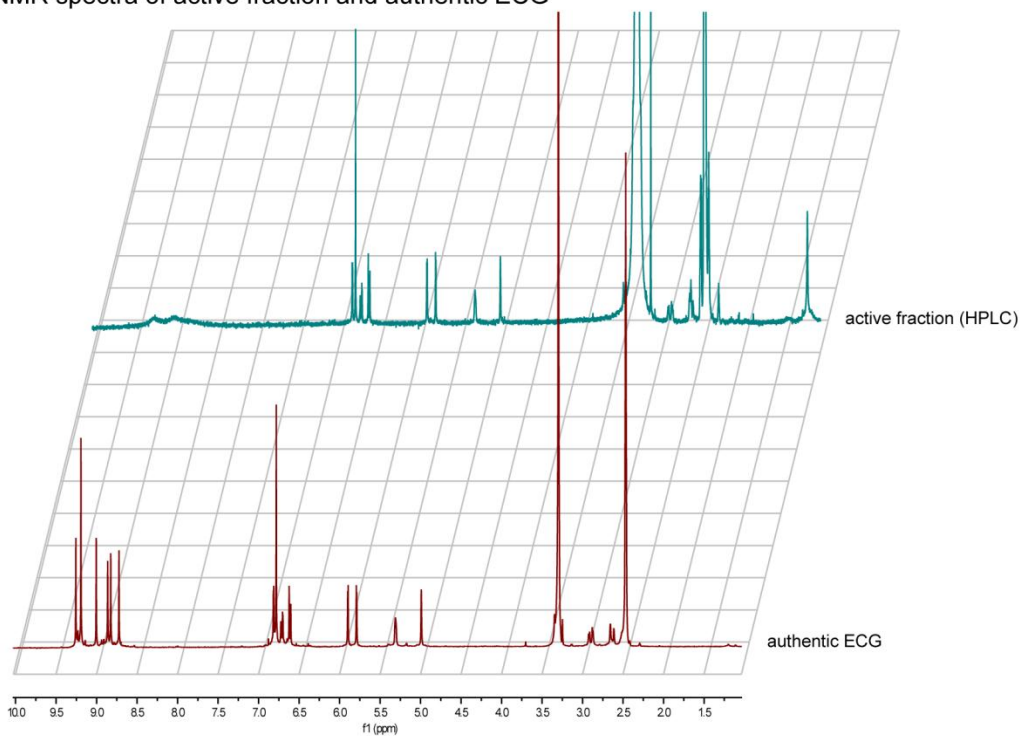


### Appendix 2.5.2 Occasional outliers in white, opaque microtiter plates.

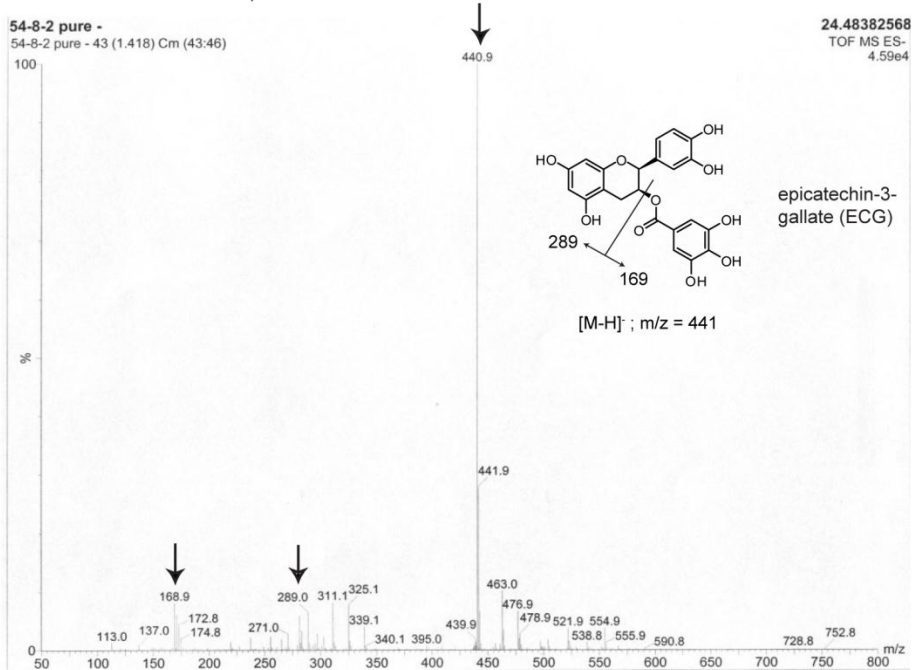
Stacks of untreated microtiter plates were monitored for fluorescence (ex. 430 nm. em. 530 nm). Note that occasional microtiter plates were monitored for fluorescence (ex. 430 nm. em. 530 nm). Note that occasional plates show significantly different fluorescence patterns and that all the plates show a “sharktooth” pattern. Representative data sets are shown for three manufacturers. Based on these results, we chose Greiner 784075 low volume plates for our experiments.

### 2.5.3. Characterization of active component from white tea and identification as (-)-epicatechin-3-gallate.

(A) <sup>1</sup>H NMR spectra of active fraction and authentic ECG



(B) ESI- MS of active fraction, consistent with the identification as ECG



**Appendix 2.5.3. Characterization of active component from white tea and identification as (-)-epicatechin-3-gallate.** (A) <sup>1</sup>H-NMR spectra of active fraction and authentic ECG. (B) ESI- MS of the active fraction.

## 2.6 References

1. Bukau B, Weissman J, Horwich A. Molecular chaperones and protein quality control. *Cell*, 125(3), 443-451 (2006).
2. Ciocca DR, Calderwood SK. Heat shock proteins in cancer: diagnostic, prognostic, predictive, and treatment implications. *Cell Stress Chaperones*, 10(2), 86-103 (2005).
3. Witt SN. Hsp70 molecular chaperones and Parkinson's disease. *Biopolymers*, 93(3), 218-228 (2010).
4. Singh VK, Utaida S, Jackson LS, Jayaswal RK, Wilkinson BJ, Chamberlain NR. Role for dnaK locus in tolerance of multiple stresses in *Staphylococcus aureus*. *Microbiology*, 153(Pt 9), 3162-3173 (2007).
5. Patury S, Miyata Y, Gestwicki JE. Pharmacological targeting of the Hsp70 chaperone. *Curr Top Med Chem*, 9(15), 1337-1351 (2009).
6. Bertelsen EB, Chang L, Gestwicki JE, Zuiderweg ER. Solution conformation of wild-type *E. coli* Hsp70 (DnaK) chaperone complexed with ADP and substrate. *Proc Natl Acad Sci U S A*, 106(21), 8471-8476 (2009).
7. Flynn GC, Pohl J, Flocco MT, Rothman JE. Peptide-binding specificity of the molecular chaperone BiP. *Nature*, 353(6346), 726-730 (1991).
8. Mayer MP, Schroder H, Rudiger S, Paal K, Laufen T, Bukau B. Multistep mechanism of substrate binding determines chaperone activity of Hsp70. *Nat Struct Biol*, 7(7), 586-593 (2000).
9. Russell R, Wali Karzai A, Mehl AF, McMacken R. DnaJ dramatically stimulates ATP hydrolysis by DnaK: insight into targeting of Hsp70 proteins to polypeptide substrates. *Biochemistry*, 38(13), 4165-4176 (1999).
10. Szabo A, Langer T, Schroder H, Flanagan J, Bukau B, Hartl FU. The ATP hydrolysis-dependent reaction cycle of the *Escherichia coli* Hsp70 system DnaK, DnaJ, and GrpE. *Proc Natl Acad Sci U S A*, 91(22), 10345-10349 (1994).
11. Jiang J, Maes EG, Taylor AB *et al.* Structural basis of J cochaperone binding and regulation of Hsp70. *Mol Cell*, 28(3), 422-433 (2007).
12. Kragol G, Lovas S, Varadi G, Condie BA, Hoffmann R, Otvos L, Jr. The antibacterial peptide pyrrolicin inhibits the ATPase actions of DnaK and prevents chaperone-assisted protein folding. *Biochemistry*, 40(10), 3016-3026 (2001).
13. Kang Y, Taldone T, Clement CC *et al.* Design of a fluorescence polarization assay platform for the study of human Hsp70. *Bioorg Med Chem Lett*, 18(13), 3749-3751 (2008).
14. Vogel M, Bukau B, Mayer MP. Allosteric regulation of Hsp70 chaperones by a proline switch. *Mol Cell*, 21(3), 359-367 (2006).
15. Swain JF, Dinler G, Sivendran R, Montgomery DL, Stotz M, Gierasch LM. Hsp70 chaperone ligands control domain association via an allosteric mechanism mediated by the interdomain linker. *Mol Cell*, 26(1), 27-39 (2007).
16. Massey AJ, Williamson DS, Browne H *et al.* A novel, small molecule inhibitor of Hsc70/Hsp70 potentiates Hsp90 inhibitor induced apoptosis in

- HCT116 colon carcinoma cells. *Cancer Chemother Pharmacol*, (2009).
17. Carter SG, Karl DW. Inorganic phosphate assay with malachite green: an improvement and evaluation. *J Biochem Biophys Methods*, 7(1), 7-13 (1982).
  18. Chang L, Bertelsen EB, Wisen S, Larsen EM, Zuiderweg ER, Gestwicki JE. High-throughput screen for small molecules that modulate the ATPase activity of the molecular chaperone DnaK. *Anal Biochem*, 372(2), 167-176 (2008).
  19. Zuck P, O'Donnell GT, Cassaday J *et al.* Miniaturization of absorbance assays using the fluorescent properties of white microplates. *Anal Biochem*, 342(2), 254-259 (2005).
  20. Kreuzsch S, Schwedler S, Tautkus B, Cumme GA, Horn A. UV measurements in microplates suitable for high-throughput protein determination. *Anal Biochem*, 313(2), 208-215 (2003).
  21. Lavery P, Brown MJ, Pope AJ. Simple absorbance-based assays for ultra-high throughput screening. *J Biomol Screen*, 6(1), 3-9 (2001).
  22. Yuan P, Walt DR. Calculation for Fluorescence Modulation by Absorbing Species and Its Application to Measurements Using Optical Fibers. *Analytical Chemistry*, 59(19), 2391-2394 (1987).
  23. Jinwal UK, Miyata Y, Koren J, 3rd *et al.* Chemical manipulation of hsp70 ATPase activity regulates tau stability. *J Neurosci*, 29(39), 12079-12088 (2009).
  24. Koren J, 3rd, Jinwal UK, Jin Y *et al.* Facilitating Akt clearance via manipulation of Hsp70 activity and levels. *J Biol Chem*, 285(4), 2498-2505 (2010).
  25. Martin YC, Kofron JL, Traphagen LM. Do structurally similar molecules have similar biological activity? *J Med Chem*, 45(19), 4350-4358 (2002).
  26. Kiselyov A, Smith L, Armstrong R. Solid support synthesis of polysubstituted tetrahydroquinolines via three-component condensation catalyzed by Yb(OTf)<sub>3</sub>. *Tetrahedron*, 54, 5089-5096 (1998).
  27. Friedman M. Overview of antibacterial, antitoxin, antiviral, and antifungal activities of tea flavonoids and teas. *Molecular nutrition & food research*, 51(1), 116-134 (2007).
  28. Chang L, Miyata Y, Ung PM *et al.* Chemical screens against a reconstituted multiprotein complex: myricetin blocks DnaJ regulation of DnaK through an allosteric mechanism. *Chem Biol*, 18(2), 210-221 (2011).
  29. Fewell SW, Day BW, Brodsky JL. Identification of an inhibitor of hsc70-mediated protein translocation and ATP hydrolysis. *J Biol Chem*, 276(2), 910-914 (2001).
  30. Fewell SW, Smith CM, Lyon MA *et al.* Small molecule modulators of endogenous and co-chaperone-stimulated Hsp70 ATPase activity. *J Biol Chem*, 279(49), 51131-51140 (2004).
  31. McKamey MR, Spitznagle LA. Chromatographic, mass spectral, and visible light absorption characteristics of toluidine blue O and related dyes. *J Pharm Sci*, 64(9), 1456-1462 (1975).
  32. Rowlands M, McAndrew C, Prodromou C *et al.* Detection of the ATPase

- activity of the molecular chaperones Hsp90 and Hsp72 using the Transcreener™ ADP assay kit. *J Biomol Screen*, 15(3), 279-286).
33. Chang L, Thompson AD, Ung P, Carlson HA, Gestwicki JE. Mutagenesis reveals the complex relationships between ATPase rate and the chaperone activities of Escherichia coli heat shock protein 70 (HSP70/DNAK). *J Biol Chem*, (2010).
  34. Wawrzynow A, Zylicz M. Divergent effects of ATP on the binding of the DnaK and DnaJ chaperones to each other, or to their various native and denatured protein substrates. *J Biol Chem*, 270(33), 19300-19306 (1995).
  35. Wisen S, Androsavich J, Evans CG, Chang L, Gestwicki JE. Chemical modulators of heat shock protein 70 (Hsp70) by sequential, microwave-accelerated reactions on solid phase. *Bioorg Med Chem Lett*, 18(1), 60-65 (2008).
  36. Salzmann M, Pervushin K, Wider G, Senn H, Wuthrich K. TROSY in triple-resonance experiments: new perspectives for sequential NMR assignment of large proteins. *Proc Natl Acad Sci U S A*, 95(23), 13585-13590 (1998).
  37. Zuiderweg ER. Mapping protein-protein interactions in solution by NMR spectroscopy. *Biochemistry*, 41(1), 1-7 (2002).



## Chapter 3

### Pharmacological Manipulation of Hsp70 by Methylene Blue

#### 3.1 Abstract

As discussed in Chapter 2, we identified inhibitors and activators of Hsp70 ATPase activity using a new high throughput screen. In this chapter, we used these molecules to study the relationship between Hsp70 and tau turnover. We hypothesized that tuning the ATPase activity of Hsp70 might control its affinity for tau, which could then translate to either its accumulation or clearance. Indeed, inhibitors led to rapid proteasomal degradation of tau in a cell-based model, while Hsp70 activators preserved tau levels. The effects of these molecules on tau stability were dependent on the levels of Hsp70, suggesting that Hsp70 is a major target of these compounds in cells. Unexpectedly, inhibition of Hsp70 did not result in widespread protein degradation; rather, only a handful of Hsp70 substrates seemed to be particularly sensitive. Also, Hsp70 inhibition did not induce a heat shock response. To explore the translational potential of these observations, we tested one of the inhibitors, methylene blue (MB) in organotypic brain slices and a mouse model of tauopathy. In both cases, MB led to rapid and substantial reductions in tau levels and, in the mouse model, it improved

cognitive functions. Based on these promising results, we explored the molecular mechanism linking MB to Hsp70 and tau degradation. Mass spectrometry, molecular modeling and point mutagenesis studies showed that MB inhibited Hsp70 by selectively oxidizing two cysteine residues, reducing its affinity for ATP. Interestingly, one of the critical reactive cysteines is only found in stress inducible Hsp70 family members and not the constitutive isoforms, such as Hsc70. Accordingly, Hsc70 was resistant to MB and mutating this cysteine to serine in Hsp70 provided resistance as well. These results suggest that stress inducible Hsp70 isoforms might have evolved to specifically respond to oxidative stress. Together, the work described in this Chapter leads to a model in which the ATPase activity of Hsp70 regulates tau stability. Further, compounds that block ATP turnover, such as MB, lead to tau degradation.

### **3.1.1 Abnormal tau causes neurodegenerative diseases**

In Alzheimer's disease (AD), the accumulation of amyloid plaques composed of A $\beta$  peptide is largely accepted as the pathogenic initiator, leading to intracellular accumulation of the microtubule associated protein tau into tangles [1,2]. However, cognitive dysfunction and neuron loss, both in AD and transgenic mice that accumulate amyloid-type pathology, are closely linked to tau deposition [3-5]. Moreover, tau pathology is found in approximately 15 other neurodegenerative diseases, some of which are caused by mutations in the tau gene itself [6]. Thus developing strategies to remove abnormal tau in symptomatic patients may be therapeutically beneficial; however, it is not yet clear which targets are best

suited to accomplish this task.

### **3.1.2 Molecular chaperones regulate the turnover of substrates, such as tau, through a poorly understood mechanism**

As discussed in more detail in Chapter 1, molecular chaperones, such as heat shock proteins Hsp70 and Hsp90, have been implicated in tau processing [7-15]. Both Hsp70 and Hsp90 utilize ATP to regulate protein refolding [16]. The details of this mechanism and the effects of nucleotide exchange on Hsp70 structure and function have been established using mutagenesis, combined with structural and biophysical studies [17,18]. Briefly, ATP binding to the nucleotide-binding domain (NBD) of Hsp70 allosterically promotes a conformational change that allows weak binding of substrate proteins in the substrate-binding domain (SBD). ATP hydrolysis to ADP then causes the C-terminal “lid” to close, facilitating high-affinity (~10-fold increase) substrate binding. When ADP is exchanged for ATP by an accessory nucleotide exchange factor (NEF), the lid opens, freeing the substrate. Despite recent progress, it still isn't clear how these biochemical features relate to the ultimate fate of substrates. How are the ATPase and substrate-binding activities of Hsp70 “decide” whether a substrate will be retained or degraded? This is one of the major questions in chaperone biology and a better understanding of this relationship could provide new therapeutic opportunities for tauopathies.

### **3.1.3 Inhibitors and activators of Hsp70 might provide new opportunities**

### **for understanding Hsp70's role in tau stability**

In contrast to the extensive work on chemical inhibitors of Hsp90 ATPase function [15,19,20], chemical modulators of Hsp70 have proven more elusive. As discussed in Chapter 2, the comparatively low intrinsic ATPase activity of Hsp70s (less than 0.2  $\mu\text{mole ATP}/\mu\text{mole}/\text{min}$ ) make low volume, high throughput screening methods challenging. In Chapter 2, we developed a sensitive, new screening assay that overcomes the weak ATPase activity of Hsp70 [21] and used this platform to identify several, first-generation inhibitors and activators. The activators included a series of dihydropyrimidines that stimulated ATP turnover. The inhibitors included myricetin, zafirlukast, and the phenothiazine, methylene blue (MB). In this Chapter, we wanted to use this suite of molecules to ask how perturbing the ATPase activity of Hsp70 would impact tau levels. In brief, we found that inhibiting Hsp70 led to rapid and dramatic degradation of tau, while stimulating Hsp70 led to tau accumulation. To further explore this relationship, we studied the mechanism of MB more closely. We found that MB oxidizes two cysteines in the stress inducible Hsp70 isoforms, leading to a loss of nucleotide-binding activity and degradation of tau in cells, brain slices and a mouse model of tauopathy. These studies substantially improve our understanding of the link between the biochemistry of Hsp70 and tau turnover. Moreover, these studies provide more clarity about how Hsp70 could be used as a drug target in tauopathy.

## 3.2 Results

### 3.2.1 Inhibiting Hsp70 leads to tau degradation, activating Hsp70 leads to tau accumulation

To explore the role of Hsp70 in tau turnover, we treated HeLa cells over-expressing human P301L tau with chemical activators and inhibitors identified in Chapter 2. The inhibitors MB and AC significantly reduced both total tau and phosphorylated tau (pTau), while treatment with the activators 115-7c or SW02 led to accumulation of these species (**Figure 3.1A**). Quantification of the blots showed that the inhibitors decreased total tau levels by up to 85% at 50  $\mu$ M (**Figure 3.1B**), while stimulating Hsp70 led to an increase of approximately 250-300% in total tau at 50 $\mu$ M (**Figure 3.1B**). The inhibitors led to dose-dependent tau degradation (**Figure 3.1C**) and the half-maximal concentrations (~ 10-15  $\mu$ M) matched well with the *in vitro* activity against Hsp70 (see Chapter 2). When inhibitors were combined and analyzed in aggregate, significant reductions in tau levels were observed in cells treated with 12.5  $\mu$ M or more of inhibitor (**Figure 3.1D**). This effect was reproducible and robust, with MB and AC (50  $\mu$ M) treatment reducing tau levels in six independent experiments (**Figure 3.1E**). These findings are significant because they suggest, for the first time, that inhibiting Hsp70, rather than stimulating this chaperone or increasing its levels, could be a therapeutic objective in clearing tau.

We next tested the response of two other disease-associated proteins to gauge the selectivity of these inhibitors for tau. We investigated  $\alpha$ -synuclein, which is

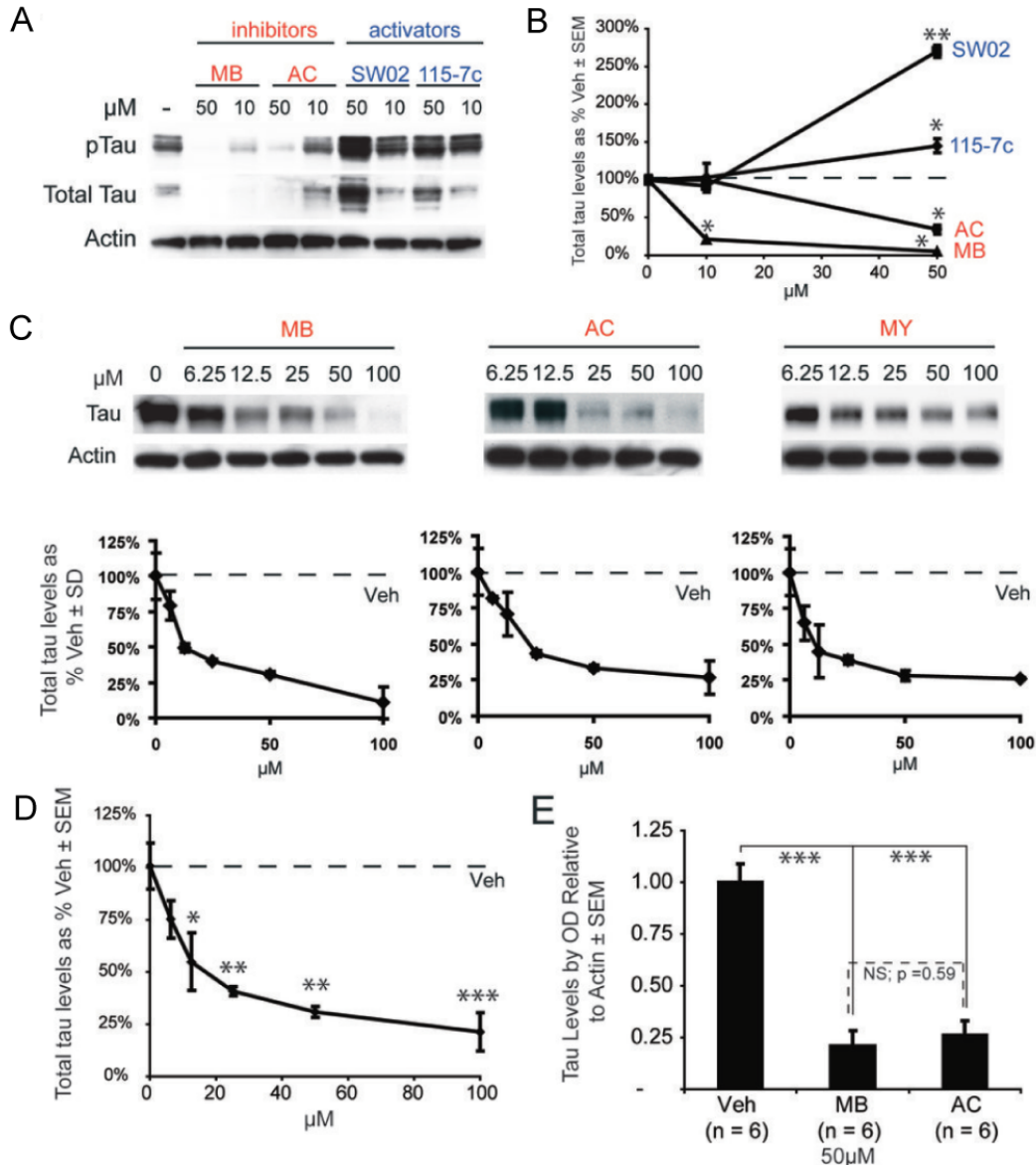


**Figure 3.1 Inhibitors of Hsp70 decrease tau levels, activators protect it.** (A) HeLa tau transfectants were treated for 24 hours with Hsp70 inhibitors (MB or AC) or activators (SW02 or 115-7c). (B) Quantification plots of the Western blots after actin normalization illustrate significant decreases in total tau levels at higher doses of MB ( $\blacklozenge$ ) or AC ( $\bullet$ ), while treatment with either 115-7c ( $\blacksquare$ ) or SW02 ( $\blacktriangle$ ) increased tau levels. Analysis was performed using replicate blots. \*\* indicates  $p < 0.01$  and \* indicates  $p < 0.05$ . (C) HeLa cells stably transfected with human 4R0N tau were treated with MB, AC or myricetin (MY) for 3 hours and harvested. Results are normalized to actin and compared to the vehicle (Veh). (D) Combining all three inhibitors for more complete statistical analysis of Hsp70 inhibition demonstrated that significant reductions in tau levels were achieved at 12.5  $\mu\text{M}$ , and significance increased with higher concentrations. \*\*\* indicates  $p < 0.001$ , \*\* indicates  $p < 0.01$  and \* indicates  $p < 0.05$ . (E) Statistical analyses using multiple experiments ( $n = 6$ ) across cell models demonstrates that MB and AC each significantly and consistently reduce tau levels at 50  $\mu\text{M}$ . Moreover, MB and AC were not significantly different from each other. \*\*\* indicates  $p < 0.001$ , \*\* indicates  $p < 0.01$  and \* indicates  $p < 0.05$ .

also an unstructured protein, but accumulates in Parkinson's disease, and we investigated TAR-DNA binding protein (TDP-43) that accumulates in a number of neurodegenerative diseases and has been identified as a cause for amyotrophic lateral sclerosis (ALS; [22-24]). We over-expressed both of these proteins in the HeLa cell line and treated with Hsp70 modifiers. Neither protein was sensitive to Hsp70 inhibitors (MB, AC or myricetin), Hsp70 activators (SW02 or 115-7c), or the Hsp90 inhibitor, 17-AAG (**Figure 3.2**). Although the underlying mechanisms are not yet clear and more work needs to be done to examine the integrity of the entire proteome, these findings suggested that tau is particularly sensitive to inhibition of Hsp70's ATPase activity. Recent work by our collaborator, the Dickey laboratory, has suggested that the survival kinase Akt is also sensitive to these treatments [25].

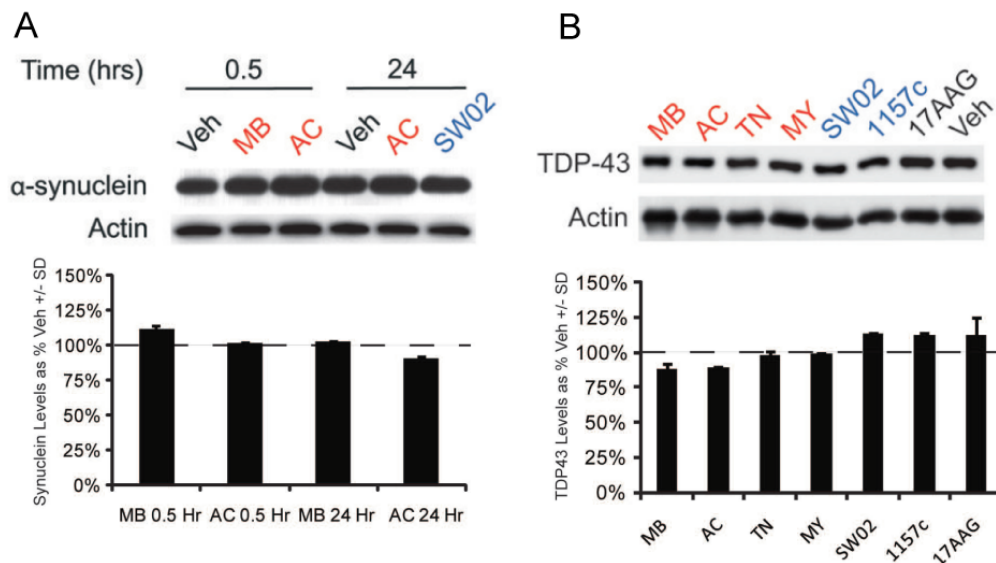


**Figure 3.2 Hsp70 modulators do not alter the levels of  $\alpha$ -synuclein and TDP-43.** (Top) HeLa cells were transfected with either  $\alpha$ -synuclein (A) or TDP-43 (B) and treated with indicated drugs (inhibitors in red, activators in blue, Hsp90 inhibitor (17AAG) and vehicle in black) for 30 minutes ( $\alpha$ -synuclein) or 24 hours (both  $\alpha$ -synuclein and TDP43). Levels of either protein were unaffected by any treatment under these conditions. (Bottom) Representative blots were quantified and expressed as % vehicle. There was no significant difference in the levels of these protein upon treatment with Hsp70 modulators.

### 3.2.2 AC causes proteasomal degradation of tau

As discussed in Chapter 1, we expected that tau stability might be linked to changes in Hsp70's nucleotide state and subsequent changes in tau binding affinity. Consistent with this idea, addition of a non-hydrolyzable nucleotide analog, ATP- $\gamma$ S, reduced affinity of Hsp70 for tau in a co-precipitation assay (**Figure 3.3A**). Moreover, co-immunoprecipitation from cells treated with Veh or AC +/- the proteasomal inhibitor, epoxomicin, showed that fewer Hsp70/tau

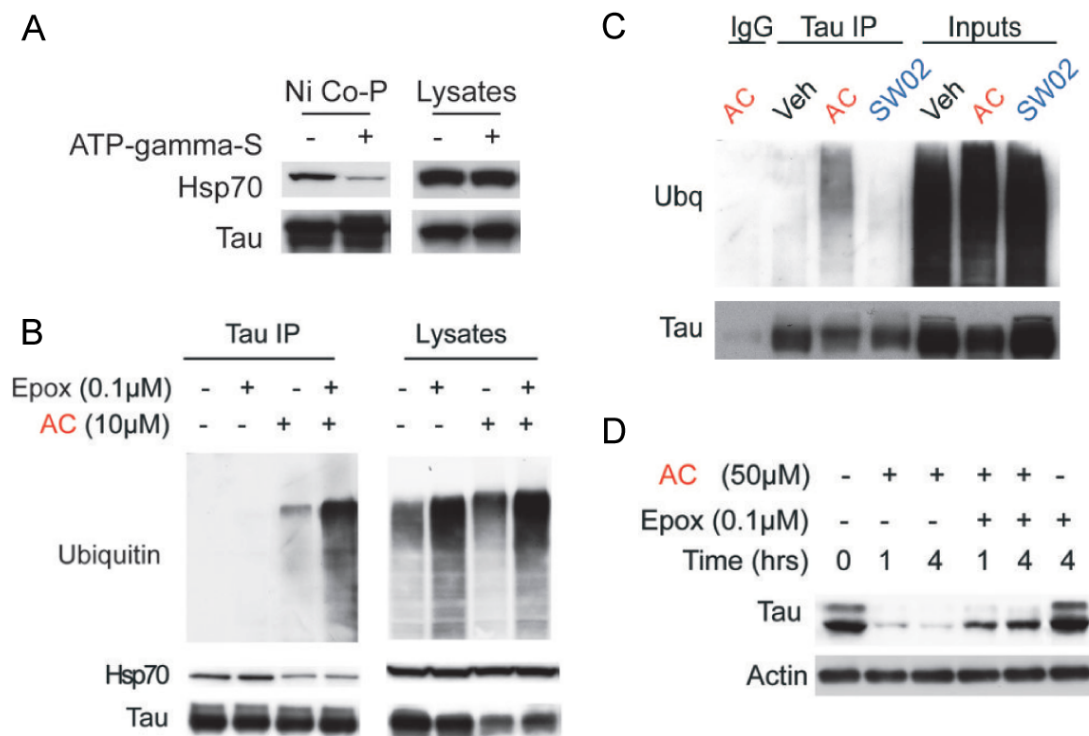


**Figure 3.3 Nucleotide state of Hsp70 regulates tau binding and inhibitor-mediated reductions in tau occur via proteasomal degradation.** (A) Lysates from cells over-expressing Hsp70 were supplemented with His-tagged tau and incubated with or without ATP-gamma-S for 30 minutes. Co-precipitation with Ni-Agarose beads (Ni Co-P) shows reduced binding of tau to Hsp70 in the presence of the non-hydrolyzable ATP analogue. (B) Ubiquitination of tau is evident in immunoprecipitates from HEK tau transfectants following treatment with AC (10 μM). Epoxomicin (Epox, 100nM) treatment for 6 hours further increased the amount of ubiquitinated tau. Hsp70 binding to tau was also reduced by AC treatment, irrespective of epoxomicin treatment. (C) Ubiquitination of tau is evident in immunoprecipitates from HEK tau transfectants following treatment with AC (10 μM), SW02 (10 μM) or vehicle (Veh) for 1hr. General IgG immunoprecipitation controlled for non-specific tau binding. (D) Tau levels 1 and 4 hours after epoxomicin (Epox; 100 nM) and AC (50 μM) treatment of HeLa tau transfectants. Actin was used to control for loading in all panels.



complexes were present following AC treatment; however ubiquitination of tau was increased (**Figures 3.3B & C**). This result suggests that AC reduces the affinity for tau and leads to its degradation. We also found that epoxomicin abrogated AC-mediated tau reductions (**Figure 3.3D**), suggesting that the loss of tau was mediated by the proteasome pathway. However, an alternative model is that tau is sequestered into insoluble or aggregated structures in response to these treatments [26]. To test this, traditional sarkosyl and SDS extractions of cell lysates treated with these compounds were performed, but no changes in insoluble tau were observed (**Figure 3.4**). Thus, while other routes of cellular clearance may contribute to tau reductions following Hsp70 inhibition, conversion into an insoluble material is not facilitated. Recently, more detail into this mechanism was provided by studies from the Duff group, in which they show that MB reduces tau levels, in part, through the autophagic pathway [27]. Together, these studies suggest that inhibition of Hsp70 leads to dual degradation of tau through the ubiquitin-proteasome system (UPS) and the macroautophagy pathway.

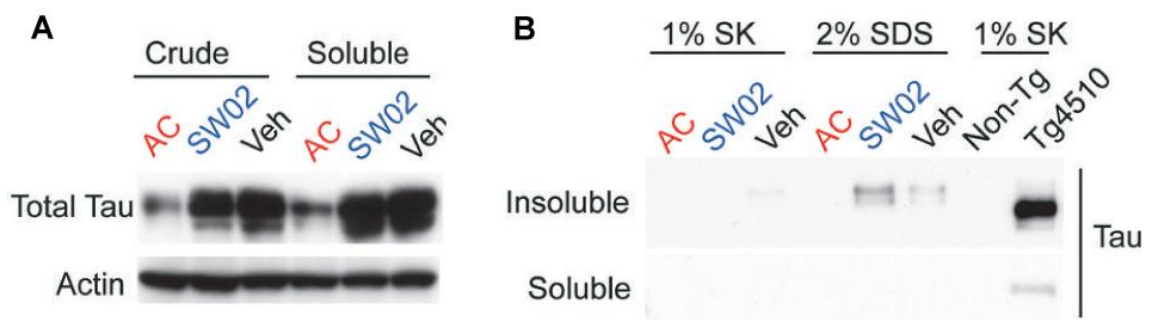


**Figure 3.4 Hsp70 modulators do not change the level of tau aggregation.** (A) Equivalent tau levels are observed in both crude and Tris-saline soluble preparations of HeLa tau transfectant lysates treated with AC (50  $\mu$ M) or SW02 (50  $\mu$ M) for 1 hour. (B) Absence of tau from soluble or insoluble fractions of sarkosyl (SK) or SDS extracts prepared from insoluble pellets. Tg4510 brain sarkosyl extract is shown as a procedural control.

### 3.2.3 Hsp70 inhibition does not cause stress response.

Genetic evidence has previously suggested that increasing the expression of Hsp70 also leads to CHIP-mediated ubiquitination and degradation of tau [10]. However, it has also been shown that Hsp70 over-expression restores tau's association with the microtubules and preserves tau levels [14]. Thus, to explore whether changes in tau levels in response to Hsp70 inhibitors are a result of

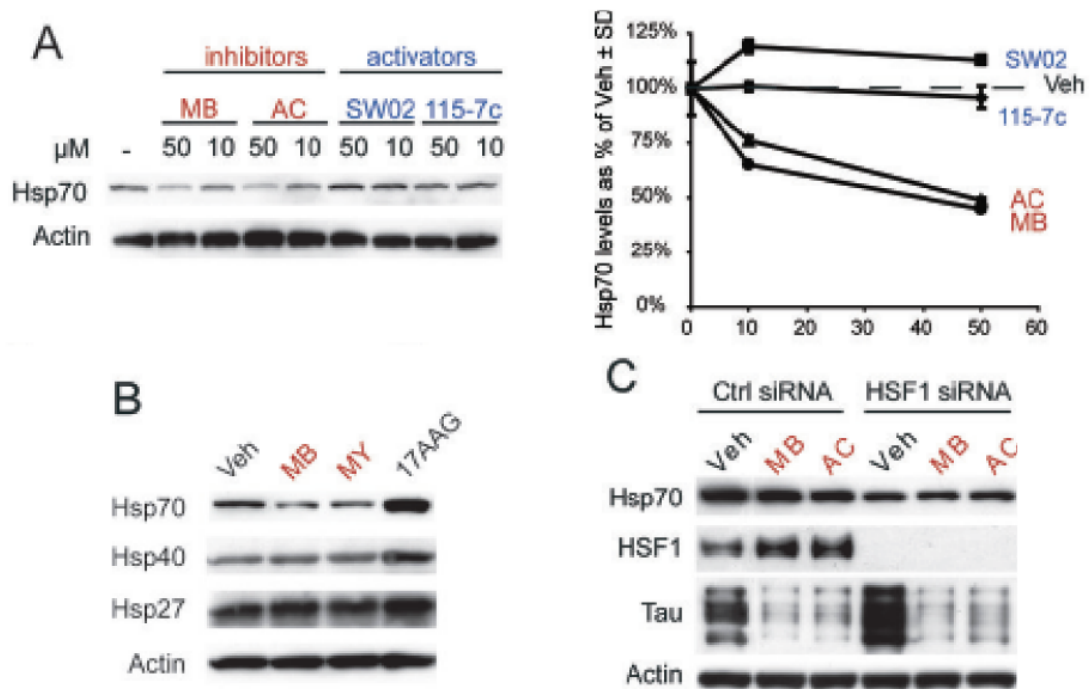


**Figure 3.5 Reductions in tau are independent of a stress response or an increase in Hsp70 expression.** (A) HeLa tau transfectants were treated for 24 hours with Hsp70 inhibitors (MB or AC) or activators (SW02 or 115-7c) and Hsp70 levels were measured by Western blot. Quantification plots of the Western blots after actin normalization illustrate decreases in Hsp70 levels after treatment with MB (◆) or AC (●), while treatment with either 115-7c (■) or SW02 (▲) had no effect. Standard deviation was derived from replicate experiments. (B) Cells were treated with MB (10μM), MY (10μM) or 17AAG (1μM) for 24 hours. Levels of Hsp70, Hsp40 and Hsp27 are shown from these lysates. (C) HeLa cells were transiently transfected with human wildtype tau and a non-silencing (Ctrl) or HSF1 siRNA. These cells were then treated with MB or AC (50 μM) for 1 hour. Reductions in tau were similar in the presence of either siRNA. (D) Statistical analyses across experiments (n = 4) showed a trend (p=0.108) for Hsp70 reduction following Hsp70 inhibition.

changes in absolute Hsp70 levels, we measured chaperone induction in response to inhibitors and activators. Using Western blots against the stress-inducible Hsp70, we found that pharmacological manipulation did not increase expression levels (**Figure 3.5A**). In fact, unlike cells treated with the Hsp90 inhibitor, 17-AAG, Hsp70 levels were actually slightly decreased or unchanged following MB and MY treatment after 24 hours, while expression of other heat shock proteins were unchanged relative to control (**Figure 3.5B**). Moreover, knockdown of HSF1 by siRNA did not abrogate the activity of MB or AC (**Figure 3.5C**). Together, these results suggest that targeting the ATPase activity of Hsp70 controls tau accumulation independent of a global stress response. This is an important finding because it suggests that the compound's effects on tau are independent of any change in Hsp70 levels.

#### **3.2.4 Overexpression of Hsp70 enhances the efficacy of Hsp70 inhibitors, suggesting that Hsp70 is a major molecular target in cells**

Both MB and MY are known to have many other potential targets and neither of these compounds are considered selective for Hsp70. However, we wondered whether their specific effects on tau stability might be directly linked to Hsp70 inhibition. To test this idea, cells were transiently transfected with myc-tagged Hsp70 and tau reductions by AC and MB were quantified (**Figure 3.6**). We found that increasing the levels of Hsp70 dramatically enhance the effectiveness of both AC and MB (tau levels were reduced 50% by only 12.5  $\mu$ M inhibitor). Interestingly, myc-Hsp70 over-expression alone only minimally affected tau

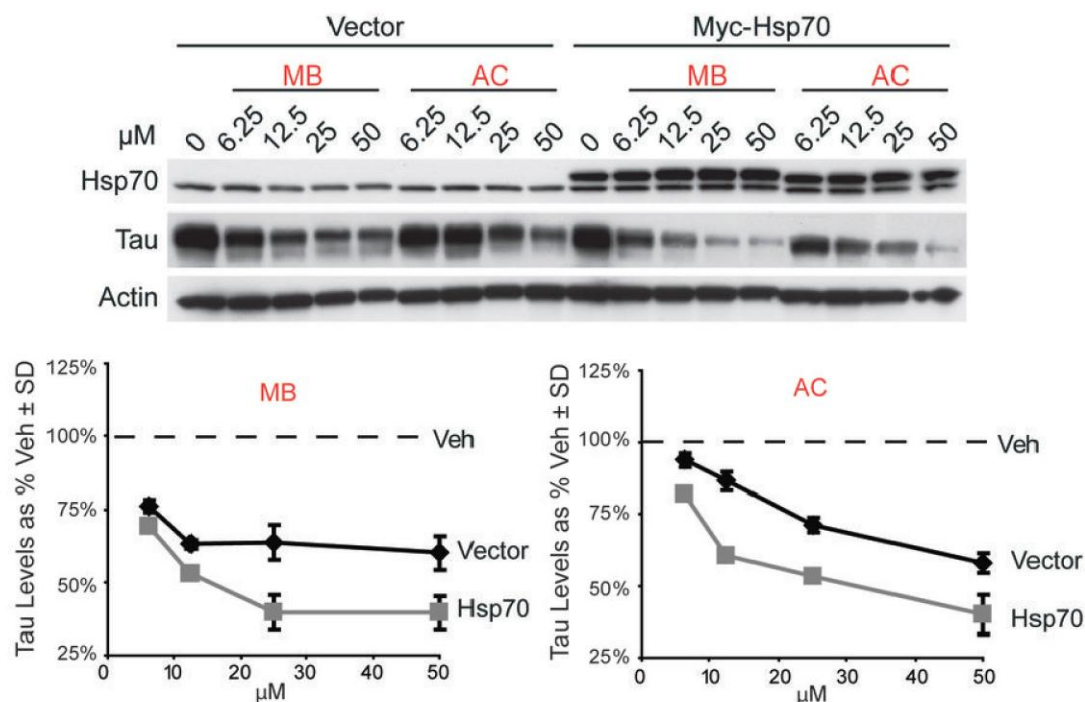


**Figure 3.6 Increasing Hsp70 levels enhances Hsp70 inhibitor efficacy.** HeLa tau transfectants were co-transfected with vector or myc-tagged Hsp70 and cells were treated with the indicated dose of MB or AC for 1hr. Consistent with a critical role for Hsp70, its over-expression dramatically improved the efficacy of MB and AC. Note that over-expression of Hsp70 alone had only mild effects on tau levels in the absence of inhibitors. Results are shown as a percent of vehicle control after actin normalization compiled from replicate experiments.

levels (**Figure 3.6**). When analyzed in aggregate, Hsp70 inhibitors at concentrations  $\geq 12.5 \mu\text{M}$  were significantly more effective at clearing tau when Hsp70 was over-expressed (**Figure 3.7A**). These findings suggest that the pool of Hsp70 is limiting for tau degradation in this specific model. Moreover, these studies suggest cells that express high levels of Hsp70, such as stressed cells, might be more sensitive to pharmacologic targeting of Hsp70. To explicitly investigate this possibility, we treated cells with celastrol, a compound that has previously been reported to robustly induce expression levels of Hsp70 [28]. HeLa cells treated for 24 hours with celasterol upregulated their Hsp70 approximately 2- to 3-fold and these cells became sensitive to normally sub-effective doses of MB (**Figure 3.7B**; 1  $\mu\text{M}$  reduced tau levels 25%). Thus, by

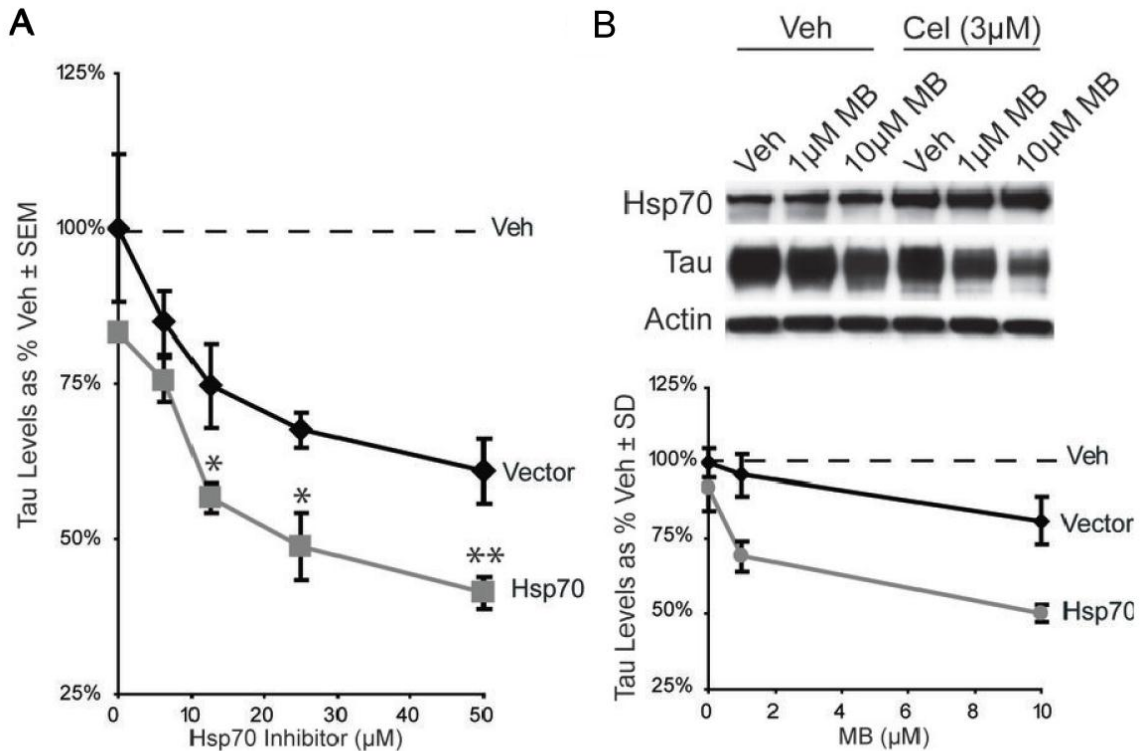


**Figure 3.7 Celastrol enhances Hsp70 inhibitor efficacy.** (A) Quantitation of both AC and MB from experiments in panel A shows over-expression of Hsp70 significantly increased Hsp70 inhibitor efficacy. Hsp70 over-expression alone did not significantly reduce tau levels. \*\* indicates  $p < 0.01$  and \* indicates  $p < 0.05$ . (C) HeLa tau transfectants were treated with  $3\mu\text{M}$  of celastrol for 24 hours and then treated with indicated concentration of MB for 1 hour. Western analysis and quantitation shows that celastrol alone has minor effects on tau levels whereas celastrol plus MB has much more potent effects than MB alone. Tau levels are represented as a % of actin by densitometry.

transiently increasing Hsp70 levels, we appeared to have produced more Hsp70/tau complexes that become sensitive to changes in nucleotide turnover.

### 3.2.5 Hsp70 inhibitors cause rapid reduction of tau levels

We hypothesized that Hsp70-tau complexes might respond to inhibitors by quickly “switching” to a degradation complex, without a requirement for new protein synthesis or other delays [29-31]. Indeed, we found that the rate of tau reduction in a stably transfected cell line was extremely fast, showing reductions within 5 minutes of treatment with MB or AC, consistent with acute enzymatic



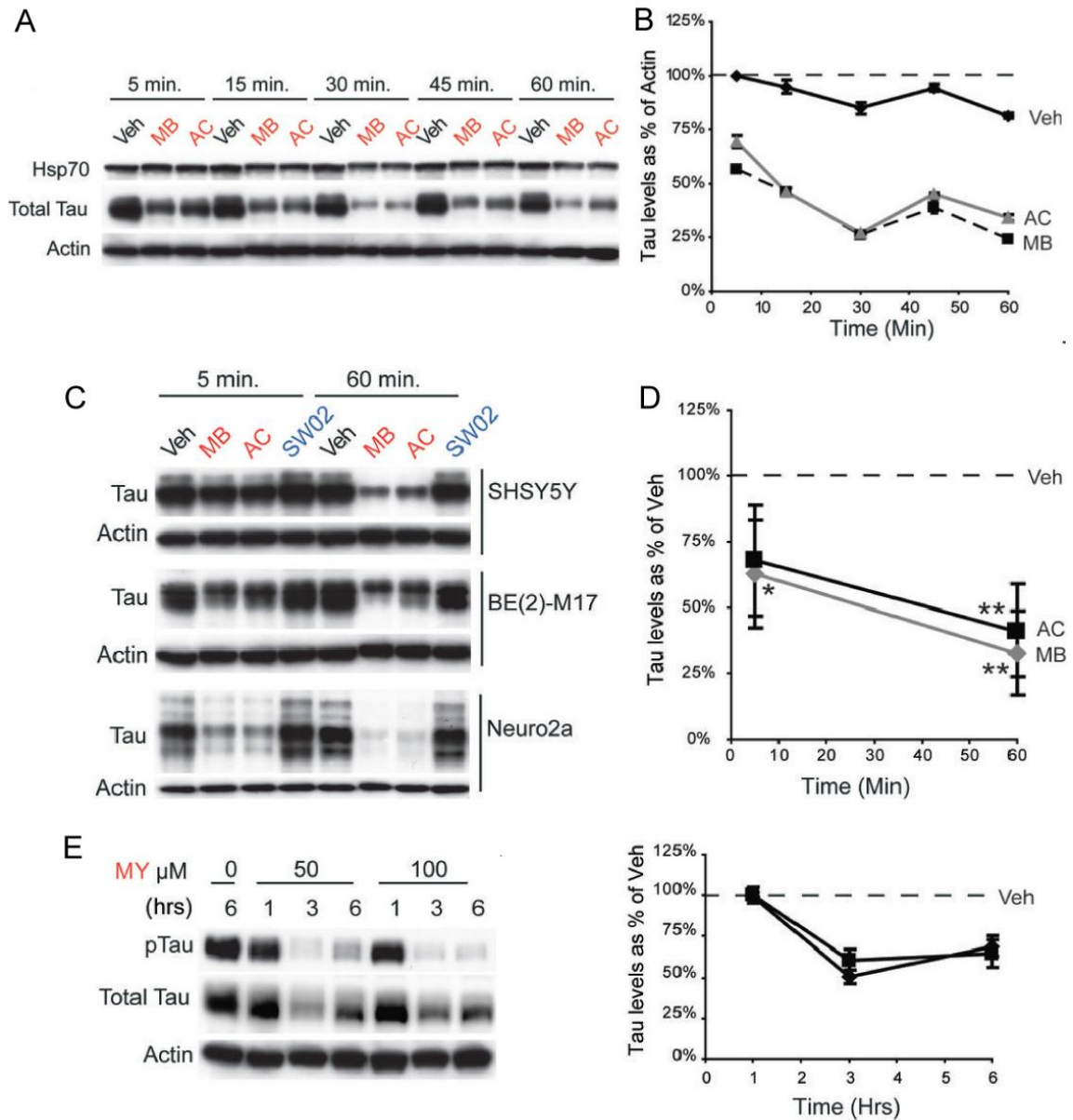


**Figure 3.8 Tau is rapidly degraded in response to Hsp70 inhibitors.** (A) Evaluation of the effects of MB and AC over 1 hour in stable tau HeLa transfectants shows rapid tau turnover in response to MB or AC. (B) Densitometric quantitation of Western data is shown as a percentage of actin levels. Greater than 50% reductions in tau levels were observed within 15 minutes and this was maintained for the hour. (C) Endogenous tau and Hsp70 levels were rapidly reduced by Hsp70 inhibitors (50  $\mu$ M) in human (SHSY5Y and BE(2)-M17) and mouse (Neuro2a) neuroblastoma cells. Similar to the results from the stably transfected HeLa cells, treatment with the activator, SW02, increased tau levels. (D) Statistical analyses across all cell lines shown reveals significant decreases in tau levels after 1 hour treatment with Hsp70 MB (gray) and AC (black). While decreases were seen within 5 minutes, significance was only achieved with MB. \*\* indicates  $p < 0.01$  and \* indicates  $p < 0.05$ . (E) Both total tau and pTau levels are rapidly reduced by myricetin (MY; 50 or 100  $\mu$ M).

inhibition and a switch in the Hsp70-directed fate of tau (**Figures 3.8A-B**). This

decline continued and the process reached a new equilibrium at approximately 60 minutes (**Figures 3.8A-B**). To test whether this rapid and dramatic loss of tau was dependent on tau over-expression, we measured endogenous tau levels in both human (BE(2)-M17 and SHSY5Y) and murine (Neuro2a) neuroblastoma cell lines (**Figure 3.8C**). In all these systems, significant decreases in tau levels were observed after 60 minutes (**Figure 3.8D**). Moreover, the flavonoid, myricetin (MY), also rapidly reduced tau levels, with reductions evident as early as 1 hour (**Figure 3.8E**). Interestingly, tau levels began to rebound after 6 hours, likely because of metabolism of the flavonoid [32]. These data suggest a model in which the inhibitors directly inhibit Hsp70 activity, leading to rapid degradation of tau through the UPS and autophagy pathways. Because of microtubule dynamics, tau might be continuously cycling between cytoskeletal and cytoplasmic compartments, providing a self-replenishing pool of Hsp70-bound tau in the cytoplasm that is sensitive to these inhibitors.

### **3.2.6 Hsp70 inhibitors reduce the level of tau mutants that are resistant to Hsp90 inhibitors**

Because tau dysfunction in AD is believed to be related to hyper-phosphorylation (as discussed in Chapter 1), we investigated whether over-expression of two kinases that are known to promote tau hyperphosphorylation at distinct residues could affect the efficacy of Hsp70 inhibitors. HeLa cells stably over-expressing human wildtype tau were transfected with either glycogen synthase kinase 3 $\beta$  (GSK3 $\beta$ ) or microtubule affinity regulating kinase 2 (MARK2/Par1) for 24 hours.

These cells were then treated with MB, AC or SW02 for 1 hour and harvested. Tau phosphorylated at S396/S404 was significantly reduced with the inhibitors, regardless of which kinase was over-expressed (**Figure 3.9A**). Interestingly, in cells over-expressing MARK2/Par1, tau phosphorylated at S262/S356 was not affected by the inhibitors, consistent with previous data suggesting that this phospho-tau species is chaperone resistant [11,20] (**Figure 3.9A**). Total tau levels were also reduced in all cases. SW02 did not increase tau levels following the short 1 hour incubation. Next, using three tau mutants that are known to cause fronto-temporal dementia with Parkinsonism linked to chromosome 17 (FTDP-17) or progressive supranuclear palsy (PSP), we investigated whether Hsp70 inhibition could facilitate their clearance similar to wildtype tau, also drawing a comparison with Hsp90 inhibition. The tau mutants P301L, V337M and R406W were all significantly reduced following inhibitor treatment, similar to wildtype levels (**Figure 3.9B**). Treating cells with the Hsp90 inhibitor, 17-AAG, caused similar reductions in wt and P301L tau after 24 hours; however V337M and R406W tau were less efficiently cleared (**Figure 3.9B**). When all 4 tau variants were analyzed in aggregate, only Hsp70 inhibition significantly reduced tau levels (**Figure 3.9B**). These findings confirm a difference in the mode-of-action of Hsp90 and Hsp70 inhibitors and they suggest that some tau mutants might be handled by distinct components of the chaperone system. More work is needed to understand which of these interactions is direct and how the Hsp70-Hsp90 system might select specific tau isoforms.



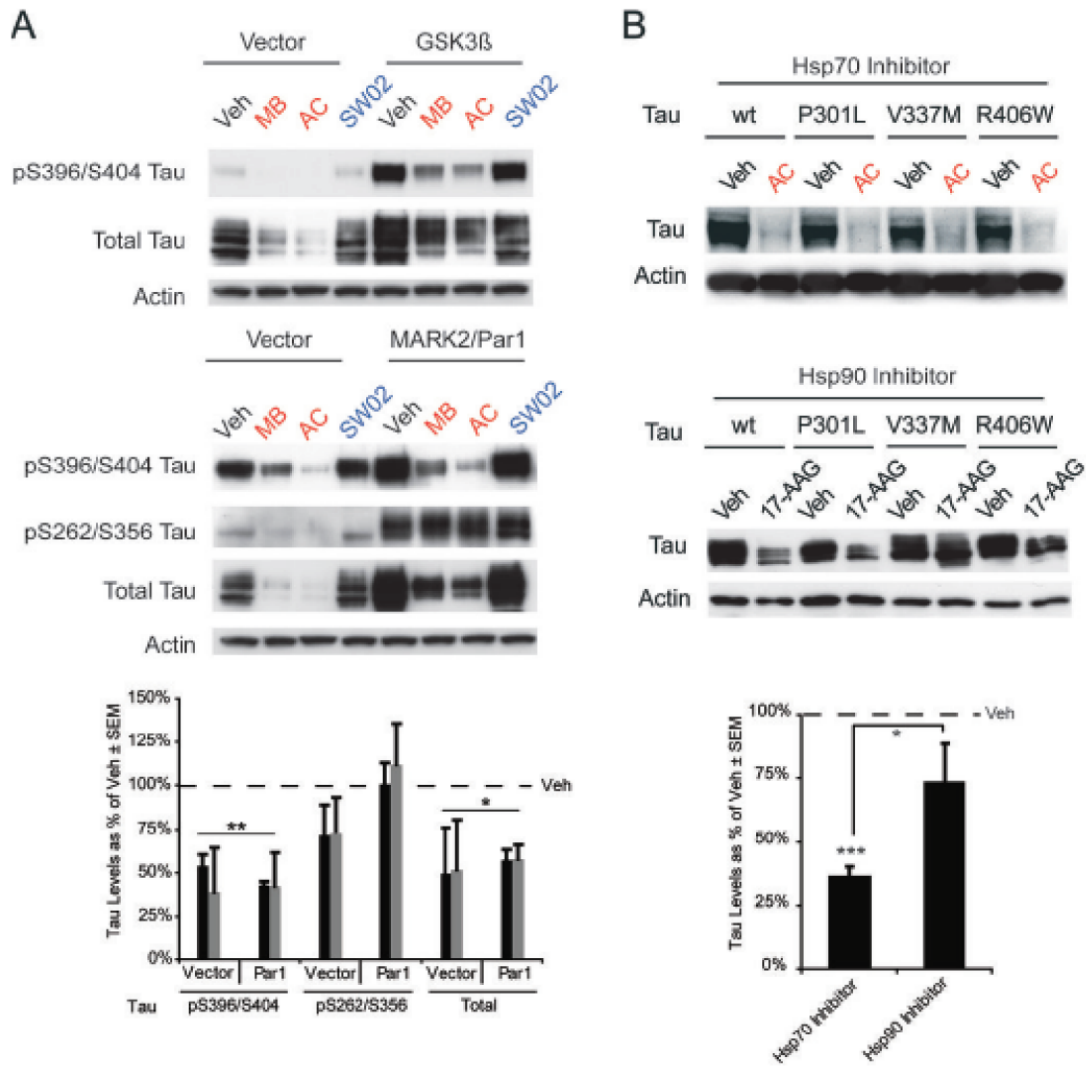


**Figure 3.9 Phospho- and mutant tau species are differentially affected by Hsp70 inhibition.** (A) Levels of indicated tau species with or without over-expression of GSK3β or MARK2/Par1 in HeLa tau transfectants treated with vehicle (Veh), MB, AC or SW02 for 1 hour. Densitometric quantitation from replicate experiments showed that tau phosphorylated at S262/S356 was resistant to Hsp70 inhibition (MB; black bars & AC; gray bars). Values are presented as tau levels as a % of vehicle treated cells ± SEM. \*\* indicates p<0.01 and \* indicates p<0.05 by student t-test. (B) The effects of Hsp70 and Hsp90 inhibitors on tau mutants suggest that at least two chaperone pathways regulate tau processing. Treatment of transfected HeLa cells with saturating amounts of the Hsp90 inhibitor, 17-AAG, caused mild reduction in the V337M and R406W mutants; whereas AC (50 μM) was able to reduce all the clinically-relevant mutants by over 90%. Statistical analysis comparing efficacy of either Hsp70 or Hsp90 inhibition against all four tau species revealed that Hsp70 inhibition significantly reduced tau levels in aggregate whereas Hsp90 inhibition did not (p = 0.243). Moreover, tau levels following Hsp70 inhibition were significantly reduced compared directly to tau levels following Hsp90 inhibition. Values are presented as tau levels as a % of vehicle treated cells ± SEM. \*\*\*indicates p<0.001 and \* indicates p<0.05 by Student t-test.

### 3.2.7 Hsp70 inhibitors reduce tau levels in a mouse model of AD

Fortunately, some of the Hsp70 inhibitors (MB and AC) we identified have well-characterized pharmacological characteristics (e.g. stability, lifetime), which we reasoned could facilitate their use in disease models. To take advantage of this property and further explore the potential of Hsp70 as a therapeutic target, we

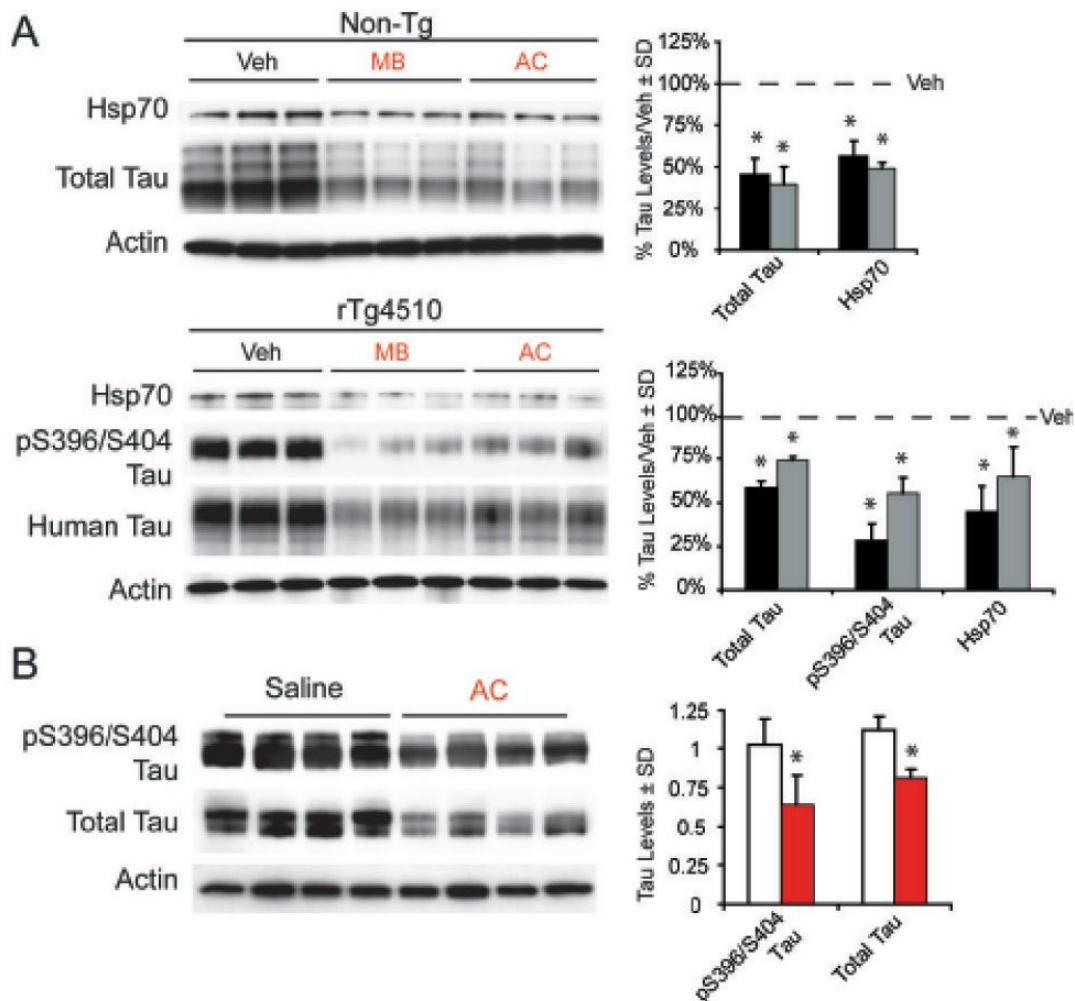


**Figure 3.10 Hsp70 inhibition reduces endogenous and over-expressed tau levels in multiple neuronal models.** (A) Levels of tau and Hsp70 are shown in cortical murine brain slices from rTg4510 mice (n = 3 slices) and wildtype littermates (n = 3 slices) that were treated with inhibitors (10  $\mu$ M) or vehicle for 3 hours. Black bars indicate AC and gray bars indicate MB as a % of vehicle treated tissue following actin normalization. (B) Eight 4 month-old rTg4510 mice injected with 2  $\mu$ l of 10 mM AC or vehicle were harvested 24 hours later. Tau levels were significantly reduced in AC-treated mice (red bars) relative to vehicle-treated mice (white bars). \* indicates  $p < 0.05$  by Student T-Test. Actin was used to control for loading in all panels.

investigated the impact of MB and AC on tau levels in organotypic brain slices from mice engineered to express mutant human tau (rTg4510) and age-matched wild type littermates. In both tissue types, tau levels were significantly reduced following three hours of treatment with either MB or AC (50 $\mu$ M; **Figure 3.10A**). Dramatic reductions in one pTau isoform linked to Alzheimer's disease, pS396/S404, were also evident in the rTg4510 model. Thus, non-dividing neurons also realized rapid reductions in tau following Hsp70 inhibition. We then directly injected AC (2  $\mu$ L of 10 mM) or saline into the hippocampi of eight 4 month-old rTg4510 mice and harvested these animals 24 hours after surgery. Remarkably, these studies revealed that AC significantly and uniformly reduced soluble tau and pS396/S404 tau levels in the hippocampus (**Figure 3.10B**). More recently, other members of the Gestwicki laboratory, in collaboration with the Dickey group (U. South Florida) found that oral delivery of MB to Tg4510 mice leads to excellent CNS exposure and ~30% reductions in soluble tau levels in the brain. Interestingly, these animals also had significantly improved performance in tests of cognitive learning and memory [33]. Together, these studies show that inhibitors of Hsp70 potently stimulate clearance of both normal and abnormal tau in brain tissue.

### **3.2.8 MB and H<sub>2</sub>O<sub>2</sub> irreversibly inhibit Hsp72 but not Hsc70**

MB has been used for the treatment of various human diseases and has a proven record of safety [34]. Thus, MB might be an especially attractive lead for drug discovery in tauopathies. For these reasons, we decided to further explore

the mechanism by which it inactivates Hsp70. Because MB has been known to directly oxidize sulfhydryls [35], we hypothesized that inhibition of Hsp70's ATPase activity by MB (see Chapter 2) may involve oxidation of cysteines. To test this idea, we treated Hsp72 with MB (200  $\mu\text{M}$ ) at 37  $^{\circ}\text{C}$  for 1 hour and then removed any remaining compound by extensive dialysis. We measured the remaining ATPase activity in the MB-treated Hsp72 using a malachite green assay [21]. Because Hsp72 is a weak ATPase, we added the stimulatory co-chaperone, DnaJ, to enhance nucleotide turnover in these experiments. Using

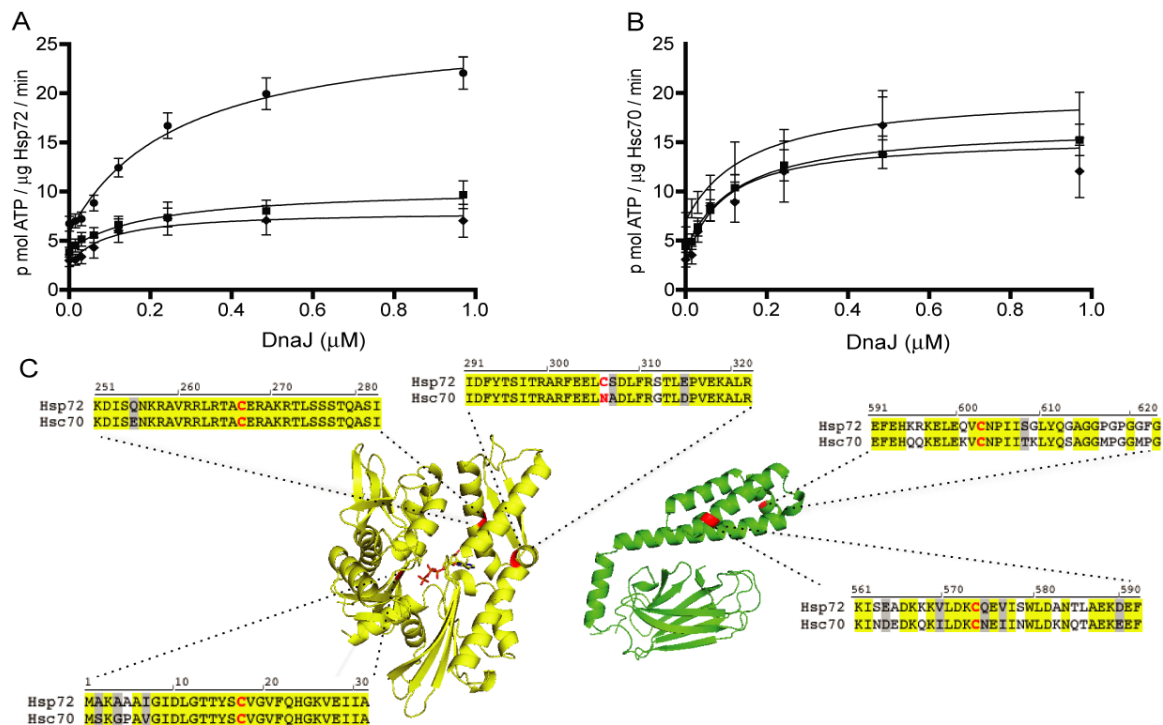


**Figure 3.11 The ATPase activity of Hsp72, but not Hsc70, is sensitive to oxidation.** (A) Purified Hsp72 (0.6  $\mu\text{M}$ ) was incubated with either MB, peroxide ( $\text{H}_2\text{O}_2$ ) or a mock control and the remaining compound removed by extensive dialysis. The stimulation of ATPase activity by the model J co-chaperone, DnaJ, was then measured. Results are the average of three experiments performed in triplicate. Error bars are standard error of the mean (SEM). (B) Human Hsc70 is resistant to oxidation. Experiments were performed as described for panel A. (C) The locations of cysteine residues (red) in Hsp72 are shown using the crystal structures of the NBD (pdb # 3JXU) and the SBD (pdb # 1DKX). In the insets, identical residues are shown in yellow, conserved residues in gray and the positions of cysteines are red. Alignments were prepared in Vector NTI (Invitrogen).

this approach, we found that MB-treated Hsp72 had dramatically reduced ATPase activity even after MB had been removed (**Figure 3.11A**). As an initial test of whether this reduced activity was related to oxidation, we treated Hsp72 with hydrogen peroxide (100  $\mu$ M) under similar conditions and found that Hsp72 was also inhibited by this treatment (**Figure 3.11A**). Cysteine residues in proteins can be progressively oxidized to sulfenic, sulfinic and then sulfonic acids [36]. Sulfenic acids, but not the other forms, are known to be readily reversible by glutathione and DTT [37]. We found that the ATPase activity of MB-treated Hsp72 was not fully recovered after exposure to DTT (1 mM) (**Appendix 3.5.1**). Thus, these results suggested that redox active compounds, such as MB, inactivate the ATPase activity of Hsp72 by irreversibly oxidizing the protein.

Initially as a control, we then tested the effects of MB on the ATPase activity of Hsc70. Unexpectedly, we found that MB had no effect on Hsc70 (**Figure 3.11B**). This result prompted us to more closely examine the chemical differences between these two well-conserved (85% identical and 94% similar) Hsp70 isoforms. Sequence alignments of the human proteins showed that Hsp72 has five cysteine residues (three in the NBD and two in the SBD) whereas Hsc70 has only four (two each in the NBD and SBD). Thus, one difference between these isoforms is that Hsp72 has a unique Cys306, which is an asparagine in Hsc70 (**Figure 3.11C**). To probe whether this sequence difference may be important, we examined the other human stress-inducible and constitutive Hsp70 isoforms. This sequence analysis revealed that Cys306 is exclusively found in stress

inducible cytosolic Hsp70 isoforms but not in constitutively expressed family members (**Appendix 3.5.2A**). Together, these results suggest that MB may oxidize at least one cysteine in Hsp72, but not Hsc70, which might selectively compromise ATPase activity.

### 3.2.9 MB oxidizes Cys306 of Hsp72

To map which cysteines in Hsp72 were oxidized by MB, we employed a well-established mass spectrometry (MS) method using dimedone (5,5-dimethyl-1,3-cyclohexanedione). Briefly, dimedone is known to react with oxidized cysteines to form stable thioethers that are readily observed in the MS spectra (**Figure 3.12A**). Accordingly, MB-treated Hsp72 was treated with dimedone and, after capping unreacted thiols with carbamidomethyl groups, we performed trypsin digestions and analyzed the resulting samples by LC-tandem MS/MS. These

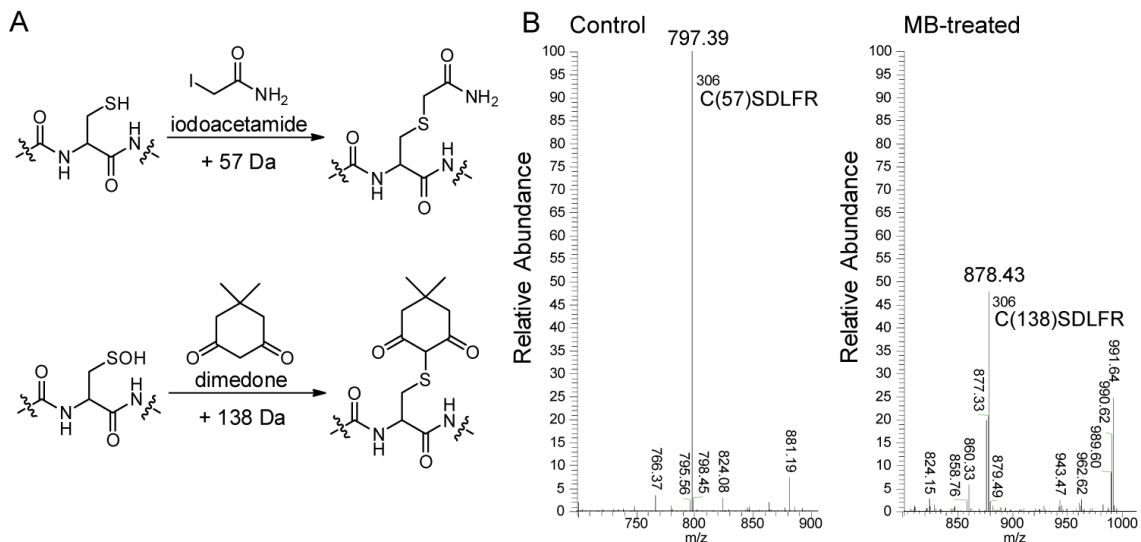


**Figure 3.12 Hsp72 is oxidized by MB at specific cysteine residues.** (A) Schematic of the specific reactions of iodoacetamide with free thiol and dimedone with sulfenic acid, producing a mass shift of +57 or +138 Da, respectively. (B) Select region of the MS/MS spectra focused on the region including the C306 fragment (CSD LFR 306-311). This fragment is 797.39 Da in the mock treated control (indicating iodoacetamide capping) and 878.43 Da in the MB treated (indicating dimedone conjugation).

experiments revealed that the mass of the fragment containing Cys306 in Hsp72 was increased by 138 Da, corresponding to the addition of a dimedone (**Figure 3.12B**). None of the other cysteines or other residues were modified, although it is important to note that the fragment containing Cys267 was not detected (likely because the nearby region is highly charged). Next, we treated Hsc70 with MB and, as expected from the ATPase experiments, found that it was resistant to dimedone (**Appendix 3.5.2B**). Thus, Hsp72 differs from Hsc70 in reactivity of its cysteines at positions 306 and perhaps 267.

### **3.2.10 Hsp72 Cys to Ser mutations confer resistance to MB**

The mass spectrometry studies suggested that MB-based oxidation of specific cysteines might be responsible for the compound's effects on Hsp72's ATPase activity. To test this idea, we mutated Cys306, Cys267 or both residues to serine by site-directed mutagenesis and purified the resulting mutant proteins. None of these substitutions had a significant effect on the global structure (**Appendix 3.5.3**) or ATPase activity of the chaperones (**Figures 3.13A-C**). Next we treated with MB and found that the ATPase activities of C267S (**Figure 3.13A**) and C306S (**Figure 3.13B**) were partially resistant to compound, while the double mutant (C267/306S) was completely immune (**Figure 3.13C**). Thus, MB appeared to exert its inhibitory effect on Hsp72 ATPase activity via oxidation of these cysteines and both residues appeared to be involved.

As discussed above, MB reduces tau levels in HeLa cells in a process that is



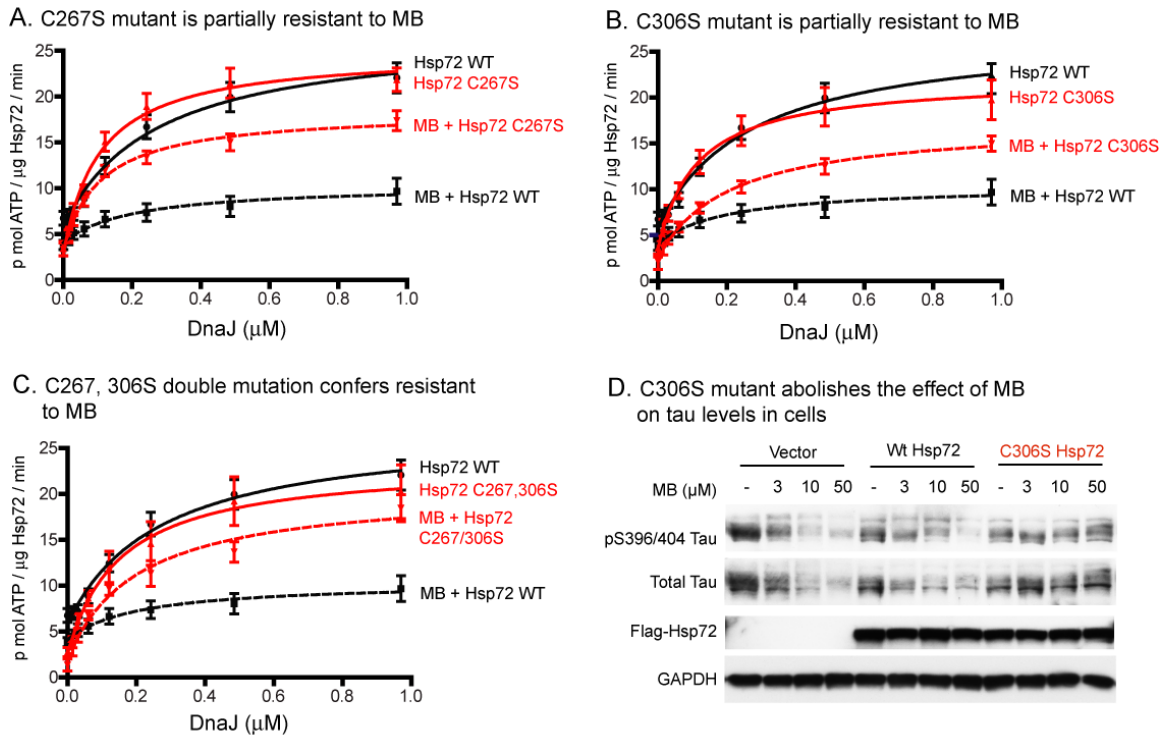


**Figure 3.13 Serine mutants of Hsp72 are resistant to MB treatment in ATPase and cell-based assays.** (A) C267S mutation confers partial resistance to MB (50  $\mu\text{M}$ ). (B) C306S confers partial resistance to MB (50  $\mu\text{M}$ ). (C) C267, 306S double mutation confers resistance to MB (50  $\mu\text{M}$ ). All of the ATPase experiments were performed at least twice in triplicate and error bars are SEM. (D) Over-expression of the C306S mutation blocks MB-mediated clearance of tau. HeLa C3 cells were transfected with vector, Flag-tagged WT Hsp72 or C306S Hsp72 mutant for 48 hours and then treated with MB for 10 minutes. Samples were analyzed by western blot and the results are representative of experiments performed in duplicate.

dependent on Hsp72 [38]. Thus, we hypothesized that over-expression of the C306S, C267S and C267/306S mutants may de-sensitize cells to MB. In fact, when HeLaC3 cells were stably transfected with Hsp72 C306S, we found that MB no longer reduced the levels of phosphorylated (pS396/404) or total tau (**Figure 3.13D**). Together, these results strongly suggest that MB acts on Hsp72 by oxidizing Cys267 and Cys306, and that this activity is important in regulating the levels of Hsp72 substrates, such as tau.

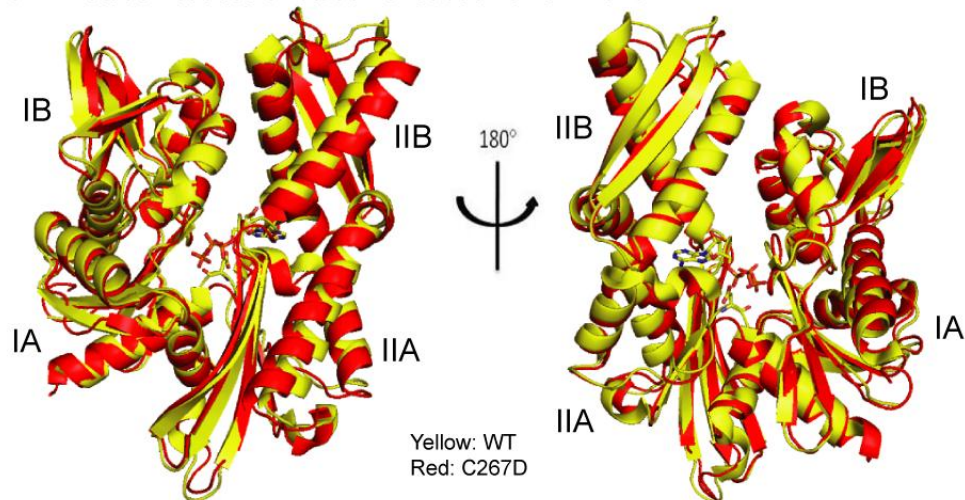
### 3.2.11 C267D mutation causes a conformational change and disrupts



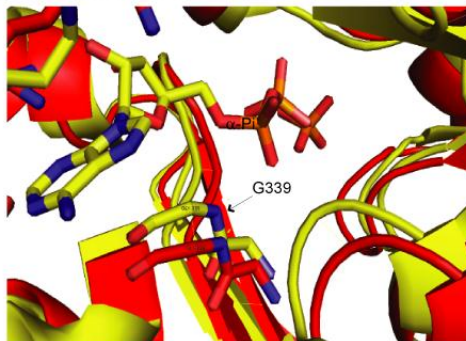
## nucleotide binding

We next wanted to understand the structural basis for the sensitivity of Hsp72 to redox stress. Accordingly, we modeled the NBD of Hsp72 containing a C267D mutation using Robetta [39], based on the structure of human Hsp72 NBD in the ADP form (3JXU) [40]. We used an aspartic acid substitution because it is considered to sterically and electronically mimic oxidized cysteines [41]. A comparison of the structures of the wild type Hsp72 NBD and the C267D Hsp72

A. C267D mutation causes a rotation of subdomains IIA and IIB



B. Displacement of Gly339



C. Displacement of Arg272

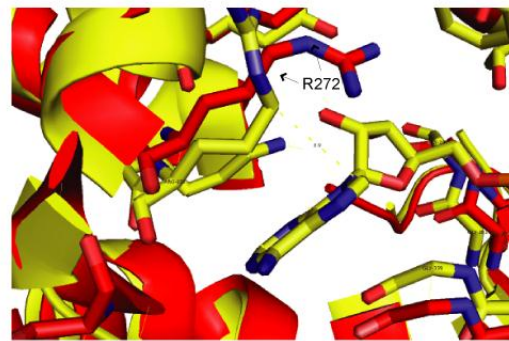
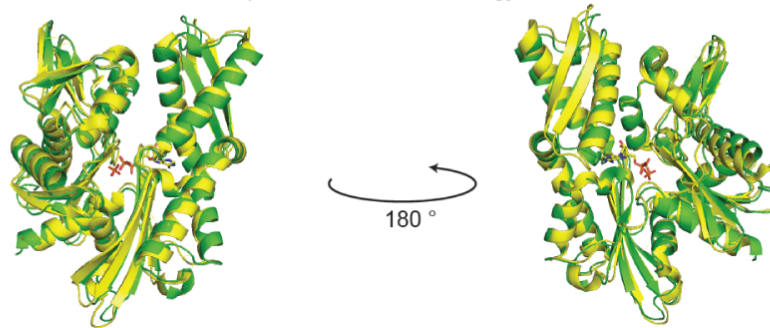


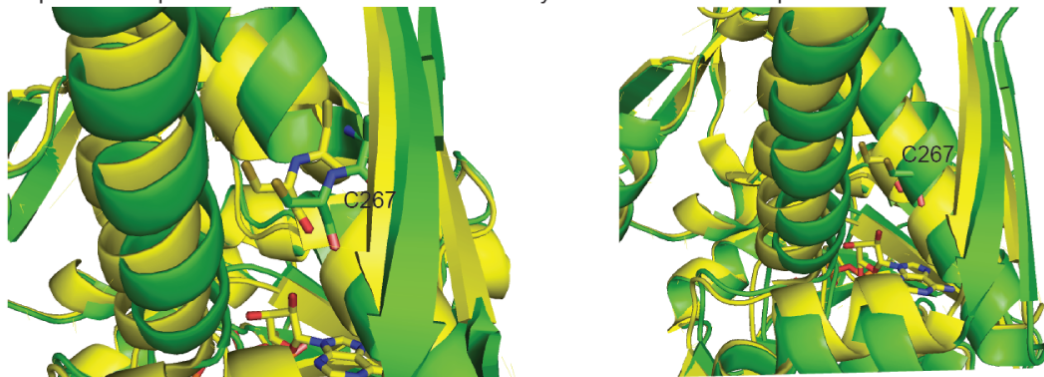
**Figure 3.14 Modeling of Hsp72 C267D reveals structural changes in residues that contact nucleotide.** (A) Overall structural alignment of Hsp72 (yellow: pdb entry 3JXU) and Hsp72 C267D Model (red: modeled from template 3JXU using Robetta Server). (B) Gly339 is shifted away from the  $\alpha$ -phosphate of nucleotide in the modeled structure. (C) Arg272 is shifted away from the adenine ring in the modeled structure.

NBD showed that they were globally very similar, with an RMSD of 1.55Å and a TM-score of 0.94 (**Figure 3.14A**). However, several residues that are specifically involved in nucleotide binding were significantly shifted. For example, Gly339,

A Overall fold is maintained in the Hsp72 C306D NBD homology model



B Hsp72 C306D pseudo-oxidation mutant shifts C267 by 3 Å into the solvent exposed cleft



C. Model for sequential oxidation of two critical cysteine “sensor” residues in Hsp72

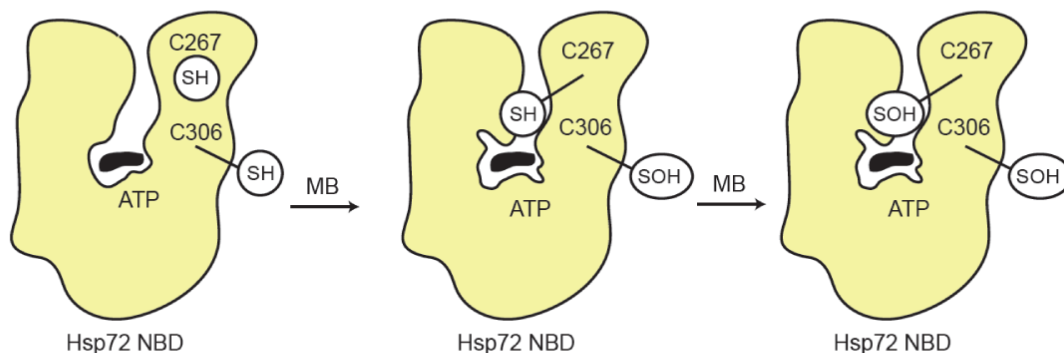


**Figure 3.15 Homology model of Hsp72 C306D NBD.** (A) Pseudo-oxidation of residue 306 does not produce global changes in the NBD fold, similar to what was seen with the C267D mutant (see Figure 3.14). Green is C306D. Yellow is wild type (PDB 3JXU). The C306D and C267D models are nearly identical (see Figure 3.12), with C306D also causing an ~25 Å total displacement of residues associated with nucleotide binding. (B) Close up that illustrates how C306D increases the solvent exposure of Cys 267, potentially enhancing its oxidation. C267 moves by ~3 Å in the C306D model. (C) Model for initial oxidation at Cys306, leading to synergistic oxidation of C267 and reduced ATP binding.

which makes a hydrogen bond interaction with the alpha phosphate group of ADP, was shifted away from the nucleotide by 1.0 Å, likely preventing the formation of this important bond (**Figure 3.14B**). Further, Arg272, which interacts with the adenine ring by pi-stacking, is significantly pulled away by regional rotations in the backbone (**Figure 3.14C**). Collectively, these changes and others (**Appendix 3.5.4**) resulted in side chain displacements totaling more than 25Å in the nucleotide binding cleft. Very similar results were seen with the C306D mutant, suggesting that these residues both contribute to conformational rearrangements (**Figure 3.15A**). Moreover, oxidation of C306 causes C267 to become significantly more solvent exposed (**Figure 3.15B**), perhaps making it more accessible to oxidation by MB. Together, these *in silico* observations suggest that oxidation of Cys267 and Cys306 in Hsp72 might damage nucleotide binding and inactivate ATP turnover. Further, these results suggest that sequential oxidation of C306 and then C267 may reinforce and promote these conformational changes (**Figure 3.15C**).

### **3.2.12 Cys to Asp mutations “phenocopies” MB treatment *in vitro* and in cells**

To test this model, we mutated Cys267 and Cys306 of Hsp72 into Asp and purified the resulting mutant proteins to study effects of pseudo-oxidation. Initial attempts to purify the mutants on ATP agarose immediately revealed that they had significantly reduced affinity for nucleotide (**Appendix 3.5.5A**), consistent with the modeled structure. Switching to size exclusion, we were able to purify

the mutants and show that they had normal circular dichroism (CD) spectra (**Appendix 3.5.5B**), suggesting that the global structure was not significantly disrupted. Finally, we analyzed them by partial proteolysis and found that they were more prone to digestion (**Appendix 3.5.5C**), suggesting that they are more flexible. Interestingly, MB treatment of wild type Hsp72 also was more prone to proteolysis (**Appendix 3.5.5C**), further enforcing the similarities between the Asp point mutants and oxidized wild type.

Next, we explored the enzymatic activity of these pseudo-oxidation mutants. In ATPase assays, we found that the C267D and C306D mutants had dramatically decreased enzymatic activity (**Figure 3.16A**), essentially behaving like Hsp72 that had been treated with MB. Next, we wanted to see if the point mutants would “phenocopy” MB treatment when over-expressed in cells. In HeLaC3 cells, we found that mutating only one of the residues, such as C306D, produced modest

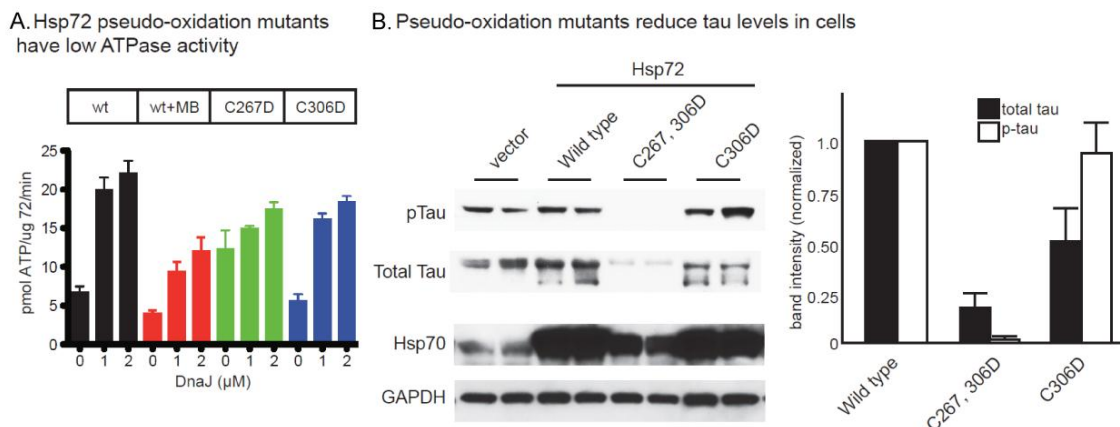


**Figure 3.16 Pseudo-oxidation mutants phenocopy MB treatment.** (A) The DnaJ-stimulated ATPase activities of purified Hsp72 mutants were reduced, resembling MB-treated wild type. These experiments were performed at least three times using two independently prepared samples. Error bars represent the standard error of the mean (SEM). (B) Over-expression of wild type Hsp72 had little effect on tau levels, but the C306D and C267/306D mutants reduced tau. The gels show two independent replicates and the quantification of band intensities includes SEM.

reductions in total tau levels and no significant effect on phosphorylated tau (**Figure 3.16B**). However, when we generated the double mutant (C267/306D), we found that its over-expression substantially reduced tau levels (**Figure 3.16B**). In contrast, over-expression of wild type Hsp72 had no effect on tau levels. Together, these findings provide strong support for MB acting through oxidation of specific cysteine residues in Hsp72 to reduce tau levels. More broadly, these studies provide a dramatic difference between Hsp72 and Hsc70 in redox sensitivity.

### **3.3 Discussion**

#### **3.3.1 Chemical modulators of Hsp70 provide insight into chaperone-mediated regulation of tau turnover**

Based on a growing body of evidence demonstrating a role for Hsp70 in modulating the stability of tau in AD, a major goal of this Chapter was to chemically modulate the ATPase activity of Hsp70 activity in order to its relationship with tau stability. We found that inhibiting Hsp70 activity dramatically reduced tau levels, while activating it preserved tau levels in the cell. In tauopathies, where the accumulation of tau is gradual over time, a rapid increase in Hsp70 levels would likely lead to a reduction in tau levels simply based on stoichiometric principles; more Hsp70 is available to bind tau, decide tau's fate, and facilitate its retention or clearance. Even if a small fraction of tau is cleared by Hsp70 normally, increasing Hsp70 expression will lead to a perceived reduction in tau simply due to the increased number of Hsp70/tau complexes.

Using new ATPase inhibitors, we impacted nucleotide turnover independent of Hsp70 protein levels. More specifically, inhibiting ATPase activity was sufficient to trigger tau turnover. Additionally, increasing the protein levels of Hsp70, either by genetic or pharmacologic methods, worked synergistically with Hsp70 ATPase inhibitors. These findings provide an interesting and somewhat unexpected model in which inhibition of Hsp70 could lead to preferential tau degradation in diseased systems that are over-loaded with tau.

### **3.3.2 Hsp70 inhibitors, unlike Hsp90 inhibitors, do not activate a stress response**

Although Hsp90 inhibitors have been studied more extensively, there is a major concern with therapeutic application of these agents because they induce expression of other heat shock proteins. This is due to the role of Hsp90 as a repressor of HSF1 (heat shock factor 1), the major transcription factor for heat shock proteins [42,43]. Certainly this outcome can be viewed as either a multi-pronged attack or a double-edged sword. HSF1 activation has been shown to have positive consequences in some models of neurodegenerative disease; however, chronic up-regulation of heat shock proteins is likely deleterious. In this work, we found that Hsp70 inhibitors did not elevate chaperone expression and that their activity is not HSF dependent. Because Hsp70 has been proposed to be part of the HSF1 repression complex [44], it isn't clear why the inhibitors do not activate a heat shock response. One compelling reason might be that these inhibitors have rather specific effects on particularly sensitive Hsp70 substrates,

such as tau and Akt [25]. HSF1 might not be one of the most sensitive Hsp70 substrates and, therefore, be immune to these allosteric inhibitors. In Chapter 5, we will discuss some of the next steps that will be required for understanding the logic of Hsp70 substrate selection.

### **3.3.3 Mechanism by which MB inhibits Hsp70**

Interestingly, one of the inhibitors that we identified in Chapter 2, MB, is non-toxic and widely used in humans for other indications, including inherited and acute methemoglobinemia, prevention of urinary tract infections, ifosfamid-induced neurotoxicity, vasoplegic adrenaline resistant shock and pediatric malaria [34]. Further, it has been explored in Phase IIb clinical trials in AD patients [45]. Because of these favorable properties, we decided to further investigate how MB might inhibit Hsp70. Our goal in that process was to gain further molecular detail into why inhibition of Hsp70 leads to degradation of tau. We considered it important to understand this mechanism to enable future translational opportunities.

Using mass spectrometry and genetic methods, we found that MB oxidizes Cys267 and Cys306 of stress inducible Hsp72 and irreversibly inhibits its ATPase activity. Importantly, treatment with MB had no effect on the constitutively expressed Hsc70. Using structural predictions, we developed a model in which oxidation of the unique Cys306 leads to increased exposure of Cys267 to oxidation and that both oxidation events contribute to loss of ATPase



activity. Oxidation of these residues did not cause global changes in structure; rather, they subtly shifted residues involved in nucleotide binding (see **Figure 3.14**). Consistent with this model, pseudo-oxidation point mutants, C267D and C306D, lacked the ability to bind ATP *in vitro* (see **Appendix 3.5.5**). We noted that Hsc70 contains the Cys267 residue, but it lacks the Cys306 residue and it was resistant to oxidation, further suggesting that oxidation of Cys306 might serve as the critical, initial sensor. Cys306 is solvent exposed in Hsp72 and, thus, would be predicted to be available for oxidation by MB or other redox stressors. Together, these findings suggest that Hsp72, and possibly other stress-inducible Hsp70 family members, are involved in sensing and responding to redox stress. Although we did not set out to understand differences between Hsp72 and Hsc70, these fortuitous findings may have important implications in tauopathy and development of new treatments because they point to a particularly strong connection between the stress-inducible Hsp70 isoforms with tau turnover. Because disruption of redox homeostasis is important in AD [46], these findings could also have implications on disease progression.

Treatments with high levels of MB are both well tolerated in cells and, moreover, MB is relatively safe in humans. On first glance, the global inactivation of Hsp72 might be hypothesized to be acutely and dramatically toxic, given the proposed roles of this chaperone in “housekeeping” activities. However, another point of view is that Hsp72 is specifically concerned with degrading only the substrates that have been damaged or misfolded [47], protecting the cytosol from the



accumulation of proteotoxic intermediates. In normal cells, the levels of such substrates may be low due to the action of other components of the protein quality controls system. However, tau is an abundant and intrinsically disordered protein [48], and thus might serve as a particularly good Hsp72 substrate. Additional work is needed to fully understand the basis for this dichotomy, but the empirical evidence currently suggests that some types of inhibition of Hsp70s are well tolerated in normal cells [49]. An important advantage of these Hsp70 inhibitors over well studied Hsp90 inhibitors is the fact that they do not cause heat shock response. This also contributes to maintaining global proteome and allows avoiding potential complications. Together, these findings provide one potential mechanism by which MB has activity in tau-related diseases, such as AD, with toxicity that is lower than might be expected.

### **3.3.4 Conclusion**

In conclusion, Hsp70 is a central component of the protein folding and triage machinery, yet the mechanisms it employs to control the fates of its substrates are not clear. Here, we used a battery of chemical modulators for Hsp70 (discovered in Chapter 2) to perturb the activity of Hsp70 and examine the consequences on tau processing. Based on these studies, we propose a model in which acute inhibition of Hsp70 might be beneficial by triggering rapid, UPS-mediated clearance of tau. Moreover, using MB as a chemical tool, we revealed that Hsp72 is specifically responsive to oxidative stress and oxidation of two sensitive cysteines inhibits ATP turnover, causing a dramatic decrease in tau

levels. Together, these results clarify the roles of endogenous Hsp70 in tau processing and suggest a promising therapeutic strategy.

### **3.4 Materials and Methods**

#### **3.4.1 Reagents, cell lines and general methods.**

Methylene blue, Azure C, thionin and myricetin were purchased from Sigma. The dihydropyrimidines 115-7c and SW02 were synthesized as described [50]. Epoxomicin and 17-AAG were acquired from A.G. Scientific. All clones were in the pcDNA3.1 vector for tau stability assays. SiRNAs (Qiagen) were transfected at 20 nM. All antibodies were diluted in 5% NFDM in TBST at 1:1000 with the exception of pS396/S404 tau, which was used at 1:100. Where pTau is indicated, pS396/S404 was the antibody used. PHF1 (pS396/S404 tau) was provided by Dr. Peter Davies. 12E8 (pS262/S356 tau) was provided by Dr. Peter Seubert. The following antibodies were purchased from the company indicated in parentheses;  $\alpha$ -synuclein (Cell Signaling), TDP43 (Protein Tech), Hsp70 and HSF1 (Assay Designs), HA (Roche), Actin (Sigma Aldrich), Hsp40 (BD Transduction Labs), Hsp27, total tau (Santacruz Biotech), total Akt (Cell Signaling) and GAPDH (BioDesign). All cell lines were obtained from ATCC and maintained according to ATCC guidelines. Stably transfected HeLa cells over-expressing wildtype 4R0N human tau were generated by clonal selection with G418 (Invitrogen).

Human Hsp72, Hsc70 and *E. coli* DnaJ were purified according to published schemes [51]. Site directed mutagenesis primers were designed based on previous reports (45) and mutagenesis of Hsp72 was carried out following the

user manual for the QuickChange site-directed mutagenesis kit (Stratagene, La Jolla, CA). The Hsp72 C267S, C306S and C267/306S mutants were expressed and purified using the same protocol as Hsp72 [51]. The Hsp72 C267D and C306D mutants were expressed as previously described [51] and purified using nickel-nitrilotriacetic acid His-Bind® resin (Novagen, Darmstadt, Germany), then buffer exchanged into a 25mM HEPES buffer (10mM KCl, 5mM MgCl<sub>2</sub> pH 7.5).

#### **3.4.2 Measurements of tau levels in cell culture.**

Cells were transfected as previously described [11,13,20]. Cell lysates and immunoprecipitates were analyzed by Western blots [20]. Briefly, cells were harvested in either Tris/NaCl buffer containing protease and phosphatase inhibitor cocktails (for co-IP) with sonication or in MPER buffer (Pierce) containing protease and phosphatase inhibitor cocktails without sonication. For sarkosyl- and SDS-insoluble protein analysis, 2 mgs of total protein were pre-cleared at 14,000 xg for 15 minutes (crude lysates) and soluble (S1) tau consisted of the supernatant from a 15 minute 60,000 xg spin. Pellets from the S1 spin were resuspended in a TBS/sucrose buffer with PMSF [12] and these pellets were incubated with either 1% sarkosyl or 2% SDS for 1 hour at 37 °C. Soluble and insoluble materials were analyzed by Western blot as previously described [20].

#### **3.4.3 Tau and Hsp70 interaction in the presence of ATP- $\gamma$ S.**

HEK cells transfected with wildtype Hsp70 were lysed in assay buffer (0.017%

Triton X-100, 100mM Tris-HCL, 20mM KCl and 6 mM MgCl<sub>2</sub>, pH 7.4), with 15 strokes of a Dounce Homogenizer B. Cell lysates was supplemented with 0.5 µg purified recombinant His-tagged human 4R Tau and treated with and without 0.5 mM ATP-γS in 500µl total volume for 30 minutes at 37°C with gentle rocking. 20 µl of samples were removed for whole lysate measures. 20µl of Ni-NT Agarose (Qiagen) were added for pull down co-precipitation of His-tagged tau/Hsp70 complexes. Samples were analyzed by western blot.

#### **3.4.4 Measurements of tau levels in brain slices and transgenic animals.**

Brain slices were prepared from 4 month old rTg4510 mice and wild type (NonTg) littermates as previously described [52] and treated with MB and AC. Briefly, mice were decapitated and brains were removed and dropped in ice-cold cutting solution. Brains were cut mid-sagittally and were sectioned horizontally in ice-cold, oxygenated cutting solution at 400 µm. Sections were immediately transferred to 50:50 (cutting solution: artificial cerebrospinal fluid, ACSF) at 27°C for 10 minutes and then equilibrated in ACSF at 37°C for 30 minutes. Sections were then transferred to warm, oxygenated ACSF containing drugs and incubated for 3 hours at 37C. Tissues were mechanically homogenized and analyzed by Western. Stereotaxic injections of AC or vehicle into eight rTg4510 mice were performed as previously described [53]. Briefly, bilateral hippocampal injections of 2 µL of either a 10 mM solution of AC in 0.9% saline or 0.9% saline only were performed using a stereotaxic rig and a 10 µL Hamilton syringe. Mice were killed 24 hours after injection and brains were harvested and analyzed by

Western blot.

#### **3.4.5 LDH Assay.**

Cells for assay were plated in designated media. Drug treatments were made in fresh Opti-MEM media. Media was collected and centrifuged to pellet dead cells. Supernatant was then added to 96-well plate in triplicate along with reagents from Cytotox96 kit (Promega) following the supplied protocol.

#### **3.4.6 Oxidation of Hsp72/Hsc70**

Protein (10  $\mu$ M) and MB (5 mM) were incubated at 37 °C for 1 hour. For H<sub>2</sub>O<sub>2</sub> oxidation, protein sample (10  $\mu$ M) was incubated with 1 mM H<sub>2</sub>O<sub>2</sub> at 37 °C for 1 hour. Treated protein samples were subsequently dialyzed against buffer A (100 mM Tris-HCl, pH 7.4, 20 mM KCl, 6 mM MgCl<sub>2</sub>) at 4°C.

#### **3.4.7 ATPase activity**

ATPase activity was measured according to the previously published method [21].

#### **3.4.8 Preparation of dimedone-modified Hsp72**

MB-treated or untreated Hsp72 (10  $\mu$ M) was incubated with 5 mM dimedone (5,5-dimethyl-1,3-cyclohexanedione) in buffer A at room temperature for 1 hour. The samples were analyzed by SDS-PAGE and stained with colloidal Coomassie blue (Invitrogen, Carlsbad, CA). Bands corresponding to Hsp72 were excised and stored at -20 °C until use.

### **3.4.9 Mass spectrometry**

In-gel digestion was performed as previously described[54]. After reduction (10 mM DTT) and alkylation (65 mM iodoacetamide) of the free cysteines at room temperature for 30 minutes, proteins were digested overnight with trypsin (Promega). Resulting peptides were resolved on a nano-capillary reverse phase column (Picofritcolumn, New Objective) using a 1% acetic acid/acetonitrile gradient at 300 nL/min and subjected to LC-tandem MS using LTQ Orbitrap XL mass spectrometer.

MS/MS spectra were searched against the database considering either carbamidomethyl- or dimedone-modified cysteine.

### **3.4.10 Modeling of Hsp72 C267D**

Hsp72 C267D was modeled using the Robetta server with the Hsp72 NBD pdb entry 3JXU as a template. Model and structure were aligned using PyMol (The PyMOL Molecular Graphics System, Version 1.4.1, Schrödinger, LLC). RMSD and TM-score were calculated using TM-align. Images and atomic distances were calculated using PyMol.

### **Notes**

This work was partially published as “Chemical manipulation of Hsp70 ATPase activity regulates tau stability” Jinwal, U.K., Miyata, Y., Koren, J.III., Jones, J.R., Trotter, J.H., Chang, L., O’Leary, J.O., Morgan, D., Lee, D., Shults, C.L., Rousaki, A., Weeber, E.J., Zuiderweg, E.R.P., Gestwicki, J.E. and Dickey, C.A. (2009) *J.*

*Neurosci*, 29 (39); 12079-12088 and “Cystein reactivity distinguishes redox signaling by the heat inducible and constitutive forms of Hsp70” Miyata, Y., Rauch, J.N., Jinwal, U.K., Thompson, A.D., Srinivasan, S., Dickey, C.A. and Gestwicki, J.E. *Chem. Biol.* (in press)

### **Author contributions**

#### Tau stability studies

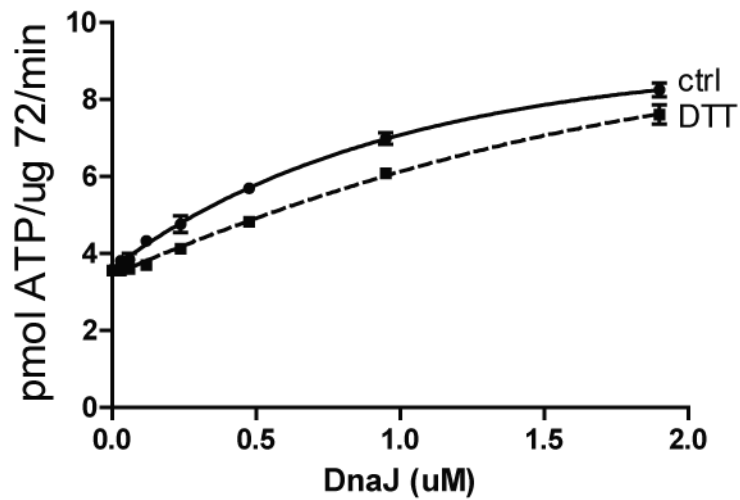
Umesh K. Jinwal, Yoshinari Miyata, Chad A. Dickey and Jason E. Gestwicki designed the experiments. The Dickey group performed the experiments.

#### Hsp72 oxidation studies

Yoshinari Miyata, Jennifer N. Rauch and Jason E. Gestwicki designed the experiments. Yoshinari Miyata, Jennifer N. Rauch, Umesh K. Jinwal and Sharan Srinivasan performed the experiments. Mass spectrometry was performed at the University of Michigan Proteomics Facility.

### 3.5 Appendices

#### 3.5.1 MB-mediated oxidation of Hsp72 is irreversible.



**Appendix 3.5.1. MB-mediated oxidation of Hsp72 is irreversible.** Hsp72 was treated with MB, dialyzed to remove the compound and then treated with DTT for 30 minutes. ATPase activity was measured as in Figure 1A. Results are the average of two experiments performed in triplicate. Error bars represent standard error of the mean.



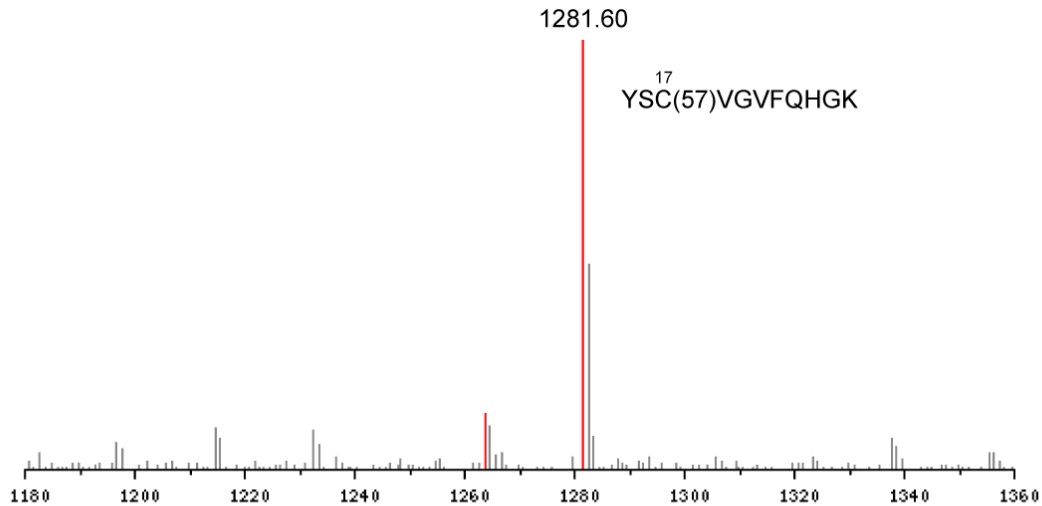
### 3.5.2 Stress inducible, but not constitutive forms of the Hsp70 family contain a unique, reactive cysteine at position 306.

A

	"Cys267"	"Cys306"	
<u>Constitutive</u>			
sp P11142 HSPA8 (Hsc70)	238 KRAVRLRRTACERAKRTLSS-STQASIEIDSLYEGID---- <td>333</td> <td></td>	333	
sp P54652 HSPA2	241 KRAVRLRRTACERAKRTLSS-STQASIEIDSLYEGVD---- <td>336</td> <td></td>	336	
sp P11021 HSPA5 (GRP78/BiP)	263 NRAVQLRREVEKAKRALSS-QHQARIEIESFYEGED---- <td>358</td> <td></td>	358	
sp P38646 HSPA9 GRP75/mortalin)	283 NMALQVRVREAAEKAKCELSS-SVQTDINLPYLTMDSSGPKHLNMKLTQAQFEGIVTDLIRRTIAPCOKAMQDAEVSKSDIGE	382	
sp P48723 HSPA13	264 KEETHRLRQAVEMVKLNLT-LHSAQLSVLLTVEEQD-----RKEPHSSDTLEPKDKLSSADHRVNSGFGFR-----	347	
<u>Stress Inducible</u>			
sp P08107 HSPA1A/B (Hsp70)	238 KRAVRLRRTACERAKRTLSS-STQASLEIDSLFEGID---- <td>333</td> <td></td>	333	
sp P17066 HSPA6	240 KRALRRLRRTACERAKRTLSS-STQATLEIDSLFEGVD---- <td>335</td> <td></td>	335	
sp P48741 HSPA7	240 KRALRRLRRTACERAKRTPLSS-STQATLEIDSLFEGVD---- <td>335</td> <td></td>	335	
sp Q0VDF9 HSPA14	236 ARAMKLTNSAEVAKHSLST-LGSANCFLDLSLYEGQD---- <td>331</td> <td></td>	331	
sp P34932 HSPA4 (Hsp110)	241 IRALLRLSQECKLKKLMSANASDLPLSIECFMNDVD----VSGTMNRGKFLMCDNLLARVEPPLRSVLEQTKLKKEDIYA	337	

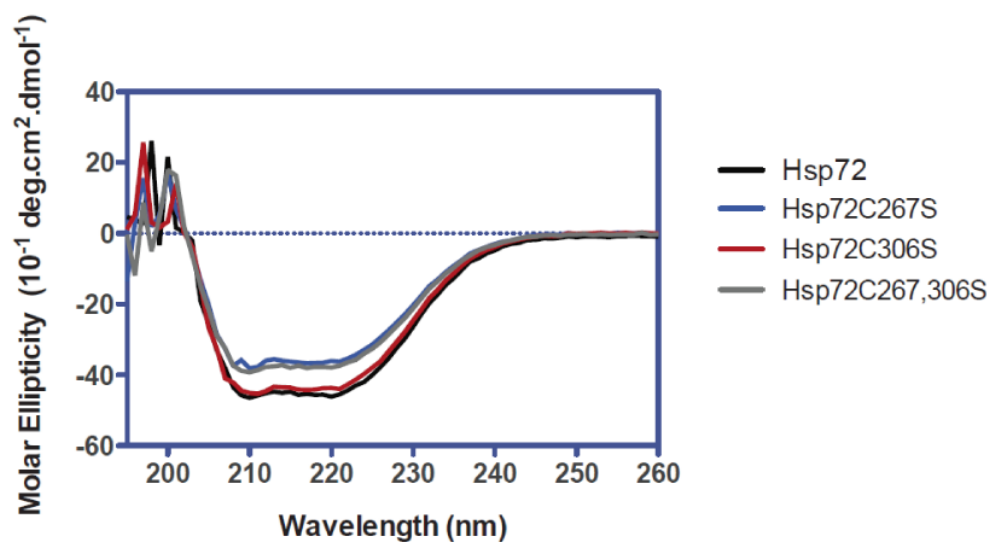
B

scan 3036; 5.1e+03



**Appendix 3.5.2 Stress inducible, but not constitutive forms of the Hsp70 family contain a unique, reactive cysteine at position 306.** (a) Sequence alignment of select human Hsp70 family members, showing conservation of cysteine 306 in stress inducible, but not constitutive forms. The 267 and 306 numbers are derived from human Hsp72 (HSP1A1). For more information see Fujikawa et al. (2010) Cell Stress Chaperones 15:193-204. (b) Representative trypsin fragment of human Hsc70 treated with MB (200  $\mu$ M), as in Fig. 2, showing that Cys17 is not oxidized. In addition, no other fragments in the Hsc70 sequence were oxidized. As discussed in the text, the fragment containing 267 was not observed in the spectra.

### 3.5.3 CD spectra of Hsp72 serine point mutants.



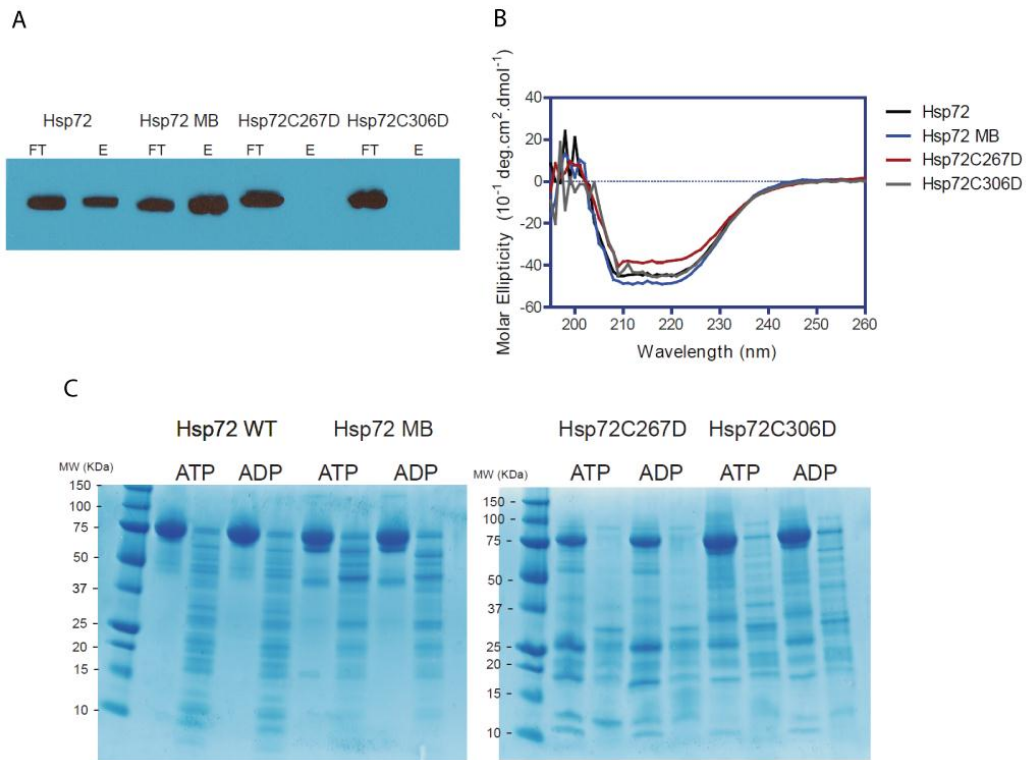
**Appendix 3.5.3 CD spectra of Hsp72 serine point mutants.** Serine point mutants Hsp72 C267S and C306S and the double mutant (C267/306S) are properly folded, as measured by circular dichroism.

**3.5.4 Hydrogen bond and hydrophobic interactions are lost in Hsp72 C267D modeled structure.**

	<u>Residue</u>	<u>3JXU</u> <u>(Å)</u>	<u>Robetta Model</u> <u>(Å)</u>	<u>ΔA</u>
Hydrogen Bond with ADP	<b>T14</b>	2.7	4.8	2.1
	<b>T14</b>	2.8	4.3	1.5
	<b>Y15</b>	2.9	4.5	1.6
	<b>G202</b>	2.7	2.3	-0.4
	<b>E268</b>	2.9	4.2	1.3
	<b>K271</b>	2.8	2.7	-0.1
	<b>S275</b>	2.5	2.3	-0.2
	<b>G339</b>	3.1	4.2	1.1
Hydrogen Bond with Phosphate	<b>T13</b>	2.5	5.1	2.6
	<b>T13</b>	2.8	4.3	1.5
	<b>T13</b>	3.1	5.5	2.4
	<b>K71</b>	2.7	1.9	-0.8
	<b>E175</b>	2.7	3.2	0.5
	<b>T204</b>	2.5	3.6	1.1
Hydrophobic Interactions	<b>Y15</b>	3.8	3.7	-0.1
	<b>G201</b>	3.8	4.0	0.2
	<b>G202</b>	3.8	3.3	-0.5
	<b>G202</b>	3.6	3.3	-0.3
	<b>G202</b>	3.8	3.7	-0.1
	<b>R272</b>	3.9	4.6	0.7
	<b>R272</b>	3.5	5.2	1.7
	<b>R272</b>	3.2	4.7	1.5
	<b>R272</b>	3.7	4.9	1.2
	<b>R272</b>	3.9	5.1	1.2
	<b>G339</b>	3.7	4.2	0.5
	<b>R342</b>	3.8	5.0	1.2
	<b>R342</b>	3.8	5.7	1.9
	<b>R342</b>	3.8	5.3	1.5
	<b>I343</b>	3.6	3.8	0.2
			<b>Total (Å) :</b>	<b>25.0</b>

**Appendix 3.5.4 Hydrogen bond and hydrophobic interactions are lost in Hsp72C267D modeled structure.**

### 3.5.5 C267D and C306D mutants have impaired ATP binding and are more flexible.



#### Appendix 3.5.5 C267D and C306D mutants have impaired ATP binding and are more flexible.

(A) Purified proteins ( $5 \mu\text{M}$ ) were treated with 1 mL of ATP-agarose, washed with 3 mL of Buffer A (25 mM HEPES, 10 mM KCl, 5 mM  $\text{MgCl}_2$ , pH 7.5) and flowthrough (FT) collected. Following three additional washes, the remaining protein was collected in the eluant (E) by washing with 3 mL of Buffer A containing 3 mM ATP. Fractions were analyzed on 1-20% Tris-Tricine gels using a polyclonal anti-Hsp72 antibody (Enzo). (B) Circular dichroism results indicate that the mutants have similar global structure to the wildtype. Likewise, MB treatment does not cause major changes in structure, as determined by this method. All proteins were used at  $2 \mu\text{M}$  in 50 mM NaF buffer. (C) Hsp70 variants ( $6 \mu\text{M}$ ) were treated with nucleotide (5 mM) for 30 minutes and then digested with trypsin for 30 min at rt. Reactions were quenched with loading dye, bands separated on 10-20% Tris-Tricine gels and imaged by Coomassie stain. Results are representative of experiments performed in duplicate.

### 3.6 References

1. Oddo S, Caccamo A, Shepherd JD *et al.* Triple-transgenic model of Alzheimer's disease with plaques and tangles: intracellular Abeta and synaptic dysfunction. *Neuron*, 39(3), 409-421 (2003).
2. Frautschy SA, Baird A, Cole GM. Effects of injected Alzheimer beta-amyloid cores in rat brain. *Proc Natl Acad Sci U S A*, 88(19), 8362-8366 (1991).
3. Roberson ED, Scearce-Levie K, Palop JJ *et al.* Reducing endogenous tau ameliorates amyloid beta-induced deficits in an Alzheimer's disease mouse model. *Science*, 316(5825), 750-754 (2007).
4. Braak H, Braak E. Neuropathological staging of Alzheimer-related changes. *Acta Neuropathol (Berl)*, 82(4), 239-259 (1991).
5. Mukaetova-Ladinska EB, Garcia-Siera F, Hurt J *et al.* Staging of cytoskeletal and beta-amyloid changes in human isocortex reveals biphasic synaptic protein response during progression of Alzheimer's disease. *Am.J.Pathol.*, 157(2), 623-636 (2000).
6. Hardy J, Orr H. The genetics of neurodegenerative diseases. *J Neurochem*, 97(6), 1690-1699 (2006).
7. Shimura H, Miura-Shimura Y, Kosik KS. Binding of tau to heat shock protein 27 leads to decreased concentration of hyperphosphorylated tau and enhanced cell survival. *J Biol Chem*, 279(17), 17957-17962 (2004).
8. Shimura H, Schwartz D, Gygi SP, Kosik KS. CHIP-Hsc70 complex ubiquitinates phosphorylated tau and enhances cell survival. *J Biol Chem*, 279(6), 4869-4876 (2004).
9. Carrettiero DC, Hernandez I, Neveu P, Papagiannakopoulos T, Kosik KS. The cochaperone BAG2 sweeps paired helical filament- insoluble tau from the microtubule. *J Neurosci*, 29(7), 2151-2161 (2009).
10. Petrucelli L, Dickson D, Kehoe K *et al.* CHIP and Hsp70 regulate tau ubiquitination, degradation and aggregation. *Hum Mol Genet*, 13(7), 703-714 (2004).
11. Dickey CA, Dunmore J, Lu B *et al.* HSP induction mediates selective clearance of tau phosphorylated at proline-directed Ser/Thr sites but not KXGS (MARK) sites. *Faseb J*, 20(6), 753-755 (2006).
12. Dickey CA, Yue M, Lin WL *et al.* Deletion of the ubiquitin ligase CHIP leads to the accumulation, but not the aggregation, of both endogenous phospho- and caspase-3-cleaved tau species. *J Neurosci*, 26(26), 6985-6996 (2006).
13. Dickey CA, Koren J, Zhang YJ *et al.* Akt and CHIP coregulate tau degradation through coordinated interactions. *Proc Natl Acad Sci U S A*, 105(9), 3622-3627 (2008).
14. Dou F, Netzer WJ, Tanemura K *et al.* Chaperones increase association of tau protein with microtubules. *Proc Natl Acad Sci U S A*, 100(2), 721-726 (2003).
15. Luo W, Dou F, Rodina A *et al.* Roles of heat-shock protein 90 in maintaining and facilitating the neurodegenerative phenotype in

- tauopathies. *Proc Natl Acad Sci U S A*, 104(22), 9511-9516 (2007).
16. Slepnev SV, Witt SN. The unfolding story of the Escherichia coli Hsp70 DnaK: is DnaK a holdase or an unfoldase? *Mol Microbiol*, 45(5), 1197-1206 (2002).
  17. Mayer MP, Schroder H, Rudiger S, Paal K, Laufen T, Bukau B. Multistep mechanism of substrate binding determines chaperone activity of Hsp70. *Nat Struct Biol*, 7(7), 586-593 (2000).
  18. Brehmer D, Rudiger S, Gassler CS *et al.* Tuning of chaperone activity of Hsp70 proteins by modulation of nucleotide exchange. *Nat Struct Biol*, 8(5), 427-432 (2001).
  19. Neckers L. Hsp90 inhibitors as novel cancer chemotherapeutic agents. *Trends Mol Med*, 8(4 Suppl), S55-61 (2002).
  20. Dickey CA, Kamal A, Lundgren K *et al.* The high-affinity HSP90-CHIP complex recognizes and selectively degrades phosphorylated tau client proteins. *J Clin Invest*, 117(3), 648-658 (2007).
  21. Chang L, Bertelsen EB, Wisen S, Larsen EM, Zuiderweg ER, Gestwicki JE. High-throughput screen for small molecules that modulate the ATPase activity of the molecular chaperone DnaK. *Anal Biochem*, 372(2), 167-176 (2008).
  22. Josephs KA, Whitwell JL, Knopman DS *et al.* Abnormal TDP-43 immunoreactivity in AD modifies clinicopathologic and radiologic phenotype. *Neurology*, 70(19 Pt 2), 1850-1857 (2008).
  23. Winton MJ, Van Deerlin VM, Kwong LK *et al.* A90V TDP-43 variant results in the aberrant localization of TDP-43 in vitro. *FEBS Lett*, 582(15), 2252-2256 (2008).
  24. Rutherford NJ, Zhang YJ, Baker M *et al.* Novel mutations in TARDBP (TDP-43) in patients with familial amyotrophic lateral sclerosis. *PLoS Genet*, 4(9), e1000193 (2008).
  25. Koren J, 3rd, Jinwal UK, Jin Y *et al.* Facilitating Akt clearance via manipulation of Hsp70 activity and levels. *J Biol Chem*, 285(4), 2498-2505 (2010).
  26. Berger Z, Roder H, Hanna A *et al.* Accumulation of pathological tau species and memory loss in a conditional model of tauopathy. *J Neurosci*, 27(14), 3650-3662 (2007).
  27. Congdon E, Wu J, Myeku N *et al.* Methylthioninium chloride (methylene blue) induces autophagy and attenuates tauopathy in vitro and in vivo. *Autophagy*, 8(4), (in press) (2012).
  28. Westerheide SD, Bosman JD, Mbadugha BN *et al.* Celastrols as inducers of the heat shock response and cytoprotection. *J Biol Chem*, 279(53), 56053-56060 (2004).
  29. Jarv J, Hedlund B, Bartfai T. Kinetic studies on muscarinic antagonist-agonist competition. *J Biol Chem*, 255(7), 2649-2651 (1980).
  30. Davidson GA, Varhol RJ. Kinetics of thapsigargin-Ca(2+)-ATPase (sarcoplasmic reticulum) interaction reveals a two-step binding mechanism and picomolar inhibition. *J Biol Chem*, 270(20), 11731-11734 (1995).

31. Ward NE, O'Brian CA. Kinetic analysis of protein kinase C inhibition by staurosporine: evidence that inhibition entails inhibitor binding at a conserved region of the catalytic domain but not competition with substrates. *Mol Pharmacol*, 41(2), 387-392 (1992).
32. Boulton DW, Walle UK, Walle T. Fate of the flavonoid quercetin in human cell lines: chemical instability and metabolism. *J Pharm Pharmacol*, 51(3), 353-359 (1999).
33. O'Leary JC, 3rd, Li Q, Marinec P *et al*. Phenothiazine-mediated rescue of cognition in tau transgenic mice requires neuroprotection and reduced soluble tau burden. *Mol Neurodegener*, 5, 45 (2010).
34. Schirmer RH, Adler H, Pickhardt M, Mandelkow E. "Lest we forget you--methylene blue...". *Neurobiol Aging*, 32(12), 2325.e2327-2316 (2011).
35. Kelner MJ, Alexander NM. Methylene blue directly oxidizes glutathione without the intermediate formation of hydrogen peroxide. *J Biol Chem*, 260(28), 15168-15171 (1985).
36. Reddie KG, Carroll KS. Expanding the functional diversity of proteins through cysteine oxidation. *Curr Opin Chem Biol*, 12(6), 746-754 (2008).
37. Poole LB, Karplus PA, Claiborne A. Protein sulfenic acids in redox signaling. *Annu Rev Pharmacol Toxicol*, 44, 325-347 (2004).
38. Jinwal UK, Miyata Y, Koren J, 3rd *et al*. Chemical manipulation of hsp70 ATPase activity regulates tau stability. *J Neurosci*, 29(39), 12079-12088 (2009).
39. Kim DE, Chivian D, Baker D. Protein structure prediction and analysis using the Robetta server. *Nucleic Acids Res*, 32(Web Server issue), W526-531 (2004).
40. Wisniewska M, Karlberg T, Lehtiö L *et al*. Crystal structures of the ATPase domains of four human Hsp70 isoforms: HSPA1L/Hsp70-hom, HSPA2/Hsp70-2, HSPA6/Hsp70B', and HSPA5/BiP/GRP78. *PLoS One*, 5(1), e8625 (2010).
41. Permyakov SE, Zernii EY, Knyazeva EL *et al*. Oxidation mimicking substitution of conservative cysteine in recoverin suppresses its membrane association. *Amino Acids*, (2011).
42. Dickey CA, Eriksen J, Kamal A *et al*. Development of a high throughput drug screening assay for the detection of changes in tau levels -- proof of concept with HSP90 inhibitors. *Curr Alzheimer Res*, 2(2), 231-238 (2005).
43. Zou J, Guo Y, Guettouche T, Smith DF, Voellmy R. Repression of heat shock transcription factor HSF1 activation by HSP90 (HSP90 complex) that forms a stress-sensitive complex with HSF1. *Cell*, 94(4), 471-480 (1998).
44. Shi Y, Mosser DD, Morimoto RI. Molecular chaperones as HSF1-specific transcriptional repressors. *Genes Dev*, 12(5), 654-666 (1998).
45. Wischik C, Betham P, Wischik D, Seng K. Tau aggregation inhibitor (TAI) therapy with Rember™ arrests disease progression in mild and moderate Alzheimer's disease over 50 weeks. In: *Alzheimer's and Dementia*. (Ed. (Eds) (2008) T167.
46. Markesbery WR. Oxidative stress hypothesis in Alzheimer's disease. *Free*

- Radic Biol Med*, 23(1), 134-147 (1997).
47. Pratt WB, Toft DO. Regulation of signaling protein function and trafficking by the hsp90/hsp70-based chaperone machinery. *Exp Biol Med (Maywood)*, 228(2), 111-133 (2003).
  48. Schweers O, Schönbrunn-Hanebeck E, Marx A, Mandelkow E. Structural studies of tau protein and Alzheimer paired helical filaments show no evidence for beta-structure. *J Biol Chem*, 269(39), 24290-24297 (1994).
  49. Yaglom JA, Gabai VL, Sherman MY. High levels of heat shock protein Hsp72 in cancer cells suppress default senescence pathways. *Cancer Res*, 67(5), 2373-2381 (2007).
  50. Wisen S, Androsavich J, Evans CG, Chang L, Gestwicki JE. Chemical modulators of heat shock protein 70 (Hsp70) by sequential, microwave-accelerated reactions on solid phase. *Bioorg Med Chem Lett*, 18(1), 60-65 (2008).
  51. Chang L, Thompson AD, Ung P, Carlson HA, Gestwicki JE. Mutagenesis reveals the complex relationships between ATPase rate and the chaperone activities of Escherichia coli heat shock protein 70 (Hsp70/DnaK). *J Biol Chem*, 285(28), 21282-21291 (2010).
  52. Mirnikjoo B, Brown SE, Kim HF, Marangell LB, Sweatt JD, Weeber EJ. Protein kinase inhibition by omega-3 fatty acids. *J Biol Chem*, 276(14), 10888-10896 (2001).
  53. Wilcock DM, Alamed J, Gottschall PE *et al.* Deglycosylated anti-amyloid-beta antibodies eliminate cognitive deficits and reduce parenchymal amyloid with minimal vascular consequences in aged amyloid precursor protein transgenic mice. *J Neurosci*, 26(20), 5340-5346 (2006).
  54. Brady GF, Galbán S, Liu X *et al.* Regulation of the copper chaperone CCS by XIAP-mediated ubiquitination. *Mol Cell Biol*, 30(8), 1923-1936 (2010).



## Chapter 4

### Exploring MKT-077 as a Scaffold for Hsp70 Modulators

#### 4.1 Abstract

As discussed in previous chapters, we have identified chemical modulators of Hsp70 by high throughput screens and used them as tools to study the role of Hsp70 in regulating client stability such as tau. To supplement these ongoing screening efforts, we also wanted to characterize the mechanism of previously known, but under-explored, Hsp70 modulators. In this Chapter, we demonstrated by NMR that an anti-cancer compound MKT-077 binds the NBD of Hsp70 at a site immediately below the nucleotide-binding region. Strikingly, the compound only bound in the presence of ADP but not ATP, establishing itself as an allosteric modulator. Biochemical studies revealed that MKT-077 stabilizes Hsp70 in an ADP-bound-like conformation, blocks J-protein-mediated stimulation of ATPase activity and increases Hsp70's affinity for substrates. All of these activities are reminiscent of an Hsp70 co-chaperone Hip (Hsp70 Interacting Protein). This observation led us to further investigate the effects of Hip overexpression and treatment with MKT-077 analogues in model systems. In cell

based assays, MKT-077 and its analogs reduced tau levels as seen for other Hsp70 inhibitors (see Chapter 3). We found that both Hip and a close analogue of MKT-077, YM1, promote ubiquitination and clearance of polyglutamine-expanded androgen receptor (polyQ-AR) in models of spinal and bulbar muscular atrophy (SBMA). Together, these studies further support a model in which the tight-affinity Hsp70 structure favors degradation of Hsp70-bound substrates. Encouraged by these promising results, we set out to optimize the compound as a possible therapeutic agent for tauopathy. Preliminary pharmacokinetic studies revealed that YM1 does not cross the blood brain barrier while a neutral analog, YM8, accumulates in brain. Accordingly, we synthesized a library of neutral derivatives and explored structure activity relationships (SAR). We found that fluorine and chlorine substitutions on the benzothiazole moiety increase affinity for Hsp70 as well as activity to reduce tau in HeLa cells. These preliminary data suggest neutral MKT-077 derivatives might have a potential to be drug leads for the treatment of tauopathy.

#### 4.1.1 MKT-077 as a candidate Hsp70 inhibitor

As discussed throughout this dissertation, Hsp70 family proteins are becoming recognized as having multiple “druggable” sites. These sites include the ATP binding site, substrate binding sites and other allosteric modulators (reviewed in [1,2]).

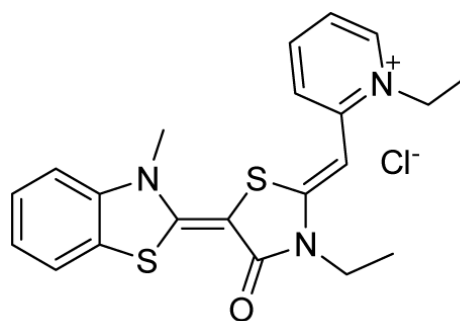


Figure 4.1 Chemical structure of MKT-077

Thus far in this thesis, we have focused on using screening approaches to identify new Hsp70 inhibitors and activators.

To supplement these unbiased screening studies, we reviewed the literature for additional compounds known to interact with Hsp70 and decided to explore a rhodacyanine dye MKT-077 (**Figure 4.1**) because its mechanism was not known. MKT-077 was originally developed as anti-cancer agent, with an  $IC_{50}$  of 0.35 – 1.2  $\mu$ M against several cancer cell lines and high selectivity toward tumor cells [3]. This selectivity is attributed to the compound's accumulation in mitochondria and its mitochondrial toxicity [3,4]. Because of these favorable properties, MKT-077 was evaluated in a Phase I trial for solid tumors but the study was discontinued due to renal toxicity [5]. While its cellular target was not known at the time of the clinical studies, it was later found to bind Hsp70 isoforms including the constitutively expressed Hsc70 and the mitochondrial resident mtHsp70 [6,7]. However, very little was known about its binding site or the mechanism by which it might impact Hsp70 function.

## **4.2 Results**

### **4.2.1 MKT-077 binds Hsc70 NBD with 1:1 stoichiometry**

Our first objective was to identify the binding site of MKT-077 on Hsc70. Previous pull-down studies had suggested that MKT-077 might bind in the nucleotide-binding domain (NBD) of mtHSP70 [6]. Based on our recent successes with NMR-based approaches to identify binding sites of Hsp70 modulators in the NBD [8-10], we used the  $^{15}\text{N}$ - $^1\text{H}$  transverse relaxation optimized spectroscopy

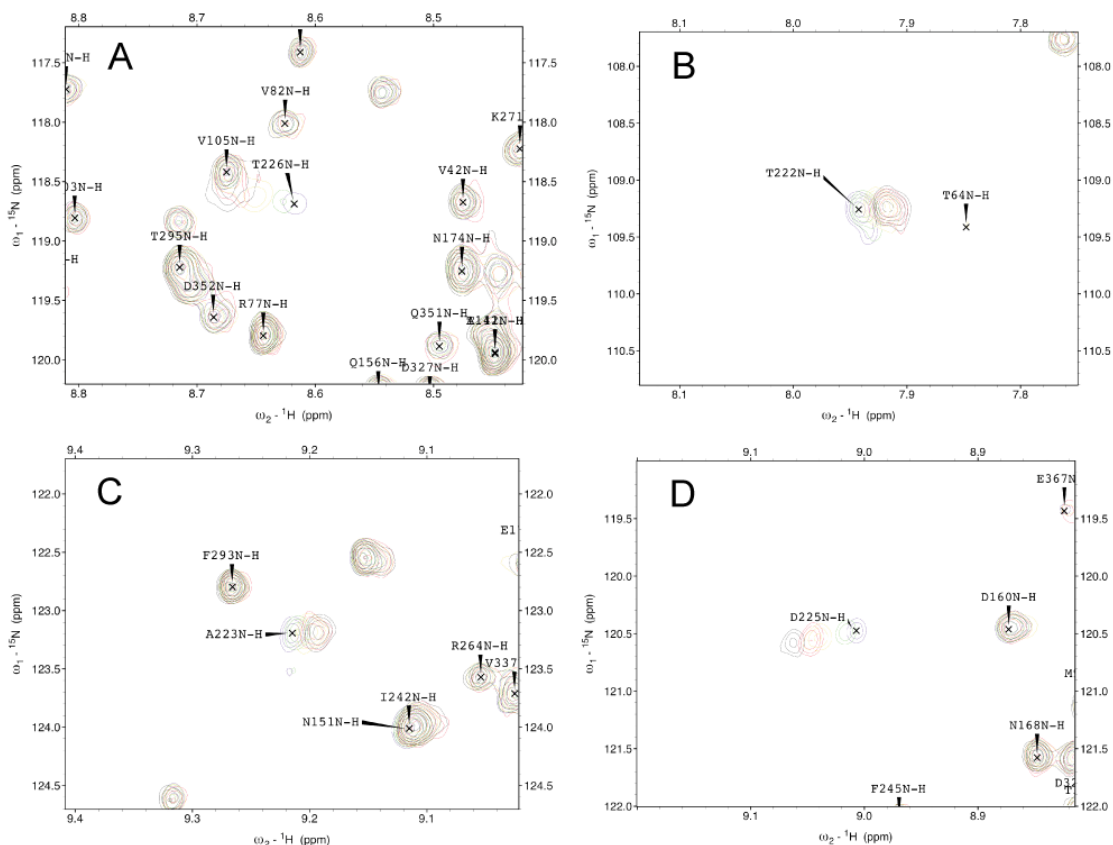


**Figure 4.2 Details of some of the chemical shift changes in the TROSY spectrum of Hsc70 NBD upon addition of MKT-077.** Ratios MKT-077/Hsc70: Blue, no MKT-077; Green, 0.25:1; Yellow, 0.5:1; Red, 0.75:1; Black, 1:1. For these, a sample of 260  $\mu\text{M}$   $^{15}\text{N}$ ,  $^2\text{H}$ -labeled Hsc70-NBD in the ADP state was used.

(TROSY) spectrum of Hsc70 NBD in the ADP state to identify the binding site of MKT-077 (**Appendix 4.5.1**). A select number of resonances show gradual chemical shift changes upon addition of MKT-077 up to a molar ratio of 1:1 (**Appendix 4.5.2 and Figure 4.2**).

#### 4.2.2 MKT-077 binds ADP-state of Hsc70 NBD

Based on these studies, the binding site of MKT-077 appeared to be in an otherwise unoccupied negatively charged pocket located on the interface of subdomains IA and IIA in the ADP-bound state (**Figures 4.3A&B**). As discussed

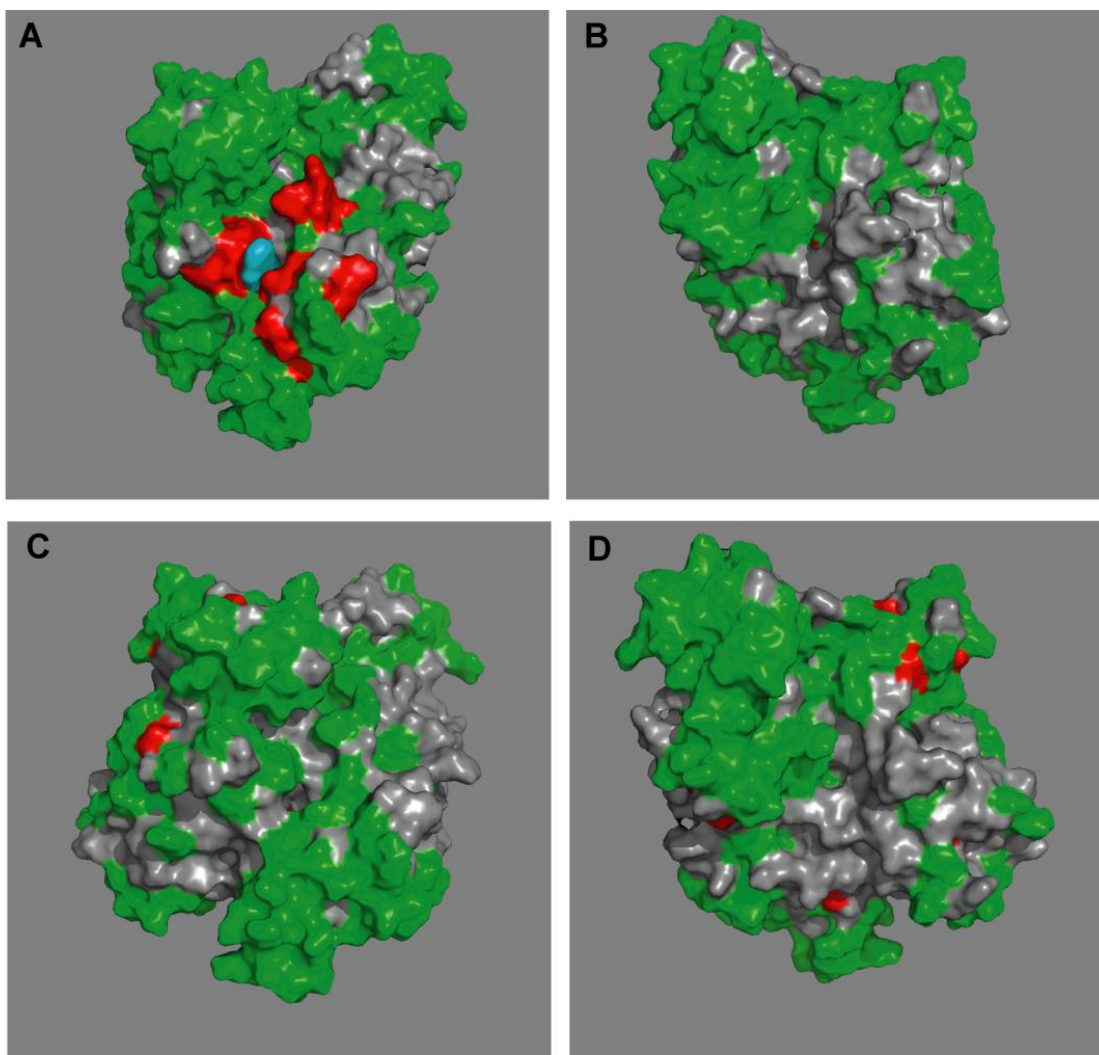


**Figure 4.3 Mapping of the chemical shift changes of MKT-077 on the structure of Hsc70 NBD (3HSC.pdb).** Panels (A) and (B): ADP state. Left and right images are rotated 180 degrees along the vertical axis with respect to each other. Color coding: Red, sites detected using 250 mM 15N-2H labeled Hsc70 NBD; Green, no changes; grey, no assignments and cannot be decided; cyan, approximate position of MKT-077 as determined by AUTODOCK. Panels (C) and (D): AMP-MPM state. Panels and color scheme as above. The figure was generated in Pymol.

in Chapter 1, Hsp70s are allosteric proteins, which show global conformational and dynamical changes on the NBD between the ADP and ATP state [11,12]. Hence, we wondered if MKT-077 would also bind to the ATP-state of the NBD. To test this idea, we titrated MKT-077 into NBD loaded with AMP-PNP or ATP and found that binding was lost (**Figures 4.3C&D**). Thus, MKT-077 only binds the ADP-bound state and not the ATP-bound state. Finally, we also monitored

MKT-077 binding to Hsc70 NBD in the apo state. Although a lack of assignments prevented definitive interpretations, MKT-077 appeared to bind to the apo-state.

#### 4.2.3 MKT-077 binds Hsc70 NBD with a $K_D$ in the low micromolar

The MKT-077-induced changes to the spectrum of Hsc70 NBD in the ADP state are in the fast-exchange limit (see **Figure 4.2**), with little or no line broadening. The largest shifts in the spectrum are approximately 20 Hz, which sets a lower limit of  $100 \text{ s}^{-1}$  for MKT-077's off-rate ( $K_D > 1 \text{ } \mu\text{M}$ , when assuming an upper limit on the diffusion-controlled

on-rate of  $10^8 \text{ M}^{-1}\text{s}^{-1}$ ).

Further, the shifts are linear over the titration interval and saturate abruptly at equivalence (**Figure 4.4**), compatible with a  $K_D < 10 \text{ } \mu\text{M}$ . Together, these

observations suggest that the affinity of MKT-077 for

Hsc70 is between 1 and  $10 \text{ } \mu\text{M}$ .

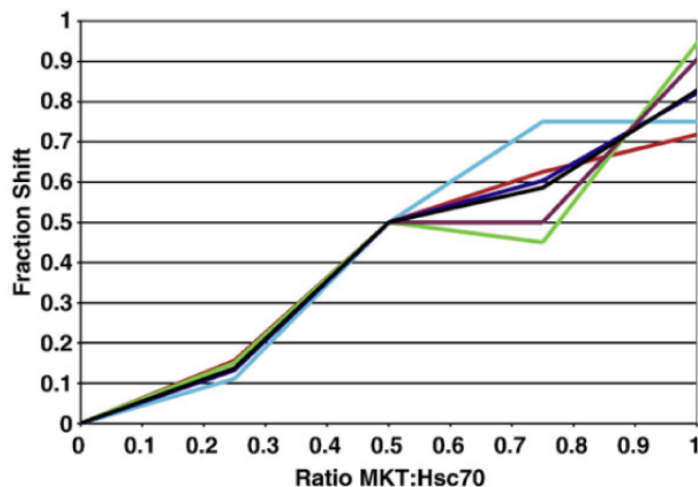


**Figure 4.4 Fractional shifts upon addition of MKT-077 in the  $^{15}\text{N}, ^2\text{H}$ -labeled Hsc70.** Cyan, T222; red, A223; blue, D225; green, H227; purple, L228; black, average. For each resonance, the shift at a molar ratio of 0.5 was defined as 50% completed.

#### 4.2.4 AUTODOCK simulations suggest how MKT-077 binds Hsc70

The TROSY studies strongly suggested a binding site immediately below the nucleotide in the NBD. Guided by these chemical shifts, our collaborator, Prof.

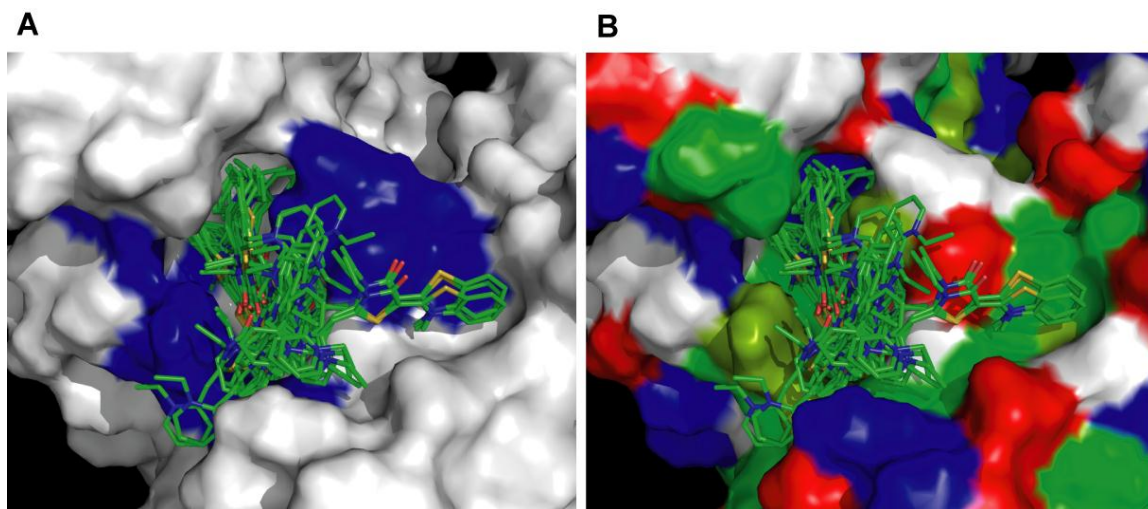


**Figure 4.5 Results of AUTODOCK.** The search box was restricted to the binding area as determined by the NMR chemical shift perturbations. (A) all dockings ranging from 4.5 – 7.0 Kcal/mole in relation to the NMR shifts in blue. (B) the same ensemble in relation to the chemical properties of the protein (green: A,C,F,I, L,M,P, V,W; dark green: T,Y; blue: H,K,R; red:D,E; white:G,N,Q,S).

Zuiderweg used AUTODOCK [13] and the crystal structure of Hsc70 NBD in complex with Hsp110 (3C7N) to obtain insight into the MKT-077 binding orientation (see **Appendix 4.5.3**). The selection of this particular Hsp70–NEF complex (there are five different complexes in the Protein Data Bank (PDB)) is based on the fact that it is the only one that contains ADP. The crystal coordinates of the NBD were minimized, equilibrated, and relaxed to 300 K using an AMBER 1175 MD protocol (see Materials and Methods). The coordinates and degrees of freedom for MKT-077 were optimized and determined from quantum mechanical calculations.

Prof. Zuiderweg next used an AUTODOCK search box localized around the NMR-determined MKT-077-binding site (**Figures 4.5A&B**). These studies yielded a variety of possible binding poses, with energies ranging between 4 and 7 kcal/mol. After culling those docking orientations to remove those with MKT-077 contacting positive residues, four possible families were identified (**Figure**



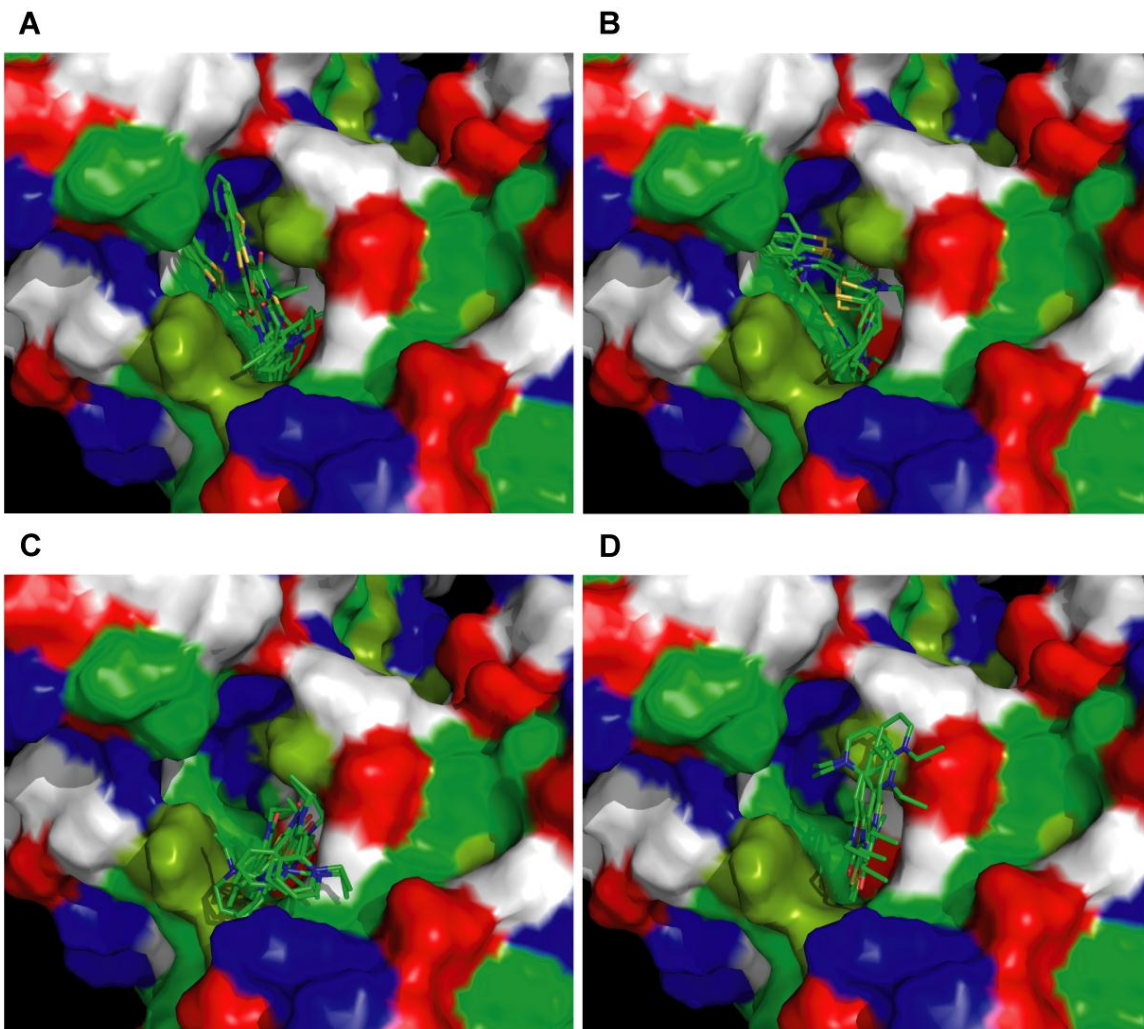


**Figure 4.6 Four families of docking poses.** (A) a family of feasible dockings with an energy of 7.03 kcal/M for its best member. (B) a family of feasible dockings with an energy of 6.32 kcal/M for its best member. (C) a family of feasible dockings with an energy of 5.36 kcal/M for its best member. (D) a family of feasible dockings with an energy of 5.25 kcal/M for its best member. The figures were generated in Pymol.

**4.6A-D).**

#### **4.2.5 The MKT-077 binding site is conserved in Hsp70 isoforms.**

All docked families are in close contact with the residues that show chemical shift perturbations, such as Glu175 and Asp206, which reside deep within the pocket and contribute to the negative electrostatic potential of the region. These residues, as well as the other residues that are in contact with MKT-077, are



100% conserved among the 13 human Hsp70 isoforms (gene name: HSPA) (see **Appendix 4.5.4**). Hence, it is more than likely that MKT-077 also binds at this site in the mitochondrial protein mtHsp70 (mortalin; HSPA9), which was earlier identified as a target [6,14].

#### **4.2.6 Analysis of the MKT-077 binding site.**

In the AUTODOCK family depicted in **Figure 4.6A**, the positive pyridinium ring is reaching into the pocket to contact Glu175 and Asp206. In the family depicted in **Figure 4.6B**, partial contact occurs. In the other families, the positive pyridinium ring is solvent-exposed. In the family depicted in **Figure 4.6D**, it is in contact with Asp225, which lines the rim of the pocket (at 2 o'clock in **Figure 4.6D**). Prior to starting additional medicinal chemistry, we wanted to further analyze these different AUTODOCK poses using the MMGB/PBSA solvation/desolvation computational protocol to determine the “best” conformation. Briefly, equilibrated 250-ps MD runs for the complexes shown in **Figure 4.6** were obtained using AMBER 11. We then used the generalized Born/Poisson Boltzmann protocol to estimate the solvation enthalpy of ligand, protein, and complex (MMGB/PBSA). These calculations demonstrated that subfamily shown in **Figure 4.6D** has the best score. In this pose, the benzothiazole ring of MKT-077 is inserted into the deep pocket composed of Pro176, Glu175, Tyr149, Ala148 and other residues (**Figure 4.7**), and the pyridinium moiety is solvent exposed. This orientation is consistent with experimental evidence in the literature; MKT-077 derivatives with larger polyaromatics in place of the pyridinium moiety are equally or more potent

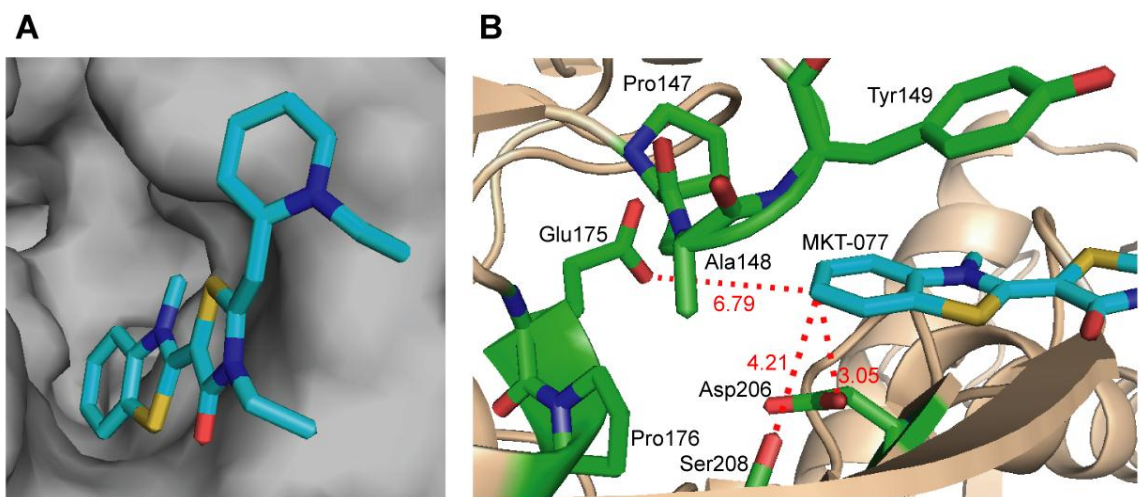


**Figure 4.7 Best docking pose of MKT-077 on Hsc70.** (A) The benzothiazole moiety is inserted into the deep pocket. (B) Amino acid residues comprising the pocket. Distances between the benzothiazole ring and some of the amino acid side chains are indicated in red (Å). Figures were prepared in PyMol.

[15]. In addition, through derivatization of the pyridinium moiety, MKT-077 could be covalently linked to Sepharose and used to bind to mtHsp70 [6,16]. Importantly, this binding site and docking pose are consistent with the NMR data (see **Appendix 4.5.5**). Together, these NMR and docking studies provide the first glimpse into where and how MKT-077 binds to Hsp70s *in vitro*.

#### 4.2.7 MKT-077 inhibits ATPase activity and stabilizes ADP-like conformation

Our next major question was focused on understanding the mechanism by which MKT-077 would impact Hsp70 function. Because other chemical modulators of Hsp70 either stimulate or inhibit its ATPase activity (Chapters 2 and 3), we first tested MKT-077 in an ATPase assay. As shown in **Figure 4.8**, MKT-077 slightly inhibited J-protein-stimulated ATPase activity of yeast Hsp70, Ssa1p, suggesting that binding of the compound allosterically blocks the interaction between Hsp70 and J-proteins. This activity is similar to what we found with other Hsp70

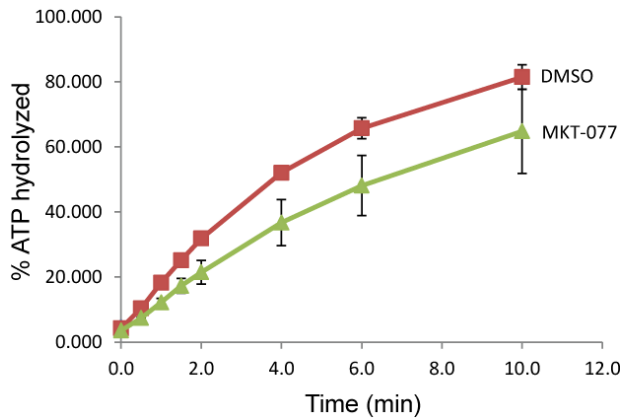


**Figure 4.8 MKT-077 inhibits J-protein-stimulated ATPase activity of yeast Hsp70 (Ssa1p).** Radio-labeled ATP was pre-bound to Ssa1p, and flash frozen. This complex was thawed in the presence of a J-protein and test compound was added after 60 secs. At the time points, aliquots were removed and developed on TLC. Results are the average of three independent experiments and errors are S.D.

inhibitors, such as MB and myricetin (see Chapters 2 and 3).

The evidence shown in **Figure 4.3** strongly suggests that MKT-077 binds preferentially to the ADP- and not the ATP-bound state of Hsc70. To test whether

this compound could stabilize the ADP-like conformation, we performed partial proteolysis

experiments. It has been previously shown that trypsin treatment of human Hsc70 yields

digestion patterns diagnostic of the chaperone's nucleotide state [17].

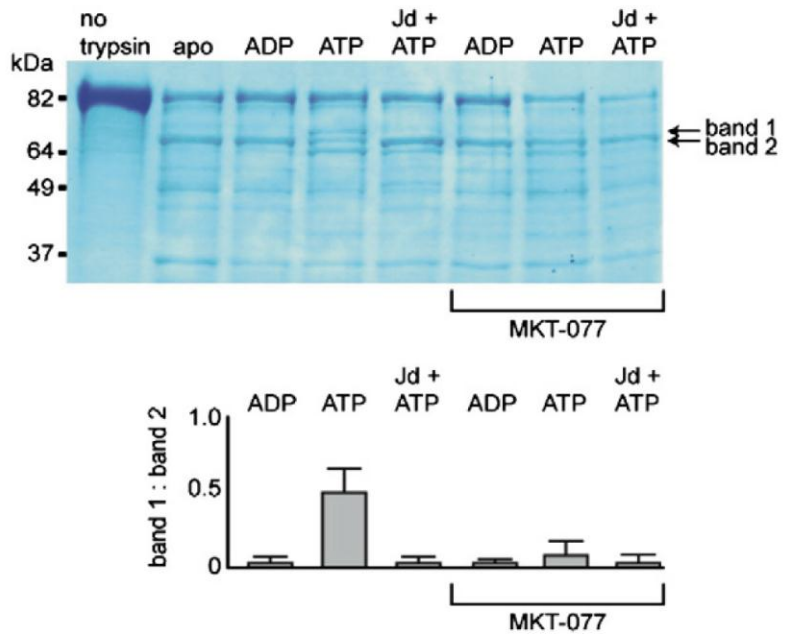


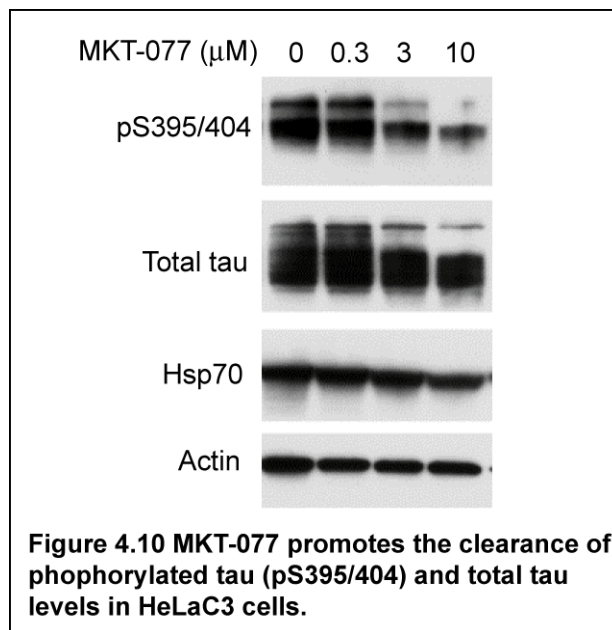
**Figure 4.9 MKT-077 favors the ADP-bound conformation of Hsc70, as measured by limited trypsin proteolysis.** Full-length Hsc70 was treated with trypsin in the presence of excess nucleotide and MKT-077. By this analysis, the ATP-bound state is characterized by the appearance of both bands 1 and 2, while the ADP-bound Hsc70 predominantly shows band 2. Addition of a J-domain (Jd) converts the ATP-like pattern into the ADP-like pattern. MKT-077 (200  $\mu$ M) suppressed the ATP-bound form and favored band 2. Bands 1 and 2 were quantified in a National Institutes of Health Image J densitometer, and the ratio of these bands (e.g., relative formation of the ATP-bound state) is shown in the bottom panel. These results are representative of experiments performed in duplicate.

Consistent with those reports, we confirmed that Hsc70 saturated with ATP was primarily cleaved into three high molecular weight bands, including prominent bands at approximately 69 kDa (band 1) and 66 kDa (band 2) (**Figure 4.9**). Conversely, treatment with ADP strongly favors band 2. Addition of the J-domain of prokaryotic DnaJ, which stimulates ATP turnover in Hsc70, converted the ATP-like pattern to an ADP-like pattern. Next, we tested whether MKT-077 could stabilize the ADP-like configuration. Addition of MKT-077 (200  $\mu$ M) largely blocked formation of band 1, consistent with the NMR data that this compound binds preferentially to the ADP-bound state of Hsc70. Together, these data support the NMR findings and suggest that MKT-077 stabilizes the ADP-bound state and inhibits steady-state ATP cycling in Hsp70s.

#### **4.2.8 MKT-077 reduces tau level in HeLa cells and is a useful compound for probing structure-function relationships in the Hsp70 system**

As discussed in Chapter 3, inhibition of Hsp70 by small molecules such as methylene blue (MB) causes enhanced clearance of tau in HeLaC3 cells. Based on this observation and the results shown above, we wondered whether MKT-077 would also lead to clearance of hyper-phosphorylated tau. **Figure 4.10** shows that the compound, indeed, reduces tau levels in HeLaC3 cells at low micromolar concentrations, comparable to the best of the previous Hsp70 inhibitors, such as MB. Together, these data suggest that MKT-077 is an allosteric modulator of Hsp70 and could serve as a lead compound for the treatment of tauopathy. Indeed, the use of these compounds as potential

tauopathy therapeutics is progressing under the direction of a postdoctoral fellow, Dr. Xiaokai Li, in the Gestwicki laboratory and initial structure-activity relationships will be discussed below. Prior to that discussion, we will first describe additional mechanistic studies on MKT-077 that were performed in

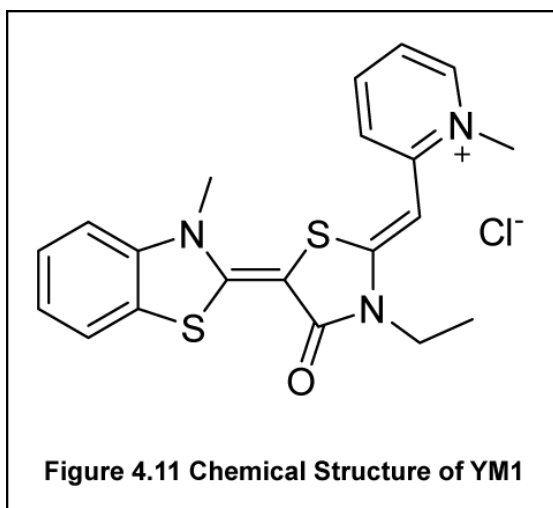


collaboration with Andrew Lieberman's group (Dept. Pathology, University of Michigan). These additional mechanistic studies were directed at forming a link between the *in vitro* effects of MKT-077 and effects of this compound in cellular and animal models, with the goal of understanding the role of nucleotide binding in dictating the fate of bound Hsp70 substrates.

#### 4.2.9 YM1 increases Hsp70 binding to denatured luciferase

One of the major questions in chaperone biology is how the structure of Hsp70 correlates to the "decision" to either fold or degrade substrates. We sought to use MKT-077 and its analogs to probe the specific role of the ADP-bound state in this decision. Further, the fact that MKT-077 stabilizes the ADP-bound form of Hsp70 is reminiscent of Hip (Hsp70 interacting protein), a co-chaperone of Hsp70. Thus, we reasoned that MKT-077 and Hip could be used to independently test the function of the ADP-bound state of Hsp70. If both of these perturbations gave

similar results, we would gain confidence in the specific role of the ADP-bound conformation.



Towards that goal, it has recently been shown that overexpression of Hip prevents the accumulation of polyglutamine (polyQ) inclusions in a cellular model [18]. However, the mechanism of this activity wasn't clear. Thus, we wondered whether MKT-077 and Hip could be combined to probe

polyQ stability *in vitro* and *in vivo*. As an initial test of this idea, we collaborated with Andrew Lieberman's group to explore the effects of MKT-077 analogs and Hip over-expression on polyQ-expanded androgen receptor (polyQ-AR). PolyQ-AR is the cause of spinal and bulbar muscular atrophy (SBMA), a progressive neurodegenerative disease that, like tauopathies, is linked to aberrant protein quality control. In these studies, we used YM1 (**Figure 4.11**), an MKT-077 derivative with excellent anti-tau activity in HeLaC3 cells (data not shown). Because of the published findings with Hip, we reasoned that the polyQ-AR system would be a particularly good model in which to study the cellular consequences of "trapping" the ADP-bound form of Hsp70s. Specifically (as discussed in Chapter 1), we hypothesized that prolonging the Hsp70-bound form of polyQ-AR (either genetically or using chemical probes) might promote ubiquitination and degradation.

To test whether YM1 could impact the apparent binding affinity of Hsp70s for substrates, we used an ELISA-like assay to measure binding to denatured luciferase. In this experiment we found that YM1 potently stimulated Hsp70 binding to its unfolded substrate, similar to what we observed with MKT-077 (**Figure 4.12A**). Next, we performed trypsin partial proteolysis studies on YM1 treated, human Hsp72 as described earlier for MKT-077. As expected, addition of YM1 (200  $\mu$ M) blocked formation of the ATP-bound form (**Figure 4.12B**).

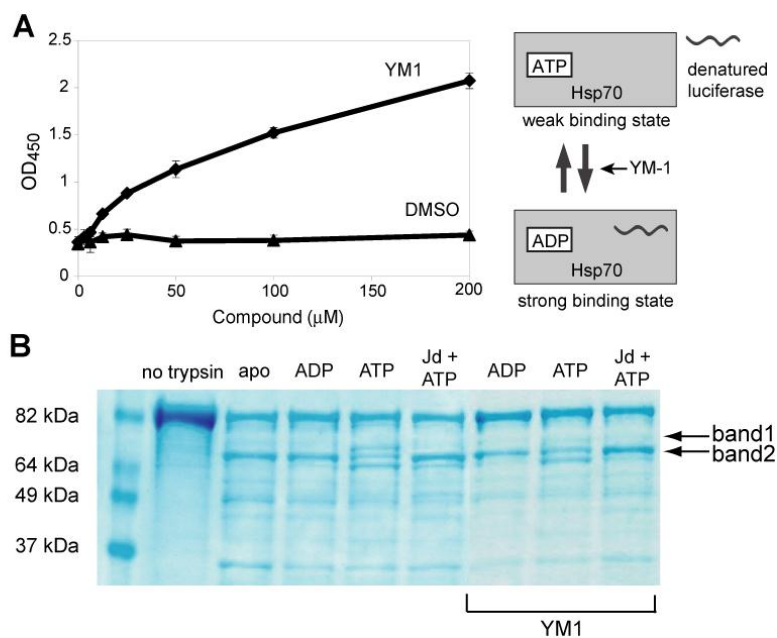


**Figure 4.12 YM1 promotes binding of Hsp70 to denatured luciferase and stabilizes ADP-bound form.** (A) ELISA plates were coated with denatured luciferase, and binding of Hsp70 was measured using an HRP-coupled anti-Hsp70 antibody. A solvent control is shown for comparison. Data are mean  $\pm$  SEM. (B) Partial trypsin proteolysis experiments show that YM1 favors an ADP-like conformation. The experiments were performed as described in Figure 4.6 using full length, human Hsp72. Results are representative of experiments performed in duplicate.

Together, these studies suggest that YM1, like MKT-077, converts Hsp70 to its tight affinity conformation.

#### 4.2.10 YM1 competes with Hip for binding

To further explore the binding of YM1 to Hsp70, we first synthesized two biotinylated probes (**Figure 4.13**). The orientation of MKT-077 bound to Hsp70, as determined by NMR, suggests that the pyridine

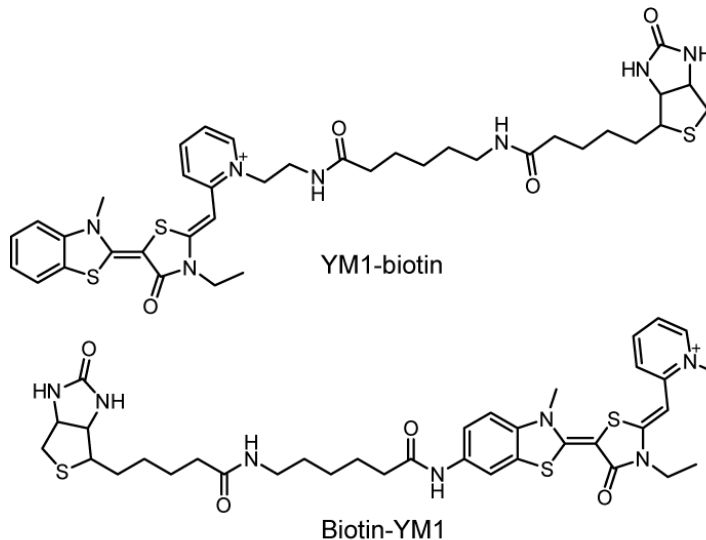


**Figure 4.13** Chemical structures of biotinylated YM1 probes.

ring should be solvent exposed (**Figure 4.8**). To test this idea, we appended a biotin tag to either the pyridine side of the YM1 (termed YM1-biotin; **Figure 4.13**) or the opposite benzothiazole (biotin-YM1), which is expected to be buried. In an ELISA-like format, we found that only the YM1-biotin probe had affinity for human Hsp72 (**Figure 4.14A**), with an apparent  $K_D$  of  $4.9 \pm 0.8 \mu\text{M}$ . This interaction

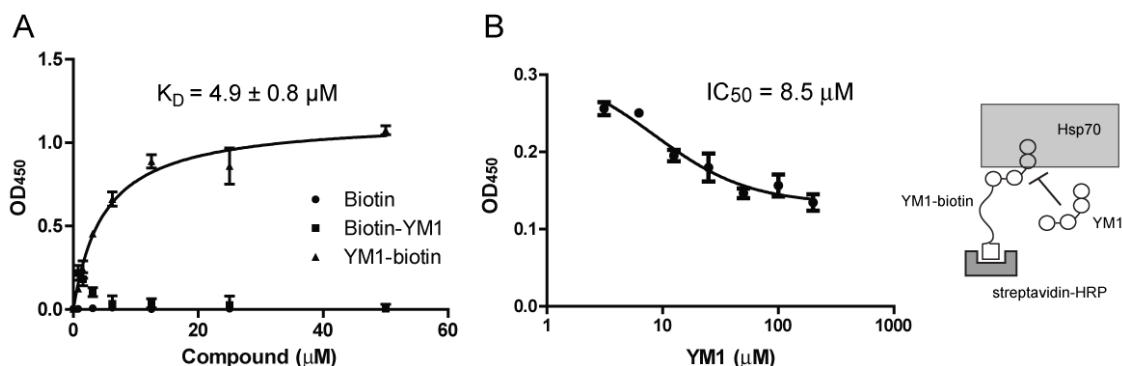


**Figure 4.14** YM1-biotin specifically binds Hsp72. (A) Binding of the biotinylated probes to Hsp70 confirms that the pyridine ring of YM1 is solvent exposed. Experiments were carried out in triplicate. Data are mean  $\pm$  SEM. (B) Binding of YM1-biotin to Hsp72 is specific and can be competed with unlabelled YM1. Experiments were carried out in triplicate. Data are mean  $\pm$  SEM.



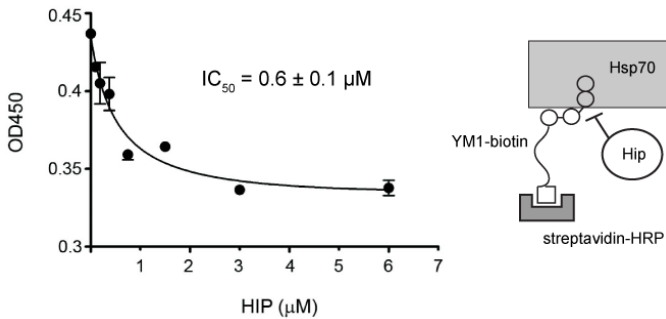


**Figure 4.15 YM-1 and Hip bind competitively to Hsp70.** Binding of YM1-biotin to immobilized Hsp70 is diminished by pre-incubation with increasing amounts of Hip. Experiments were carried out in triplicate. Data are mean  $\pm$  SEM.

appeared to be specific, because unlabelled YM-1 could compete for binding (**Figure 4.14B**). This platform not only provided insight into YM-1 binding to Hsp70, but also allowed us to test whether the

co-chaperone, Hip, could compete with YM-1. Using purified Hip, we found that it could indeed block binding of the YM-1-biotin probe (**Figure 4.15**), suggesting that these natural and synthetic co-chaperones utilize a similar contact surface. Based on these data, we propose that YM-1 acts similarly to Hip; favoring accumulation of the ADP-bound form of Hsp70 and increasing its apparent affinity for substrates.

#### 4.2.11 Hip and YM1 promote clearance of AR112Q

To test the effect of Hip on polyglutamine proteins, we over-expressed Hip with AR containing 112 glutamines (AR112Q). In this model, aggregation and misfolding of the polyQ AR is dependent on the addition of androgen receptor ligands, such as R1881 [19]. We found that Hip over-expression promoted clearance of soluble and RIPA-insoluble AR112Q after addition of R1881 (**Figure 4.16A**). Further, this co-chaperone diminished the frequency of androgen-dependent intranuclear inclusions in cells stably expressing tetracycline-inducible AR112Q (**Figures 4.16B&C**). Loss of AR112Q was mediated, in part, by the

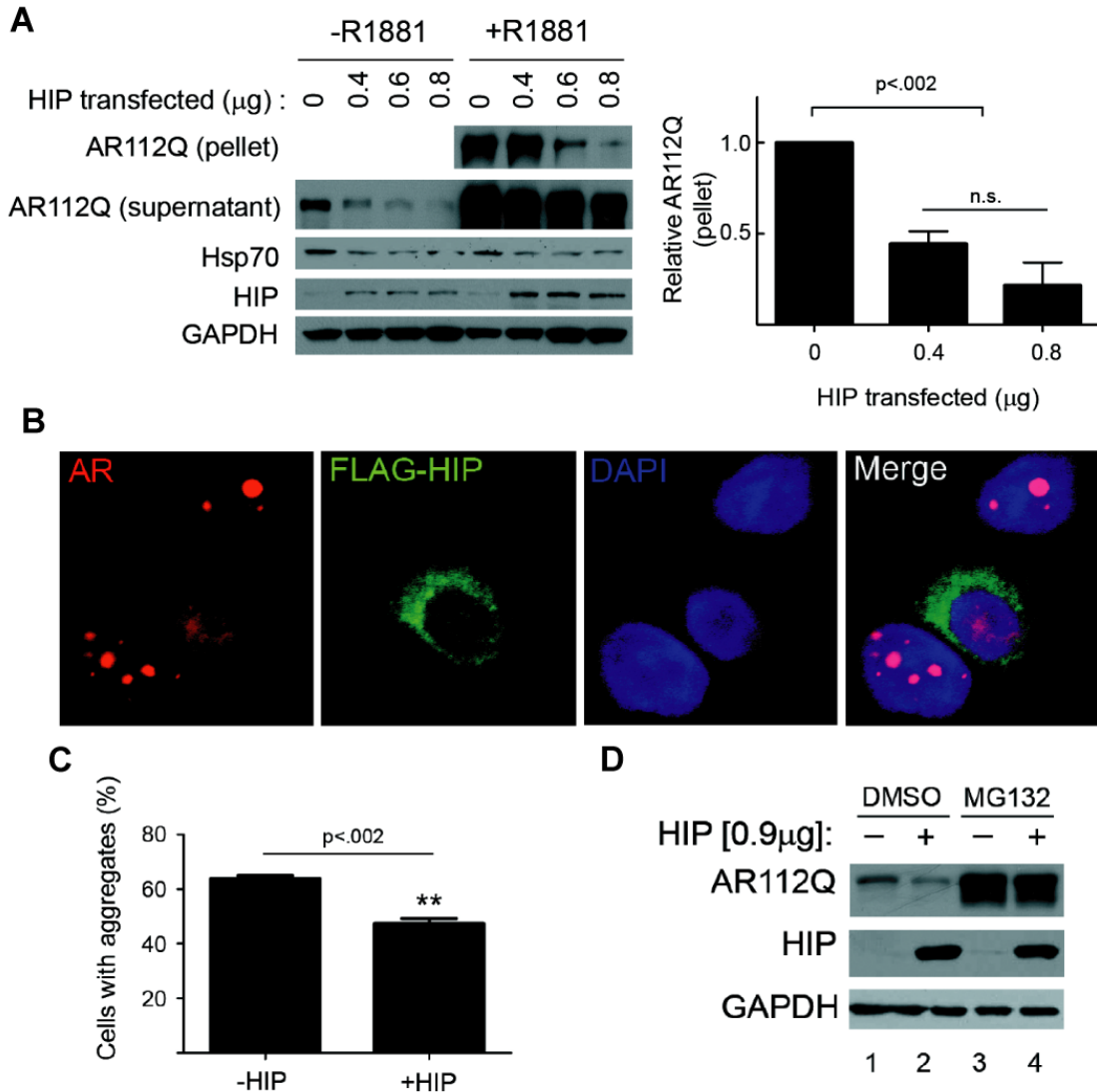
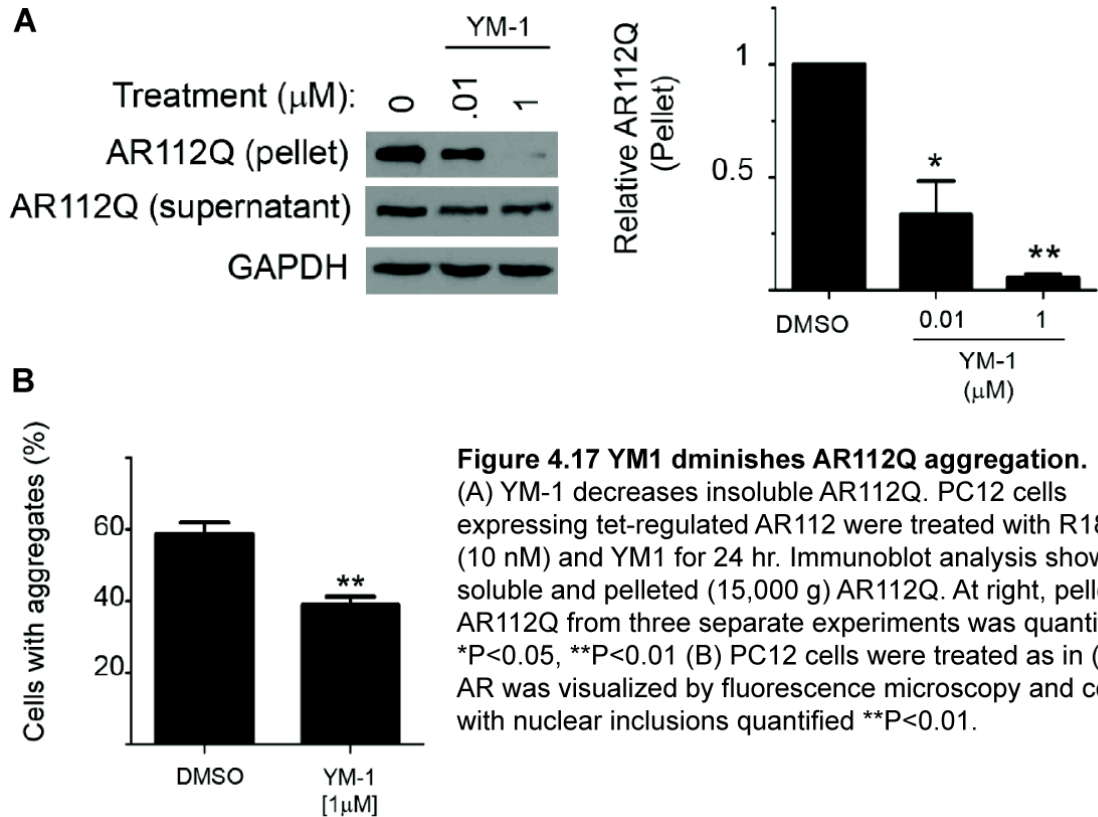


**Figure 4.16 Hip promotes clearance of AR112Q via proteasomal degradation.** (A) Hip promotes AR112Q clearance. HeLa cells transiently expressing AR112Q and increasing amounts of Hip were treated with R1881 (10 nM) for 24 hr. Lysates were separated into supernatant and 15,000 g pellet fractions, then analyzed by western blot (left). At right, pelleted AR from three experiments was quantified. n.s. = not significant. (B) Hip diminishes AR112Q aggregates. PC12 cells expressing tet-regulated AR112Q were transfected with FLAG-Hip, then treated with doxycycline and R1881 (10 nM) for 24 hr. AR and FLAG-Hip were visualized by confocal microscopy. (C) The expression of Hip significantly decreased the frequency of polyQ AR intranuclear inclusions. Data are mean  $\pm$  SEM. (D) Hip promotes AR112Q degradation. HeLa cells were co-transfected with AR112Q and Hip, then treated with R1881 (10 nM) for 24 hr prior to 8 hr treatment with MG132 (10 nM).

proteasome, because it could be suppressed by MG132, a proteasome inhibitor (Figure 4.16D). We conclude that Hip over-expression enhanced ubiquitination and degradation of polyQ AR. Next, we tested YM1 in the same system. Similar



to Hip over-expression, YM1 diminished polyQ AR levels in tet-inducible PC12 cells. To explore whether both the soluble and insoluble forms of AR112Q were sensitive to this treatment, we added YM1 and separated these fractions. We found that YM1 significantly decreased the accumulation of RIPA-insoluble AR112Q (**Figure 4.17A**) and diminished the occurrence of AR intranuclear inclusions in the presence of ligand (**Figure 4.17B**), suggesting a strong effect on the clearance of aggregated polyQ AR. In contrast, treatment with YM1 only slightly diminished the levels of soluble AR112Q. These results suggest that unfolded AR species, such as those found in aggregates, were most sensitive to YM1 under these conditions.

#### 4.2.12 YM1 enhances clearance of polyQ AR via proteasomal degradation.

We postulated that YM1 exerted these effects by increasing polyQ AR degradation. To test this notion, we induced AR112Q expression in tet-regulated PC12 cells in the presence of R1881 for 48 hrs. This protocol allows for robust polyQ expression, followed by ligand-dependent unfolding. Then, the media was replaced to shut off transgene expression and cells were incubated for an additional 72 hrs with YM1 or a solvent control (**Figure 4.18A**). In this experiment, YM1 significantly promoted the clearance of AR112Q as reflected by the loss of immunofluorescence staining (**Figure 4.18B**). Immunoblot analysis revealed that YM1 promoted the clearance of both RIPA-insoluble AR112Q and the high

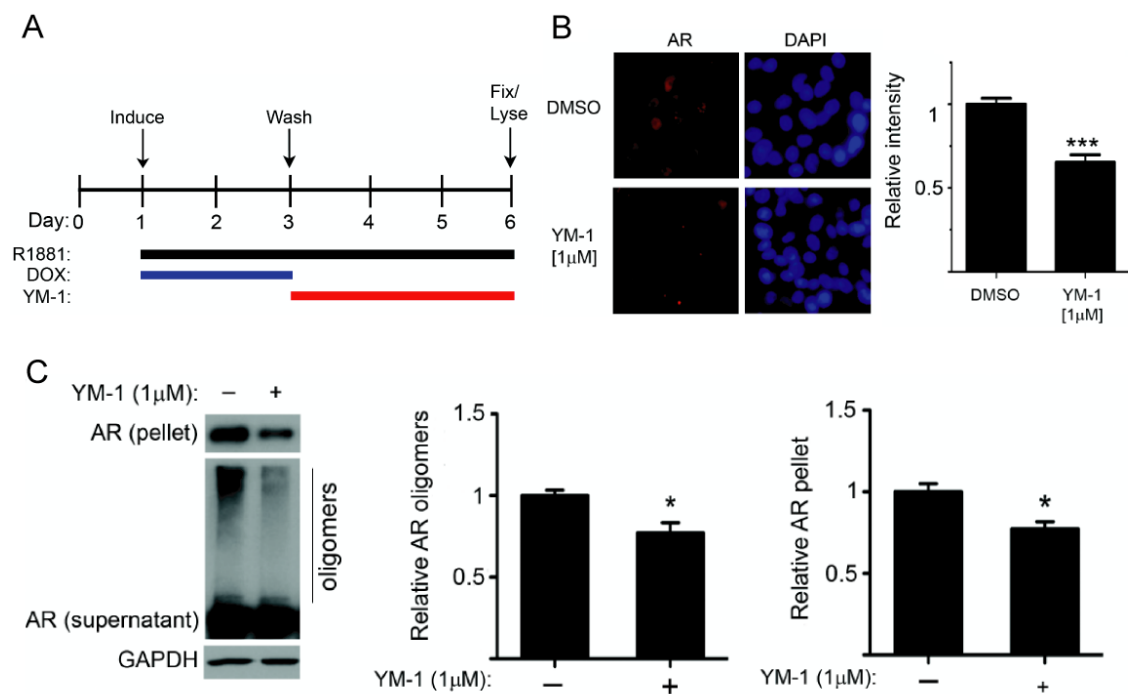


**Figure 4.18 YM1 promotes clearance of AR112Q.** (A) Experimental time-line for analysis of AR112Q degradation. PC12 cells were induced to express AR112Q in the presence of R1881 (10 nM) for 48 hr, then washed to remove doxycycline to turn off the transgene. Cells were incubated an additional 72 hr in the presence or absence of YM1. (B) YM1 promotes AR112Q clearance. Cells were treated as in (A) and stained for AR. Quantification of field signal intensity (right) shows significant decrease in the presence of YM1. \*\*\* $P < 0.001$  (C) YM1 promotes clearance of insoluble and oligomeric AR112Q. Lysates were prepared from cells treated as in (A). Immunoblot shows decreased AR112Q monomer in the 15,000 g pellet and diminished high MW oligomers in the soluble fraction after ultracentrifugation. Quantification of signal intensity at right (mean  $\pm$  SEM). \* $P < 0.05$

molecular weight oligomers that remained in the soluble fraction after ultracentrifugation (**Figure 4.18C**). These oligomers formed in a hormone-dependent manner and were detected only in cells expressing the polyQ AR (**Appendix 4.5.6**). The effects of YM1 were blocked by MG132 (**Figure 4.19A**), indicating that YM1 promoted proteasomal degradation of polyQ AR. Unlike Hsp90 inhibitors, such as geldanamycin, YM1 exerted these effects without increasing the expression of the stress-responsive molecular chaperones, such

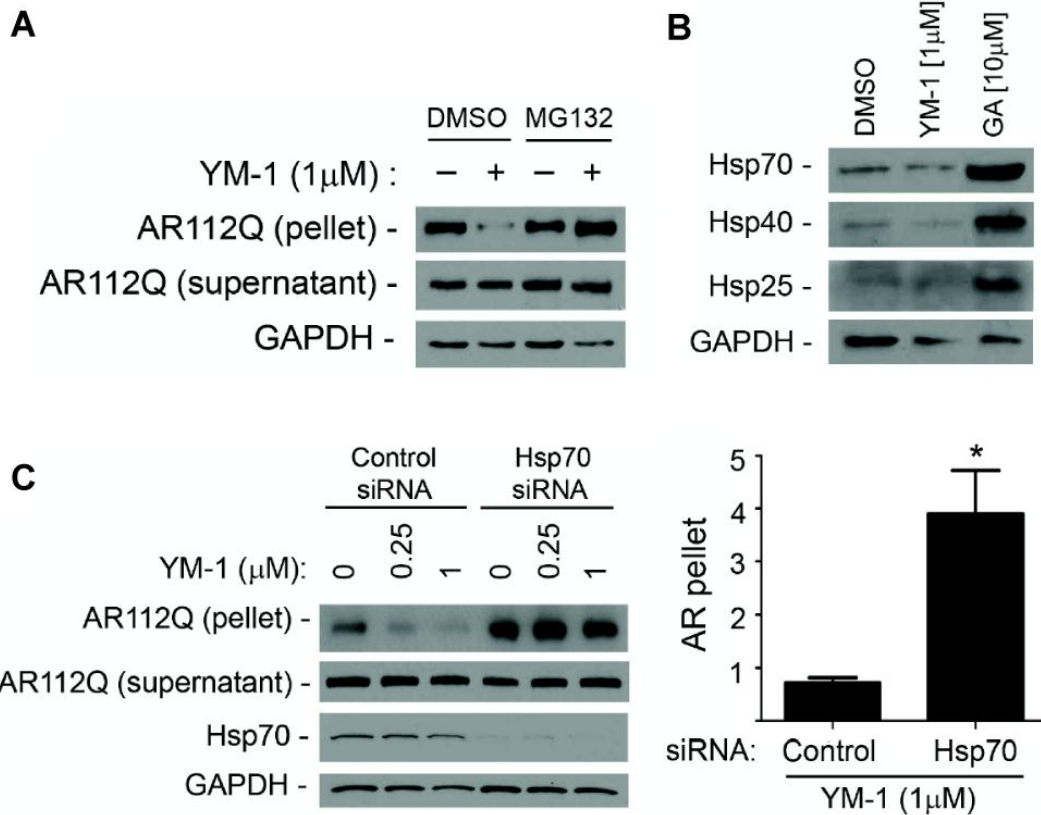


**Figure 4.19 YM1 promotes proteasomal degradation of AR112Q in an Hsp70 dependent manner.** (A) YM1 promotes AR112Q degradation. Immunoblot of AR112Q in supernatant and pellet shows that effects of YM1 are blocked by 24 hr treatment with MG132 (10  $\mu$ M). (B) YM1 does not induce a stress response. HeLa cells treated with vehicle, YM1, or geldanamycin (GA) for 24hr were probed for expression of inducible Hsp70, Hsp40, and Hsp25. (C) YM1 effects are dependent upon Hsp70. PC12 cells expressing tet-regulated AR112Q were transfected with siRNAs targeted at inducible Hsp70 or non-targeted control. Effects of YM1 on pelleted AR112Q are shown on left and quantified on right. \*P<0.05.



as Hsp70, Hsp40 or Hsp25 (**Figure 4.19B**). This result is consistent with our previous data showing that chemical modulators of Hsp70 do not induce a stress response (Chapter 3). Notably, the activity of YM1 was dependent on Hsp70, because siRNA knock-down reduced its potency (**Figure 4.19C**), further supporting this chaperone as its critical cellular target.

#### 4.2.13 YM1 rescues AR aggregation phenotype in *D. melanogaster*

We next wondered whether the reduced accumulation of polyQ AR observed in

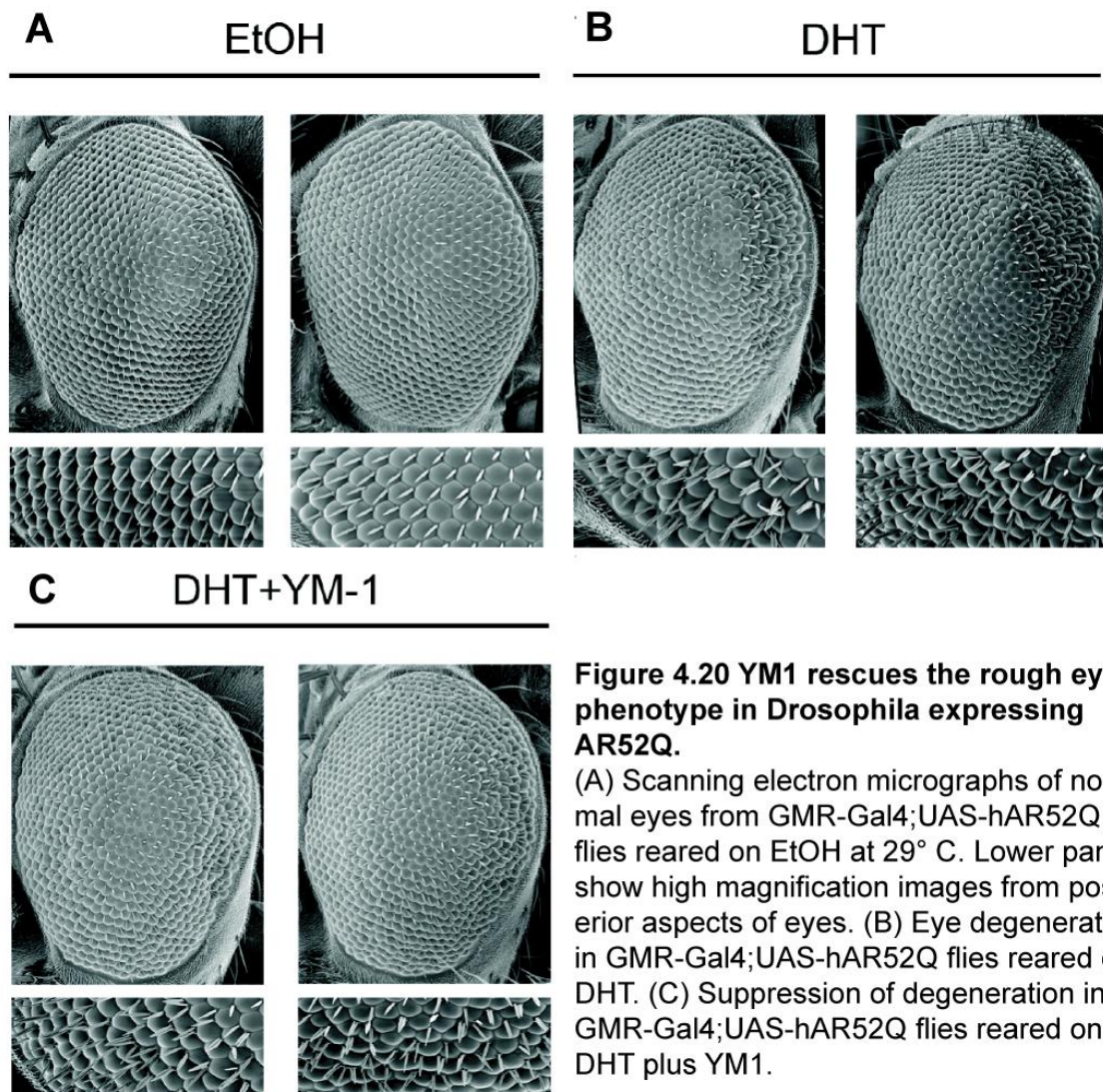


**Figure 4.20 YM1 rescues the rough eye phenotype in *Drosophila* expressing AR52Q.**

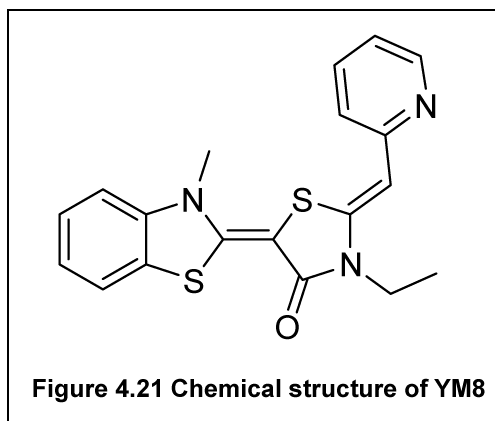
(A) Scanning electron micrographs of normal eyes from GMR-Gal4;UAS-hAR52Q flies reared on EtOH at 29° C. Lower panels show high magnification images from posterior aspects of eyes. (B) Eye degeneration in GMR-Gal4;UAS-hAR52Q flies reared on DHT. (C) Suppression of degeneration in GMR-Gal4;UAS-hAR52Q flies reared on DHT plus YM1.

cells would abrogate proteotoxicity in disease models. We turned to a *Drosophila melanogaster* model of SBMA in which the UAS/Gal4 system drives expression of a polyglutamine expanded human AR (hAR52Q) and AR aggregation is promoted by addition of dihydroxytestosterone (DHT) [19]. When hAR52Q was expressed by the eye-specific *GMR* promoter, flies exhibited a DHT-dependent rough eye phenotype characterized by ommatidial degeneration and extranumerary inter-ommatidial bristles, particularly in the posterior aspects of the eye (**Figures 4.20A&B**). We found that DHT-dependent eye degeneration in this line was relatively modest, and was partially rescued by rearing flies on YM1 (**Figure 4.20C**).

From these studies, we concluded that stabilizing the ADP-bound form of Hsp70, by either application of YM1 or over-expression of HiP, leads to enhanced proteasomal degradation of polyQ-expanded AR. This is an exciting result because, for the first time, it links a specific Hsp70 structure to a specific cellular outcome. Mechanistic work on this chemical series is being continued by Dr. Xiaokai Li in both the polyQ and tau systems.

#### 4.2.14 YM8 is BBB permeable

A key feature of any good chemical probe for Hsp70 is selectivity and potency. Moreover, to ask questions about proteostasis in animal models of



neurodegenerative disease, these ideal probes should be permeable to the blood-brain barrier (BBB). Encouraged by the initial results with MKT-077 and YM1, we next explored pharmacological properties of this rhodocyanine scaffold, with the goal of increasing BBB permeability, selectivity and potency.

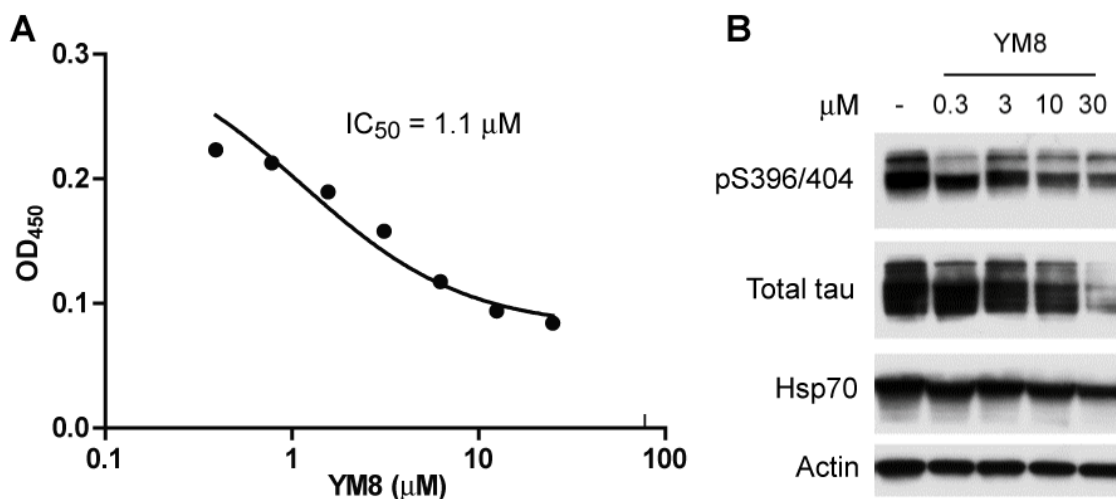
It has been shown that MKT-077 does not enter the CNS and it was suggested that its hydrophilic property and positive charge might prevent it from crossing the BBB [20]. Thus, we wondered whether removing the positive charge would improve BBB permeability. Moreover, we reasoned that this change would not impact binding to Hsp70 because the charged region was located in the solvent exposed area, based on our earlier NMR and docking studies. To test this idea, we synthesized a neutral version of MKT-077, YM8 (**Figure 4.21**), and investigated its distribution in CD-1 mice in collaboration with Duxin Sun's group (Univ. of Michigan, College of Pharmacy). Briefly, mice were injected intravenously with either YM1 or YM8 and their distribution was assessed after 10 and 60 minutes.

Strikingly, a large amount of YM8 was found in the brain after 10 minutes (**Table 4.1**). This was in contrast to YM1, which showed no distribution in the brain. Importantly, YM8

**Table 4.1 Distribution of YM1 and YM8 in CD-1 mice**

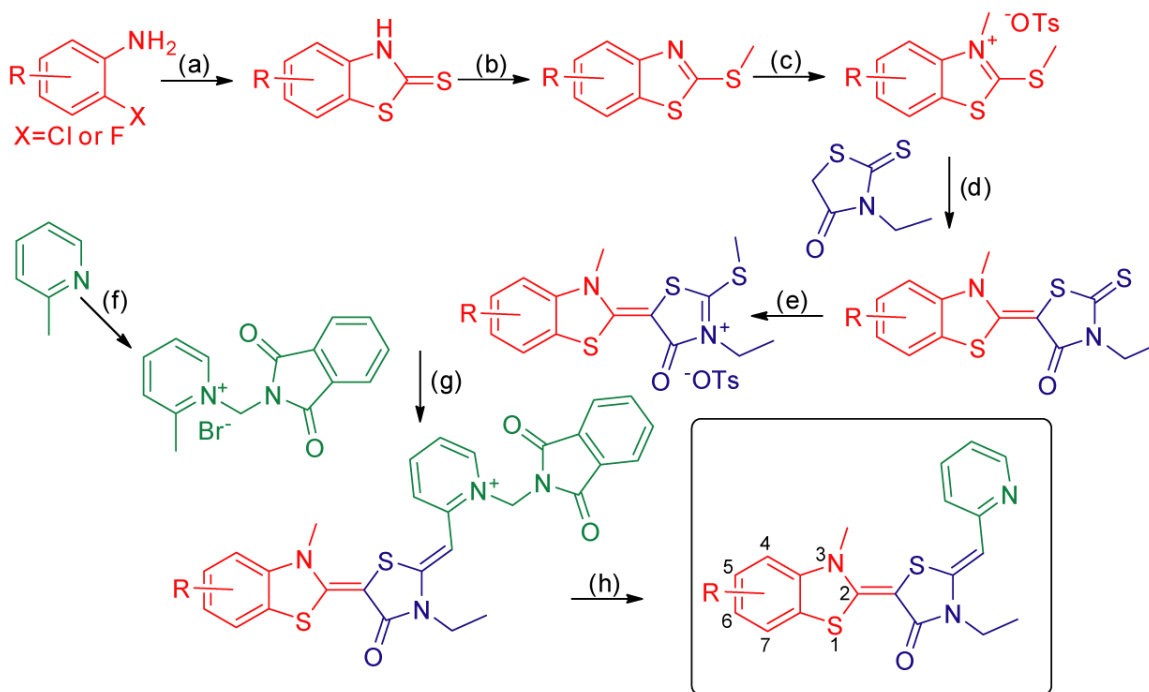
Time (min)	YM1 (20 mg/kg)		YM8 (10 mg/kg)	
	10	60	10	60
Plasma (ng/mL)	359	324	1600	14.8
Brain (ng/g)	0	0	23268	0
Liver (ng/g)	13472	5768	1453	124
Heart (ng/g)	38126	31205	50772	1814
Fat (ng/g)	9	99	332	349
Lung (ng/g)	10242	8333	290186	526171
Kidney (ng/g)	74378	63231	7232	55
Spleen (ng/g)	35868	19663	409	0





**Figure 4.22 YM8 competes with YM1-biotin and reduces tau levels. (A)** Experiments were carried out in triplicate. Data are mean  $\pm$  SEM. **(B)** YM8 reduces both phosphorylated and total tau levels in HeLaC3 cells.

retained its ability to bind Hsp70 shown by the ELISA-like assay using YM1-biotin and to reduce tau levels in cells (**Figure 4.22**). Further, these data suggest that neutral derivatives of MKT-077 are BBB permeable Hsp70 inhibitors.

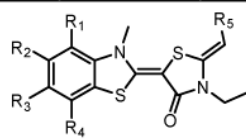
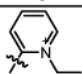
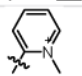
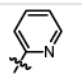
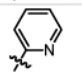
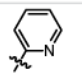
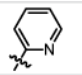
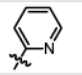
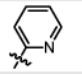
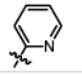
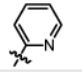
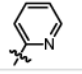
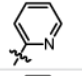
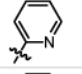
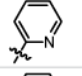
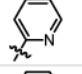
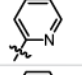
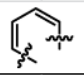
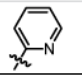


**Figure 4.23 Synthetic scheme for uncharged MKT-077 derivatives.** (a) potassium ethylxanthate, DMF, 140 °C, 4 h; (b) MeI, triethylamine, EtOH, 90 °C, 1 h; (c) p-TsOMe, anisole, 125 °C, 4 h; (d) triethylamine, MeCN, 25 °C, 4 h; (e) p-TsOMe, DMF, 135 °C, 3 h; (f) N-(bromomethyl)phthalimide, EtOH, 90 °C, 3 h; (g) triethylamine, MeCN, 70 °C, 3 h; (h) 30 % aqueous ammonium hydroxide, MeOH, 25 °C, 1 h.

## 4.2.15 Synthesis and evaluation of neutral MKT-077 derivatives

To further improve potency, we set out to build a library of neutral MKT-077

**Table 4.2 Chemical structures of neutral MKT-077 derivatives and their activity**

compound ID						YM1-biotin	DnaK-luciferase
	R <sub>1</sub>	R <sub>2</sub>	R <sub>3</sub>	R <sub>4</sub>	R <sub>5</sub>	IC <sub>50</sub> (μM)	EC <sub>50</sub> (μM)
MKT-077	H	H	H	H		12.4	n/a <sup>a</sup>
YM1	H	H	H	H		8.2	n/a <sup>a</sup>
YM8	H	H	H	H		1.3	1.4
1	F	H	H	H		5.5	n/a <sup>a</sup>
2	H	F	H	H		1.5	1.6 <sup>b</sup>
3	H	H	F	H		0.6	1.7
4	H	H	H	F		3.5	0.5
5	Cl	H	H	H		n/a <sup>a</sup>	1.7
6	H	Cl	H	H		n/a <sup>a</sup>	0.7
7	H	H	Cl	H		0.9	0.5
8	H	H	H	Cl		1.5	n/a <sup>a</sup>
9	H	H	NH <sub>2</sub>	H		2.8	> 25
10	H	H	NO <sub>2</sub>	H		>25	>25
11	H	H	CF <sub>3</sub>	H		n/a <sup>a</sup>	1.7
12	H	H	H	CF <sub>3</sub>		n/a <sup>a</sup>	4.6
13	H	OMe	H	H		2.8	n/a <sup>a</sup>
14			H	H		3.3	n/a <sup>a</sup>

<sup>a</sup> IC<sub>50</sub>/EC<sub>50</sub> could not be obtained due to artifacts

<sup>b</sup> Degree of stimulation was very weak

derivatives. General synthetic scheme is shown in **Figure 4.23**. Based on the docking model shown in **Figure 4.7**, we first focused on modifications at the benzothiazole moiety. Specifically, we synthesized compounds with halogen groups at C-4 ~ C-7 to explore the space around the ring, those with substitutions at C-6 to explore potential interactions with Asp206 and Ser208, and those with substitutions at C-1/C-2 to add a little diversity to the series. Subsequently, we tested them in ELISA-like YM1-biotin and DnaK-luciferase assays. The results are shown in **Table 4.2**. IC<sub>50</sub> and EC<sub>50</sub> values for some of the compounds could not be obtained (indicated as n/a) usually due to poor solubility. These two assays were complementary to each other in evaluating the collection and provided insight into structure-activity relationships. The data suggest that (1) electron withdrawing groups at R<sub>2</sub> and R<sub>3</sub> are favorable (2) substitutions at R<sub>3</sub> is better than those at R<sub>2</sub> and (3) chlorine has an optimum size for R<sub>3</sub> substitutions. Interestingly, C-5 and C-6 (see **Figure 4.23**) are known to be oxidized by cytochrome P450 *in vivo* [21,22]. Therefore, substitutions at these positions may improve not only affinity for Hsp70 but also *in vivo* stability. Next, we explored

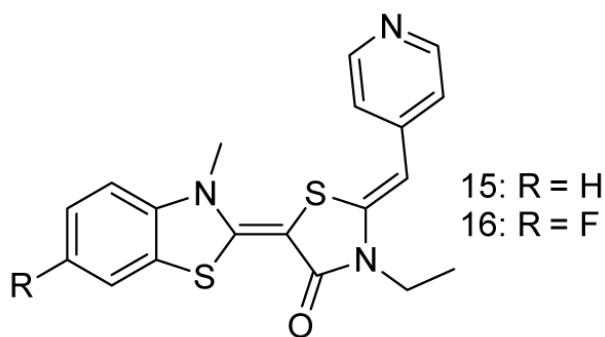


**Figure 4.24** Chemical structures of compounds **15** and **16**

whether the position of the nitrogen atom on the pyridine ring is important. We synthesize compounds **15** and **16** (**Figure 4.24**), and tested them in the same assay. Changing the

orientation of the pyridine ring altered compounds solubility and  $IC_{50}/EC_{50}$  values for compound **15** could not be obtained. Compound **16** showed  $IC_{50}$  and  $EC_{50}$  values of 22.7 and 7.7  $\mu M$ , respectively. These results suggest that having a nitrogen atom at *para* position to the methylene group significantly reduces the compounds'

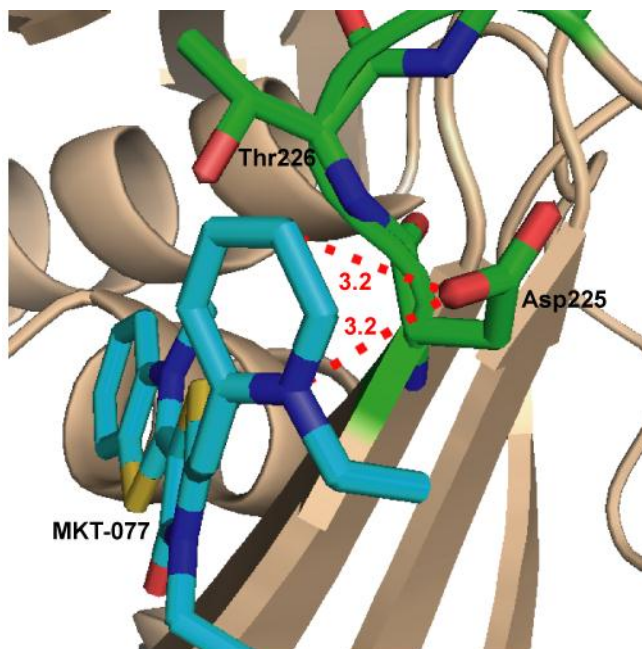


**Figure 4.25** Potential contacts between the pyridinium moiety of MKT-077 and Hsc70. Asp223 is in proximity to the quaternary nitrogen atom. Distances between the nitrogen and Asp223 are indicated in red (Å). Figure was prepared in PyMol.

activity and that the orientation of the pyridine ring in the original scaffold is critical. The model suggests that the quaternary nitrogen might have an electrostatic interaction with Asp223 (**Figure 4.25**). Interestingly, in this model, the “*para*” position would have the same distance from the aspartate. Thus, contributions from these potential contacts to the affinity would be expected to be similar. At this point, the apparent difference between “*ortho*” and “*para*” compounds in their affinity for Hsp70 cannot be explained based on our current model. We currently hypothesize that it is due to reduced solubility of *para* substituted derivatives.

## 4.3 Discussion

### 4.3.1 MKT-077 binds Hsp70 at an interface of two lobes and stabilizes its ADP form

Based on the literature suggesting Hsp70 as a major cellular target of the anti-cancer agent MKT-077, we set out to study the interaction between the compound and Hsc70 using NMR and computer simulations. TROSY spectra indicated that MKT-077 binds at the interface between lobe I and lobe II, which is immediately below the nucleotide binding pocket. Interestingly, it only bound the ADP-form of Hsc70 but not the ATP-form. The Zuiderweg laboratory recently showed that Hsp70 NBD subdomains change their relative orientations between the different allosteric states (**Appendix 4.5.3**) [11]. In detail, it was found (a) that the relative orientations of the subdomains of the *T. thermophilus* DnaK in the ADP state resemble, in solution, those of Hsc70 complexed with a nucleotide exchange factor as seen in a crystal and (b) that the relative orientations of the subdomains of the *T. thermophilus* DnaK in the AMP-PNP state resemble, in solution, those of Hsc70 NBD in crystal, irrespective of the latter's nucleotide state. In this context, the MKT-077 binding pocket is “open” in the ADP state and “closed” in the ATP state (**Appendix 4.5.3**), which is consistent with our observation that MKT-077 only binds to the ADP form of Hsp70. In addition, we found that MKT-077 actually stabilizes the ADP state and reduces tau levels in cells. These results suggest a new model of Hsp70 biology in which prolonged retention of substrates on Hsp70 promotes their degradation. This model needs further testing, but it suggests an exciting link between structure-and-function that

could significantly help the design and discovery of new Hsp70-targeted therapeutics.

#### **4.3.2 MKT-077 analogs serve as an artificial co-chaperone and promote clearance of AR112Q.**

It has been known that the co-chaperone Hip stabilizes the ADP-form of Hsp70, which has high affinity for substrates [23] and that Hip over-expression enhances clearance of misfolded polyglutamines [18]. Thus, we hypothesized that MKT-077 and its analogs might have similar effects on client proteins. To test this idea, we worked with Prof. Lieberman's group to explore the effects of Hip over-expression and YM1 treatment in models of SBMA. We showed that YM1 competes with Hip for binding to Hsp70 and they both prevent aggregation and promote proteasomal degradation of AR112Q in cells. Importantly, this effect was dependent on Hsp70. Further, YM1 suppressed disease phenotypes in a *Drosophila melanogaster* model of SBMA. Together, these results support the model that "dwell time" on Hsp70 impacts the fate of bound substrates (as discussed in Chapter 1). The critical off-rate of substrates is likely affected by many factors including the levels of the client, availability of co-chaperones and the intrinsic affinity of the substrate. Since MKT-077 derivatives force Hsp70 into high affinity conformation, they might represent useful tools in "tuning" Hsp70's affinity and studying this concept.

### **4.3.3 Structure-based design leads to the development of high-affinity MKT-077 derivative with BBB permeability.**

Small molecule therapeutics targeting the brain must be able to penetrate the BBB. Despite their potency in cells and in a *Drosophila* model, MKT-077 derivatives cannot be used as therapeutic agents or *in vivo* chemical probes for tauopathies or polyglutamine expansion disorders due to their lack of BBB permeability [20]. Because lipophilicity is one of the major factors that contributes to BBB partitioning, we hypothesized that removing the positive charge from the pyridine moiety might be beneficial. Indeed, a neutral analog of MKT-077/YM1, YM8, was found in mouse brain 10 minutes after intravenous injection (**Table 4.1**). In our biochemical assay, YM8 showed binding affinity for Hsp70 that is comparable to YM1. Our attempt to observe binding of YM8 to Hsc70 NBD by NMR was not successful likely due to the compound's poor solubility (data not shown). These findings led us to focus our next effort on improving the potency and solubility of neutral derivatives. Based on the docking structure, we designed and synthesized 16 derivatives and explored their structure activity relationships using two complementary biochemical assays. Although extensive medicinal chemistry efforts have been made on MKT-077 and analogous lipophilic cationic dyes as anti-cancer and anti-malarial agents, we found that there is still room for improvement particularly at the aromatic ring of benzothiazole moiety. Together, these results suggest that neutral MKT-077 analogs might represent promising leads for the treatment of tauopathy.

## **4.4 Materials and Methods**

### **4.4.1 Reagents and cell lines**

Unless otherwise specified, all reagents were purchased from Sigma (St. Louis, MO). HeLa cells were from the American Type Culture Collection. PC12 cells expressing tet-inducible forms of the AR were from Dr. Diane Merry (Thomas Jefferson University) [24]. Phenol red-free Dulbecco's modified Eagle's medium was from Invitrogen (Carlsbad, CA), charcoal-stripped calf serum was from Thermo Scientific Hyclone Products (Waltham, MA) and horse serum was from Invitrogen. Fugene 6 was from Roche (Indianapolis, IN), and DHT and MG132 were from Sigma (St. Louis, MO). Geldanamycin and the anti-72/73-kDa Hsp70 (N27F3-4), stress inducible Hsp70, Hsp40, Hsp25 and HIP antibodies were from Enzo Life Sciences (Plymouth Meeting, PA). The AR (N-20), FLAG, and GAPDH antibodies were from Santa Cruz Biotechnology (Santa Cruz, CA), Sigma, and Abcam (Cambridge, MA) respectively. The HRP-tagged secondary antibodies were from Biorad, and the Alexa Flour 594 and 488 conjugated secondary antibodies were from Invitrogen. Plasmid encoding Hip was from GeneCopoeia and modified by the addition of a triple FLAG tag. Hsp70 siRNAs were ON-TARGETplus SMART pool rat HSPA1A or non-targeting control (Dharmacon).

### **4.4.2 Protein preparation**

The plasmid for the expression of bovine Hsc70 NBD (100% identical with the human protein) was a generous donation by Dr. D. B. McKay (Stanford School of Medicine, Stanford, CA). It was expressed in *E. coli* strain BL21 (DE3). The cells



were inoculated from a freshly transformed Petri dish of a 2 mL LB culture, grown until  $OD_{600}=0.4$ , transferred to a 100 mL flask of M9 media, and grown until  $OD_{600}=0.4$  in order to increase the yield of the induction. Subsequently, the cells were centrifuged and transferred to a 1 L M9 medium containing 98%  $D_2O$ , 2 g/L protonated [ $^{13}C$ ] glucose, and 1 g/L  $^{15}NH_4Cl$ . The expression was induced by isopropyl- $\beta$ -D-thiogalactopyranoside to 0.5 mM at  $OD_{600}=0.8$ . Harvested cells were removed by centrifugation and disrupted mechanically by a French press. Cell debris was removed by centrifugation, and the supernatant was loaded onto a DEAE-52 column and eluted with 150 mM KCl. The Hsc70 fractions were dialyzed against 20 mM Hepes (pH 7.0)/25 mM KCl/10 mM ethylenediaminetetraacetic acid (EDTA). EDTA was precipitated by the addition of 25 mM  $MgCl_2$  in the dialyzed protein pool, yielding 5 mM free  $Mg^{2+}$ . The precipitate of (Mg) EDTA was removed by centrifugation. The supernatant was loaded onto an ATP-agarose affinity column and eluted with 3 mM ADP. The protein was concentrated by using Amicon concentrators. The protein was, at all times, stabilized with protein inhibitors and kept at 4 °C.

#### **4.4.3 NMR assignment**

For the assignment of the protein's NMR spectrum, we used a  $^{15}N,^{13}C,^2H$ -labeled 280  $\mu M$  Hsc70 NBD sample that contained 5 mM  $MgCl_2$ , 25 mM KCl, 20 mM Tris-HCl, 10 mM ADP, 5 mM  $K_3PO_4$ , 0.005% sodium azide, and 10% (vol/vol)  $D_2O$  (pH 7.2). The experiments were performed at 26 °C on an 800 MHz Varian Inova NMR spectrometer equipped with a triple-resonance cold probe. The

protein backbone resonances were assigned from three-dimensional HNCA, HN(CO)CA, HNCO, HN(CA)CO, HNCACB, and HN(CO)CACB TROSY data. All spectra were processed with NMR Pipe [25] and converted into SPARKY [26]. The SPARKY program was used to peakpick the spectra. The peak-pick lists were manually curated to obtain consistent NH root labeling throughout the different spectra. Assignments were made from these curated lists using the automatic assignment program SAGA [27]. Alternative assignments as produced by SAGA were evaluated and further checked using SPARKY. Only assignments of stretches of more than two connected spin systems were retained. By and large, they corresponded to the previous manual assignments for this protein domain [12].

The  $^1\text{H}$  spectrum of MKT-077 in  $\text{H}_2\text{O}$  was assigned using double quantum filtered – correlated spectroscopy and rotating frame Overhauser effect spectroscopy acquired on a 500-MHz Bruker Avance spectrometer. The rotating frame Overhauser effect spectroscopy spectra confirmed the trans configuration of the pyridinium ring and the nitrogen in the oxothiazolidine moiety over the double bond as shown in **Figure 4.1**.

#### **4.4.4 NMR titrations**

Hsc70 NBD samples of 80 – 240  $\mu\text{M}$  in 5 mM  $\text{MgCl}_2$ , 25mM KCl, 20 mM Tris-HCl, 10 mM ADP, 5 mM  $\text{K}_3\text{PO}_4$ , 0.005% sodium azide and 10% (vol/vol)  $\text{D}_2\text{O}$  (pH 7.2) were used for the titrations, using 4 mM solutions of MKT-077 in water (neutral pH) as titrant. The results of two titrations are reported here. Using a

sample of 80  $\mu\text{M}$   $^{15}\text{N}$ -labeled Hsc70 NBD, MKT-077 was added to ratios of 1:1 and 2:1. Duplicate TROSY spectra of 8 hours each were recorded for each titration step. Using a triple-labeled 270  $\mu\text{M}$  sample of Hsc70 NBD, MKT-077 was titrated to ratios of 0.25:1, 0.5:1, 0.75:1 and 1:1. Duplicate TROSY spectra of 4 hours each were recorded for each titration step. The shifts upon the addition of the drugs were manually recorded in SPARKY and were mapped on the crystal structure coordinates of Hsc70 NBD (3HSC.pdb) using Pymol [28].

#### **4.4.5 Docking computations**

AUTODOCK-4 [13] was used for the docking of MKT-077 to Hsc70 NBD. The initial structure for MKT-077 was minimized in Jaguar (Schrödinger, LLC) at the B3LYP/6-31G\* level. Standard charging methods within AUTODOCK leave MKT-077 uncharged. To obtain better charging models, we used the Antechamber [29] suite in AMBER [30]. In one round of computations, we use Gasteiger charging as afforded by Antechamber, and just added +1 to the charge of the pyridinium nitrogen. We also used AM1-BCC charges as computed in AMBER. AM1-BCC predicts considerable polarization over the remainder of the conjugated molecule which also seems more realistic than the charge pattern in Gasteiger in which polarization is absent. The AMBER-charged models were hand-edited into the AUTODOCK. pdbqt files.

All available crystal structures for the NBD of Hsc70 conform to the closed (ATP) state [11]. These structures cannot be used for docking because MKT-077 does not bind to this state. In absence of a “true” high-resolution structure for the open

ADP state, we chose one of the available crystal structures of Hsc70 in complex with a nucleotide exchange factor. According to the NMR analysis of a bacterial Hsp70 in the ADP and ATP state, Hsc70 in complex with a nucleotide exchange factor is a likely representation of the ADP state [11]. We chose Hsc70 in complex with yeast Hsp110 (3C7N.pdb [31]) as our model, because it is the only complex that contains ADP and Mg<sup>++</sup>. We discarded the coordinates of Hsp110 in the docking computations. In order to relieve possible strain exerted by crystal and/or Hsp110, the extracted Hsc70 NBD coordinates were relaxed using restrained minimization and equilibration in AMBER (see below). The coordinates of the equilibrated protein, including ADP and Mg<sup>++</sup> were used for the AUTODOCK runs.

The AUTODOCK gridbox was located on the interface of the four subdomains IA-IB-IIA-IIB with a 0.2 Å resolution. We used a Lamarckian genetic algorithm with the following parameters : the GA runs were set to 100, the size of the initial population to 1500, the maximum number of evaluations was set to long, the maximum number of top individuals that automatically survive was set to 1, the rate of gene mutation was set to 0.02, the rate of crossover was 0.8, the GA crossover mode was twopt, the mean of Cauchy distribution for gene mutation was set to 0, the variance of Cauchy distribution for gene mutation was set to 1 and the number of generations for picking worst individuals was set to 10. The calculations were performed on a Macintosh computer. The docked structures were clustered and evaluated by hand using Pymol.

#### 4.4.6 Molecular dynamics

The crystal structure coordinates of Hsc70 in complex with yeast Hsp110, ADP,  $\text{SO}_4^{2-}$  and  $\text{Mg}^{++}$  ions (3C7N.pdb) were used as a starting point. The coordinates of Hsp110 and  $\text{SO}_4^{2-}$  ions were removed. The NBD, ADP and Mg coordinates were minimized in 1000 steps using a hybrid forcefield (ff99SB for the protein, gaff for metal ions and a gaff-derived forcefield [32] for ADP) in the Amber 11 program suite [30]. The coordinates were restrained to the X-ray coordinates with a force constant of  $5 \text{ kcal/Mol/\AA}^2$ . Subsequently we carried out a molecular Langevin dynamics equilibration run in implicit generalized Born solvent with 0.1 M ionic strength, running from 0 - 300 K over 10 ps. The same hybrid forcefield was used. The dynamics equilibration was restrained by 940 CA-CA distances in the 2-5 Å range, 2952 CA-CA distances in the 10-20 Å range, and 742 restraints between protein CA atoms and all atoms of ADP and  $\text{Mg}^{++}$  in the 1-15 Å range. The restraints had as lower bounds the actual distances as computed from the PDB file, and as upper bounds the actual distance + 1 Å, enforced by a parabolic potential of  $20 \text{ kcal/Mol/\AA}^2$ . The calculations were performed on an Apple MacBookPro5.1 computer equipped with a 64-bit 2.4 GHz Intel Core 2 Duo processor, running Mac OS X10.6.6.

#### 4.4.7 Docking evaluation

The AUTODOCK solutions with “energies” of 7.03, 6.32, 5.36 and 5.25 kcal/M were evaluated using AMBER (vs. 11) in the following way. Hydrogen-atoms were re-attached to the coordinates of the docked MKT-077 molecules and the

double and aromatic bonds were reassigned in the Pymol Builder module. These coordinates were converted to AMBER .prepi and forcefield modification files using the Amber Antechamber suite. We used AM1-BCC charging for MKT-077. In order to carry out a proper MD-based binding energy evaluation, it is necessary to run the simulations using explicit solvation. For a molecule the size of Hsc70 NBD (380 residues) such computations become too time consuming for our labs, which do not have access to specialized super computers. Hence, we decided to carry out restrained MD simulations on a docking site consisting of Hsc70 residues 12-13 + 69-83 + 143-158 + 172-177 + 196-211 + 219-229 + 316-323 and the Mg<sup>++</sup> ion, which was extracted from the equilibrated pdb files (see **Appendix 4.5**). Four different docked MKT-077 poses, corresponding to the best members of each of the four families shown in **Figure 4.7**, were added to the site (not simultaneously). Identical protocols were followed for the four computational series. The “complexes” were solvated with ~6500 TIP3P waters in a 12 Å<sup>3</sup> periodic box. After a minimization step, a molecular dynamics temperature ramp running from 0 - 300 K over 50 ps was carried out. The same hybrid force field was used as described above. This run was restrained by 3790 restraints between N, HN, CA, C' and O backbone atoms of the reduced binding site, 55 Mg<sup>++</sup> - CA restraints, and ~2600 MKT - CA restraints based on the minimized structure (depending on family member). All restraints were defined within a 1.0 Å range and enforced with a 20 Kcal/Mol/Å<sup>2</sup> gradient. Subsequently, a density equilibration (for 50 ps, with pressure relaxation time of 1 ps) and general equilibration (for 100 ps, with pressure relaxation time of 2 ps) with the

same restraints followed. These equilibration steps were followed by a production run of 250 ps restrained MD computations at 300 K. In the production runs, the MKT restraints were removed, while all others remained.

The binding enthalpies were calculated using the MM-GB/PBSA protocol [13] as implemented in the Amber 11 release, using 100 frames of the last 50 ps of the molecular dynamics production runs. The calculations were performed on an Apple MacBookPro5.1 computer equipped with a 64-bit 2.4 GHz Intel Core 2 Duo processor, running MacOS X10.6.6.

#### **4.4.8 Partial proteolysis**

The partial proteolysis protocol was adapted from a previously described method [33]. Briefly, Hsc70 (6  $\mu$ M) in 40 mM HEPES buffer (20 mM NaCl, 8 mM MgCl<sub>2</sub>, 20 mM KCl, 0.3 mM EDTA, pH 8.0) was incubated with 1 mM nucleotide (ADP or ATP), either a buffer control or compound (200  $\mu$ M) and a J-domain (residues 2-108, 24  $\mu$ M) when noted. Samples were incubated at room temperature for 30 minutes. The trypsin (SIGMA Ec 3.4.2.1.4) was added to a final concentration of 0.9  $\mu$ M and the samples were incubated for another 30 minutes at room temperature. The reaction was then quenched with the addition of 25  $\mu$ l of 3x SDS loading buffer (240 mM Tris, 6 % w/v SDS, 30 % v/v glycerol, and 16 % v/v  $\beta$ -mercaptoethanol, 0.6 mg/ml bromophenol blue, pH 6.8) and heated to 95 °C for 3 minutes. Bands were separated by 12 % SDS-PAGE and stained with Coomassie blue.

#### **4.4.9 Luciferase binding assay**

Binding of Hsp70 to immobilized firefly luciferase was performed as described in Chapter 2. YM1 was added from a stock solution of 2.5 mM and diluted to a final DMSO concentration of 4%. All results were compared to an appropriate solvent control. Experiments were performed in triplicate.

#### **4.4.10 Hip competition binding assay**

Human Hsp72 and Hip were purified as previously described [33,34] and the Hsp70-binding assay was carried out using an adaptation of a previously described assay (Chapter 2). Briefly, Hsp72 (2.3  $\mu$ M) was immobilized on ELISA plates (ThermoFisher brand, clear, non-sterile, flat bottom). The treated wells were pre-incubated with Hip (0 – 6  $\mu$ M) for 5 min prior to addition of biotin-labeled YM1. The labeled probe was incubated in the wells for 2 hrs at room temperature, followed by three washes with 150  $\mu$ L TBST and incubation with 100  $\mu$ L 3% BSA in TBST for 5 min. The BSA solution was discarded and the wells were incubated with streptavidin-horseradish peroxidase for 1 hr. Following three additional washes with TBST, the wells were incubated with 100  $\mu$ L TMB substrate (Cell Signaling Technology, Danvers, MA) for 30 min. After addition of stop solution, the absorbance was read in a SpectraMax M5 plate reader at 450 nm. Results were compared to control wells lacking Hsp70. Experiments were performed in triplicate and at least two independent trials were performed for each condition.



#### **4.4.11 Cell culture and transfection**

HeLa cells were grown in phenol red-free DMEM supplemented with 10% charcoal/dextran-stripped fetal calf serum. Cells were transfected with 3  $\mu$ L Fugene 6 and 1  $\mu$ g DNA. Twenty four hours post-transfection, cells were pooled and replated, then treated as indicated. PC12 cells were grown in phenol red-free DMEM supplemented with 5% charcoal/dextran-stripped fetal calf serum, 10% charcoalstripped horse serum, G418 (Gibco) and hygromycin B (Invitrogen). AR expression was induced with 0.5  $\mu$ g/mL doxycycline (Clontech). PC12 cells were transfected by electroporation with the Lonza Nucleofector kit. HEK293 cells were grown in DMEM and transfected using  $\text{Ca}^{2+}$ -phosphate.

#### **4.4.12 Analysis of protein expression**

Cells were washed with PBS, harvested, and lysed by sonication in RIPA buffer containing phosphatase and proteinase inhibitors. For analysis of oligomers, cells were lysed in high salt lysis buffer (20mM Hepes, pH 7.5, 400mM NaCl, 5 mM EDTA, 1 mM EGTA, 1% NP-40). Lysates were centrifuged at 4°C for 15 min at 15,000 g and protein concentration was determined by a BCA protein assay. Samples for oligomer analysis were subjected to ultracentrifugation at 100,000 g for 30 min at 4°C. Protein samples were electrophoresed through 10% SDS-polyacrylamide or 4%-20% gradient gels and transferred to nitrocellulose membranes using a semi-dry transfer apparatus. Immunoreactive proteins were detected by chemiluminescence. Signal intensity was normalized to GAPDH, and densitometric analysis was performed using ImageJ (NIH).

#### **4.4.13 Immunofluorescence**

PC12 cells were transfected with 3xFLAG-Hip as indicated. Following induction and small molecule treatment, cells were fixed, stained and mounted using Vectashield mounting medium with DAPI (Burlingame, CA). Fluorescence images were captured using a Zeiss Axio Imager.Z1 microscope, and nuclear signal intensity was quantified by ImageJ (NIH). Data are from at least 3 fields per condition in 3 experiments. Confocal microscopy was performed using a Zeiss LSM 510-META Laser Scanning Confocal Microscopy system.

#### **4.4.14 Drosophila stocks and phenotypes**

The following strains were used in this study: White Canton-S (wild type), BG380-Gal4 [35], GMR-Gal4 [36], OK371-Gal4 [37], HIPEY14563 (Bloomington), HIP-REY01382 (Bloomington). UAS-hAR52Q flies were provided by Ken-ichi Takeyama [19]. Drosophila stocks were maintained on standard cornmeal agar media at 25°C and experimental flies were kept at 29°C. Food was supplemented with 1 mM DHT, 1 mM YM1, or vehicle controls once cooled to <50°C. The eclosion phenotype was scored by marking existing pupal cases at 10 days post addition of parents. Following 7 days at 29°C, the percentage of marked pupal cases that failed to eclose was determined for 200-800 flies of each condition. Scanning electron micrographs were captured by the University of Michigan Microscopy & Image Analysis Core on 1 - 2 day old GMRGal4; UAS-hAR52Q flies reared on food supplemented as indicated.

#### **4.4.15 Statistics**

Statistical significance was assessed by ANOVA with Newman-Keuls multiple comparison test, or unpaired Student's *t*-test using the software package Prism 5 (GraphPad Software). *P* values less than 0.05 were considered significant.

#### **4.4.16 Pharmacokinetic sampling**

Female CD-1 mice (25-30 g in body weight) were purchased from Charles River Laboratories (Wilmington, MA). Mice were treated with 6 mg/kg YM8 through the tail-vein injection. The plasma and tissues (brain, heart, liver, lung, spleen, kidney, intestine, fat and muscle) were collected at 0.016, 0.08, 0.16, 0.25, 0.5, 1, 2, 4, 6, 13, 18, 24 and 48h after drug administration. Whole blood samples were drawn through the cardiac puncture using a heparinized syringe with a 22 gauge needle, followed by centrifugation at 3,000 g for 10min at 4°C to obtain plasma. Collected tissues were washed with PBS, immediately frozen using liquid nitrogen, and stored at -80 °C until further analysis. For urine and feces analysis, mice were placed in metabolism chambers to collect urine and feces at 18, 24 and 48h post-administration of YM8. Collected samples were stored at -80 °C until further analysis.

#### **4.4.17 Extraction of YM8**

Tissue and feces homogenates were prepared by adding PBS (1:5 w/v, homogenate/PBS) and homogenized for 3 min. Urine was also diluted with PBS (1:5 w/v, homogenate/PBS) without homogenization. YM8 was extracted from

100  $\mu$ l aliquot of samples by adding 300  $\mu$ l of acetonitrile containing 50 ng/ml IS, followed by vortexing for 3 min. The supernatant was collected and subjected to LC-MS/MS analysis.

#### **4.4.18 LC-MS/MS analysis**

The separation of YM8 and internal standard was performed using Agilent 1200 HPLC system (Agilent Technologies, Santa Clara, CA) and Zobax SB-C18 column (2.1  $\times$  50 mm, 3.5  $\mu$ m) (Agilent Technologies). The compounds were eluted with a fixed gradient of 20% water with 0.1%(v/v) glacial acetic acid and 80% of acetonitrile with 0.1%(v/v) glacial acetic acid. After injecting 10  $\mu$ l of samples into HPLC system, the elution was performed over 2 min at a flow rate of 0.4 ml/min. The YM8 and MKT-077 eluents were detected using QTRAP 3200 mass spectrometer (Applied Biosystems/MDS Sciex, Foster City, CA) equipped with an electrospray ionization source (ESI). The temperature of ESI was set at 650°C and curtain gas, gas 1, and gas 2 were set to 30, 50, and 50 units, respectively. A positive voltage at 5500 V was applied through ESI to convert the eluents to ions in the form of  $MH^+$ . The ions were detected using a MRM mode. The ion transitions from the precursor ion ( $m/z$  368) to the fragment ion ( $m/z$  =222) and from the precursor ion ( $m/z$  396) to the fragment ion ( $m/z$ =175) were used to detect YM8 and IS, respectively.

#### **4.4.19 Calibration standards of YM8 for LC-MS/MS analysis**

Eight stock solutions of YM8 ranging from 50-50,000 ng/ml were prepared in

acetonitrile. Then, eight calibration standards, ranging from 5 to 5,000 ng/ml, were prepared for each sample origin by spiking 10  $\mu$ l of stock solution into 90  $\mu$ l of plasma blanks or homogeneous tissue blanks, including brain, heart, lung, liver, spleen, kidney, fat, muscle, urine, or feces. YM8 was extracted from an aliquot of homogenate (100  $\mu$ l) by adding 300  $\mu$ l of acetonitrile containing 50 ng/ml IS, followed by vortexing for 3 min. The supernatant was collected and subjected to LC-MS/MS analysis. For each tissue, the ratio of AUC of YM8 to AUC of IS versus the concentration of YM8 was used to generate a standard curve, through which an unknown YM8 concentration in samples was determined.

#### **4.4.20 Pharmacokinetic analysis**

The plasma concentration data were analyzed by compartmental pharmacokinetic analysis using WinNonlin software (Pharsight). Akaike Information Criterion (AIC) was used as measures of goodness of fit based on maximum likelihood for the PK models.

#### **4.4.21 Plasma protein binding**

A protein plasma binding assay was conducted using Rapid Equilibrium Dialysis (RED) device (Pierce). The experiment was performed according to the protocol provided by the manufacturer. In brief, 200  $\mu$ l aliquot of plasma sample containing 5  $\mu$ M of YM8 was added into the sample chamber and 350  $\mu$ l of buffer was added to the buffer chamber. The buffer membrane with a cutoff of 8,000 kD was placed in between two chambers. After covering the chambers with a gas-

permeable membrane, the sample was placed on a shaker and incubated at 37 °C for 4hrs. At the end of incubation, 50 µl were aspirated from both sample and a buffer chamber. The extraction of YM8 from performed by adding 150 µl of ice-cold acetonitrile containing 50 ng/ml of IS in to the aspirate. After centrifugation at 14,000 rpm for 5 min, supernatants were collected and subjected to LC-MS/MS analysis. The unbound fraction was calculated according to equation 1:

$$\% \text{ bound} = 100 - \left( \frac{\text{amount of YM8 in bufer}}{\text{amunt of YM8 in plasma}} \right) \times 100 \quad (1)$$

where the amount of YM8 was defined as the ratio of YM8 peak area to IS peak area.

#### 4.4.22 Synthesis of MKT-077 and YM1

MKT-077 and YM1 were synthesized as previously described [38].

YM1: <sup>1</sup>H δ (DMSO) 8.67 (1H, d, *J* = 6.3 Hz), 8.26 (1H, t, *J* = 8.2 Hz), 8.04 (1H, d, *J* = 8.6 Hz), 7.87 (1H, d, *J* = 7.8 Hz), 7.61 (1H, d, *J* = 8.2 Hz), 7.49 (1H, t, *J* = 7.4 Hz), 7.42 (1H, t, *J* = 7.4 Hz), 7.30 (1H, t, *J* = 7.4 Hz), 5.96 (1H, t), 4.14 (3H, s), 4.10, (2H, q, *J* = 7.4, 6.7 Hz), 4.04 (3H, s), 1.26 (3H, t, *J* = 6.7 Hz). <sup>13</sup>C δ (DMSO) 163.80, 154.42, 150.60, 150.51, 145.33, 142.67, 140.33, 127.01, 125.61, 123.53, 122.80, 122.06, 118.69, 111.72, 84.19, 78.26, 45.18, 38.23, 34.48, 11.87.

#### 4.4.23 Synthesis of biotinylated YM1 probes

YM1-biotin and Biotin-YM1 were synthesized by coupling of corresponding aminated YM1 derivatives and 6-((Biotinoyl)amino)hexanoic acid using standard peptide coupling methods.

YM1-biotin:  $^1\text{H}$   $\delta$  (DMSO) 8.57 (1H, d,  $J = 6.9$  Hz), 8.27 (2H, m), 8.06 (1H, d,  $J = 9.5$  Hz), 7.86 (1H, d,  $J = 7.8$  Hz), 7.77 (1H, m), 7.61 (1H, d,  $J = 8.1$  Hz), 7.48 (1H, t,  $J = 6.9$  Hz), 7.43 (1H, t,  $J = 6.4$  Hz), 7.29 (1H, t,  $J = 7.8$  Hz), 6.42 (1H, s), 6.37 (1H, s), 6.18 (1H, s), 4.60 (2H, m), 4.29 (1H, t,  $J = 5.4$  Hz), 4.17 (2H, m), 4.11 (1H, m), 4.04 (3H, s), 3.53 (2H, m), 3.08 (1H, m), 2.97 (2H, dd,  $J = 6.1, 5.4$  Hz), 2.80 (1H, d,  $J = 4.7, 12.0$  Hz), 2.03 (4H, m), 1.59 – 1.23 (16H).

Biotin-YM1:  $^1\text{H}$   $\delta$  (DMSO) 8.65 (1H, d,  $J = 6.4$  Hz), 8.24 (1H, t,  $J = 7.8$  Hz), 8.15 (1H, s), 8.02 (1H, d,  $J = 8.3$  Hz), 7.76 (2H, m), 7.57 (2H, m), 7.40 (1H, t,  $J = 5.9$  Hz), 6.42 (1H, s), 6.36 (1H, s), 5.94 (1H, s), 4.29 (1H, m), 4.18 – 4.06 (6H), 4.01 (3H, s), 3.08 (1H, m), 3.02 (2H, m), 2.81 (1H, dd,  $J = 4.9, 11.7$  Hz), 2.31 (2H, t,  $J = 6.9$  Hz), 2.03 (2H, t,  $J = 7.3$  Hz), 1.65 – 1.18 (16H).

#### 4.4.24 Synthesis of neutral MKT-077 derivatives

Synthetic procedure of neutral MKT-077 derivatives have been previously described [39]. See **Figure 4.23** for the general procedure.

YM8:  $^1\text{H}$  NMR (400 MHz, dmso)  $\delta$  8.53 (d,  $J = 3.7$  Hz, 1H), 7.66 (m, 2H), 7.35 (d,  $J = 8.9$  Hz, 2H), 7.22 (m, 1H), 7.14 (d,  $J = 6.6$  Hz, 1H), 6.95 (s, 1H), 6.18 (s, 1H), 3.96 (s, 1H), 3.89 (d,  $J = 6.9$  Hz, 1H), 1.20 (t,  $J = 6.6$  Hz, 3H).

Compound 1:  $^1\text{H}$  NMR (401 MHz, dmso)  $\delta$  8.52 (d,  $J = 4.4$  Hz, 1H), 7.63 (dd,  $J = 10.6, 4.7$  Hz, 1H), 7.49 (d,  $J = 7.6$  Hz, 1H), 7.18 (m, 3H), 6.96 (m, 1H), 6.23 (s, 1H), 4.05 (s, 3H), 3.90 (q,  $J = 7.1$  Hz, 2H), 1.20 (t,  $J = 7.0$  Hz, 3H).

Compound **2**:  $^1\text{H}$  NMR (401 MHz, dmsO)  $\delta$  8.54 (s, 1H), 7.64 (d,  $J = 10.0$  Hz, 2H), 7.28 (dd,  $J = 25.2, 8.1$  Hz, 2H), 6.97 (d,  $J = 15.1$  Hz, 2H), 6.21 (s, 1H), 3.91 (d,  $J = 18.1$  Hz, 5H), 1.20 (s, 3H).

Compound **3**:  $^1\text{H}$  NMR (500 MHz, dmsO)  $\delta$  8.52 (d,  $J = 4.3$  Hz, 1H), 7.63 (m, 2H), 7.31 (dd,  $J = 8.8, 4.1$  Hz, 1H), 7.21 (m, 2H), 6.94 (m, 1H), 6.18 (s, 1H), 3.93 (s, 3H), 3.88 (q,  $J = 6.9$  Hz, 2H), 1.19 (t,  $J = 6.9$  Hz, 3H).

Compound **4**:  $^1\text{H}$  NMR (401 MHz, dmsO)  $\delta$  8.54 (d,  $J = 4.8$  Hz, 1H), 7.64 (td,  $J = 7.8, 1.7$  Hz, 1H), 7.39 (dd,  $J = 8.2, 5.8$  Hz, 1H), 7.26 (d,  $J = 8.0$  Hz, 1H), 7.19 (d,  $J = 8.2$  Hz, 1H), 7.04 (t,  $J = 8.7$  Hz, 1H), 6.96 (dd,  $J = 6.8, 5.4$  Hz, 1H), 6.23 (s, 1H), 3.95 (s, 3H), 3.90 (dd,  $J = 14.1, 7.0$  Hz, 2H), 1.21 (t,  $J = 7.0$  Hz, 3H).

Compound **5**:  $^1\text{H}$  NMR (400 MHz, dmsO)  $\delta$  8.54 (d,  $J = 4.2$  Hz, 1H), 7.64 (m, 2H), 7.36 (d,  $J = 8.0$  Hz, 1H), 7.27 (d,  $J = 8.0$  Hz, 1H), 7.14 (t,  $J = 7.8$  Hz, 1H), 6.98 (m, 1H), 6.26 (s, 1H), 3.99 (s, 3H), 3.91 (m, 2H), 1.21 (t,  $J = 6.9$  Hz, 3H).

Compound **6**:  $^1\text{H}$  NMR (401 MHz, dmsO)  $\delta$  8.55 (d,  $J = 4.3$  Hz, 1H), 7.65 (m, 2H), 7.46 (s, 1H), 7.25 (d,  $J = 8.0$  Hz, 1H), 7.18 (d,  $J = 8.2$  Hz, 1H), 6.95 (m, 1H), 6.22 (s, 1H), 3.90 (m, 5H), 1.20 (t,  $J = 7.0$  Hz, 3H).



Compound 7:  $^1\text{H}$  NMR (400 MHz, dmso)  $\delta$  8.53 (d,  $J = 4.9$  Hz, 1H), 7.80 (d,  $J = 2.1$  Hz, 1H), 7.62 (m, 1H), 7.37 (dd,  $J = 8.7, 2.1$  Hz, 1H), 7.30 (d,  $J = 8.8$  Hz, 1H), 7.24 (d,  $J = 8.0$  Hz, 1H), 6.95 (ddd,  $J = 7.3, 5.0, 1.0$  Hz, 1H), 6.19 (s, 1H), 3.92 (s, 3H), 3.89 (d,  $J = 7.1$  Hz, 2H), 1.20 (t,  $J = 7.1$  Hz, 3H).

Compound 8:  $^1\text{H}$  NMR (400 MHz, dmso)  $\delta$  8.53 (s, 1H), 7.64 (t,  $J = 7.7$  Hz, 1H), 7.38 (t,  $J = 8.1$  Hz, 1H), 7.25 (m, 4H), 6.96 (s, 1H), 6.23 (s, 1H), 3.92 (m, 6H), 1.21 (t,  $J = 6.7$  Hz, 3H).

Compound 9:  $^1\text{H}$  NMR (400 MHz, dmso)  $\delta$  8.51 (d,  $J = 3.9$  Hz, 4H), 7.60 (t,  $J = 7.2$  Hz, 1H), 7.22 (d,  $J = 7.0$  Hz, 4H), 7.08 (d,  $J = 8.9$  Hz, 1H), 6.91 (m, 1H), 6.86 (s, 1H), 6.65 (d,  $J = 7.8$  Hz, 1H), 6.12 (s, 3H), 3.88 (s, 10H), 1.19 (t,  $J = 7.0$  Hz, 1H).

Compound 10:  $^1\text{H}$  NMR (401 MHz, dmso)  $\delta$  8.61 (s, 1H), 8.55 (d,  $J = 5.4$  Hz, 1H), 8.21 (dd,  $J = 9.4, 2.1$  Hz, 1H), 7.65 (t,  $J = 7.6$  Hz, 1H), 7.43 (d,  $J = 9.4$  Hz, 1H), 7.27 (d,  $J = 7.7$  Hz, 1H), 6.98 (m, 1H), 6.27 (s, 1H), 3.99 (s, 3H), 3.92 (m, 2H), 1.21 (t,  $J = 6.9$  Hz, 3H).

Compound 11:  $^1\text{H}$  NMR (400 MHz, dmso)  $\delta$  8.54 (d,  $J = 4.1$  Hz, 1H), 8.11 (s, 1H), 7.65 (ddd,  $J = 9.2, 8.6, 5.2$  Hz, 2H), 7.45 (d,  $J = 8.5$  Hz, 1H), 7.26 (d,  $J = 8.0$  Hz, 1H), 6.96 (m, 1H), 6.23 (s, 1H), 3.97 (s, 3H), 3.91 (q,  $J = 7.0$  Hz, 2H), 1.21 (t,  $J = 7.0$  Hz, 3H).

Compound **12**:  $^1\text{H}$  NMR (400 MHz, dms $\text{o}$ )  $\delta$  8.55 (d,  $J = 4.4$  Hz, 1H), 7.76 (d,  $J = 7.5$  Hz, 1H), 7.60 (m, 3H), 7.48 (d,  $J = 7.2$  Hz, 1H), 7.26 (d,  $J = 7.9$  Hz, 1H), 6.97 (m, 1H), 6.25 (s, 1H), 3.97 (s, 3H), 3.90 (m, 3H), 1.21 (t,  $J = 6.9$  Hz, 3H).

Compound **13**:  $^1\text{H}$  NMR (401 MHz, dms $\text{o}$ )  $\delta$  8.54 (d,  $J = 4.9$  Hz, 1H), 7.62 (td,  $J = 7.8, 1.8$  Hz, 1H), 7.54 (d,  $J = 8.5$  Hz, 1H), 7.24 (d,  $J = 8.0$  Hz, 1H), 6.94 (t,  $J = 5.6$  Hz, 2H), 6.77 (dd,  $J = 8.5, 2.2$  Hz, 1H), 6.17 (s, 1H), 3.95 (s, 3H), 3.89 (q,  $J = 7.1$  Hz, 2H), 3.83 (s, 3H), 1.20 (t,  $J = 7.0$  Hz, 3H).

Compound **14**:  $^1\text{H}$  NMR (500 MHz, dms $\text{o}$ )  $\delta$  8.55 (d,  $J = 4.4$  Hz, 1H), 8.45 (d,  $J = 8.5$  Hz, 1H), 8.03 (d,  $J = 8.0$  Hz, 1H), 7.79 (q,  $J = 8.5$  Hz, 2H), 7.63 (m, 2H), 7.55 (t,  $J = 7.3$  Hz, 1H), 7.28 (d,  $J = 7.9$  Hz, 1H), 6.98 (t,  $J = 5.8$  Hz, 1H), 6.25 (s, 1H), 4.21 (s, 3H), 3.93 (q,  $J = 6.5$  Hz, 2H), 1.23 (t,  $J = 6.8$  Hz, 3H).

Compound **15**:  $^1\text{H}$  NMR (500 MHz, dms $\text{o}$ )  $\delta$  8.42 (d,  $J = 4.9$  Hz, 2H), 7.70 (d,  $J = 7.7$  Hz, 1H), 7.39 (q,  $J = 8.2$  Hz, 2H), 7.29 (d,  $J = 5.1$  Hz, 2H), 7.17 (t,  $J = 7.3$  Hz, 1H), 6.01 (s, 1H), 3.94 (s, 3H), 3.88 (q,  $J = 7.2$  Hz, 2H), 1.18 (t,  $J = 7.0$  Hz, 3H).

Compound **16**:  $^1\text{H}$  NMR (401 MHz, dms $\text{o}$ )  $\delta$  8.43 (dd,  $J = 4.7, 1.5$  Hz, 2H), 7.68 (dd,  $J = 8.3, 2.6$  Hz, 1H), 7.40 (dd,  $J = 9.0, 4.2$  Hz, 1H), 7.29 (dd,  $J = 4.8, 1.5$  Hz, 2H), 7.22 (td,  $J = 9.0, 2.7$  Hz, 1H), 6.02 (s, 1H), 3.92 (s, 3H), 3.88 (q,  $J = 7.1$  Hz, 2H), 1.18 (t,  $J = 7.0$  Hz, 3H).

## Notes

This work was partially published as “Allosteric Drugs: The Interaction of Antitumor Compound MKT-077 with Human Hsp70 Chaperones” Rousaki A., Miyata, Y., Jinwal, U., Dickey, C.A., Gestwicki, J.E., Zuiderweg, E.R.P. *J.Mol.Biol.* (2011) 411, 614-632 and “Allosteric activation of Hsp70 binding promotes polyglutamine androgen receptor clearance and rescues toxicity in a *Drosophila* model of SBMA” Wang, A.M., Miyata, Y., Klinedinst, S., Peng, H., Chua, J.C., Komiyama, T., Pratt, W.B., Osawa, Y., Collins, C.A., Gestwicki, J.E. and Liberman, A.P. *Nat. Chem. Biol.* (in press)

## Author contributions

### NMR studies

Aikaterini Rousaki, Jason E. Gestwicki and Erik R.P. Zuiderweg designed the experiments. Aikaterini Rousaki, and Erik R.P. Zuiderweg performed the NMR and simulation experiments. Yoshinari Miyata synthesized MKT-077 and performed the partial proteolysis. Umesh K. Jinwal performed tau stability assay. ATPase assay for MKT-077 was performed by Sandlin P. Seguin from Jeffrey Brodsky's group at University of Pittsburgh.

### PolyQ AR studies

Adrienne M Wang, Yoshinari Miyata, Susan Klinedinst, Hwei-Ming Peng, Jason C. Chua, William B. Pratt, Yoichi Osawa, Catherine A. Collins, Jason E. Gestwicki and Andrew P. Lieberman designed the experiments. Adrienne M Wang, Susan Klinedinst, Hwei-Ming Peng, Jason C. Chua performed biological

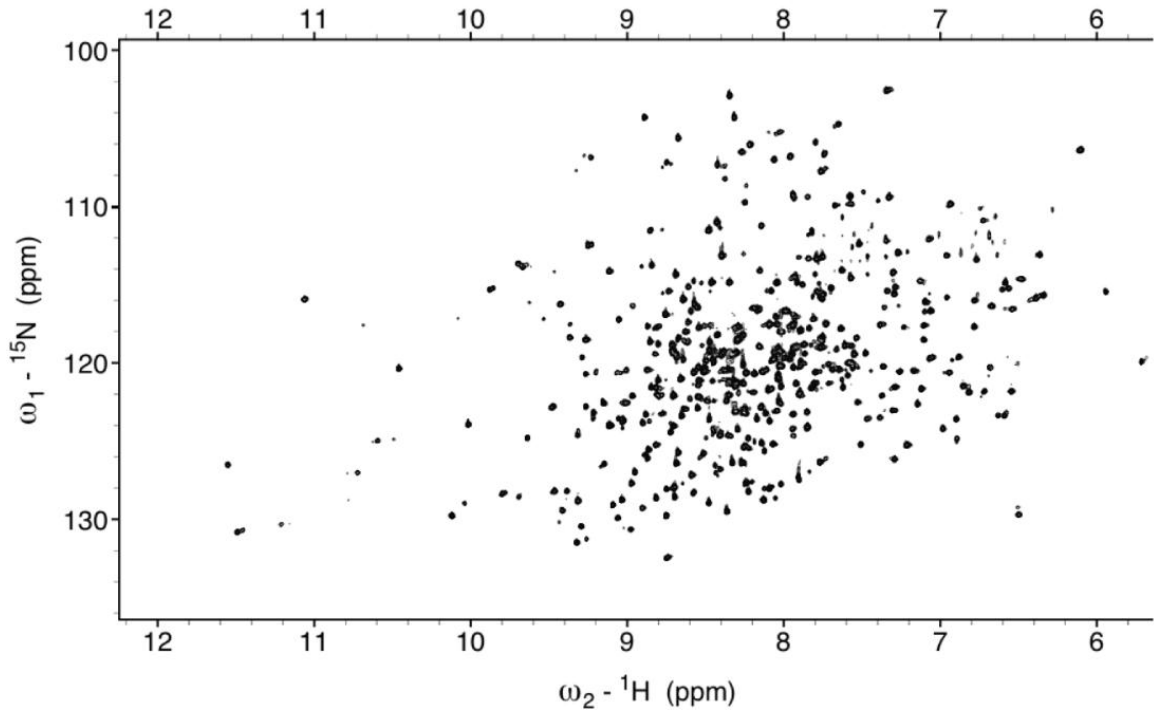
experiments. Yoshinari Miyata synthesized compounds, developed assays and performed biochemical characterizations.

Neutral MKT-077 derivatives studies

Yoshinari Miyata, Xiaokai Li, Hsiu-Fang Lee, Duxin Sun and Jason E. Gestwicki designed the experiments. Yoshinari Miyata and Xiaokai Li synthesized compounds and performed assays. Hsiu-Fang Lee performed pharmacokinetic experiments.

## 4.5 Appendices

### 4.5.1 800 MHz $^1\text{H}$ - $^{15}\text{N}$ TROSY spectrum of 250 $\mu\text{M}$ $^{15}\text{N}$ , $^2\text{H}$ , $^{13}\text{C}$ Hsc70 NBD in the ADP state (residues 1-387).



Appendix 4.5.1 800 MHz  $^1\text{H}$ - $^{15}\text{N}$  TROSY spectrum of 250  $\mu\text{M}$   $^{15}\text{N}$ ,  $^2\text{H}$ ,  $^{13}\text{C}$  Hsc70 NBD in the ADP state (residues 1-387).

## 4.5.2 Compilation of chemical shift changes in the $^{15}\text{N}$ - $^1\text{H}$ TROSY spectra.

1	2	3	4	5	6	7	8	9	10	11	12	13	14	15	16	17	18	19	20	21	22	23	24	25	26	27	28
1	2	3	4	5	6	7	8	9	10	11	12	13	14	15	16	17	18	19	20	21	22	23	24	25	26	27	28
1	2	3	4	5	6	7	8	9	10	11	12	13	14	15	16	17	18	19	20	21	22	23	24	25	26	27	28
31	32	33	34	35	36	37	38	39	40	41	42	43	44	45	46	47	48	49	50	51	52	53	54	55	56	57	58
31	32	33	34	35	36	37	38	39	40	41	42	43	44	45	46	47	48	49	50	51	52	53	54	55	56	57	58
31	32	33	34	35	36	37	38	39	40	41	42	43	44	45	46	47	48	49	50	51	52	53	54	55	56	57	58
61	62	63	64	65	66	67	68	69	70	71	72	73	74	75	76	77	78	79	80	81	82	83	84	85	86	87	88
61	62	63	64	65	66	67	68	69	70	71	72	73	74	75	76	77	78	79	80	81	82	83	84	85	86	87	88
61	62	63	64	65	66	67	68	69	70	71	72	73	74	75	76	77	78	79	80	81	82	83	84	85	86	87	88
91	92	93	94	95	96	97	98	99	100	101	102	103	104	105	106	107	108	109	110	111	112	113	114	115	116	117	118
91	92	93	94	95	96	97	98	99	100	101	102	103	104	105	106	107	108	109	110	111	112	113	114	115	116	117	118
91	92	93	94	95	96	97	98	99	100	101	102	103	104	105	106	107	108	109	110	111	112	113	114	115	116	117	118
121	122	123	124	125	126	127	128	129	130	131	132	133	134	135	136	137	138	139	140	141	142	143	144	145	146	147	148
121	122	123	124	125	126	127	128	129	130	131	132	133	134	135	136	137	138	139	140	141	142	143	144	145	146	147	148
121	122	123	124	125	126	127	128	129	130	131	132	133	134	135	136	137	138	139	140	141	142	143	144	145	146	147	148
151	152	153	154	155	156	157	158	159	160	161	162	163	164	165	166	167	168	169	170	171	172	173	174	175	176	177	178
151	152	153	154	155	156	157	158	159	160	161	162	163	164	165	166	167	168	169	170	171	172	173	174	175	176	177	178
151	152	153	154	155	156	157	158	159	160	161	162	163	164	165	166	167	168	169	170	171	172	173	174	175	176	177	178
181	182	183	184	185	186	187	188	189	190	191	192	193	194	195	196	197	198	199	200	201	202	203	204	205	206	207	208
181	182	183	184	185	186	187	188	189	190	191	192	193	194	195	196	197	198	199	200	201	202	203	204	205	206	207	208
181	182	183	184	185	186	187	188	189	190	191	192	193	194	195	196	197	198	199	200	201	202	203	204	205	206	207	208
211	212	213	214	215	216	217	218	219	220	221	222	223	224	225	226	227	228	229	230	231	232	233	234	235	236	237	238
211	212	213	214	215	216	217	218	219	220	221	222	223	224	225	226	227	228	229	230	231	232	233	234	235	236	237	238
211	212	213	214	215	216	217	218	219	220	221	222	223	224	225	226	227	228	229	230	231	232	233	234	235	236	237	238
241	242	243	244	245	246	247	248	249	250	251	252	253	254	255	256	257	258	259	260	261	262	263	264	265	266	267	268
241	242	243	244	245	246	247	248	249	250	251	252	253	254	255	256	257	258	259	260	261	262	263	264	265	266	267	268
241	242	243	244	245	246	247	248	249	250	251	252	253	254	255	256	257	258	259	260	261	262	263	264	265	266	267	268
271	272	273	274	275	276	277	278	279	280	281	282	283	284	285	286	287	288	289	290	291	292	293	294	295	296	297	298
271	272	273	274	275	276	277	278	279	280	281	282	283	284	285	286	287	288	289	290	291	292	293	294	295	296	297	298
271	272	273	274	275	276	277	278	279	280	281	282	283	284	285	286	287	288	289	290	291	292	293	294	295	296	297	298
301	302	303	304	305	306	307	308	309	310	311	312	313	314	315	316	317	318	319	320	321	322	323	324	325	326	327	328
301	302	303	304	305	306	307	308	309	310	311	312	313	314	315	316	317	318	319	320	321	322	323	324	325	326	327	328
301	302	303	304	305	306	307	308	309	310	311	312	313	314	315	316	317	318	319	320	321	322	323	324	325	326	327	328
331	332	333	334	335	336	337	338	339	340	341	342	343	344	345	346	347	348	349	350	351	352	353	354	355	356	357	358
331	332	333	334	335	336	337	338	339	340	341	342	343	344	345	346	347	348	349	350	351	352	353	354	355	356	357	358
331	332	333	334	335	336	337	338	339	340	341	342	343	344	345	346	347	348	349	350	351	352	353	354	355	356	357	358
361	362	363	364	365	366	367	368	369	370	371	372	373	374	375	376	377	378	379	380	381	382	383	384	385	386		
361	362	363	364	365	366	367	368	369	370	371	372	373	374	375	376	377	378	379	380	381	382	383	384	385	386		

### Appendix 4.5.2 Compilation of chemical shift changes in the $^{15}\text{N}$ - $^1\text{H}$ TROSY spectra.

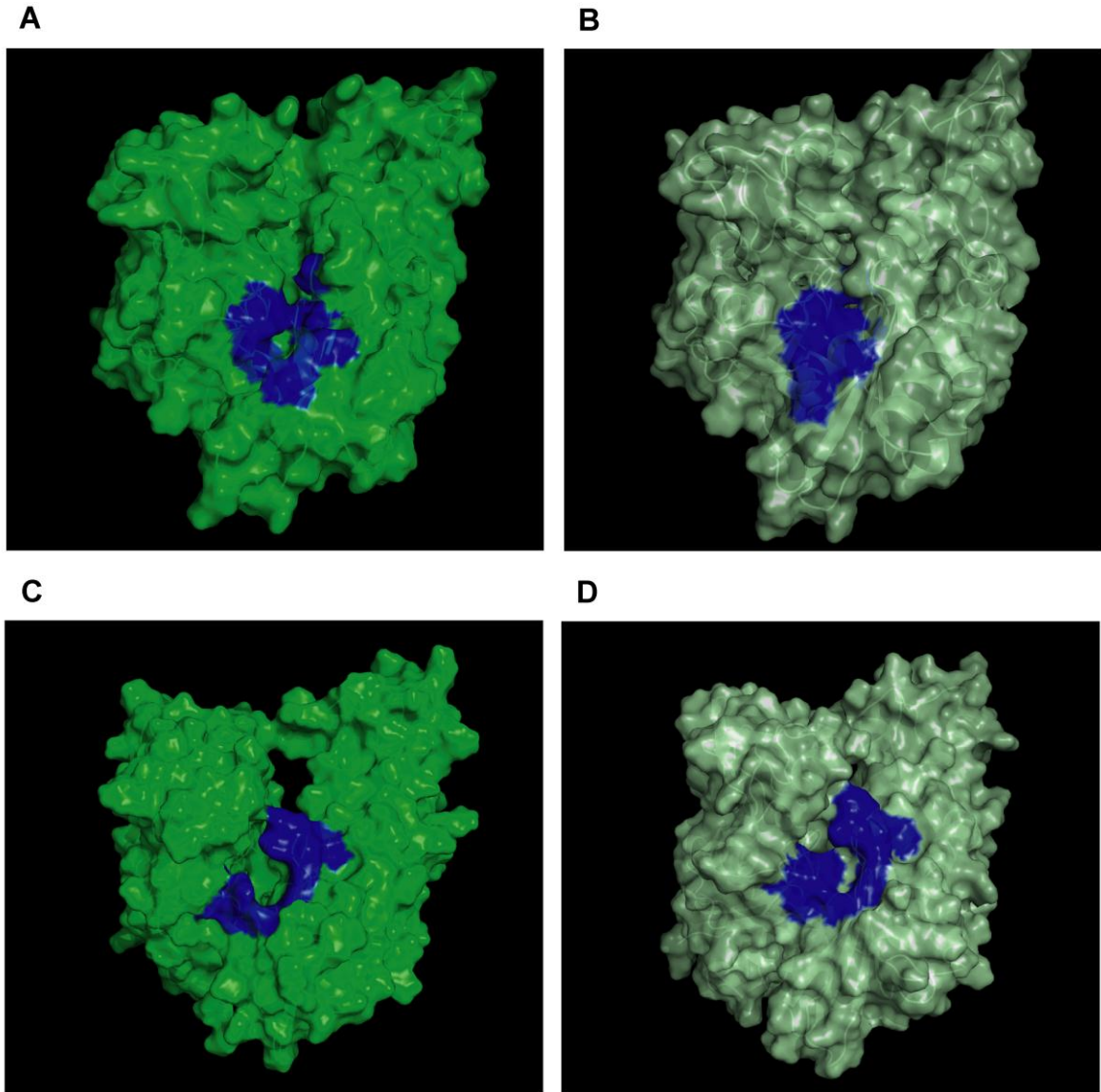
Top line: 80  $\mu\text{M}$   $^{15}\text{N}$ -labeled Hsc70 NBD in the presence of 10 mM ADP, with 80  $\mu\text{M}$  MKT-077.

Middle line: 250  $\mu\text{M}$   $^{15}\text{N}$ - $^2\text{H}$  labeled Hsc70 NBD in the presence of 10 mM ADP, with 120  $\mu\text{M}$  MKT-077.

Bottom line: 120  $\mu\text{M}$   $^{15}\text{N}$ -labeled Hsc70 NBD in the presence of 2 mM AMPPNP, with 240  $\mu\text{M}$  MKT-077.

Green, no changes; yellow, small changes; red, large changes; grey, no assignments; cyan, cannot tell because of overlap.

### 4.5.3 Nucleotide-dependent conformational changes in Hsp70 NBD



**Appendix 4.5.3 Nucleotide-dependent conformational changes in Hsp70 NBD.** Top: Changes in the overall architecture of the NBD of DnaK of *Thermos Thermophilus* in solution. (A) The open ADP state; (B) the closed AMPPNP (ATP) state. The MKT contact residues of Hsc70 NBD are projected on these conformations in blue. Bottom: Changes in the overall architecture of the NBD of human Hsc70 in the crystal. (C) The (equilibrated) crystal structure of Human Hsc70 NBD-ADP in complex with yeast Hsp110 (3C7N) resembles the solution open state. (D) The (equilibrated) crystal structure of isolated Hsc70 NBD-ADP resembles the solution closed (ATP) state. The figure was generated in PyMol.

#### 4.5.4 Hsc70 (HSPA8) residues in contact with the five MKT-077 docking families, shown in the context of the human Hsp70 (HSPA) paralogs.

	11	12	13	14	15						69	70	71	72	73	74	75	76		80	81	82	83	84													
HSPA8	L	G	T	T	Y						D	A	K	R	L	I	G	R		D	A	V	V	Q													
HspA1A	L	G	T	T	Y						D	A	K	R	L	I	G	R		D	P	V	V	Q													
HspA1L	L	G	T	T	Y						D	A	K	R	L	I	G	R		D	P	V	V	Q													
Hspa2	L	G	T	T	Y						D	A	K	R	L	I	G	R		D	A	T	V	Q													
HSPA5	L	G	T	T	Y						D	A	K	R	L	I	G	R		D	P	S	V	Q													
HSPA6	L	G	T	T	Y						D	A	K	R	L	I	G	R		D	T	T	V	Q													
HSPA9	L	G	T	T	N						A	T	K	R	L	I	G	R		D	P	E	V	Q													
HSP12A	F	G	T	T	S						Y	A	A	R	D	F	Y	H		P	N	E	A	K													
HSPA12b	F	G	T	T	S						Y	T	A	R	D	Y	Y	H		P	E	E	A	R													
HSPA13	L	G	T	T	Y						D	A	K	R	F	I	G	K		A	E	E	L	E													
HSPA14	L	G	C	T	S						K	V	K	Q	I	L	G	R		D	P	Q	A	Q													
	145	146	147	148	149	150	151	152	153	154	155	156			173	174	175	176	177																		
HSPA8	T	V	P	A	Y	F	N	D	S	Q	R	Q			I	N	E	P	T																		
HspA1A	T	V	P	A	Y	F	N	D	S	Q	R	Q			I	N	E	P	T																		
HspA1L	T	V	P	A	Y	F	N	D	S	Q	R	Q			I	N	E	P	T																		
Hspa2	T	V	P	A	Y	F	N	D	S	Q	R	Q			I	N	E	P	T																		
HSPA5	T	V	P	A	Y	F	N	D	S	Q	R	Q			I	N	E	P	T																		
HSPA6	T	V	P	A	Y	F	N	D	S	Q	R	Q			I	N	E	P	T																		
HSPA9	T	V	P	A	Y	F	N	D	S	Q	R	Q			I	N	E	P	T																		
HSP12A	T	V	P	A	<i>I</i>	W	K	Q	P	A	K	Q			A	L	E	P	E																		
HSPA12b	T	V	P	A	<i>I</i>	W	K	Q	P	A	K	Q			A	L	E	P	E																		
HSPA13	S	V	P	A	E	F	D	L	K	Q	R	N			I	N	E	P	T																		
HSPA14	T	V	P	F	D	F	G	E	K	Q	K	N			I	H	E	P	S																		
	202	203	204	205	206	207	208			220	221	222	223	224	225	226	227	228	229	230			318	319	320												
HSPA8	G	G	T	F	D	V	S			K	S	T	A	G	D	T	H	L	G	G			E	K	A												
HspA1A	G	G	T	F	D	V	S			K	A	T	A	G	D	T	H	L	G	G			E	K	A												
HspA1L	G	G	T	F	D	V	S			K	A	T	A	G	D	T	H	L	G	G			E	K	A												
Hspa2	G	G	T	F	D	V	S			K	S	T	A	G	D	T	H	L	G	G			E	K	A												
HSPA5	G	G	T	F	D	V	S			K	A	T	N	G	D	T	H	L	G	G			Q	K	V												
HSPA6	G	G	T	F	D	V	S			K	A	T	A	G	D	T	H	L	G	G			E	K	A												
HSPA9	G	G	T	F	D	I	S			K	S	T	N	G	D	T	F	L	G	G			Q	K	A												
HSP12A	G	G	T	V	D	L	T			K	A	T	G	G	P	Y	G	S	L	G			R	D	L												
HSPA12b	G	G	T	V	D	L	T			K	A	S	G	G	P	Y	G	A	V	G			E	A	L												
HSPA13	G	G	T	L	D	V	S			R	A	M	S	G	N	N	K	L	G	G			Q	Q	V												
HSPA14	G	T	S	L	S	L	S			L	S	T	N	T	D	D	N	I	G	G			R	G	L												

Appendix 4.5.4 Hsc70 (HSPA8) residues in contact with the five MKT-077 docking families, shown in the context of the human Hsp70 (HSPA) paralogs. The alignment was carried out in BLAST-P. Red, contacts with 4 or 5 families; orange, contacts with 2 families; yellow, contacts with 1 family. The residues that showed chemical shifts are shown in italic. Numbering is for Hsc70 (HSPA8).



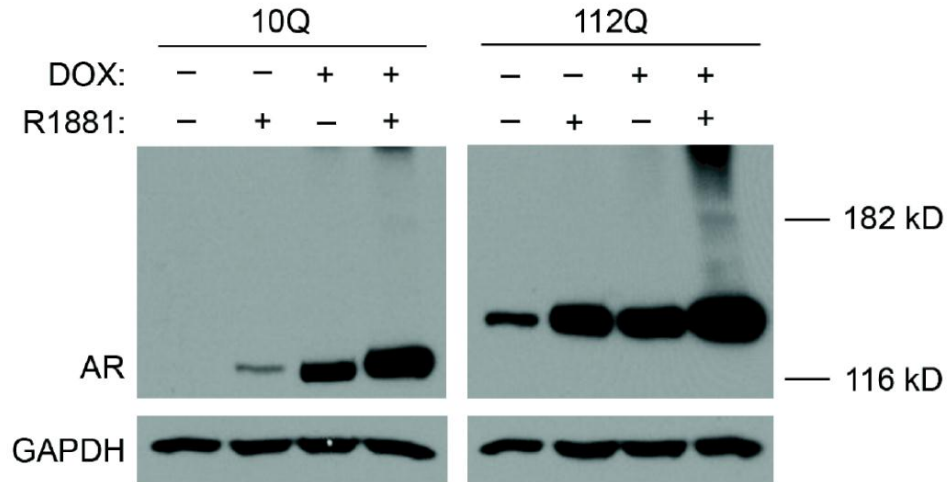
**4.5.5 Residues with chemical shift changes and their distances from MKT-077 in the orientation modeled by AUTODOCK**

NMR residues	Distance from MKT-077 (Å)
Gln84	>5.0
Thr140	>5.0
Ala142	>5.0
Val143	>5.0
Val144	>5.0
Ala148	4.0
Thr222	2.3
Ala223	2.1
Asp225	2.8
Thr226	3.0
His227	4.8
Leu228	>5.0

**Appendix 4.5.5 Residues with chemical shift changes and their distances from MKT-077 in the orientation modeled by AUTODOCK.**

Distances between the residues and closest non-hydrogen atom on MKT-077 were calculated using PyMol.

**4.5.6 Hormone and glutamine length-dependent polyQ AR oligomerization in Tet-ON PC12 cells**



**Appendix 4.5.6 Hormone and glutamine length-dependent polyQ AR oligomerization in Tet-ON PC12 cells.** PC12 cells were induced to express AR10Q (left panel) or AR112Q (right panel) with doxycycline (0.5  $\mu\text{g}/\mu\text{l}$ ) and treated with R1881 (10nM) for 48 hours. Lysates were analyzed after ultracentrifugation at 100,000 g for 30 min. High MWAR112Q oligomers are seen by western blot in the presence of ligand.

## 4.6 References

1. Evans CG, Chang L, Gestwicki JE. Heat shock protein 70 (hsp70) as an emerging drug target. *J Med Chem*, 53(12), 4585-4602 (2010).
2. Patury S, Miyata Y, Gestwicki JE. Pharmacological targeting of the Hsp70 chaperone. *Curr Top Med Chem*, 9(15), 1337-1351 (2009).
3. Koya K, Li Y, Wang H *et al.* MKT-077, a novel rhodacyanine dye in clinical trials, exhibits anticarcinoma activity in preclinical studies based on selective mitochondrial accumulation. *Cancer Res*, 56(3), 538-543 (1996).
4. Modica-Napolitano JS, Koya K, Weisberg E, Brunelli BT, Li Y, Chen LB. Selective damage to carcinoma mitochondria by the rhodacyanine MKT-077. *Cancer Res*, 56(3), 544-550 (1996).
5. Propper D, Braybrooke J, Taylor D *et al.* Phase I trial of the selective mitochondrial toxin MKT 077 in chemo-resistant solid tumours. *Annal of Oncology*, 10, 923-927 (1999).
6. Wadhwa R, Sugihara T, Yoshida A *et al.* Selective toxicity of MKT-077 to cancer cells is mediated by its binding to the hsp70 family protein mot-2 and reactivation of p53 function. *Cancer Res*, 60(24), 6818-6821 (2000).
7. Tikoo A, Shakri R, Connolly L *et al.* Treatment of ras-induced cancers by the F-actin-bundling drug MKT-077. *Cancer J*, 6(3), 162-168 (2000).
8. Chang L, Bertelsen EB, Wisen S, Larsen EM, Zuiderweg ER, Gestwicki JE. High-throughput screen for small molecules that modulate the ATPase activity of the molecular chaperone DnaK. *Anal Biochem*, 372(2), 167-176 (2008).
9. Chang L, Miyata Y, Ung PM *et al.* Chemical Screens against a Reconstituted Multiprotein Complex: Myricetin Blocks DnaJ Regulation of DnaK through an Allosteric Mechanism. *Chem Biol*, 18(2), 210-221 (2011).
10. Wisen S, Bertelsen EB, Thompson AD *et al.* Binding of a Small Molecule at a Protein-Protein Interface Regulates the Chaperone Activity of Hsp70-Hsp40. *Acs Chemical Biology*, 5(6), 611-622 (2010).
11. Bhattacharya A, Kurochkin AV, Yip GN, Zhang Y, Bertelsen EB, Zuiderweg ER. Allostery in Hsp70 chaperones is transduced by subdomain rotations. *J Mol Biol*, 388(3), 475-490 (2009).
12. Zhang Y, Zuiderweg ER. The 70-kDa heat shock protein chaperone nucleotide-binding domain in solution unveiled as a molecular machine that can reorient its functional subdomains. *Proc Natl Acad Sci U S A*, 101(28), 10272-10277 (2004).
13. Morris GM, Huey R, Lindstrom W *et al.* AutoDock4 and AutoDockTools4: Automated docking with selective receptor flexibility. *J Comput Chem*, 30(16), 2785-2791 (2009).
14. Chiba Y, Kubota T, Watanabe M *et al.* Selective antitumor activity of MKT-077, a delocalized lipophilic cation, on normal cells and cancer cells in vitro. *J Surg Oncol*, 69(2), 105-110 (1998).
15. Kawakami M, Koya K, Ukai T *et al.* Structure-activity of novel rhodacyanine dyes as antitumor agents. *J Med Chem*, 41(1), 130-142 (1998).

16. Kawakami M, Suzuki N, Sudo Y, Shishido T, Maeda M. Development of an enzyme-linked immunosorbent assay (ELISA) for antitumor agent MKT 077. *Analytica Chimica Acta*, 362(2-3), 177-186 (1998).
17. Buchberger A, Theyssen H, Schroder H *et al.* Nucleotide-induced conformational changes in the ATPase and substrate binding domains of the DnaK chaperone provide evidence for interdomain communication. *J Biol. Chem.*, 270(28), 16903-16910 (1995).
18. Howarth JL, Glover CP, Uney JB. HSP70 interacting protein prevents the accumulation of inclusions in polyglutamine disease. *J Neurochem*, 108(4), 945-951 (2009).
19. Takeyama K, Ito S, Yamamoto A *et al.* Androgen-dependent neurodegeneration by polyglutamine-expanded human androgen receptor in *Drosophila*. *Neuron*, 35(5), 855-864 (2002).
20. Tatsuta N, Suzuki N, Mochizuki T *et al.* Pharmacokinetic analysis and antitumor efficacy of MKT-077, a novel antitumor agent. *Cancer Chemother Pharmacol*, 43(4), 295-301 (1999).
21. Kashiya E, Hutchinson I, Chua MS *et al.* Antitumor benzothiazoles. 8. Synthesis, metabolic formation, and biological properties of the C- and N-oxidation products of antitumor 2-(4-aminophenyl)benzothiazoles. *J Med Chem*, 42(20), 4172-4184 (1999).
22. Henriksen G, Hauser AI, Westwell AD *et al.* Metabolically stabilized benzothiazoles for imaging of amyloid plaques. *J Med Chem*, 50(6), 1087-1089 (2007).
23. Hohfeld J, Minami Y, Hartl FU. Hip, a novel cochaperone involved in the eukaryotic Hsc70/Hsp40 reaction cycle. *Cell*, 83(4), 589-598 (1995).
24. Walcott JL, Merry DE. Ligand promotes intranuclear inclusions in a novel cell model of spinal and bulbar muscular atrophy. *J Biol Chem*, 277(52), 50855-50859 (2002).
25. Delaglio F, Grzesiek S, Vuister GW, Zhu G, Pfeifer J, Bax A. NMRPipe: a multidimensional spectral processing system based on UNIX pipes. *J Biomol NMR*, 6(3), 277-293 (1995).
26. Goddard TD, Kneller DG. SPARKY 3. (Ed.^(Eds) (University of California, San Francisco, CA., 2000)
27. Crippen GM, Rousaki A, Revington M, Zhang Y, Zuiderweg ER. SAGA: rapid automatic mainchain NMR assignment for large proteins. *J Biomol NMR*, 46(4), 281-298 (2010).
28. DeLano W. The PyMOL Molecular Graphics System (Ed.^(Eds) (DeLano Scientific, San Carlos, CA, USA., 2002)
29. Wang JM, Wang W, Kollman PA, Case DA. Automatic atom type and bond type perception in molecular mechanical calculations. *Journal of Molecular Graphics & Modelling*, 25(2), 247-260 (2006).
30. Case DA, Cheatham TE, 3rd, Darden T *et al.* The Amber biomolecular simulation programs. *J Comput Chem*, 26(16), 1668-1688 (2005).
31. Schuermann JP, Jiang JW, Cuellar J *et al.* Structure of the Hsp110 : Hsc70 nucleotide exchange machine. *Molecular Cell*, 31(2), 232-243 (2008).

32. Meagher K, Redman L, Carlson H. Development of polyphosphate parameters for use with the AMBER force field. *Journal of Computational Chemistry*, 24, 1016-1025 (2003).
33. Chang L, Thompson AD, Ung P, Carlson HA, Gestwicki JE. Mutagenesis reveals the complex relationships between ATPase rate and the chaperone activities of Escherichia coli heat shock protein 70 (Hsp70/DnaK). *J Biol Chem*, 285(28), 21282-21291 (2010).
34. Kanelakis KC, Murphy PJ, Galigniana MD *et al.* hsp90 interacting protein Hip does not affect glucocorticoid receptor folding by the hsp90-based chaperone machinery except to oppose the effect of BAG-1. *Biochemistry*, 39(46), 14314-14321 (2000).
35. Budnik V, Koh YH, Guan B *et al.* Regulation of synapse structure and function by the Drosophila tumor suppressor gene dlg. *Neuron*, 17(4), 627-640 (1996).
36. Freeman M. Reiterative use of the EGF receptor triggers differentiation of all cell types in the Drosophila eye. *Cell*, 87(4), 651-660 (1996).
37. Mahr A, Aberle H. The expression pattern of the Drosophila vesicular glutamate transporter: a marker protein for motoneurons and glutamatergic centers in the brain. *Gene Expr Patterns*, 6(3), 299-309 (2006).
38. Takasu K, Inoue H, Kim HS *et al.* Rhodacyanine dyes as antimalarials. 1. Preliminary evaluation of their activity and toxicity. *J Med Chem*, 45(5), 995-998 (2002).
39. Nishigaki J. New rhodacyanine intermediate and synthesis of pigment using the same. In: *Patent Abstracts of Japan*. (Eds) (Japan, 2004)

## Chapter 5

### Conclusions and Future Directions

#### 5.1 Conclusions

The heat shock protein 70 (Hsp70) is a major regulator of proteostasis and, thus, has been thought to have an important role in protein misfolding diseases. As discussed in Chapter 1, genetic evidence had previously suggested Hsp70's role in tau processing; however, its potential as a therapeutic target had not been explored largely due to the scarcity of chemical tools. This thesis work focused on developing chemical modulators of Hsp70 and using them to better understand the relationship between Hsp70's function and tau stability.

When the Gestwicki laboratory started in 2005, there were only a few small molecules known to interact with Hsp70 and they were poorly characterized [1]. In order to rapidly identify new chemical scaffolds with affinity for Hsp70, Lyra Chang, a former graduate student in the group, developed the first HTS method for the ATPase activity of Hsp70 [2]. When I started my graduate studies, I worked with Lyra to transition from 96- to 384-well format, enabling the screening of larger, diverse libraries. Because the original HTS method was colorimetric and there was a significant loss of sensitivity in 384-well plates, Lyra and I took

advantage of the intrinsic fluorescence properties of white microtiter plates and converted the colorimetric assay to a fluorescence mode. Using this method, we then screened both diversity and focused compound libraries and identified new inhibitors and activators (Chapter 2). Based on the protocol that Lyra and I developed, the Gestwicki laboratory continues to actively use this screening platform. For example, two other lab members recently completed a screen of 100,000 compounds to identify additional Hsp70 inhibitors. Moreover, other academic and industrial colleagues have adapted this method, suggesting that it is a robust approach. Thus, I think that one of my major contributions over the past 4.5 years has been the careful development of this HTS protocol.

Another goal for my thesis was to characterize the mechanism of newly discovered Hsp70 inhibitors and use these compounds to clarify the potential of Hsp70 as a drug target in tauopathies. With a battery of Hsp70 chemical modulators in hand from the HTS efforts, I collaborated with the Dickey group to “tune” the ATPase activity of Hsp70 and study the impact on tau. Because overexpression of Hsp70 had been known to reduce tau levels [3], we initially expected that Hsp70 activators would have the same effect. Surprisingly, we observed the opposite result! Inhibitors reduced tau levels while the activators promoted accumulation. This is an important finding because it strongly supported the idea that Hsp70 is a double-edged sword and it suggested that the kinetics of ATP turnover may be a critical factor in making triage decisions. Based on the findings described in this thesis, further studies on the mechanisms

of Hsp70-mediated quality control are a major objective of the Gestwicki laboratory.

The third major objective of my thesis was to characterize the mechanism of new Hsp70 inhibitors. Subsequent mechanistic study on one of the inhibitors, methylene blue (MB), serendipitously revealed a significant difference between stress inducible Hsp72 and constitutively expressed Hsc70 in responding to oxidative stress (Chapter 3). Although I did not originally intend to study redox reactivity in Hsp70 variants, this work took an interesting and potentially important turn. To our knowledge, this is the first evidence showing that Hsp72 and Hsc70 have distinct functions under stress conditions. Further, these results could have a major impact on drug discovery for AD because MB is currently in Phase III trials.

Although my work on the MB mechanism was quite interesting and unexpected, this scaffold was not amenable to medicinal chemistry; thus, I set out to develop more potent Hsp70 inhibitors that were based on the MKT-077 scaffold. MKT-077 initially caught my attention during the preparation of a review of known Hsp70 inhibitors because it has potent anti-cancer activity and it has been explored in Phase I clinical trials [4-6]. However, despite the promise of this scaffold, little work on its binding site or mechanism had been explored, which motivated me to further study this system. Using NMR and molecular modeling, we showed that MKT-077 binds Hsp70 at a site immediately below the nucleotide



binding pocket. Further, we found that the compound stabilizes the ADP state of Hsp70 and increases its affinity for substrates. This finding was significant because its functional effect on Hsp70 was different from any other Hsp70 modulators we had developed at the time. This novel mechanism led us to use MKT-077 derivatives as chemical tools to study the relationship between Hsp70's affinity for substrates and their stability. Using an MKT-077 analog and the co-chaperone Hip, which has the same *in vitro* effects on Hsp70 as MKT-077, we showed that increasing Hsp70's affinity for clients leads to proteasomal degradation of polyQ AR. Together, these results demonstrate that chemical probes for Hsp70 are powerful tools in studying complex chaperone biology and provide insight into how triage decisions are made.

Finally, we showed that an uncharged MKT-077 derivative, YM8, can cross the blood-brain barrier (BBB) while maintaining its binding to Hsp70 and activity to reduce tau in HeLa cells. Because BBB permeability is often the major hurdle in developing central nervous system (CNS) targeting drugs, these results suggest strong promise of this chemical scaffold for the treatment of tauopathy. To improve potency and metabolic stability, we synthesized 16 member library of uncharged MKT-077 analogs based on the docking model. We found that fluorine and chlorine substitutions at C-5 and C-6 on the benzothiazole ring increase the compound affinity for Hsp70 *in vitro*, consistent with the docking results. While more structure activity relationship (SAR) and pharmacokinetic analyses are needed, these favorable properties warrant further development as

a drug lead.

When I started in the Gestwicki laboratory, there were only a few Hsp70 modulators known and the methods for HTS were still under development. My major contributions to the field (described in this thesis) were the development of 384-well methods for HTS (Chapter 2), development of the first model linking Hsp70's ATPase activity to substrate fate (Chapter 3) and the development of the first potent and well-characterized Hsp70 inhibitors (Chapter 4). Together, this work significantly advanced the field and, collectively, these studies strongly indicate that Hsp70 is a potential therapeutic target for tauopathies. However, these studies are really only the beginning. In the next sections, I will discuss some ideas for how the work of Chapter 2-4 might provide a framework for further exploring Hsp70 as a drug target.

## **5.2 Future Directions**

### **5.2.1 Identifying co-chaperones that are involved in “low affinity” and “high affinity” complexes**

Although components of the “folding” and “degradation” complexes have been suggested [7], little is known about what is responsible for switching between them. Because the results in Chapters 3 and 4 suggest that substrate dwell time may be an important factor in determining substrate fate, it is likely that ATP- and ADP- forms of Hsp70 have different co-chaperone interactomes. Specifically, it is expected that the ADP state has more interactions with degradation factors.

Other members of the Gestwicki laboratory recently identified molecular chaperones that are associated with soluble and aggregation-prone polyQ fragments using chemical probes and mass spectrometry [8]. Furthermore, Andrea Thompson, a graduate student in our group, recently used MB and mass spectrometry to identify what molecular chaperones are interacting with tau when it is targeted for degradation (Thompson, *et al.* unpublished data). I think that an important next step is to take a similar strategy to explore how MKT-077 changes the co-chaperones bound to Hsp70 in the ADP-like conformation. Specifically, mass spectrometry in the presence of the compound may identify the components of the Hsp70 chaperone complex in the high affinity state (**Figure 5.1**). Based on currently available data, for example, we expect to find an E3 ligase such as CHIP in this state. In contrast, “pro-folding” factors such as HOP might be enriched in the control sample (i.e. no MKT-077). This work could be supplemented with other compounds, such as 115-7c, and point mutants in Hsp70. The results obtained in this proposed experiment might further clarify the

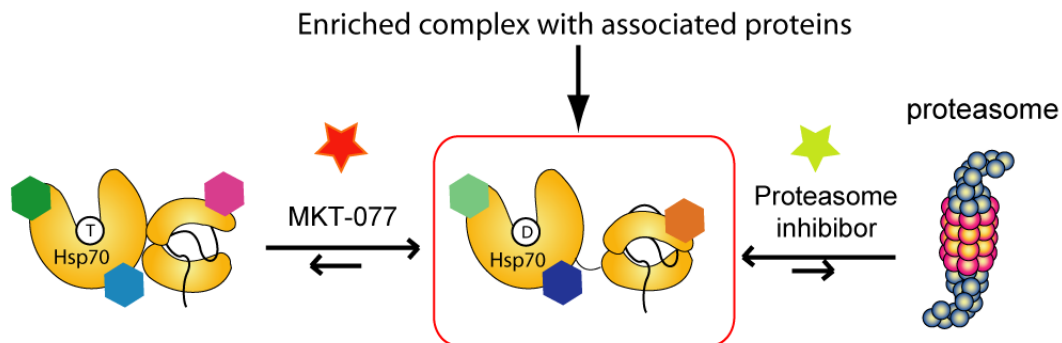


**Figure 5.1 Utilizing chemical probes to identify chaperone complexes in the high-affinity ADP-state.** Hsp70 interacts with various “pro-folding” and “degradation” factors. We can use MKT-077 to stall Hsp70 in the ADP-state, inhibit proteasome to enrich for intermediate complexes and conduct mass spectrometry analysis to identify proteins associated with this particular nucleotide states.

relationship between nucleotide state and recruitment of degradation factors.

### 5.2.2 Identifying modulators of protein-protein interactions

As discussed in Chapter 1, another strategy to alter tau stability is to modulate protein-protein interactions within the Hsp70 chaperone complex. Even within the same co-chaperone family, individual isoforms have been known to have different effects on tau (e.g. BAG1 and BAG2). Accordingly, it will be beneficial to build a library of chemical modulators that specifically block each chaperone/co-chaperone interaction. To date, we have extensively used the ATPase activity of Hsp70 as readout to identify chemical modulators; however, other members of our group recently showed that ATPase activity does not necessarily correlate with other Hsp70 functions [9]. Therefore, it will be useful to look at specific physical interactions between Hsp70 and its co-chaperones. For examples, Srikanth Patury in our group developed a flow cytometry-based binding assay

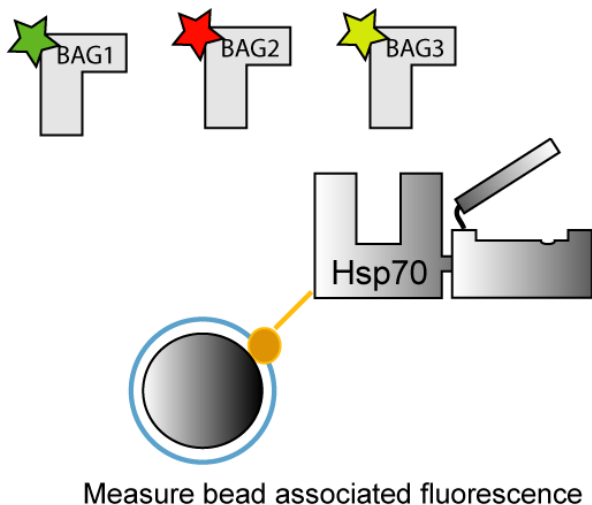
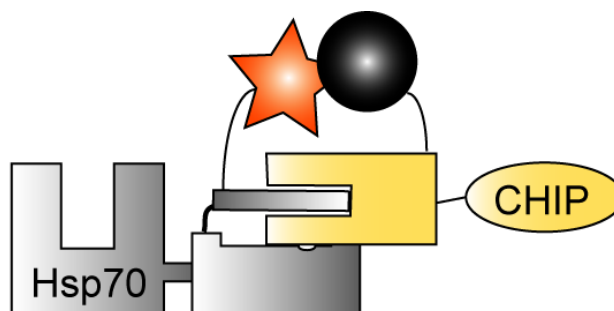


**Figure 5.2 Flow cytometry assay.** Hsp70 is immobilized on a bead and its interactions with fluorescent labeled binding partners are measured.

platform to monitor the interaction between Hsp70 and the BAG proteins (**Figure 5.2**). This platform is amenable to HTS and, thus, it may be used to screen for small molecules that perturb the interaction.

In addition, Matt Smith,

another graduate student in the laboratory, developed a FRET-like assay to measure binding of Hsp70 to CHIP (Figure 5.3). In this assay,



binding partners are labeled either with a fluorophore or a

**Figure 5.3 FRET-like binding assay.** Hsp70 and its binding partner are labeled with a fluorophore and a quencher, respectively. The protein-protein interaction can be measured by fluorescence quench.

quencher and the binding event can be monitored by quenching of the fluorescent signal. This assay has successfully been used to investigate spergualin analogs, which have been speculated to block the interaction (data not shown). These methods are generally applicable to other Hsp70/co-chaperone combinations and may provide an avenue for developing small molecule modulators of the protein-protein interactions.

### 5.2.3 Optimizing neutral MKT-077 derivatives as drug leads

Although we developed BBB permeable MKT-077 derivatives that reduce tau levels in cells, they need to be further optimized in order to be tested in animals. For example, YM8 is not a very stable compound; 80% of the compound is gone within 10 minutes in mouse liver microsome (Lee, et al. unpublished data). Mass spectrometry experiments indicated that YM8 is extensively oxidized at the benzothiazole and pyridinium moieties. In addition, YM8 has poor solubility, which makes administration into animals difficult. For other benzothiazole compounds, it has been suggested that C-5 and C-6 are oxidized by cytochrome

P450 [10,11]. Therefore, it will be interesting to test our uncharged MKT-077 derivatives with substituents at those positions (compounds **2**, **3**, **6**, **7**) in the microsome stability assay. Because our *in vitro* studies demonstrated that these compounds are more potent than the original scaffold (YM8), these substitutions may confer higher overall *in vivo* efficacy. Currently, Dr. Xiaokai Li is synthesizing compounds with a variety of substituents at C-5 and C-6. We expect that these molecules may provide further insight into the interaction between the MKT-077 scaffold and Hsp70, which would help us design more potent Hsp70 inhibitors. Furthermore, we plan to explore potential contacts between the pyridinium moiety and the protein by synthesizing compounds with substituents on the ring as well as other basic heterocycles such as pyrimidine and imidazole. By incorporating both binding and pharmacokinetic data, we expect to develop a drug lead with low to mid nano molar affinity and enhanced stability. Binding of best compounds to Hsp70 will be further characterized by NMR and other methods available in our laboratory. Finally, a candidate compound will be tested in a mouse model of tauopathy.

### **5.3 Final Thoughts**

The last few years have been very exciting for the Gestwicki laboratory as we started to understand some aspects of Hsp70 functions and to demonstrate its potential as a therapeutic target. Importantly, much of our progress and contribution to the field of chaperone biology owe to the chemical probes described throughout this thesis and others developed in our group. It is

noteworthy that all this was made possible by interdisciplinary collaborations with others inside and outside our laboratory. Because Hsp70 chaperone machinery is multifunctional by nature and is regulated by multiple co-chaperones, which exponentially adds complexity, chemical biology approach seems to be a perfect fit for studying this system. The more chemical probes we develop and more people use them in a variety of biological systems, the better we understand the biology of Hsp70.

## 5.4 References

1. Brodsky JL, Chiosis G. Hsp70 molecular chaperones: emerging roles in human disease and identification of small molecule modulators. *Curr Top Med Chem*, 6(11), 1215-1225 (2006).
2. Chang L, Bertelsen EB, Wisen S, Larsen EM, Zuiderweg ER, Gestwicki JE. High-throughput screen for small molecules that modulate the ATPase activity of the molecular chaperone DnaK. *Anal Biochem*, 372(2), 167-176 (2008).
3. Petrucelli L, Dickson D, Kehoe K *et al.* CHIP and Hsp70 regulate tau ubiquitination, degradation and aggregation. *Hum Mol Genet*, 13(7), 703-714 (2004).
4. Koya K, Li Y, Wang H *et al.* MKT-077, a novel rhodacyanine dye in clinical trials, exhibits anticarcinoma activity in preclinical studies based on selective mitochondrial accumulation. *Cancer Res*, 56(3), 538-543 (1996).
5. Wadhwa R, Sugihara T, Yoshida A *et al.* Selective toxicity of MKT-077 to cancer cells is mediated by its binding to the hsp70 family protein mot-2 and reactivation of p53 function. *Cancer Res*, 60(24), 6818-6821 (2000).
6. Tikoo A, Shakri R, Connolly L *et al.* Treatment of ras-induced cancers by the F-actin-bundling drug MKT-077. *Cancer J*, 6(3), 162-168 (2000).
7. Arndt V, Rogon C, Hohfeld J. To be, or not to be--molecular chaperones in protein degradation. *Cell Mol Life Sci*, 64(19-20), 2525-2541 (2007).
8. Walter GM, Smith MC, Wisén S *et al.* Ordered assembly of heat shock proteins, Hsp26, Hsp70, Hsp90, and Hsp104, on expanded polyglutamine fragments revealed by chemical probes. *J Biol Chem*, 286(47), 40486-40493 (2011).
9. Chang L, Thompson AD, Ung P, Carlson HA, Gestwicki JE. Mutagenesis reveals the complex relationships between ATPase rate and the chaperone activities of Escherichia coli heat shock protein 70 (Hsp70/DnaK). *J Biol Chem*, 285(28), 21282-21291 (2010).
10. Henriksen G, Hauser AI, Westwell AD *et al.* Metabolically stabilized benzothiazoles for imaging of amyloid plaques. *J Med Chem*, 50(6), 1087-1089 (2007).
11. Kashiyama E, Hutchinson I, Chua MS *et al.* Antitumor benzothiazoles. 8. Synthesis, metabolic formation, and biological properties of the C- and N-oxidation products of antitumor 2-(4-aminophenyl)benzothiazoles. *J Med Chem*, 42(20), 4172-4184 (1999).